

WELCOME

The Organizing Committee kindly welcomes you at the International Conference “Functional materials and nanotechnologies” **FM&NT-2012**. The conference is organised by Institute of Solid State Physics, University of Latvia in co-operation with National Research programme in Materials Science and Information Technologies of Latvia.



The purpose of the conference is to bring together scientists, researchers, engineers and students from universities, research institutes and related industrial companies working in the field of advanced material science, energy and materials technologies.

Scientific topics of the conference

Multifunctional Materials:

Advanced inorganic, organic and hybrid materials; ferroics; multiscale and multiphenomenal material modelling and simulation;

Nanotechnologies:

Progressive methods, technologies and design for investigation of nanoparticles, nanostructures, nanocomposites, thin films and coatings;

Energy:

Perspective materials and technologies for renewable and hydrogen energy, fuel cells, photovoltaics and developing diverse energy systems.

International Organizing Committee

- **Andris Sternberg (chairperson)**, Institute of Solid State Physics, University of Latvia, Latvia
- **Juras Banys**, Vilnius University, Lithuania
- **Gunnar Borstel**, University of Osnabrück, Germany
- **Niels E. Christensen**, University of Aarhus, Denmark
- **Robert A. Evarestov**, St. Petersburg State University, Russia
- **Claes-Goran Granqvist**, Uppsala University, Sweden
- **Dag Høvik**, The Research Council of Norway, Norway
- **Marco Kirm**, Institute of Physics, University of Tartu, Estonia
- **Jiri Kulda**, Institut Laue-Langevin, France
- **Witold Łojkowski**, Institute of High Pressure Physics, Poland
- **Ergo Nommiste**, University of Tartu, Estonia
- **Ingólfur Torbjörnsson**, Icelandic Centre for Research, Iceland
- **Marcel H. Van de Voorde**, University of Technology Delft, The Netherlands

International Program Committee

- **Līga Grinberga (chairperson)**, Institute of Solid State Physics, University of Latvia
- **Eugene Kotomin**, Max Planck Institute for Solid State Research, Germany
- **Martins Rutkis**, Institute of Solid State Physics, University of Latvia, Latvia
- **Inta Muzikante**, Institute of Solid State Physics, University of Latvia, Latvia
- **Līga Berzina-Cimdina**, Institute of Biomaterials and Biomechanics, Riga Technical University, Latvia
- **Janis Grabis**, Institute of Inorganic Chemistry, Riga Technical University, Latvia
- **Linards Skuja**, Institute of Solid State Physics, University of Latvia, Latvia
- **Maris Springis**, Institute of Solid State Physics, University of Latvia, Latvia
- **Ilmars Zalite**, Institute of Inorganic Chemistry, Riga Technical University, Latvia
- **Janis Zicans**, Institute of Polymers, Riga Technical University

Local Committee

Līga Grinberga, Anatolijs Sarakovskis, Jurgis Grube, Maris Kundzins, Anastasija Jozepa, Anna Muratova, Raitis Siatkovskis, Andris Fedotovs, Dmitrijs Bocarovs, Sniedze Abele, Mikus Voss, Andris Sivars, Peteris Lesnicenoks, Virginija Liepina.

The Organizing Committee sincerely hopes that the conference will give all the participants new insights into the wide spread development of functional materials and nanotechnologies and will enhance the circulation of information released at the meeting.

On behalf of FM&NT-2012 organizers thank you all for coming and we wish you most successful and enjoyable conference.

The book of abstracts has been published thanks to the financial support from ERAF project „Atbalsts starptautiskās sadarbības projektiem zinātnē un tehnoloģijās LU Cietvielu fizikas institūtā” Nr.2010/0204/2DP/2.1.1.2.0./10/APIA/VIAA/010.



ĪEGULDĪJUMS TAVĀ NĀKOTNĒ

Edited by: Andris Sternbergs (ISSP UL), Līga Grinberga (ISSP UL)
Typesetting: Anatolijs Sarakovskis (ISSP UL), Jurgis Grube (ISSP UL)
Printed by SIA “Latgales Druka”
ISBN: 978-9984-45-496-2
Institute of Solid State Physics, University of Latvia
8 Kengaraga Street, LV-1063, Riga, Latvia
Phone: +371-67187816
Fax: +371-67132778
e-mail: issp@cfi.lu.lv
web: <http://www.cfi.lu.lv>
Riga, 2012

In Memoriam
Dr. habil. phys. Inta Muzikante
(08.01.1951-15.02.2012)

Inta was born in Valmiera, a town in the northern part of Latvia. She attended school in Sigulda and high school in Riga. While at the high-school, Inta decided to study natural sciences. After graduating from high-school in 1969 she entered the physics section of the Physics and Mathematics department of University of Latvia and obtained her university degree in 1974.



In parallel with University studies, Inta started to work at Semiconductor Physics Research Lab at University of Latvia. After graduating she was offered a position at the Physical Energetics institute of Latvian Academy of Sciences, in the laboratory of prof. Edgars Silinsh, one of the internationally most known Latvian physicists. Inta started a research of electronic and photoelectric processes in organic crystals and thin films. This was a novel field, pioneered both internationally and in Latvia by professors E. Silinsh, O. Neilands and J. Freimanis. It may be stated that Inta stood at the cradle of this research field and stayed faithful to it all of her life. Her work was very successful and within few years she advanced from research assistant to researcher and then leading research scientist. First scientific topic was studies of the mechanism of charge carrier photogeneration and separation in organic molecular crystals. In 1983 for a work titled "Charge carrier photogeneration and trapping processes in organic molecular crystals" Inta obtained her Ph.D. degree (USSR Candidate of Sciences degree).

The major part of I.Muzikante's research activities has been devoted to investigation of electronic states in organic thin films and multilayers. Studies of electrophysical properties and energy structure of the wide class of organic compounds, such as isolators, semiconductors and conductors have been done. During these studies the complex application of conventional space charge limited current method (SCLC), differential method of SCLC, thermally modulated SCLC and thermally stimulated current was provided for local trapping state investigation. These investigations are of great importance for application in studies of organic light-emitting diodes and organic solar cells. In I.Muzikante's work for the first time the existence and asymmetry of trapping states of quadrupolar origin in pentacene thin films was experimentally confirmed.

In the last decade I. Muzikante has broadened her scientific scope. The organic materials with photochromic effect became important part of her research because of their possibility of being employed in optical storage of data and molecular switching devices. Reversible trans/cis photoisomerization of azobenzene and indandione derivatives in self-assembled monolayers, LB multilayers and polymer films were studied.

A turning point in Inta's life was the re-establishment of independent Republic of Latvia in 1991: the previously tightly closed international borders opened, and she was free to visit and work in the most important international scientific centers. During this period she stayed and worked at Potsdam University and the Center of Macromolecular Chemistry in Germany, South Bank University, London and Manchester University in UK, Ecole Supérieure de Physique et de Chemie Industrielles, P.& M.Curie University, and Angers University in France and at the Vilnius University in Lithuania.

After the passing away of prof. E.Silinsh in 1998, Inta took over the duties of the Head of Laboratory. In spite of the Latvian science going through hard times due to inadequate funding, she managed to preserve the labs core staff and to further develop its scientific potential, while also continuing an active research work herself. In 1998 she obtained the Dr.Habil degree for the work "Electronic processes and states in organic molecular crystals and Langmuir-Blodgett multistructures". Inta's research was highly recognized by awarding her in 1999 the recently established and prestigious Edgar's Silinsh prize in physics by Latvian Academy of Sciences. During this and the subsequent period, another of her many talents started to shine through: her particular skill to find capable young people from the best high-schools in Latvia and to motivate them for the research work. Several of these students have now become researchers in her lab. With Inta's demise, 4 PhD students lost their supervisor.

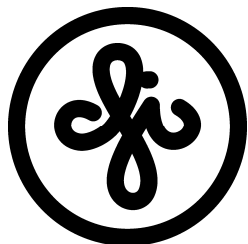
Inta's research and organizational work gained even more momentum after her lab transferred to the Institute of Solid State Physics in 2003. At her new home Inta rapidly acquired the respect and sympathies of their new colleagues. Her duties of the Head of Laboratory and of Leading research scientist were soon supplemented by the tasks of the Institute deputy director for research. In 2006 Inta was elected as Corresponding Member of Latvian Academy of Sciences, and subsequently elected to full Academy membership in 2008. She has authored more than 240 research papers. Inta started to give lecture courses to the physics students of University of Latvia and took up even more duties. She served as a guest editor in international journals, as an expert in European Commission, and as a representative for Latvia in a number of European scientific programs and projects.

With passing away of Inta Muzikante, the Latvian and international science community has lost an excellent scientist and a talented science organizer. However, more important and above all of her excellent professional achievements: all of us who knew her will remember her as a helpful and cordial friend.

A special section devoted to Inta Muzikante is organized at FM&NT-2012.

Organizing committee of FM&NT-2012

Information about the conference



Publishers of the conference papers



Conference hotels



Exhibitors at the conference



America's Leading Manufacturer of Engineered and Advanced Material Products



Armgate is a supplier of analytical equipment and turn-key laboratories for universities, scientific research and independent laboratories, oil refinery and production enterprises, metrology centers in the three Baltic States. Armgate offers the supply and full scale service of equipment, as well as individual task solution of each client. Armgate believes in long-term relations with its customers, providing comprehensive technical support over the life cycle of the equipment. Long-term experience and a team of qualified specialists enable to solve any tasks even in the tightest time-scales. Armgate has the exclusive right to sell and provide service for equipment of such high quality world-class manufacturers:



Shimadzu Corporation (Japan) - leading laboratory equipment with such analytical equipment systems, as HPLC, LCMS, GC, GCMS, UV/VIS, FTIR, AAS, ICP spectrometers, TOC, analytical scales and other systems. Web: <http://eu.shimadzu.de/>



Wesemann GmbH & Co produces the highest quality laboratory furniture and among the leading laboratory furniture producers in Germany over 40 years. All furniture complies to the newest safety and quality requirements set for laboratory furniture. Web: <http://www.wesemann-international.com/>



Rigaku corporation – among the world leaders in the fields of X-ray spectrometry, diffraction, optics, as well as small instrumentation technology, molecule and protein crystallography. Web: <http://www.rigaku.com>



Anton Paar GmbH produces high-end measuring and laboratory instruments for industry and research. It is the world leader in the measurement of density, concentration and CO₂ and in rheometry. Anton Paar GmbH is owned by the Santner Foundation. Web: <http://www.anton-paar.com/>



Armfield Ltd specialises in the design and manufacturing of laboratory equipment for engineering education and miniature scale research. Most equipment is self-contained and requires minimum preparation time. Web: <http://www.armfield.co.uk>



Hitachi High – Tehnologies Hitachi High-Technologies in Europe handles a wide variety of products - from computers and peripherals to scientific instruments and systems, electronic devices, and industrial machinery and materials. Web: <http://www.hht-eu.com/cms/home.html>



GE phoenix|x-ray is the product-line of GE Sensing & Inspection Technologies for high-resolution 2D X-ray inspection, as well as 3D failure analysis and 3D metrology with Computed Tomography. Web: <http://www.phoenix-xray.com>



Beneq focuses on equipment and technology for functional coatings. Products include equipment for thin film Atomic Layer Deposition, functional coating on glass and ceramics, as well as laboratory equipment for functional nanoparticle synthesis and deposition. Web: <http://www.beneq.com/>



Renishaw is a global company with core skills in measurement, motion control, spectroscopy and precision machining. Renishaw products are used such applications as machine tool automation, co-ordinate measurement, Raman spectroscopy, machine calibration, position feedback, CAD/CAM dentistry, stereotactic neurosurgery and medical diagnostics. Web: <http://www.renishaw.com/>



NT-MDT enjoys a 20-year history in instrumentation created specifically for nanotechnology research, leading the field in originality, quality, and high tech development.

We strive for next-generation SPM technology. Web: <http://www.ntmdt.com/>



Oxford Applied Research is a supplier of UHV and HV components and systems for the deposition and characterisation of thin films. Our speciality lies in providing unique solutions to common deposition challenges. <http://www.oaresearch.co.uk/>



Angstrom Engineering was founded in 1992 and has quickly grown into a global company with a reputation for providing high-quality machines and unparalleled customer service. Our PVD equipment is created by our highly-skilled engineering team and is used by a variety of researchers in world-class labs in countries around the world. Web: <http://www.angstromengineering.com/>

phone: +371 67 976 780

e-mail: armgate@armgate.lv

www.armgate.eu



Right from the beginning, which is now more than fifty years ago, Bruker has been driven by a single idea: to provide the best technological solution for each analytical task. Today, worldwide more than 5400 employees are working on this permanent challenge at over 90 locations on all continents. Bruker systems cover a broad spectrum of applications in all fields of research and development and are used in various industrial production processes for the purpose of ensuring quality and process reliability.

- **Bruker AXS** - Developer and manufacturer of high-quality analytical X-ray systems and complete solutions for material analysis. As a high technology enterprise, Bruker AXS define technological trends and standards in order to open up new fields of application. XRD and XRF spectrometers, Profilers and AFM, Scratchers and more.
- **Bruker Optics** - offers the most advanced FT-IR, FT-NIR, Raman, TD-NMR and TeraHertz spectrometers to meet all your demanding application requirements. The countless innovations found in our spectrometers, epitomize our philosophy of think forward.
- **Bruker Biospin** –Equipment for NMR and EPR spectroscopy and preclinical MRI research. World leading developer of NMR solutions starting from table top instruments up to enhanced customized scientific solutions.
- **Bruker Daltoncs** – GC and mass spectrometers as powerful tool for a wide variety of applications with different analytical challenges.

To better serve customers in Baltic countries Bruker has established a branch office Bruker Baltic OU in 2010. Company Bruker Baltic OU provides full service off all equipment included in Bruker portfolio starting from customer visits, including demos in demo labs, quoting, instalation, customer training, warranty and after warranty service.

Contacts:

Bruker Baltic OÜ

Address: Pärnu mnt 141, Tallinn 11314, Estonia

Phone: +372 6899000

Fax: +372 6899009

e-mail: info@brukerbaltic.com

internet: www.bruker.com

SIA *Saint-Tech* - Latvian company focused on research equipment supply to different application laboratories. For our short history we have realized some turnkey projects for laboratory furniture and high-end laboratory equipment in Latvia and Estonia.

Our partners are world known suppliers of innovative laboratory and research equipment. Starting up our company we brought to Latvian market new famous brands which were not presented to Latvian scientists in past.

Not long time ago we released our new webpage what easily could be called by first Latvian laboratory equipment portal (www.saint-tech.eu).

We would be happy to offer you appropriate solution for your research needs.



Atomic Force Microscopes

New approach PPL lithography tools



Xradia x-ray microscopes



Nano particle deposition systems



Tabletop SEMs



Confocal and optical microscopes

**Please contact us: vadim@saint-tech.lv, ph. +371 29706045
www.saint-tech.eu**

Photonics Tools

- Optomechanics
- Motion Controls
- Tunable Lasers
- Advanced Imaging
- OCT Systems
- Optics
- Fibers



You Speak, We Listen.....

THORLABS

www.thorlabs.com
scandinavia@thorlabs.com

April 17	
16:00	Registration
17:00	Welcome party
18:30	

Nanomaterials
Multifunctional materials
Energy
Session devoted to Inta Muzikante

Plenary - 40 min
<u>Invited - 30 min</u>
Oral - 20 min

April 18			
8:00	Registration		
9:00	Opening		
9:30	M.Kirm		
10:10	D.Høvik		
10:40	Technical information		
10:50	Conference photo		
Coffee 11:00 - 11:30			
×	HALL 1	×	HALL 2
11:30	Züttel	11:30	Trepakov
12:00	Montone	12:00	Azamat
12:30	Pasquini	12:20	Rodny
13:00	Fursikov	12:50	Suchocki
13:20	Vilciauskas	13:10	Aleksanyan
Lunch 13:40 - 14:50			
×	HALL 1	×	HALL 2
14:50	D'yachkov	14:50	Shugai
15:10	Krasnenko	15:10	Omelkov
15:30	Shunin	15:30	Kaminska
15:50	Maksimenko	15:50	Dolgov
16:10	Kuzhir	16:10	Churmanov
16:30	Andzane	16:30	Lojkowski
Coffee&snacks 16:50 - 17:20			
Poster session 17:20 - 19:00			

April 19			
8:00	Registration		
×	HALL 1	×	HALL 2
8:50	Technical info	8:50	Technical info
9:00	Christensen	9:00	Kulda
9:30	Granqvist	9:30	Sozanska
10:00	Ozolins	9:50	Bykov
10:30	Butikova	10:10	Albertini
		10:30	Mannsberger
Coffee 10:50 - 11:20			
11:20	R. Evarestov	11:20	Sokovnin
		11:40	Strazdina
12:00	Kulkova	12:00	Salak
12:20	Mironova-Ulmane	12:20	Fitting
		12:40	Dovbeshko
12:40	Zvejnieks	13:00	El Mourabit
13:00	Timoshenko	13:20	Kangur
Lunch 13:40 - 15:00			
15:00	Excursion & Conference dinner		
22:30			

DURING THE CONFERENCE THE EXHIBITION OF SEVERAL COMPANIES WILL BE HELD

April 20			
×	HALL 1	×	HALL 2
9:00	Sternberg	9:00	Bandura
		9:20	Zhukovskii
9:10	Nunzi	9:40	Bagaturyants
9:40	Jursenas	10:10	Kalnins
10:10	Juska	10:30	Kotomin
10:40	Rutkis	10:50	Mastrikov
11:00	Kampars	11:10	Gryaznov
Coffee 11:30 - 12:00			
12:00	Valkunas	12:00	Ma
12:30	Gulbinas	12:20	Eglitis
12:50	Ozols	12:40	Brik
13:10	Teteris	13:00	Dauletbekova
		13:20	Flerov
Lunch 13:40 - 14:50			
14:50	Kholkin	14:50	Chubarov
15:20	Romanova	15:10	Peterlevitz
15:40	Abele	15:30	Lähderanra
16:00	Lancere	15:50	Shvartsman
		16:10	Mikhaleva
HALL 1			
Closing			
Goodbye refreshments 16:30 - 17:30			

Plenary presentations (in alphabetic order)

R. Evarestov	BaTiO₃ based Nanostructures: Nanolayers, Nanotubes, Nanowires	Page 30
M. Kirm	Challenges and Contribution of Estonian Research Community at European Infrastructures – MAX-IV Lab, ESS and CERN and Facilitating Industrial Access Using the Sciencelink Project	Page 31

Invited presentations (in alphabetic order)

A. Bagaturyants	Atomistic Multiscale Simulation of Nanostructured Materials for Photonic Applications	Page 34
N.E. Christensen	Quasiparticle Electronic Structures of Thermoelectric Pbx (X=S,Se,Te)	Page 35
C.G. Granqvist	Nanothermochromics for Energy Efficient Fenestration	Page 36
D. Høvik	Strategic Research Programmes within Nanotechnology and Advanced Materials in Norway	Page 37
A.L. Kholkin	Piezoelectric Biomaterials: Structure, Properties, Applications	Page 38
J. Kulda	Neutron Spectroscopy of Nanoscale Materials	Page 39
A. Montone	Hydrogen Cycling Effect on MgH₂ Nanocomposites	Page 40
V. Ozolins	Using Lone s² Pairs to Design Crystalline Compounds with Minimal Thermal Conductivity	Page 41
L. Pasquini	Magnesium Nanoparticles for Hydrogen Storage: Structure, Kinetics and Thermodynamics	Page 42
P. Rodnyi	Scintillating Ceramics Based on Zinc Oxide	Page 43
V. Trepakov	Polaronic Excitons in KTN: Optical Absorption and Photo-EPR Manifestations	Page 44
A. Züttel	Storage of Renewable Energy in Synthetic Fuels	Page 45

Oral presentations (in alphabetic order)

S. Abele	The Story of Polymer Monoliths: From USA to Europe and to Latvia	Page 48
E. Aleksanyan	Luminescence Properties of Re³⁺- Doped Hafnia and Zirconia Thin Films Grown by Atomic Layer Deposition Method	Page 50
J. Andzane	Application of Ge Nanowire Mass Sensor for Graphene Exfoliation	Page 51
D.V. Azamat	EPR Studies of Transition Metal Impurities in SrTiO₃	Page 52
A. Bandura	First-Principles LCAO Calculations of Single-Walled ZrO₂ Nanotubes	Page 53
M.G. Brik	Simulation of Lattice Constants for Cubic Crystals	Page 54
J. Butikova	Processing of Amorphous Si by Pulsed Laser Irradiation at Different Wavelengths	Page 55
I. Bykov	Measurements of Mechanical, Electrical and Optical Properties of Modern Nanostructures with AFM-Based Methods	Page 56
M. Chubarov	High Quality Epitaxial r-BN Grown by CVD	Page 57
V.N. Churmanov	Low-Energy Charge Transfer Excitations in NiO Nanocrystals	Page 58
P.N. D'yachkov	Linear Augmented Cylindrical Wave Method for Nanotubes	Page 59
A. Dauletbekova	Colour Centers and Structural Damage in LiF Induced by 150 MeV Kr ions	Page 60
L. Dolgov	Fluorescence of TiO₂:Sm³⁺ Composite Stimulated by Plasmon Waves	Page 61
G. Dovbeshko	Vibrational Spectra of Opal-Based Photonic Crystals	Page 62
R.I. Eglitis	<i>Ab initio</i> Calculations for the <i>H</i> Centers in SrF₂, as Well as Surface <i>H</i> Centers in BaF₂ and <i>F</i> Centers Aggregation in BaF₂ and CaF₂	Page 63
H.J. Fitting	Ion Beam Mixing for Gradual SiO_x Interfaces	Page 64

I. Flerov	Fluorides and Oxyfluorides with Elpasolite-Cryolite Structure: Order-Disorder Phase Transitions and Barocaloric Efficiency	Page 65
P.V. Fursikov	Hydrogen Sorption Behavior of Nanostructured Mg Alloys with Ni and RE	Page 66
D. Gryaznov	<i>Ab initio</i> Thermodynamic Calculations of Oxygen Vacancies in Perovskites: the Case Study of (La,Sr)(Co,Fe)O_{3-δ} and SrTiO_{3-δ}	Page 67
J.R. Kalnin	One-dimensional Diffusion in Heterogeneous Medium	Page 68
A. Kaminska	Recovery of Radiative Transitions of Ce³⁺ Ions in Gadolinium Gallium Garnet Crystal Using High Hydrostatic Pressure	Page 69
T. Kangur	Micro- and Nanostructured Silica Surfaces as Cell Substrates	Page 70
E.A. Kotomin	First Principles Calculations of Structural Stability for Complex Perovskites	Page 71
V. Krasnenko	<i>Ab initio</i> Modeling of the Benzene Molecule Adsorption on Graphene	Page 72
S. Kulkova	<i>Ab initio</i> Study of Metal-Zirconia Interfaces	Page 73
P. Kuzhir	Microwave and THz Probing of Multi-Walled CNT / Polymer Composites <i>versus</i> CNT Oxidation Treatment, Average Outer Diameter and Number of Shells	Page 74
E. Lähderanta	Magnetic Properties of Carbon Nanoparticles	Page 75
L. Lancere	Commercial and Prosthetic PMMA Surface Wettability Regulation	Page 76
W. Lojkowski	Microwave Solvothermal Synthesis of Highly Biocompatible Nano Hydroxyapatite	Page 77
C.-G. Ma	<i>Ab initio</i> Calculations of Structural, Elastic, Electronic and Thermodynamic Properties for Cubic Perovskites CsMF₃ (M=Ca, Cd, Hg, Pb)	Page 78
S.A. Maksimenko	Influence of Deformation of Carbon Nanotube Based Polymer Composites on Their Electromagnetic Properties	Page 79
M. Mannsberger	XPS analysis of carbon nanostructures	Page 80
Yu.A. Mastrikov	First Principles Study of Oxygen Vacancies in Perovskite Solid Solutions	Page 81

E. Mikhaleva	Caloric Effects and Phase Transitions in Ferroelectric-Ferromagnetic Composites $(x)\text{La}_{0.7}\text{Pb}_{0.3}\text{MnO}_3-(1-x)\text{PbTiO}_3$	Page 82
N. Mironova-Ulmane	Crystal Field Analysis of Energy Levels for the Off-center Ni^{2+} Ions in MgO	Page 83
S.E. Mourabit	Stability of mesoporous silicas under acidic conditions	Page 84
S.I. Omelkov	The Luminescence of Pr^{3+}-Doped LiBaAlF_6 Crystals	Page 85
A.C. Peterlevitz	Synthesis and Characterization of Magnetic Nanodiamond Films	Page 86
M. Romanova	PbS Nanodots in ZrO_2 Thin-film Matrix as a Possible Material for Microdosimetry of Ionizing Radiation	Page 87
A.N. Salak	Thermal Behaviour and Hydration Dynamics of Layered Double Hydroxide Zn-Al Pyrovanadate	Page 88
A. Shugai	Luminescent Protection Against Defect Creation in $\text{Lu}_3\text{Al}_5\text{O}_{12}:\text{Ce}$	Page 89
Y. Shunin	Electromagnetic Properties in CNT and Graphene Based Nanostructures	Page 90
V.V. Shvartsman	Converse Magnetoelectric Effect in $\text{CoFe}_2\text{O}_4/\text{BaTiO}_3$ Core-Shell Composites	Page 91
S.Yu. Sokovnin	Production of Metal Oxide Nanopowders Using Pulsed Electron Beam in Low Pressure Gas	Page 92
A. Sozańska	Modern Raman Techniques– Probing the Nanoworld	Page 93
I. Strazdina	Hydrogen Influence on ITO Layer Sputtering on Polymeric Film Using HIPIMS	Page 94
A. Suchocki	The High-Pressure Studies of Structural and Optical Properties of ZnO Bulk and Nano-Crystals	Page 95
J. Timoshenko	Lattice Dynamics and Structural Disorder in Rhenium Trioxide: Reverse Monte Carlo Study	Page 96
L. Vilčiauskas	First Principles Molecular Dynamics Studies of Proton Transport Mechanisms in Phosphorus Oxoacids	Page 97
Yu.F. Zhukovskii	First Principles Calculations on Properties of the Rutile-Based TiO_2 Nanowires with Ti-atom Centered Symmetry Axes	Page 98
G. Zvejnieks	Microscopic Approach to the Kinetics of Pattern Formation of Charged Molecules on Surfaces	Page 99

Invited presentations in the session devoted to Inta Muzikante

S. Jursenas	In Search for Efficient Blue-Light Emitters	Page 102
G. Juška	Reduced Langevin Recombination in Organic Solar Cells	Page 103
J.M. Nunzi	Plasmonic Organic Electronic Devices	Page 104
L. Valkunas	Coherent Dynamics and Dissipative Relaxation of Excitations in Molecular Aggregates	Page 105

Oral presentations in the session devoted to Inta Muzikante

V. Gulbinas	Excited State Dynamics of PPI Dendrimers Functionalized with 4-(4'-ethoxybenzoyloxy)salicylaldehyde Chromophores	Page 108
V. Kampars	Influence of Specific and Non-Specific Solvent Effects on Frontal MO of DMABI System	Page 109
A. Ozols	Holographic Studies of Photoinduced Anisotropy in Molecular Glassy Films Containing Diphenylamine Based Azochromophores	Page 110
M. Rutkis	Assessment of Quantum Chemical and Experimental Methods for Ionization Energy and Electron Affinity Evaluation of Organic Thin Films	Page 111
J. Teteris	Optical Field-Induced Surface Relief Formation on Chalcogenide and Azo-Benzene Polymer Films	Page 112

Poster presentations

Po-1	D. Erts	INTERREG project “Technet_nano” – National network of clean rooms and research facilities in nanotechnology making accessible innovation resources and services to SMEs in the BSR
Po-2	E. Blokhin	A New Approach to the Engineering of <i>Ab initio</i> Materials Simulations on an Example of CRYSTAL, VASP and WIEN2K Packages
Po-3	E. Blokhin	Joint Theoretical-Experimental Study of Iron Impurities and Oxygen Vacancies in SrTiO₃
Po-4	A. Pishtshev	A Comparative Study of Structural Energetics and Chemical Bonding in Ca-Based Dielectric Materials: An Integrated View from First-Principles Calculations
Po-5	E. Klotins	Treatment of Excitons by Discrete Variable Representation
Po-6	K. Bergfelds	Modelling of Turbulent Silicon Melt Flow in Purifying Process with Electron Beam
Po-7	K. Janisels	Phase Shapes and Melt Motion 3D Modeling for FZ Silicon Single Crystal Growth Process
Po-8	J. Gabrusenoks	Lattice Dynamics of WOCl₄
Po-9	A. Bystrova	Hydroxyapatite OH-Channels for Proton Transferring Aimed to Surface Charging
Po-10	A. Bakulin	The Investigation of Chemical Bonding at Metal-Ceramic Interfaces
Po-11	R.I. Eglitis	<i>Ab initio</i> Calculations of SrTiO₃, BaTiO₃, PbTiO₃, CaTiO₃, BaZrO₃, SrZrO₃ and PbZrO₃ (001), (011) and (111) Surfaces as Well as Nb Impurity Segregation Towards the SrTiO₃ Surface
Po-12	P. Zhgun	Electronic Structure and Lattice Dynamics of ScF₃ from <i>Ab Initio</i> LCAO Calculations
Po-13	A.V. Sorokin	First Principles Calculations of Defective ZnO Crystals: The Role of Symmetry and Phonons
Po-14	A. Useinov	<i>Ab Initio</i> Calculations of Hydrogen Impurities in ZnO
Po-15	F. Muktepavela	The Role of Nanopowder Particle Surfaces and Grain Boundary Defects in the Sintering of ZnO Ceramics

Po-16	R. Zabels	Shear Banding Mechanism of Plastic Deformation in LiF Irradiated With Swift Heavy Ions
Po-17	A.S. Kuprin	Effects of Deuterium Ion Implantation on the Hardness TiN-based Nanocrystalline Films
Po-18	H.J. Fitting	Electron Beam Charging of Semi-Insulating Samples
Po-19	S. Bellucci	New Materials for Neutron Shielding Based on Boron Enriched Unfired Phosphate Ceramics
Po-20	M. Palatnikov	Mechanical Properties of Nb₂O₅ and Ta₂O₅ Ceramics
Po-21	M. Palatnikov	The Effect of Feed Charge Grain Size on the Electrical Characteristics of the Li_{0.03}Na_{0.97}Ta_{0.05}Nb_{0.95}O₃ Perovskite Ceramics
Po-22	M. Palatnikov	Conoscopic Microscopy Studies of Optical Homogeneity of the LiNbO₃:Mg Crystals
Po-23	M. Livinsh	Influence of Lithium Substitution on Structure, Electric and Pyroelectric Properties of Sodium Niobate Ceramic
Po-24	I. Smeltere	Ultrasonication as a Method of Investigation of the Mechanical Properties of Doped Hafnium Barium Titanate
Po-25	I. Smeltere	The Effect of BaTiO₃ on Dielectric and Ferroelectric Properties of Lead-Free Ceramics Based on KNN
Po-26	M. Dunce	Phase Transitions in Li, K and Ag Modified Na_{1/2}Bi_{1/2}TiO₃-SrTiO₃-PbTiO₃ Solid Solutions
Po-27	Š. Svirskas	Dynamics of Phase Transition in 0.4Na_{0.5}Bi_{0.5}TiO₃-(0.6-X)SrTiO₃-xPbTiO₃ Solid Solutions
Po-28	M. Kinka	Investigation of Ferroelectric Phase Transition in Ba₂Nd_(1-x)Pr_(x)FeNb₄O₁₅ Ceramics Using Ultrasonic Spectroscopy
Po-29	M. Kinka	Dielectric Properties of CoFe₂O₄ and NiFe₂O₄ Ceramics
Po-30	D. Jablonskas	Dielectric Properties of 0.98Pb(Mg_{1/3}Nb_{2/3})O₃ – 0.02La(Mg_{2/3}Nb_{1/3})O₃ Crystal
Po-31	R. Mackeviciute	Dielectric properties of Pb(Fe_{2/3}W_{1/3})+1%MnO₂ ceramics
Po-32	R. Grigalaitis	Dielectric Spectra of Relaxor PMN-PT Ceramics
Po-33	V. Dimza	Dopant (Mn, Co, Fe) Effects on the Structure and Dielectric Properties in (Ba, Pb)TiO₃ Ceramics
Po-34	M. Kundzins	The Changes of Relaxor Behaviour of PLZT8/65/35 Ceramics at Doping with 3d Elements

Po-35	A. Kalvane	Physical Properties of Ba_{0.95}Pb_{0.05}TiO₃+0.1%Co₂O₃ Ceramic
Po-36	O. Malyshkina	Magnetic Properties and Microstructure of Modified Lead Ferrotantalate Ceramics
Po-37	S. Rucevskis	Static Analysis of Piezoelectric Composite Structure Based on Thermal Analogy Method
Po-38	V. Serga	Extractive-Pyrolytic Method for FePt Alloy Production
Po-39	J. Dec	Relaxing Polar Nanoregions and Creeping Domain Walls in the Strontium-Barium Niobate Uniaxial Relaxor Crystal
Po-40	E. Dauksta	Influence of Laser Radiation on Electrical Properties of CdZnTe Crystal
Po-41	K. Bormanis	Microstructure and Mechanical Properties of High-Pressure Li_xNa_{1-x}Ta_yNb_{1-y}O₃ Solid Solution Perovskite Ceramics
Po-42	K. Bormanis	Heat Capacity and Dielectric Properties of the PNN-PT Ferroelectric Ceramics
Po-43	K. Bormanis	Relaxation of Polarisation at the Broad Phase Transition in Doped PMN Ferroelectric Ceramics
Po-44	B. Sorkin	The Ferroelectric Polarization Effects in the Surface Superconductivity
Po-45	A. Kovalovs	Active Vibration Control of Structure with an Optimum Placement of Macro-Fiber Composite Actuators
Po-46	A. Kovalovs	Non-destructive Technique for Determination of Material Properties
Po-47	N. Ponomarenko	Dimensional Effects of Microstructure and Sample Geometry of NiZn-Ferrites
Po-48	J. Purans	DC Magnetron Sputter Deposition of Zinc Oxide Based n- and p-Type Transparent Conductor Thin Films
Po-49	G. Kucinskis	Synthesis and Electrochemical Performance of Li₂FeSiO₄ Cathode Material for Lithium Ion Batteries
Po-50	G. Bajars	Characterization of LiFePO₄/C Composite Thin Films Using Electrochemical Impedance Spectroscopy
Po-51	A. Lūsis	Influence of Moisture on the Functional Properties of Physically and Chemically Modified Technical Textiles
Po-52	E. Pentjuss	Electrochemical Impedance and Moisture Contents of Glass Fabric

Po-53	S. Vihodceva	Cotton Fabric Surface Modification by Sol-Gel Deposition of ZnO Thin Films
Po-54	A. Salundi	Elaboration of High Performance Electro-Optical Films by Sol-Gel Method
Po-55	M. Part	Novel Methods in Synthesis of Microtubes and Composite Materials via Sol-Gel Route
Po-56	M. Umalas	Synthesis of Polymeric Titanium and Zirconium Precursors to Preparation of Fine Binary Carbide Systems
Po-57	M. Paalo	Preparation and Characterization of Transparent Fiber Electrodes Based on CNT-s Metal Oxides
Po-58	K. Luse	Color Representation Dependence on Printing Technology
Po-59	S. Fomins	Print Materials Colorimetric Changes Due To Illumination
Po-60	M. Ozolinsh	The Minimum Motion Techniques to Determine Lutein and Zeaxanthin Macular Pigment Optical Density Using CRT and Different Spectral Emission Light Emission Diode Light Sources
Po-61	R. Trukša	Leds Brightness Modulation Application in Anomaloscope and Heterochromatic Flicker Tests
Po-62	J. Vamze	Expression of Interleukins and Defensins in the Experimental Rabbit Bone Tissue after Implantation of Different Biomaterials
Po-63	U. Gertners	The Impact of Light Polarization on the Direct Relief Forming Processes in As₂S₃ Thin Films
Po-64	A. Gerbreders	UV Optical Record and Electron Beam Lithography in Polymer Films
Po-65	J. Aleksejeva	Photoinduced Phenomena in Azo-Dyed Gelatin Films
Po-66	V. Kalkis	Thermosetting Materials of Radiation Modified High Density Polyethylene/Iron Ferrite Nanocomposites
Po-67	I. Kaulachs	Non-Planar Phthalocyanine for Improved Optical Coverage in Bulk Heterojunction Solar Cell
Po-68	L. Khenkin	Iron Complexes Embedding Influence on PMAA Hydrogel Cross-Linking
Po-69	R. Vålbe	Preparation of R-Methyl Imidazolium-Sodium Hexaflorosilicate Complex Crystals

Po-70	M. Barczak	Structural and Surface Properties of SBA-15 and SBA-16 Mesoporous Materials Functionalized With Different Groups
Po-71	D. Lapidus	Molecular Dynamics of Amylin 10-29 Amyloid Formation
Po-72	I. Liepina	Molecular Dynamics of Amyloid Formation of Two Abl-SH3 Domain Peptides
Po-73	K. Ozols	Influence of Laser Radiation on Electrical Resistivity of Polyisoprene/Nanostructured Carbon Composites
Po-74	K. Pudzs	Electrical Properties and Morphology of Pentacene Thin Films Evaporated on Different Temperature Substrate
Po-75	I. Reinholds	Mechanical and Structural Properties of Polyolefin/Iron Ferrite Magnetic Nanocomposites
Po-76	R. Fedorovskis	Synthesis and Use of Methacrylic and Styrenic Monoliths as Stationary Phases in HPLC
Po-77	G. Vaivars	Synthesis Tri-Metallic Platinum Group Metal Electrocatalysts Using Organometallic Chemical Vapour Deposition Technique for Methanol Oxidation
Po-78	A. Jershova	Formation of Nanosized Strontium Substituted Hydroxyapatites
Po-79	S. Gluhihs	Two Thin Polymer Sheets Identification of Flexural Modulus
Po-80	L. Bauermeistere	Determination of Cerium Oxidation State in Cerium Substituted Hydroxyapatites
Po-81	A. Andersone	Role of Paramagnetic Polyconjugated Clusters In Lignin Antioxidant Activity
Po-82	R. Karpicz	Temperature Induced Color Changes in Photoluminescent Polymer/Dye Blends
Po-83	A. Tokmakovs	Nonlinear Optical Properties of Low Molecular Organic Glasses Formed by Triphenyl Modified Chromophores
Po-84	I. Mihailovs	Hyper-Rayleigh Scattering and Two-Photon Luminescence of Phenylamine–Indandione Chromophores
Po-85	A. Freidzon	Multiscale Approach to the Structure and Spectra of Nile Red Adsorbed on Polystyrene Nanoparticles
Po-86	A. Bulanovs	Luminescence and Structural Properties of Thermally Evaporated Benzanthrone Dyes Thin Films
Po-87	L. Grigorjeva	Near-Band Luminescence of CdZnTe Detector Crystals

Po-88	D. Millers	Induced Short-lived Absorbtion in PLZT Electrooptical Ceramics
Po-89	K. Smits	Oxygen Vacancies and RE Ion Agglomeration Caused Up-Conversion Luminescence Quenching Prevention in Zirconia
Po-90	J. Grube	Concentration Impact on Er³⁺ Green Luminescence Decay Kinetics in NaLaF₄
Po-91	G. Doke	Photoluminescence and Energy Transfer in Nd³⁺ and Er³⁺ Doped NaLaF₄ Material
Po-92	A. Sarakovskis	Up-Conversion Luminescence in Erbium Doped Cubic and Hexagonal NaYF₄
Po-93	A. Dauletbekova	Absorption Spectra of Irradiated LiYF₄ Crystals at 15K
Po-94	A. Dauletbekova	Radiation Defects in LiF Crystals Irradiated with 56 MeV Ar Ions
Po-95	R. Kassymkanova	LiF Crystals Doped With Polyvalent Cations: Transformation of Oxygen-Containing Impurity Induced by Irradiation
Po-96	S. Zazubovich	Ultraviolet Luminescence and Creation of Defects under UV Irradiation of Lead Tungstate Crystals Doped with Trivalent Rare-Earth Ions
Po-97	L. Maksimov	Fluctuations in an Inorganic Glass Forming System Capable to Liquid-Liquid Phase Separation
Po-98	A.N. Trukhin	Absorption and Luminescence in Amorphous 95%SiO₂ 5%GeO₂ Films with Fluorine Fabricated by SPCVD. If GeODC(I) exist
Po-99	A. Svagere	Measurements of SiO₂ Glass Surface Parameters by Methods of Microscopy
Po-100	T. Shalapska	VUV Excited luminescence and Energy Transfer in LiGdP₄O₁₂:Eu³⁺
Po-101	V. Skvortsova	Optical Properties of Irradiated Yttrium Aluminum Garnet
Po-102	L. Shirmane	Raman Scattering Study of YVO₄:Eu³⁺ Nanocrystals
Po-103	L. Shirmane	Time-Resolved Luminescence Properties of YVO₄:Eu³⁺ Nanocrystals
Po-104	P. Rodnyi	Transparent Ceramics Based on Barium Fluoride with Ultra Fast Scintillation Decay Time
Po-105	S. Kaemmer	Advances in Combined Atomic Force and Raman Microscopy
Po-106	K. Salma-Ancane	Raman Spectroscopy of Some Biogenic Carbonates

Po-107	A.I. Popov	Effect of Aging on the Luminescence of Pure and Doped CdI₂
Po-108	A.I. Popov	VUV Synchrotron Radiation Spectroscopy of PLZT Ceramics
Po-109	N. Mironova-Ulmane	Raman Spectroscopy Study of the Antiferromagnetic-Paramagnetic Phase Transition in Nickel Oxide
Po-110	D. Gnatyuk	Modification of Photoluminescence and Absorption Properties of Surface Functional CdTe Single Crystal Layer under Laser Irradiation
Po-111	K. Utt	Preparation and Optical Properties of YSZ:Sm³⁺ Microrolls
Po-112	V. Liepina	Preparation of Persistent Strontium Aluminate Phosphor by Solar Induced Solid State Synthesis
Po-113	D. Berzins	EPR Spectra of the Mn²⁺ Ion in the Oxyfluoride Glass Ceramics Containing BaF₂ Nanocrystalline Phase
Po-114	A. Fedotovs	Characteristics of the Mn²⁺ EPR Spectra in the Oxyfluoride Glass Ceramics Containing SrF₂ Nanocrystals
Po-115	M. Polakovs	Gallstones Studies by EPR and EDX Spectroscopy
Po-117	A. Kuzmin	Electronic Excitations in NiWO₄ Using VUV Synchrotron Radiation
Po-118	A. Kuzmin	X-ray Absorption Spectroscopy of Cu-doped WO₃ for Use in Electrochemical Metallization Cell Memory
Po-119	A. Kuzmin	First Principles LCAO Study of Copper Tungstate CuWO₄
Po-120	A. Kalinko	X-ray Absorption Spectroscopy Study of Local Atomic Structure and Lattice Dynamics in Copper Nitride Cu₃N
Po-121	A. Anspoks	X-ray Absorption Spectroscopy of Local Structure and Lattice Dynamics in Multiferroic MnWO₄ and Mn_{1-c}Co_cWO₄
Po-122	A. Anspoks	X-ray Absorption Spectroscopy of the Local Atomic Structure in PbS Quantum Dots
Po-123	P. Kulis	Nanocrystals for Solar Cell Applications
Po-124	V. Malyshev	Metallothermic Synthesis of Nanocrystalline Powders and Nanorods of Chromium Silicides
Po-125	S.Yu. Sokovnin	Production of Nanopowders Using Nanosecond Electron Beam from Gas and Liquid Precursors

Po-126	V.O. Mats	The Effects of Cold Deformation and Electron Irradiations of Zr-1%Nb Alloy on Temperature Range Deuterium Desorption
Po-127	J. Katkevics	Deposition of Cu and Pt Nanoparticles on the Surface of Metallic Aluminum and Impedance Spectra of these Complex Electrodes
Po-128	J. Liepins	Zirconia Nanoparticles as Submicro-Level Label for Biological Applications
Po-129	R. Poplauskis	Optical Properties of Metal Nanoparticle Arrays Deposited Through Ultrathin Anodized Aluminum Membranes
Po-130	I. Segal	Superparamagnetic Iron Oxide Based Nanostructures Bearing Organosilicon Heterocyclic Choline Analogues as Original Approach to Double Pro-Drugs
Po-131	G. Kronkalns	Synthesis of Ferrite Nanoparticles for the Magnetic Fluids of Various Practical Applications
Po-132	V. Sints	Nonisothermal Transport of Ferrocolloid Particles through Porous Membrane under Transversal Magnetic Field
Po-133	M. Maiorov	Direct and Indirect Determination of the Ferrite Nanoparticles Size Distribution
Po-134	M. Maiorov	The Relaxation Time of the Ferrofluid Optical Anisotropy as an Indicator of the Ferrite Nanoparticles Fractionation
Po-135	A. Mezulis	Sedimentation of Suspended Nanoparticles
Po-136	Z. Alute	Characterization of Au Nanodots and Azobenzene Derivative Films by Kelvin Probe Force Microscopy
Po-137	M. Biednov	Optical Properties of Nanostructured Ag-Al₂O₃ Granular Thin Films
Po-138	E. Elksnis	Diamond synthesis using Plasma Chemical Vapour Deposition method
Po-139	L. Gerca	Deposition and Characterization of Graphene Oxide Films Obtained by Langmuir-Blodgett Technique
Po-140	G. Dobeles	Structure of Nanoporous Carbon Materials for Supercapacitors
Po-141	U. Joost	Effect of Annealing Temperatures and Substrate Surface Treatment on the Properties of Nickel Containing Titania Thin Sol-Gel Films
Po-142	P. Akishin	Characterization of Elastic and Dissipative Nanocomposite Material Properties via Using of Small Dimension Specimens

Po-143	J. Pilipavicius	Synthesis of Silica-Carbon Nanotube Composite Materials and Their Application for Laser Systems
Po-144	J. Zicans	Mechanical and Electrical Properties of Pe Nanocomposites with Carbon Nanotubes
Po-145	J. Zicans	The Effect of Nanosize ZnN on the Structure and Properties of the Selected Polymer Blend Composites
Po-146	M. Antsov	Measurement of Static Friction Force of Complex Shaped ZnO Nanowires on a Flat Surface
Po-147	L. Jasulaņeca	Mechanical Properties of Antimony Sulfide Nanowires
Po-148	G. Kunakova	Properties and Applications of Well-Ordered and Individual V-VI Group Semiconductor Nanowires
Po-149	R. Meija	Improved Method of Nanowire Disconnection for Application in NEM Switches
Po-150	A. Pastare	Au Electrodeposition into AAO Pores and on the Bi₂S₃ Nanowires
Po-151	P. Ščajev	Carrier Dynamics in Nanostructures of Ternary AlGaN with Tunable Bandgap
Po-152	S. Stepina	Evaluation of Polymer-Nanostructured Carbon Composites Response to Chemical Stimuli
Po-153	M. Knite	Sensing Effects in Polymer/Thermoexfoliated Graphite and Polymer/Multiwall Carbon Nanotube Composites
Po-154	A. Linarts	Completely Hyperelastic Pressure Sensing Mat with Structurally Integrated Piezoresistive Sensors
Po-155	E. Liepa	Effect of the Plasticizers on Chemoresistivity of Polyvinylacetate-Nanostructured Carbon Composite
Po-157	V. Duka	Molecular Dynamics 1,4-DHP-Lipid as a Gene Transfection Agent
Po-158	O. Krievs	Investigation of Electric Properties of Nanocomposites in Frequency Domain – Compact Measurement Data Representation
Po-159	S. Čornaja	Glycerol Oxidation by Molecular Oxygen in Presence of Novel Supported Platinum Catalysts

Po-160	P. Nanni	Cobalt Cementation in Ethanol-Water System: Kinetics and Morphology of Metal Aggregates
Po-161	M. Baitimirova	Structure and Zeta-Potential Analysis of Particulate Matter
Po-162	O. Lisovski	Quantum Chemical Simulations of Doped TiO₂ Nanotubes for Photocatalytic Hydrogen Generation
Po-163	J. Kazeroovskis	Atomic and Electronic Properties of Ni Filament Encapsulated Inside Single-walled Carbon Nanotubes of Different Chiralities
Po-164	J. Begens	Quantum Chemical Simulations of Doped SrTiO₃ Nanotubes for Application in Photocatalytic Reactions
Po-165	V. Gopeyenko	Parametric Simulation of CNT <i>dc</i>- and <i>ac</i>-Conductivity for Various Nanotube Chiralities
Po-166	E.K. Shidlovskaya	Cluster Embedding Method for Quantum-Chemical Simulation of Nanodevices
Po-167	P. Nazarovs	Finite Temperature Effects in Single-Parameter Non-Adiabatic Electron Pumps
Po-168	J. Timoshenko	Modeling of Non-Adiabatic Quantum Pumping
Po-169	P. Merzlyakov	Analysis of Void Superlattice Formation in CaF₂
Po-170	G. Zvejnieks	Atomistic Theory of Mesoscopic Pattern Formation Induced by Bimolecular Surface Reactions between Oppositely Charged Molecules
Po-171	D. Zablotsky	Numerical Investigation of the Stability of Photoinduced Microconvective Structures in Ferrofluid Layers
Po-172	V. Kuzovkov	The Non-equilibrium Charge Screening Effects in Diffusion-Driven Systems
Po-173	V. Kuzovkov	The Anderson Localization Problem, the Fermi–Pasta–Ulam Paradox and the Generalized Diffusion Approach
Po-174	V. Kuzovkov	Light Induced Self Assembly of Switchable Colloids
Po-175	T. Plank	Institute of Physics, University of Tartu in Baltic Sea Region Cooperation Network Technet_nano – New Challenges for Academia and Industry
Po-176	A. Knoks	Magnetic and Electric Field Effects on the Growth of Ferrite Films in Spray Pyrolysis Process
Po-177	J. Kleperis	Light Sensitivity Enhancement of TiO₂ Thin Films with Ferrite Nanoparticles Using Multi-source Spray Pyrolysis Method

Po-178	I. Liepina	Preparation and Photoactivity of Electrophoretic TiO₂ Coating Films
Po-179	I. Narkevica	Structural studies of titanium oxide after thermal treatment
Po-180	P. Lesnicenoks	Hydrogen Adsorption in Zeolite Studied with Sievert and Thermogravimetric Methods
Po-181	O.M. Morozov	Threshold Character of Temperatures on Hydrogen Desorption from the Mg-V Composite
Po-182	A.V. Zvjagintseva	Boron – the Extrinsic Trap for Atoms of Hydrogen in Electrochemical Systems
Po-183	M. Vanags	Comparison of Electrodes with Smooth and Nanostructured Surfaces in Pulse and DC Electrolysis
Po-184	J. Hodakovska	Measuring In-Plane and Through-Plane Conductivities of Polymer Electrolyte Membranes
Po-185	R. Drunka	Synthesis and Photocatalytic Properties of Modified TiO₂ Nanotubes
Po-186	A. Cvetkov	EPM Fine-Disperse Platinum Coating on Powder Carriers
Po-187	G. Kolosovska	Quantification of Impurities in Solar Silicon
Po-188	P. Onufrievs	p-n Junction in Intrinsic Semiconductor Formed by Laser Radiation
Po-189	V. Garaev	Properties of the Nafion Membrane Impregnated With Hydroxyl Ammonium Based Ionic Liquids
Po-190	G. Barinovs	Multiscale Modeling of Silicon Crystal Growth: From Molecular Dynamics to Macroscopic Features
Po-191	D. Bocharov	<i>Ab initio</i> Modeling of Uranium Nitride Grain Boundary Interfaces
Po-192	F.U. Abuova	<i>Ab initio</i> Calculations of Bulk and Surface Defects in MgF₂ Crystals
Po-193	A. Gopejenko	Quantum Chemical Simulation on Binding Energies of Pair- and Triple-Wise Defects in Fcc-Fe Lattice for ODS Steels
Po-194	A. Zarins	Influence of SiO₂ Admix on Radiolysis of Powders of Li₄SiO₄
Po-195	M. Halitovs	Comparison of Tritium Accumulation in Various Divertor Tiles Depending on the Geometrical Positioning in the Divertor Structure
Po-196	J. Kalnacs	Methane Emissions by Combustion of Biomass

Po-197	J. Kalnacs	Characterisation of Biomass Ashes
Po-198	O.I. Davarashvili	Growth and Properties of Strained Epitaxial Nanolayers of Lead Selenide

Abstracts of the plenary presentations

BaTiO₃ based Nanostructures: Nanolayers, Nanotubes, Nanowires

R. Evarestov

Department of Chemistry, Quantum Chemistry Division, St. Petersburg State University, Russia

e-mail: re1973@re1973.spb.edu

The first-principles LCAO calculations with hybrid HF-KS exchange correlation functional and the structure optimization are performed on the cubic BaTiO₃ based nanostructures: diperiodic (2D) layers with the periodicity in (001) and (110) planes, monopерiodic (1D) nanotubes (with the square morphology), monopерiodic (1D) nanowires with the translation axis along [001] and [110] directions. The convergence of the results with the nanosystem size increasing is studied under stoichiometric condition.

2D layers. BaTiO₃ (001) slabs, being consisted of even number of atomic planes with BaO and TiO₂ terminations, obey stoichiometry. Oxygen-terminated (110) slabs with odd number of planes can be converted to stoichiometric sheets by removing extra oxygen atoms from surface planes. The converged results for the surface energy of 1.28 J/m², 1.22 J/m², and the values for the formation energy of 24 kJ/mol, 33 kJ/mol are obtained for the (001) and (110) slabs consisting of 10 formula units.

1D nanotubes. The comparison of the surface and formation energies for the nanotubes rolled up from two (2L) and four (4L) planes (both with Ti and Ba terminations for the outer nanotube shell) is made. The monopерiodic unit cell consisting of 300 atoms was used to model the nanotubes with chiralities (60,0), (30,30) and (30,0), (15,15), respectively. The smallest surface energy (1.1 J/m²) and the smallest formation energy (130 kJ/mol) were found for both 2L Ba terminated and 4L Ti terminated (30,0) nanotubes, respectively. The strain energy is about of -10 kJ/mol in the first case and +10 kJ/mol in the second case. The strain and formation energies of 4L nanotubes at chirality (*n,n*) are noticeably greater than those at chirality (*n,0*) for the both terminations.

1D nanowires. [001] nanowires were constructed using $n \times n \times 1$ supercells of the bulk crystal and removing the periodical boundary conditions in the [100] and [110] directions. For $n = 4$ (80 atoms in 1D unit cell) the surface and formation energies of [100] nanowire are 1.52 J/m² and 122 kJ/mol, respectfully. The results obtained for [110] nanowires are close to those for [001] nanowires of the equivalent size, except that their formation energy is slightly larger.

Acknowledgments

Author thanks St. Petersburg State University for the support (grant 12.37.142.2011).

Challenges and Contribution of Estonian Research Community at European Infrastructures – MAX-IV Lab, ESS and CERN and Facilitating Industrial Access Using the Sciencelink Project

M. Kirm

Institute of Physics, University of Tartu, Estonia

e-mail: marco.kirm@ut.ee

In 2010 the Estonian Roadmap of Research Infrastructures [1] consisting of 20 selected infrastructure objects was compiled after the careful analysis of 50 proposals by a special working group. The research infrastructures are „facilities", "resources" and related "services" needed for the development of leading-edge research in the most efficient manner as well as for knowledge transmission. In Estonia it will be used in long term (10-20 years) planning and they have to be of national importance, either new or in a need of upgrading.

Among these 20 objects there are the activities of Estonian scientists foreseen at several large scale European facilities. Among the funded objects are an Estonian beam-line at the MAX-IV Lab [2] and participation in the European Spallation Source [3], both located near Lund in south Sweden. In these facilities the Estonian researchers plan to develop own research equipment like the soft X-ray beam-line, at MAX-IV storage ring, with the end station for the gas and solid phase spectroscopy in order to investigate electronic structure and properties. The neutron science community is under formation with the main challenge to build-up knowledge needed by training young researchers, develop connections with neutron scientist in other countries and join the consortia setting up equipment covering our research interest. In CERN there is a well established scientific cooperation in high energy physics at CMS. Here we are targeting knowledge and innovation transfer, where industries from Estonia can participate in the upgrade of CERN research infrastructures. The number of Baltic Sea Region projects: Science Link and Technet_Nano with the involvement of all Baltic countries provide access of local SME's to large scale and specialized facilities (cleanrooms) for increasing their innovation potential. The Estonian strategy along with activities foreseen at European large scale facilities and cooperation possibilities will be discussed.

References

1. <https://www.etis.ee/Portaal/infrastruktuur.aspx?lang=en>
2. <http://www.maxlab.lu.se/maxlab/max4/index.html>
3. <http://ess-scandinavia.eu/>

Abstracts of the invited presentations

Atomistic Multiscale Simulation of Nanostructured Materials for Photonic Applications

A. Bagaturyants, M. Alfimov

Photochemistry Center, Russian Academy of Sciences, ul. Novatorov 7a, build. 1, Moscow 119421 Russia

e-mail: sasha@photonics.ru

Atomistic multiscale simulation is applied to hierarchically constructed nanostructured materials, in which the structure of a lower level of scale is built into the structure of a higher level of scale. The development of nanostructured materials for optical chemical gas sensors is considered as an example. The functionality of such a material is provided by a photoactive molecule (indicator molecule, IM) such that it changes its optical response (mostly, luminescence) upon interaction with a target molecule (detected or analyte molecule, AM). IM represents the lowest level of the hierarchy and is built into a local structure forming a receptor center (RC), which in its turn is built into a nanoparticle (NP). An NP may bear many RCs. Finally, nanoparticles are assembled into a layer or a multilayered structure (nanoparticle assembly, NPA). The goal of simulation in this case is to predict the optical properties of the entire structure (sensing material) and its response to various AMs. Direct calculations in real time and space scales are impossible with the currently available computational resources. Instead, a multiscale approach is used, in which simulations and calculations at each level of scale are performed using methods and approximations appropriate for the corresponding scale, while the results of modeling the structure and properties of a material at a lower level are transferred as input data to the next, higher level of scale. The main steps of such modeling are considered: modeling at the molecular level, modeling at the supramolecular level, and modeling at the level of nanoparticles. Problems arising at each step of modeling are analyzed, and current approaches to their solution are discussed. The possibilities of modern atomistic simulation methods are considered using specific examples.

Quasiparticle Electronic Structures of Thermoelectric Pbx ($X=S,Se,Te$)

A. Svane¹, N.E. Christensen¹

¹Department of Physics and Astronomy, Aarhus University, DK-8000 Aarhus, Denmark

e-mail: nec@phys.au.dk

A thermoelectric material's potential to convert heat into electricity is quantified by the thermoelectric figure of merit $ZT=S^2T\sigma/\kappa$, where T is the temperature, S the Seebeck coefficient, σ and κ the electrical and thermal conductivities. A high figure of merit requires large S and σ values, but small thermal conductivity. The thermal conductivity has contributions from electrons (κ_e) and phonons (κ_l), and for electrons it is difficult to simultaneously maximize σ and minimize κ_e (Wiedemann-Franz "law" for metals). Therefore materials for thermoelectrics are often semiconductors (doped), and nanostructured (to reduce the thermal conductivity), nanowires, nanodots. Lead telluride, $PbTe$, has for many years been known to be a good thermoelectric material with ZT up to 1.3-1.5 at high temperatures, but lately it has been realized that new doping and alloying has made it possible to reach even higher values, close to $ZT=2$ using the lead chalcogenides [1,2]. A materials "design" for such applications requires that the electronic structures, the electron-phonon and phonon-phonon interactions [3] are well understood and accurately modeled. The present work is focused on the electronic structures, and it is shown that conventional density-functional calculations are not sufficiently accurate, and therefore quasiparticle bands are calculated in the quasiparticle self-consistent GW approximation (QSGW, van Schilfgaarde, Kotani and Faleev) including spin-orbit coupling [4]. The semiconducting gap is formed between states of L_6 symmetry (L_{6+} and L_{6-}), which is the reason why these materials are semiconductors even in the local-density approximation (LDA). Closer inspection reveals that the order of the L_6 states is reversed in the LDA, and this leads to the wrong sign of the band gap deformation potentials. With QSGW both sign and magnitude of the deformation potentials are in agreement with experiment. Also, the details of the electronic structures which have particular relevance in connection with thermoelectric applications of these materials are discussed.

References

1. D. Parker and D. J. Singh Phys. Rev. B **82**, 035204 (2010)
2. Y. Pei, X. Shi, A. Lalonde, H. Wang, L. Chen, and J. Snyder, Nature **473**, 69 (2011)
3. O. Delaire et al., Nature Materials **10**, 614 (2011)
4. A. Svane, N. E. Christensen, M. Cardona, A. N. Chantis, M. van Schilfgaarde, and T. Kotani, Phys. Rev. B **81**, 245120 (2010)

Nanothermochromics for Energy Efficient Fenestration

C.G. Granqvist

Department of Engineering Sciences, The Ångström Laboratory, Uppsala University, Uppsala, Sweden

e-mail: claes-goran.granqvist@angstrom.uu.se

Thermochromic technology can be employed for regulating the solar energy throughput in “smart” windows with the object of achieving energy efficiency in buildings. Thin films of vanadium dioxide (VO_2) give an appropriate starting point for developing this functionality; they have a significantly higher infrared transmittance below a “critical” temperature τ_c than above this temperature as a result of a reversible structural transformation. However VO_2 films cannot be used without modification for three main reasons: (i) the modulation of solar transmittance ΔT_{sol} is too small at τ_c , (ii) the luminous transmittance T_{lum} is too low, and (iii) τ_c is $\sim 68^\circ\text{C}$ and hence too high for normal buildings-related applications. I describe how these three problems can be met to a large degree and thus how thermochromic fenestration for energy efficient buildings can come closer to practical realization. In particular, I discuss how nanothermochromics—involving VO_2 -based nanoparticle composites rather than thin films—make it possible to significantly improve ΔT_{sol} as well T_{lum} , how magnesium doping of VO_2 can give further enhancements of T_{lum} , and how tungsten doping (and to some extent also magnesium doping) can bring τ_c to a normal comfort temperature. Finally, I outline how thermochromics may be combined with electrochromics and vacuum insulation in order to create novel “super fenestration” for buildings with radically improved energy performance and a high degree of indoor comfort.

Strategic Research Programmes within Nanotechnology and Advanced Materials in Norway

D. Høvik, V. Skagestad

The Research Council of Norway

e-mail: dah@rcn.no

In the end of 2011 The Research Council of Norway (RCN)'s Programme on Nanotechnology and New Materials (NANOMAT) was concluded after ten years of pioneering activity. The external final evaluation of NANOMAT, conducted by the international consulting firms DAMVAD of Denmark and Econ Pöyry of Norway, concluded that it has succeeded in building knowledge and capacity, coordinating national research communities and developing research groups in the areas of the ethical, legal and social aspects of biotechnology, nanotechnology, and HSE (health, safety and environment).

Education in the field was given a major boost during the NANOMAT programme period as well. All of the largest educational institutions in Norway introduced their own study programmes in nanotechnology at the bachelor, master and doctoral levels. NANOMAT was also very active on international co-operation, as being one of the key partners within the ERA NET MATERA, where also Latvia participated.

NANOMAT was established as a follow up of the external evaluation of RCN, an earlier RCN programme within basic materials science, plus initiatives from the Norwegian universities and largest research institutes. During the NANOMAT programme the Norwegian Government through RCN invested more than Euro 95 mill. In addition, the project partners, mainly from the industry, have invested almost Euro 24 mill.

When a national research programme comes to an end, there is no automatic start-up of a new programme with the same economic funding per year. In 2006 the Research Council of Norway completed a national strategy on Nanoscience and Nanotechnology, which was handed over to the Ministry of Science and Education. In 2009 RCN started an open process where relevant stakeholders from the academy, research institutes, industry and others were asked about priorities and directions for a new programme on nanotechnology and advanced materials. Based upon these processes and the evaluation of NANOMAT, the new strategic programme NANO2021 was established this year with a 10 years programme period and an annual programme budget of appr. Euro 12.5 mill. More insights into NANOMAT, NANO2021 and the process of establishing the Norwegian Government's national strategy on nanotechnology will be given.

Piezoelectric Biomaterials: Structure, Properties, Applications

A.L. Kholkin, A. Heredia, E. Bosne, I.K. Bdikin, M. Wojtas, A. Geraldés, E. Seyedhosseini,
V.V. Bystrov, A. Rudnitskaya, I. Delgadillo

University of Aveiro, Portugal

e-mail: kholkin@ua.pt

One of the key aspects of biological systems is the intricate relationship between chemical and electrical functionality, ranging from piezoelectricity in amino acid derivatives and calcified tissues to the complicated dynamics of ionic channels and flexoelectricity in cellular membranes [1]. Traditionally, it was believed that the polarization or piezoelectricity in biological systems are unambiguously defined by the structure, and cannot be tuned by external electric fields. In other words, many biomaterials possess piezoelectricity, but ferroelectricity is rather rare. With the recent advances in Scanning Probe Microscopy it has become possible to investigate local piezoelectricity and ferroelectricity in artificial biological materials such as amino acid microcrystals [2] and peptide nanotubes [3]. These biomaterials have the potential to replace some inorganic piezoelectrics in sensors and actuators and can be used, e.g., as naturally biocompatible components in medical implants where bioelectromechanical actuation or charge redistribution is required.

In this presentation, recent advances in the fabrication and investigation of artificial biopiezoelectrics and bioferroelectrics will be presented. It will be shown that some of them possess high piezoelectric effect (>50 pm/V) and, in addition, polarization can be switched by the external electric field. The smallest amino acid glycine is shown to possess ferroelectric properties and phase transition at about 200 °C. These studies open up a set of interesting possibilities regarding the role of piezoelectricity and ferroelectricity in–protein formation, as well as emerging properties in peptides from the biophysical point of view.

Acknowledgements

The work was partly supported by the EU ITN project “Nanomotion” and EU-Brazil STREP “PodiTrodi”.

References:

1. “Electromechanics on the Nanometer Scale: Emerging Phenomena, Devices, and Applications, *Materials Research Bulletin*, Sept. 2009, S. V. Kalinin, N. Setter and A. L. Kholkin, Eds.
2. A. Heredia et al. *Adv. Funct. Mater.* (in print).
3. A. L. Kholkin et al. *ACS Nano* **4**, 610 (2010).

Neutron Spectroscopy of Nanoscale Materials

J. Kulda

Institut Laue-Langevin, BP 156X, 38042 Grenoble Cedex 9, France

The traditional image of neutron inelastic scattering is usually connected with studies elementary excitations - phonons and magnons - in condensed matter, possibly using large single crystals as samples. In this talk we shall concentrate on recent trends, making use of more advanced instrument configurations, characterized by simultaneous data acquisition over large ranges in the momentum-energy space and marked by applications to materials containing inhomogeneities on the nanometer scale. While neutron scattering cannot investigate individual objects on this scale, due to its inherent flux limitations, it is highly efficient to establish energy spectra and correlation functions in space and time characterizing the nano-objects and their ensembles. Spectroscopy of adsorbed molecules at levels equivalent to 10 μg of hydrogen, freezing-in of polar nanoregions in relaxor ferroelectrics and molecular nanomagnets are just a couple of examples to be cited, which illustrate applications making use of recent instrumentation developments at the ILL.

Hydrogen Cycling Effect on MgH₂ Nanocomposites

A. Montone¹, A. Aurora¹, D.M. Gattia¹, M.V. Antisari¹

¹ENEA Research Center of Casaccia, Technical Unit for Material Technologies (UTTMAT) Via Anguillarese, 301 –
00123 (Rome) Italy

e-mail: amelia.montone@enea.it

MgH₂ is a very attractive material for safe and cheap solid-state hydrogen storage, due to a high theoretical gravimetric capacity, to the reversibility of the reaction with hydrogen and to a relatively low cost. Nanostructured composite materials obtained by ball milling MgH₂ with different additives (Fe, Nb₂O₅ or carbon-based materials) [1] were studied by a microstructural and kinetic point of view. The evolution of MgH₂ ball-milled during a sequence of hydrogen absorption and desorption reactions at different experimental conditions was explored by the Scanning Electron Microscopy (SEM) and by the analysis of the kinetic curves, in order to derive information about the reaction rates and the rate limiting step. The main features coming up by the cycling procedure was the presence of micrometric structures protruding from the particle surface and of hollow particles constituted by empty nanometric MgO shell box. Despite the microstructural evolution, the kinetics slightly changes in terms of H₂ capacity and sorption rate. Focusing the attention to the application of these metallic hydrides inside tanks for hydrogen storage, studies were carried out with MgH₂-based pellets prepared with the addition of Nb₂O₅ and carbon based materials [2]. The sorption kinetic of the pellets was studied revealing the material to have a similar kinetic with respect to the powder. SEM observations of the inner core of the pellets, before and after the cycling process, were performed. The effects of air exposure were also investigated.

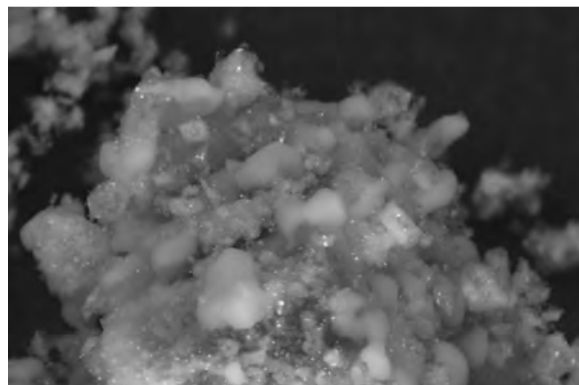


Fig.1 Secondary Electron image of ball-milled MgH₂ with Nb₂O₅ as additive after cycling.

References

1. A. Montone, A. Aurora, D. Mirabile Gattia, M. Vittori Antisari, J. Alloy. Compd, 509 Suppl. 2, (2011). S580-S583
2. S. Garrier, A. Chaise, P. de Rango, P. Marty, B. Delhomme, D. Fruchart, S. Miraglia, Int. J. Hydrogen Energy 36 (2011) 9719

Using Lone s^2 Pairs to Design Crystalline Compounds with Minimal Thermal Conductivity

V. Ozolins¹, M. Nielsen², J. Heremans²

¹Department of Materials Science and Engineering, University of California, Los Angeles, California 90095, USA

²Department of Physics, Ohio State University, Columbus, Ohio, USA

e-mail: vidvuds@ucla.edu

Good thermoelectric materials should possess a combination of seemingly incompatible properties, such as high electronic mobility and low lattice thermal conductivity. Therefore, search for crystalline materials with glass-like thermal conductivity has been an active field of research. Several cubic I-V-VI₂ semiconductors, the paradigm for which is AgSbTe₂, have been shown to exhibit minimal values of lattice thermal conductivity at ambient temperatures when the phonon mean free path equals the interatomic distance. These modes are due to the existence of highly polarizable lone s^2 electron pairs on the group V cations. Hybridization and repulsion between the lone pairs and the valence p electrons on group VI anions tends to favor locally distorted bonding configurations and may lead to unstable phonons. We present the results of first-principles density functional theory (DFT) calculations of phonon dispersion and electron-phonon interactions in cubic I-V-VI₂ semiconductors, where the group I elements are Cu, Ag, Au or alkali metals, the group V elements are P, As, or Bi, and the group VI elements are S, Se, or Te. Compounds that have only marginally stable phonons have extremely large Grüneisen parameters that result in a thermal conductivity limited by Umklapp processes to values at the amorphous limit above 200 K. Following the ab initio calculation, we synthesized AgSbTe₂, AgSbSe₂, AgBiTe₂, NaSbTe₂, NaSbSe₂, and NaBiTe₂ and report their thermal conductivity and specific heat: in all cases, the experiments confirm the theory.

Magnesium Nanoparticles for Hydrogen Storage: Structure, Kinetics and Thermodynamics

L. Pasquini¹, F. Boscherini¹, A. Montone², M.V. Antisari², E. Bonetti¹

¹Department of Physics and CNISM, University of Bologna, Italy

²ENEA, C.R. Casaccia, Rome, Italy

e-mail: luca.pasquini@unibo.it

The widespread interest in novel light-element solid-state hydrogen (H) storage media has triggered the investigation of a quite impressively variety of candidate materials. In alternative to the synthesis of new compounds, an interesting strategy consists in the engineering of nanostructures with a large specific area of properly functionalized surfaces. Nanoparticles (NPs) of light metal hydrides are appealing in this sense because their fine size and large surface area can lead to radically improved H-sorption kinetics. Moreover, the possibility that surface and/or interface effects alter the thermodynamics of the H-metal interaction could pave the way towards tunable hydride forming materials.

In this work we focus on magnesium-based NPs with metal/oxide core/shell morphology, synthesized by inert gas condensation and surface decorated by in situ post-evaporation of transition metal clusters [1-6]. The structure and morphology of the NPs are characterized by electron microscopy, including high-resolution observations. The kinetics and thermodynamics of H-sorption are investigated using standard laboratory techniques as well as *in situ* experiments of X-ray diffraction and absorption, that allow a correlation with ongoing structural transformations. In this respect we address several features like the irreversible formation of intermetallic phases, the H-induced reversible transition between these phases, and the possible formation of hollow nanoparticles driven by hydrogenation at sufficiently high temperature.

References

1. L. Pasquini et al., Appl. Phys. Lett. **94**, 041918 (2009)
2. E. Callini, L. Pasquini, E. Piscopiello, A. Montone, M. Vittori Antisari, E. Bonetti., Appl. Phys. Lett. **94**, 221905 (2009)
3. E. Callini, L. Pasquini, L.H. Rude, T.K. Nielsen, T.R. Jensen, E. Bonetti, J. Appl. Phys. **108**, 073513 (2010)
4. L. Pasquini et al., Phys. Rev. B **83**, 184111 (2011)
5. L. Pasquini, A. Montone, E. Callini, M. Vittori Antisari, E. Bonetti., Appl. Phys. Lett. **99**, 021911 (2011)
6. L. Pasquini et al., J. Nanopart. Res. **13**, 5727 (2011)

Scintillating Ceramics Based on Zinc Oxide

P. Rodnyi

Saint-Petersburg State Polytechnical University, Russia

e-mail: Rodnyi@tuexph.stu.neva.ru

Zinc oxide has a unique combination of properties of a semiconductor material with a significant fraction of ionic bonding. Powdered ZnO is known to be an effective phosphor, while thin ZnO films are used as particle detectors in deuterium–tritium generators [1]. It was recently proposed to use ZnO optical ceramics as scintillators [2]. The scintillators based on ZnO show a high radiation hardness and sufficient stopping power.

Densification of different ZnO powders into ceramics was realized by uniaxial hot pressing method [2]. Ceramics were prepared from a commercial zinc oxide powders (Alfa Aesar Company) with initial particle sizes within 120÷160 nm and from the highly purified powders produced in Russia with initial particle sizes within 300÷600 nm. The sample preparation conditions (temperature, pressure, gaseous medium, etc.) were varied so as to obtain the optical ceramics with maximum transparency and light yield (LY).

Obtained ZnO and ZnO:Zn ceramics of 24 mm diameter and 1.0 mm thickness exhibit high transmission up to 45% in the region of maximum wavelength of X-ray induced luminescence (520 nm); an absolute LY about 29000 photons/MeV; and very good linearity of the relative light output in a 10÷662 keV energy range. The decay constant of the ZnO ceramics is about 1.1 μ s. The level of afterglow is about 0.01% at 10 ms after an X-ray excitation pulse. These characteristics show that ZnO ceramics is a promising scintillator for use in X-ray computed tomography (CT).

In ZnO:Ga ceramics the long-wavelength emission band is suppressed and excitonic emission peaked at 385 nm predominates. Excitons in the doped ceramics possess subnanosecond decay time of scintillations, such a short decay time is very important for the Positron Emission Tomography (PET) which operates in the time-of-flight mode.

It is shown that in ZnO, ZnO:Zn and ZnO:Ga luminescence centers are zinc vacancies V_{Zn} , oxygen vacancies V_O and excitons localized on the donors, respectively.

References

1. A. Beyerle, J.P. Hurley, and L. Tunnele, Nucl. Instr.Meth. Phys. Res. A 299, 458 (1990).
2. E.I. Gorokhova, P.A. Rodnyi, K.A. Chernenko et al., Optical Materials, 78, 85 (2011).

Polaronic Excitons in KTN: Optical Absorption and Photo-EPR Manifestations

V. Trepakov^{1,2}, R. Yusupov³, I. Gracheva³, A. Rodionov³, P. Syrnikov², A. Gubaev⁴, A. Dejneka¹,
L. Jastrabik¹, M. Salakhov³

¹Institute of Physics AS CR, Na Slovance 2, 182 21 Prague, Czech Republic

²Ioffe Physical-Technical Institute RAS, 194 021 St-Petersburg, Russia

³Kazan (Volga Region) Federal University, 420 008 Kazan, Russia

⁴Institute for Physical Chemistry Muenster University, D 48 140 Germany

e-mail: trevl@fzu.cz

The “quantum paraelectrics” KTaO_3 and SrTiO_3 can be considered as systems close to the quantum mechanical limit at low temperatures. In such systems, unlike in the classical case, the phase transitions can be achieved by tuning not the temperature, but the other parameters, such as pressure, electric and magnetic field, chemical composition, impurity doping. The giant photodielectric effect recognized in SrTiO_3 and KTaO_3 [1-3], where UV light irradiation at low temperatures strongly enhances the dielectric constant is another example. Qualitatively, this phenomenon has been assigned to the inhomogeneous polar state induced by photocharge carriers, but understanding of their microscopic nature had not been achieved.

We report on results of low-T studies of optical absorption and photo-EPR of KTN ($\text{KTa}_{1-x}\text{Nb}_x\text{TaO}_3$, $x=0.004\div 0.02$) crystals. It was found that UV light irradiation results in a broad absorption band in NIR region. Together with photoconductivity and photoluminescence experiments it provides the broad hint of strong localization of the charge carriers in the form of Nb^{4+} electronic polarons. Strict verification and characterization of photo-polaronic states is provided by the x-band photo-EPR experiments. So, photo-EPR spectrum of KTN with $x = 0.012$ reveals the anisotropic component originated from the axial centres with $S = 1$, $g_{\parallel} = 0.82 \pm 0.04$, $g_{\perp} = 0.52 \pm 0.04$, and $D = 0.44 \pm 0.03 \text{ cm}^{-1}$ attributed to the polaronic excitons $\text{Nb}^{4+}\text{-O}^-$ with activation energy $E_{a1} \sim 3.7 \text{ meV}$ for internal dynamics and destruction energy $E_{a2} \sim 52 \text{ meV}$. Namely $\text{Nb}^{4+}\text{-O}^-$ polaronic excitons manifest themselves via the wide absorption band at $\sim 0.7 \text{ eV}$, which arises in the KTN under UV illumination.

References

1. M. Takesada, T. Yagi, M. Itoh, D. Koshihara, J. Phys. Soc. Jpn. **72**, 37 (2003)
2. T. Hasegawa, S. Mouri, Y. Yamada, K. Tanaka, Ibidem **72**, 42 (2003)
3. I. Katayama, Y. Ishikawa, K. Tanaka, Phys. Rev. B **67**, 100102 (2003)

Storage of Renewable Energy in Synthetic Fuels

A. Züttel

EMPA Materials Science & Technology, Div. Hydrogen & Energy, Dübendorf, Switzerland

e-mail: andreas.zuetzel@empa.ch

The world wide energy demand increases just as rapidly as the average temperature of the atmosphere. The reserves of fossil fuels worldwide are limited and the combustion of the carbon fuels leads to a severe increase of the CO₂ concentration in the atmosphere. The latter is responsible for the climate change. The future of the industrialized world, i.e. the economy as well as the society, is determined by the ability to change from fossil fuels as energy carriers to renewable energy. The main difference between the fossil period and the future is the requirement of producing synthetic energy carriers.

Hydrogen as an energy carrier opens the path to a society based on renewable energy. The storage of hydrogen in metals and complex hydrides as stable compounds offers a great volumetric storage density, however the gravimetric storage density is limited to less than 20mass% in the materials. In order to replace fossil fuels without scarification on energy density synthetic fuels based on hydrogen e.g. NH₃ or C₈H₁₈ have to be developed [1]. The latter also represents a effective CO₂ sink for the atmosphere.

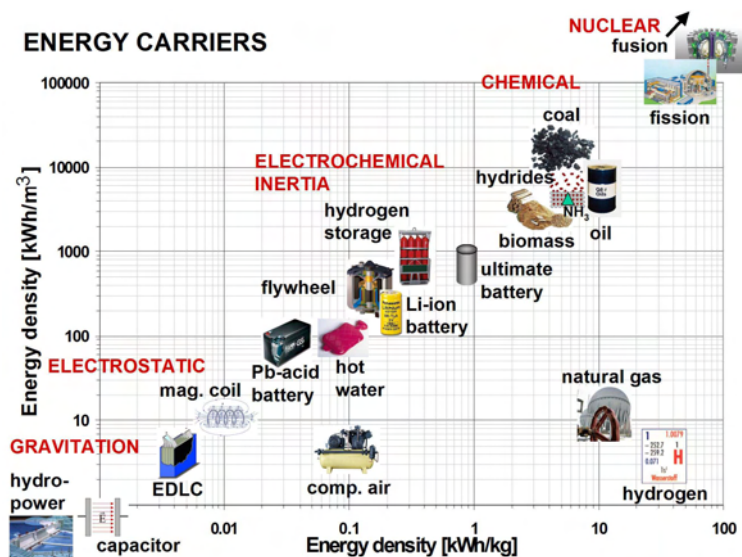


Fig. 1: Volumetric vs. gravimetric energy density of important energy carriers.

References

1. A. Züttel et al. Phil. Trans. R. Soc. A (2010) 368, 3329–3342

Abstracts of the oral presentations

The Story of Polymer Monoliths: From USA to Europe and to Latvia

S. Abele¹, Z. Walsh², P. Smejkal³, O. Yavorska², Z. Zanriba¹, R. Fedorovskis¹, R. Poplausks⁴,
D. Erts⁴, I. Susinskis⁵, K. Kuprevics⁵, J. Hmelnickis⁵, F. Foret³, M. Macka²

¹Faculty of Chemistry, University of Latvia, Riga, Latvia

²Dublin City University, Dublin 9, Ireland

³Institute of Analytical Chemistry, ASCR, v.v.i., 60200 Brno, Czech Republic

⁴Institute of Chemical Physics, University of Latvia, Riga, Latvia

⁵"Grindeks", JSC, Riga, Latvia

e-mail: silvija.abele@lu.lv

Separation technologies - gas chromatography (GC), liquid chromatography (LC), ion chromatography (IC), capillary electrophoresis (CE) - are used to extract, separate, detect and quantify compounds in pharmaceutical, biochemical and petrochemical industries. Chromatographic research over many years has focused on the development of new stationary phases. Originally the predominant technology used was that of the packed column but the invention of monolithic columns in 1992 by Svec, Fréchet, and co-workers has pioneered the use of rigid, porous monoliths based on organic polymers [1] as alternative column materials for high performance liquid chromatography (HPLC).

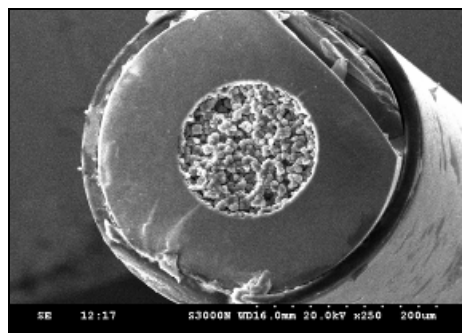


Fig.1. SEM image of polymer monolith in fused silica capillary, 100 μm i.d., magnification 250 x

The monolith is formed in situ as a continuous bed within the capillary (Fig.1) or other type of mold and therefore can be covalently bound to the capillary wall. Monolithic materials as stationary phases offer several advantages in comparison to particle packed columns (improved mechanical stability, spatial control, range of different pore size and different surface chemistries available). A lot of efforts are devoted to studies of monolithic materials in many research groups, as there has been a growing demand for new and more selective chromatographic materials.

In the present work thermal polymerisation and photoinitiated polymerisation have been studied for the synthesis of methacrylic and styrenic monoliths [2, 3]. Examples of chromatographic separations of proteins [2, 3] or pharmaceutical compounds using styrenic or methacrylic monoliths are demonstrated.

References

1. F. Svec, J. M. J. Fréchet, *Anal. Chem.*, 1992, 64, 7, 820–822
2. Z. Walsh, P. A. Levkin, V. Jain, B. Paull, F. Svec, M. Macka, *J. Sep. Sci.*, 2010, 33, 61–66
3. S. Abele, P. Smejkal, O. Yavorska, F. Foret, M. Macka, *The Analyst*, 2010, 135, 477–481

Luminescence Properties of Re^{3+} - Doped Hafnia and Zirconia Thin Films Grown by Atomic Layer Deposition Method

E. Aleksanyan^{1, 2}, M. Kirm¹, E. Feldbach¹, K. Kukli^{1, 3}, S. Lange¹, I. Sildos¹, A. Tamm¹

¹Institute of Physics, University of Tartu, Estonia

²Yerevan Physics Institute, Yerevan, Armenia

³University of Helsinki, Department of Chemistry, Finland

e-mail: aeduard@fi.tartu.ee

In order to achieve good spatial resolution needed for micro-imaging of ionizing radiation based techniques it is necessary to use a scintillator as a thin film. As it has been shown for ALD grown hafnia and zirconia films [1], the performance of such films strongly depends on growth methods and parameters. In this work luminescence of Sm, Eu and Er ions as well as intrinsic (STE) emission in ALD grown HfO_2 and ZrO_2 was investigated using time-resolved luminescence spectroscopy under VUV-XUV excitation and cathodoluminescence. The 300 keV ions were implanted into the films, which were annealed to restore host lattice [2]. The ALD grown $\text{ZrO}_2:\text{Er}_2\text{O}_3$ nanolaminates [3] were also spectroscopically investigated and results compared with the ion-implanted samples.

Our investigations under XUV excitation revealed that at low temperatures Sm^{3+} , Eu^{3+} and Er^{3+} ions possess characteristic f-f lines superposed by STE emission with considerable intensity, which has the asymmetric shape peaked at about 4-4.5 eV. Such wide bandwidth in all ion-implanted films is due to superposition of several bands of excitonic origin, attributed to radiative recombination of STE at perfect sites or perturbed ones near different defects. At RT STE emission is quenched and the emission in the region of 2.5-3.5 eV was revealed. In Y-stabilized zirconia [4] such bands were attributed to recombination emission at centers distorted by presence of oxygen vacancy. In $\text{ZrO}_2:\text{Er}_2\text{O}_3$ nanolaminates at room temperatures non-radiative relaxation channels cause complete quenching of excitonic and defect related luminescence and only rather weak f-f transitions were observed. Relaxation and energy transfer processes will be discussed for studied samples.

References

1. J. Aarik, H. Mändar, M. Kirm, L. Pung, *Thin Solid Films*, **466**, 41 (2004)
2. S. Lange, V. Kiisk, V. Reedo, M. Kirm, J. Aarik, I. Sildos, *Optical Materials* **28**, 1238 (2006)
3. A. Tamm, M. Heikkilä, M. Kemell et al., *Thin Solid Films*, **519**, 666 (2010)
4. L. Grigorjeva, D. Millers, A. Kalinko, V. Pankratov, K. Smits, *Journal of Europ. Cer. Soc.* **29**, 255 (2009).

Application of Ge Nanowire Mass Sensor for Graphene Exfoliation

J. Kosmaca¹, J. Andzane¹, J.D. Holmes², D. Erts¹

¹University of Latvia, Raina blvd. 19, Riga, LV-1586, Latvia

²Department of Chemistry, National University Ireland, Cork, Ireland

e-mail: Jana.Andzane@lu.lv

As a novel material with several unique features, graphene, since it was discovered, caused recently an increasing number of related researches. Graphene may be described as 2D allotrope form of carbon – the thinnest material in the world with hundreds of properties which are unique or superior to other materials.

Graphene properties are strongly dependent on purity and number of single layers of the sample. Thickness of individual graphene samples has to be determined and after that samples with appropriate layers can be used for applications [1]. Best quality graphene is obtained by mechanical exfoliation of pyrolytic graphite although thickness of samples are unpredictable and number of layers has to be determined in each graphene flake before application.

Here we present simple and accurate method for graphene flake selection from the pyrolytic graphite surface and determination of the number of layers in it *in situ* by using a nanowire-based nanoelectromechanical tool. This method is based on adhesion between the nanowire material and carbon, which is stronger than carbon cohesion and thus allows to place the selected graphene flake on the certain area of the single-clamped nanowire. Then the mass of the graphene flake can be accurately calculated from the difference between resonant frequencies of empty and loaded nanowire [2]. Knowing flake's mass, geometry and interplanar spaces between the graphite layers, it is possible to estimate the number of layers in it. Then using the same tool the selected graphene sample with certain number of layers can be placed in defined position on the substrate for further applications.

References

1. A.K. Geim, *Graphene: Status and Prospects*, Science, 324, **5934**, (2009).
2. J. Zhou et al, *Nanowire as pico-gram balance at workplace atmosphere*, Solid State Communications, **139** (2006).

EPR Studies of Transition Metal Impurities in SrTiO₃

D.V. Azamat¹, A.G. Badalyan², J. Lancok¹, V.A. Trepakov^{1,2}, L. Jastrabik¹, A. Dejneka¹

¹Institute of Physics AS CR, 182 21, Prague 8, Czech Republic

²Toffe Physical-Technical Institute, Russian Academy of Sciences, 194021, St. Petersburg, Russia

Transition-metal doped perovskites continue to attract significant attention as promising materials for a wide range of applications from actuators, ferroelectric nonvolatile memory and modern optical devices to anodes for solid-electrolyte and solid-oxide fuel cells. The development of perovskite-based semiconductor devices relies on controlling the point defects, such as oxygen vacancies and transition metal impurities. Strontium titanate, the incipient ferroelectric with perovskite structure, has become in the focus of interest in attempt to combine magnetic and ferroelectric properties of the material. In this work we use electron paramagnetic resonance (EPR) spectroscopy for the accurate determination of different oxidation states and local environment of manganese and chromium impurities in SrTiO₃. Trivalent manganese ions in SrTiO₃ crystals look like a model ones to study exchange-coupled systems in mixed-valent manganese oxides.

The single crystals of SrTiO₃ were grown in Furuuchi Chemical Corporation by use of Verneuil technique through the melting of SrTiO₃ and 0.5% wt of MnO/Cr₂O₃ crystalline powders. EPR spectra originating from the $S = 2$ ground state of Mn³⁺ ions are shown to belong to the three distinct types of Jahn-Teller centres. The present results indicate the strong covalent reduction of the density of unpaired spins (Fermi term) at the manganese nucleus for the various types of centers.

When crystals of SrTiO₃ are heavily doped with fourvalent manganese (or trivalent chromium) there is a tendency for the impurity ions to form exchange coupled pairs. The EPR spectra indicate the formation of exchange-coupled transition-metal dimer centers lying along the $\langle 110 \rangle$ directions (in the next nearest neighbor position).

First-Principles LCAO Calculations of Single-Walled ZrO₂ Nanotubes

A. Bandura¹, R. Evarestov¹

¹Department of Chemistry, Quantum Chemistry Division, St. Petersburg State University, Russia

e-mail: andrei@ab1955.spb.edu

Nanotubes of zirconia have been recently synthesized by different techniques such as template-assistant deposition, hydrothermal treatment and anodization methods. The diameter of fabricated ZrO₂ nanotubes (ZNT) vary from tens to hundred of nanometres. Experimental observations give evidences that the atomic structure of ZNT may correspond to cubic, tetragonal, and monoclinic phases of bulk zirconia, or to be a mixture of all mentioned structures. In this work, for the first time, we theoretically analyse the structure and stability of ZNT obtained by folding of layers in three low-pressure zirconia phases. All calculations are made using hybrid PBE0 LCAO approach via the CRYSTAL-2009 computer code.

We have optimized the atomic structure of thin slabs corresponding to all possible low-index surfaces in cubic, tetragonal and monoclinic ZrO₂ phases, which are compatible with orthogonality condition between supposed helical and translational vectors. Considered nanosheets include up to 12 atomic planes, depending on the parent phase and surface indexes. Taking into account atomic reconstruction, the final number of 2D structures proved to be less than the total number of considered surfaces. Accordingly, the faces (110), (111) of the cubic phase, (001), (110) of the tetragonal phase, and (100), (-101) of monoclinic phase were chosen as generic for single-walled ZNTs.

The initial structures of nanotubes have been obtained by rolling up the relaxed or reconstructed ZrO₂ slabs. Different ZNT chiralities compatible with the 2D symmetry of parent nanosheets have been considered. Positions of all atoms have been optimized to obtain the most stable ZNT structure with preserving the rototranslational symmetry. Basing on the formation and strain energy estimations we found that the most stable tubes with thin (one ZrO₂ layer) walls have hexagonal (cubic (111) face) morphology. The tubes with walls composed by two ZrO₂ layers most probably have lepidocrocite (tetragonal (001) face) morphology. The tubes with thicker walls can possess a different structure originated from cubic or tetragonal phases.

Acknowledgments

The authors are grateful for the support to RBRF (grant 11-03-00466a).

Simulation of Lattice Constants for Cubic Crystals

M.G. Brik¹, I.V. Kityk²

¹Institute of Physics, University of Tartu, Riia 142, Tartu 51014, Estonia

²Electrical Engineering Department, Czestochowa University of Technology, Armii Krajowej 17, Czestochowa, Poland

e-mail: brik@fi.tartu.ee

It has been recognized for a long time that the crystal lattice constants (LCs) are determined by properties of the particular ions, such as ionic radii, electronegativity, oxidation state etc [1]. Up to now, two methods were used to calculate and/or predict the LCs of crystals: i) experimental X-ray diffraction technique and ii) theoretical *ab initio* calculations. However, both methods are time-consuming. So there exists a strong demand for a reliable and quick estimation of the structural parameters, using empirical model and statistical analysis of the LCs for a large number of iso-structural crystalline materials.

In the present work, we considered 85 crystals with general chemical formula A_2XY_6 ($A=K, Cs, Rb, Tl$; X =tetravalent cation, $Y=F, Cl, Br, I$), crystallizing in the $Fm-3m$ space group. For this group of crystals, we derived the following equation, which links together their lattice constants a (expressed in Å) with ionic radii R (measured in Å) dimensionless electronegativities χ :

$$a = 1.96325(R_A + R_X) + 0.98102(R_X + R_Y) + 0.07593(\chi_Y - \chi_X) + 0.57901$$
 [2].

Fig.1 illustrates good agreement between the experimental and predicted LCs; the studied compounds are grouped into 4 categories depending on the nature of the Y anion (fluorides, chlorides, bromides, iodides). The mean error of the model's prediction is 1.05 % only, which is comparable with the accuracy of the experimental determination of the LCs.

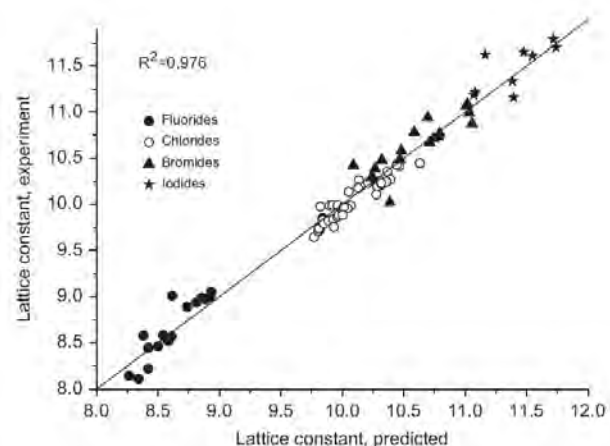


Fig.1 Comparison between the predicted and experimental lattice constants for the A_2XY_6 compounds. The axes units are Å.

References

1. L. Pauling, The Nature of the Chemical Bond, 3rd ed., Cornell University Press, Ithaca, 1960.
2. M.G. Brik, I.V. Kityk, J. Phys. Chem. Solids **72**, 1256 (2011)

Processing of Amorphous Si by Pulsed Laser Irradiation at Different Wavelengths

I. Tale, J. Butikova, G. Marcins, A. Muhins, B. Polyakov, A. Voitkans

Institute of Solid State Physics, University of Latvia, Latvia

e-mail: but@latnet.lv

Polycrystalline silicon is a promising material for various thin film electronic devices. There have been the attempts of using laser crystallized poly-Si to increase the efficiency of thin film solar cells. The second field of interest is using laser-treated silicon as an active layer in thin-film transistors for large area liquid crystal displays [1].

In this study, a-Si thin films deposited on SiO₂-coated Si/SiO₂ wafers have been processed by the 2nd and the 3rd harmonics of Nd:YAG laser, as well as by KrF excimer laser. Surface modification of amorphous silicon layers have been investigated scanning electron microscopy before and after chemical etching of processed silicon films.

The order of a grain size in polycrystalline Si samples prepared by successive crystallization in the lateral growth regime is of 1 μm. It varies with the laser fluence.

At an initial stage, a pulsed laser processing results in nucleation of Si nanocrystals which starts from unmolten silicon islands. Nanocrystals are growing near the a-Si layer surface. Si nanocrystals obtained during the pulsed laser processing can be used as seed particles for the following laser stimulated processing to produce poly-Si layer.

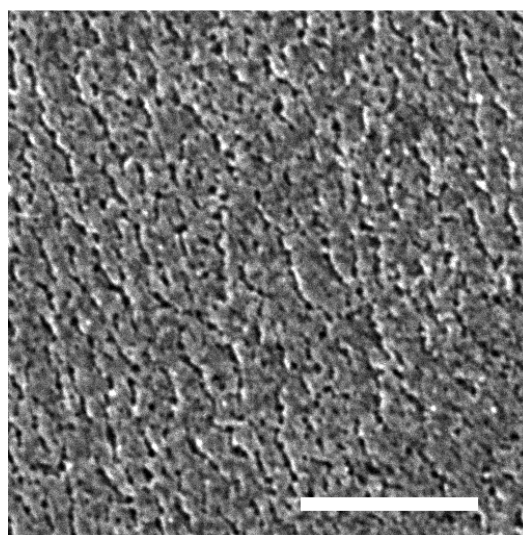


Fig.1. Lateral crystal growth after laser irradiation (355 nm) of the amorphous Si sample. Scale bar 3 μm

Acknowledgements

I.T, J.B., A.M., B.P., A.V. are supported by the ERAF project Nr.2010/0252/2DP/2.1.1.1.0/10/APIA/VIAA/009

References

1. K. Brendel et al., Thin Solid Films **427**, 86 (2003)

Measurements of Mechanical, Electrical and Optical Properties of Modern Nanostructures with AFM-Based Methods

I. Bykov

NT-MDT Co., Zelenograd, Moscow, Russia

e-mail: ivan_bykov@ntmdt.ru

Scanning Probe Microscopy gives an opportunity to carry out studies of spatial, physical and chemical properties of objects with the typical dimensions of less than a few nanometers. Owing to its multifunctionality, availability and simplicity, Atomic-Force Microscope (AFM) has become one of the most prevailing “tools for nanotechnology” nowadays. The next step towards the new functionality should be combining with various other modern research methods. Besides the extending the measurements to specific conditions: vacuum, liquids, low and high temperatures, etc the combination of AFM with other methods has given an opportunity of going beyond the limits of traditional methods and carry out researches (mechanical, electric, optical properties) with the highest resolution.

Possibility to operate with AFM in low vacuum conditions provides increased Q- factor of the cantilever, better sensitivity, accuracy of low-force measurements and elimination of influence of adhesion and contaminations.

Quantitative measurements of elastic properties (soft polymers, biology, graphene and other) require further development of standard AFM modes. The calculation of real tip shape, detailed analysis of contact area and correct model of interaction – considered of all these aspects we can achieve the true information about surface.

Using of diamond probe instead of silicon cantilever becomes very important while studying of mechanical properties of relatively hard materials. Elastic modulus, hardness, strength, crack-resistance and even the elastic conductivity can be measured highly doped semiconductor diamond probe.

Simultaneously with AFM, confocal Fluorescence and Raman measurements provide information about sample chemical composition, crystal structure and its orientation, presence of impurities and defects, macromolecular conformation, and so on. By using a specially prepared sharp needle tip, in TERS mode we can multiply the Raman signal strength by a few orders of magnitude from a precisely scanned, localized spot on the surface several nanometers in diameter. Even single molecules can be detected and recognized by their spectra. Lateral resolution of Raman (TERS) and fluorescence maps is no longer limited by light diffraction and can be less than 15 nm.

High Quality Epitaxial r-BN Grown by CVD

M. Chubarov, H. Pedersen, H. Högberg, A. Henry

Department of Physics, Chemistry and Biology, Linköping University SE-581 83 Linköping, Sweden

e-mail: mihails.cubarovs@liu.se

Hexagonal (h-BN) and rhombohedral (r-BN) are the two sp^2 -hybridized phases of boron nitride. They differ only by their stacking sequence, where h-BN has ABAB stacking and r-BN has ABCABC stacking. This makes phase identification by XRD in Bragg-Brentano configuration difficult. Both phases are interesting as semiconductor and optoelectronic thin film materials in the UV range given a bandgap of around 6 eV [1]. For growth of such materials, thermal CVD has often been the choice of technique and from these studies the literature reports on growth of h-BN [2].

From hot wall CVD and with triethyl boron and ammonia as precursors, we demonstrate epitaxial growth of high quality r-BN films on Al_2O_3 (0001) substrates with an AlN buffer layer grown by *in-situ* nitridization [3]. Pole figure measurements confirm that the deposited phase is r-BN with a twinned growth behavior. Further, our studies on the influence of the process parameters (temperature (Fig. 1), N/B-ratio, B/H₂-ratio and carrier gas composition) show that epitaxial r-BN film can only be deposited in a narrow process window and that a thin strained AlN buffer layer is needed to support epitaxial growth.

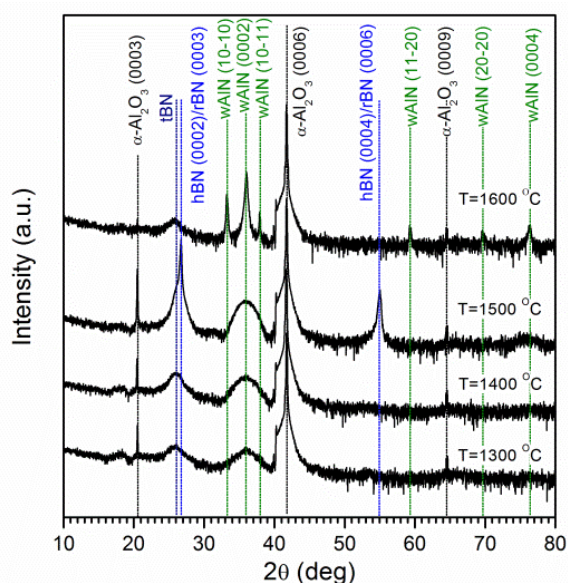


Fig. 1 Growth temperature influence on the sp^2 BN film quality. The growth was done with H₂ as carrier gas, at 100 mbar, B/N of 615 and B/H₂ of 0.02%.

References:

1. M. G. Silly, P. Jaffrennou, J. Barjon, J.-S. Lauret, F. Ducastelle, A. Loiseau, E. Obraztsova, B. Attal-Tretout, and E. Rosencher, Phys. Rev. B 75, 085205 (2007)
2. Y. Kobayashi, T. Nakamura, T. Akasaka, T. Makimoto, N. Matsumoto, J. Crystal Growth 298, 325 (2007)
3. M. Chubarov, H. Pedersen, H. Högberg, V. Darakchieva, J. Jensen, P. O. Å. Persson, A. Henry, Phys. Status Solidi RRL 5, 397 (2011)

Low-Energy Charge Transfer Excitations in NiO Nanocrystals

V.I. Sokolov¹, V.A. Pustovarov², V.N. Churmanov², V.Yu. Ivanov², A.Ye. Yermakov¹,
M.A. Uimin¹, N.B. Gruzdev¹, P.S. Sokolov³, A.N. Baranov³, A.S. Moskvina⁴

¹Institute of Metal Physics UD RAS, Yekaterinburg, Russia

²Yeltsin Ural Federal University, Yekaterinburg, Russia

³Lomonosov Moscow State University, Moscow, Russia

⁴Department of Theoretical Physics, Institute of Natural Science, Ural Federal University, Yekaterinburg, Russia

e-mail: chenov@olympus.ru

Explaining the electronic properties of transition metal monoxides is one of the long-standing problems in the condensed matter physics. Main goal of our paper is to show with NiO as an example that the photoluminescence excitation (PLE) spectroscopy of the nanocrystalline materials appears to be a novel informative technique for inspection of different charge transfer transitions.

In this paper we have performed a comparative analysis of photoluminescence and photoluminescence excitation spectra of NiO poly- and nanocrystals in the spectral range 2-5.5 eV. The PL spectra for both types of samples have a very similar spectral shape with broad emission bands centered at about 2.5 eV. The PLE spectra reveal two PLE bands peaked near 3.7 and 4.6 eV with a dramatic rise in the low-temperature PLE spectral weight of the 3.7 eV PLE band in the nanocrystalline NiO as compared with its polycrystalline counterpart. In frames of a cluster model approach [1-2] we assign the 3.7 eV PLE band to the low-energy bulk-forbidden p-d ($t_{1g}(\pi)$ - e_g) charge transfer (CT) transition which becomes the allowed one in the nanocrystalline state while the 4.6 eV PLE band is related with the bulk allowed d-d (e_g - e_g) CT transition scarcely susceptible to the nanocrystallization. For the first time we succeeded to distinctly separate contributions of the low-energy p(π)-d and d-d CT transitions to the fundamental absorption of NiO and show that NiO is close to the intermediate regime of the Zaanen-Sawatzky-Allen scheme.

Acknowledgments

This work was supported in part by the program of development of Yeltsin Ural Federal University.

References

1. Moskvina A.S., Phys. Rev. B **65**, 205113 (2002)
2. Pisarev R.V., Moskvina A.S., Kalashnikova A.M. and Rasing Th., Phys. Rev. B **79**, 235128 (2009)

Linear Augmented Cylindrical Wave Method for Nanotubes

P.N. D'yachkov

Kurnakov Institute of General and Inorganic Chemistry, Russian Academy of Sciences, Moscow, Russia

In the terms of muffin-tin and DFT theory, we developed a linear augmented cylindrical wave (LACW) method for electronic structure of the single- and double-wall nanotubes. We calculated the band structures of the nanotubes up to the chiral (100, 99) tubule. The electronic spectrum of nanotubes is governed by the electrons movement in interatomic space of cylindrical layers, by scattering on the atomic spheres, and tunneling between the layers. A model for electronic structure of nanotubes embedded in a crystal matrix is developed too. The LACW-Green function theory is elaborated for the nanotubes with point defects. A first-principles numerical method for calculation of the electronic structure of the point impurities in the single-walled carbon nanotubes based on a Green's function technique is developed. The host nanotubes electron Green's function is calculated using a linear augmented cylindrical wave theory. The Green's function of the impurities is calculated in the terms of matrix Dyson equation. The impurities are described by the single-site perturbed muffin-tin potentials in otherwise perfect nanotubes with the rotational and helical symmetries. Due to the account of these symmetry properties, the method is developed applicable to any tubule including the chiral nanotubes with point defects independent of the number of atoms in translational unit cell of the host systems. Finally, a relativistic version of the LACW method is elaborated and applied to calculating the spin-orbit coupling effects in the armchair nanotubes.

Acknowledgments

This study was performed in the frames of the Program "Researches and developments on priority directions of scientific-technological complex of Russia in 2007-2012". It was supported by RFBR (11-03-00691).

References

1. P.N. D'yachkov and D.V. Makaev, Phys. Rev. B 76, 195411 (2007).
2. P.N. D'yachkov and D.V. Makaev, Phys. Rev. B 74, 155442 (2006).
3. P.N. D'yachkov and D.V. Makaev, Phys. Rev. B 71, 081101 (2005).
4. P.N. D'yachkov, D. Z. Kutlubaev, and D.V. Makaev, Phys. Rev. B 82, 035426 (2010).
5. P.N. D'yachkov, D. Z. Kutlubaev, Phys. Rev. B (in press).

Color Centers and Structural Damage in LiF Induced by 150 MeV Kr ions

A. Russakova¹, A. Dauletbekova¹, K. Schwartz², J. Maniks³, A. Akilbekov¹, V. Lisitsin⁴,
M. Zdorovets⁵

¹L.N. Gumilyov Eurasian National University, Astana, Kazakhstan

²GSI Helmholtz Zentrum für Schwerionenforschung, Darmstadt, Germany

³Institute of Solid State Physics, University of Latvia, Riga, Latvia

⁴Tomsk Polytechnic University, Tomsk, Russia

⁵Institute of Nuclear Physics, Kazakhstan

e-mail: arussakova@gmail.com

Color centers and structural damage was investigated in LiF crystals irradiated at room temperature with 150 MeV ⁸⁴Kr ions with a beam current of 10 nA/cm² in the fluence range 10¹¹ - 10¹⁴ ions/cm² at the cyclotron accelerator DC-60 (Astana, Kazakhstan).

UV-VIS spectroscopy was utilized to study the concentration of electron color centers (F and F_n) as a function of fluence (Φ). A saturation of F centers occurs at Φ ~ 10¹³ ions/cm² but due to strong aggregation of single F centers, at higher fluences their concentration decreases. A rapid increase of F_n centers begins at fluences above 10¹² ions/cm² (details about the mechanism can be found in [1, 2]).

The ion-induced modifications of structure on the irradiated surfaces and cross-sections of samples were investigated using scanning electron microscope JSM-7500F (JEOL). The structural defects were revealed by chemical etching. At the fluence of 10¹¹ ions/cm², SEM imaging revealed mainly formation of etchable ion tracks. Above this fluence, severe structural modifications in the irradiated layer were observed which include the ion-induced formation of dislocations and grains with nano-scale dimensions. The intensity of nanostructuring depends on fluence and energy loss of ions. Nanostructuring dominates in the near-surface region whereas formation of dislocations prevails in the tail part of ion range where the energy loss of ions decreases below the threshold for track core damage.

References

1. K. Schwartz, M. V. Sorokin, A. Lushchik et al, Nucl. Instr. Meth **B** 266, 2736 (2008)..
2. A. Dauletbekova, A. Akilbekov, M. Zdorovets, Phys. Status Solidi B **247**, 1227 (2010).

Fluorescence of $\text{TiO}_2:\text{Sm}^{3+}$ Composite Stimulated by Plasmon Waves

L. Dolgov, V. Kiisk, S. Pikker, A. Loot, I. Sildos

Institute of Physics, University of Tartu, Estonia

e-mail: dolgov@fi.tartu.ee

Metal oxides with rare earth dopants are perspective fluorescent materials because of several reasons. Rare earth ions in metal oxide matrices are chemically stable and do not suffer from photobleaching in contrast to organic fluorophores. Rare earth fluorescence can serve as a marker of surrounding metal oxide crystal structure [1]

or work as a sensor if metal oxide pores are filled by exterior gas [2]. On the other hand, rare earth fluorescence can provide gained signal in the metal oxide active optical fibers [3] and laser resonators [4]. Recently we demonstrated that direction, polarization and intensity of fluorescence can be tuned for rare earth ions, which are incorporated in the layered metal-dielectric structure [5]. Fluorescent $\text{TiO}_2:\text{Sm}^{3+}$ film was deposited on the gold-plated glass,

which was attached to the base of semi-cylindrical prism. The emitted light penetrates especially effective through the gold film to the prism at the definite resonance angles. It is caused by coupling of Sm^{3+} fluorescence with surface plasmons induced at the gold surface. Such coupled part of emission becomes strongly polarized and directional. Here we demonstrate that surface plasmons can stimulate Sm^{3+} ions by such a way to get about 10 % of non-linear emission growth over the pumping (Fig. 1). It opens attractive possibilities for generation of coherent plasmons and plasmon coupled lasing effects.

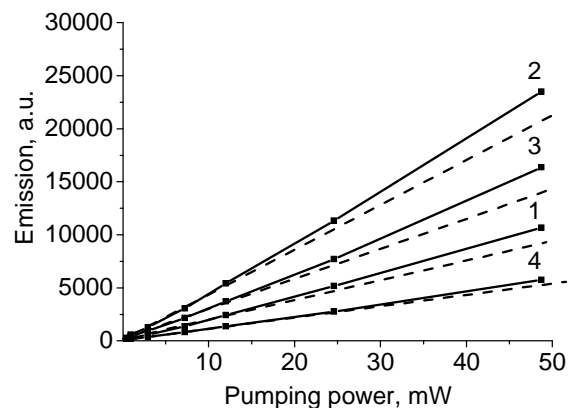


Fig. 1. Emission vs. pumping for the different spectral bands of Sm^{3+} : 1) 578 nm; 2) 615 nm; 3) 665nm; 4) 728 nm. Angle of detection is 60° . Experimental solid lines deviate from dashed linear dependence.

Acknowledgments

This work was supported by Nanotwinning project FP7-INCO-2011-6 and ERDF Centre of Excellence "Mesosystems: Theory and Applications", TK114.

References

1. V. Kiisk, V. Reedo, M. Karbowiak, M.G. Brik, I. Sildos, *J. Phys. D: Appl. Phys.* **42**, 125107 (2009)
2. V. Reedo, S. Lange, V. Kiisk, A. Lukner, T. Tatte, I. Sildos, *Proc. of SPIE* **5946**, 1-6 (2005)
3. A. Marques, R. Almeida, *J. Non-cryst. Solids* **353(27)**, 2613-2618 (2007)
4. H. Hsu, C. Cai, A. Armani, *Opt. Express* **17(25)**, 23265 (2009)
5. L. Dolgov, V. Kiisk, I. Sildos, *Book of FMNT 2011 abstracts* 52 (2011)

Vibrational Spectra of Opal-Based Photonic Crystals

G. Dovbeshko¹, O. Fesenko¹, V. Boyko¹, V. Romanyuk², V. Moiseyenko³, V. Gorelik⁴, L. Dolgov⁵,
V. Kiisk⁵, I. Sildos⁵

¹Institute of Physics, NASU, Kyiv, Ukraine

²Institute for Physics of Semiconductors NASU, Kyiv, Ukraine

³Dnipropetrovsk National University, Dnipropetrovsk, Ukraine

⁴P.N. Lebedev Physical Institute of RAS, Moscow, Russia

⁵Institute of Physics, University of Tartu, Tartu, Estonia

e-mail: gd@iop.kiev.ua

Periodicity of structural units in photonic crystals, particularly in silica opals, is dependent strongly on the shape and packing type of their globules. Infrared (IR) and Raman scattering (RS) spectroscopy allow identify the framework of silicates in the globules by the signal from bridging oxygen breathing mode of the SiO₄ rings [1].

Hereby we represent the synthetic silica opals prepared by Stöber method and investigated by methods of IR and RS spectroscopy. It was obtained opals with globules 230-270 nm arranged in periodical domains 50-250 μm. Similar features in RS and IR spectra of opal and fused quartz testify about the major amorphous structure of these materials, but there are several distinctions in their spectra:

- quartz IR absorption bands of Si-O-Si stretching vibrations at 1060-1250 cm⁻¹ were red-shifted by 6-10 cm⁻¹ and became twice narrower for opal, which testify about decreasing of phonon location zone in globular opal in comparison with crystalline quartz;
- twice increase of IR intensity for the stretching vibrations at 440 cm⁻¹ for opal;
- IR band at 650-750 cm⁻¹ and RS bands at 650-750 cm⁻¹ and near 997 cm⁻¹ together with shoulder at 304 cm⁻¹ suggest the presence of a small amount of cristobalite and tridymite phases in the major amorphous opal globules. These bands could be assigned to defects in SiO₂, namely Si-H, Si-O [1].

Using of light confinement effects in opal for optical sensing along with plasmonic effects can be perspective. Our first experiments with doping of colloidal gold and biological molecules into opal led to drastic changes in RS and practically did not influence IR spectra [2].

Acknowledgments

This work was supported by Ukrainian-Russian project STCU #5525 and partially by Nanotwinning project FP7-INCO-2011-6 and ERDF Centre of Excellence TK114.

References

1. L. Skuja, J. Non-Cryst. Solids **239**, 16 (1998).
2. V. Boyko, G. Dovbeshko, O. Fesenko, V. Gorelik, V. Moiseenko, V. Romanyuk, T. Shvets, P. Vodolazky, Mol. Cryst. Liq. Cryst **535**, 30 (2011).

***Ab Initio* Calculations for the *H* Centers in SrF₂, as Well as Surface *H* Centers in BaF₂ and *F* Centers Aggregation in BaF₂ and CaF₂**

R.I. Eglitis¹, H. Shi², R. Jia³, L. Yue⁴, X. He³

¹Institute of Solid State Physics, University of Latvia, Latvia

²School of Science, Beijing Institute of Technology, 100081, Beijing, PR China

³Department of Mathematics and Natural Sciences, Bergische Universität Wuppertal, Wuppertal, Germany

⁴Fachbereich Physik, Universität Osnabrück, Osnabrück, Germany

e-mail: reglitis@yahoo.com

The ground state of *H*-center systems for the SrF₂ crystal is simulated with two different arrangements, which are oriented along either [100] or [111] axes [1]. The calculations are performed by using density functional theory (DFT) with hybrid exchange potentials, namely DFT-B3PW. The energy difference between *H* centers with different orientations shows that the *H*-center oriented in the [111] direction in alkaline earth fluorides is the most stable configuration.

Two different configurations of surface *H*-centers are investigated carefully in BaF₂ [2]. Both surface *H*-center systems have strong relaxations because of the surface effect. In the configuration that the interstitial fluorine atom is within the surface, the unpaired electron is almost equally distributed onto the two atoms of the *H*-center, which is quite different from the bulk *H*-center case.

The association energy calculations on *R* centers (a defect composed of three *F* centers) in BaF₂ and CaF₂ [3, 4] indicates stable aggregation of isolated *F* centers. During *F*-center aggregation, a considerable chemical bond covalency between two neighbor fluorine vacancies with trapped electrons forms. Our calculations show that the *F*-center transfer barrier is equal to 1.83 eV in BaF₂, whereas the *F*-center diffusion barrier is equal to 1.67 eV in CaF₂ [3, 4].

References

1. L. Yue, R. Jia, H. Shi, X. He and R. I. Eglitis, J. Phys. Chem. A **114**, 8444 (2010)
2. H. Shi, R. Jia and R. I. Eglitis, Phys. Rev. B **81**, 195101 (2010)
3. H. Shi, R. Jia and R. I. Eglitis, Solid State Ionics **187**, 1 (2011)
4. H. Shi, L. Chang, R. Jia and R. I. Eglitis, J. Phys. Chem. C **116**, 4832 (2012)

Ion Beam Mixing for Gradual SiO_x Interfaces

H.J. Fitting¹, L.F. Kourkoutis², B. Schmidt³

¹University of Rostock, Physics Dept., D-18051 Rostock, Germany

²School of Applied Physics, Cornell University, Ithaca, NY 14853, USA

³Ion Beam Physics, Research Center Dresden-Rossendorf, POB 510119, D- 01314 Dresden, Germany

e-mail: hans-joachim.fitting@uni-rostock.de

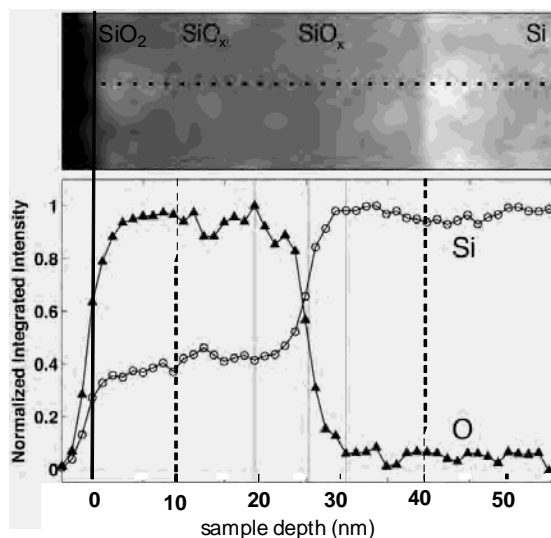
Scanning transmission electron microscopy (STEM) and energy filtered transmission electron microscopy (EFTEM), see [1], in combination with electron energy loss spectroscopy (EELS), and cathodoluminescence (CL) have been used to investigate Si⁺ ion beam mixing and Si nanocluster formation at the interface of amorphous silicon dioxide layers to crystalline Si substrate.

Thin amorphous, thermally grown SiO₂ layers of 28 nm thickness, wet oxidized at 1100 °C on Si substrate, have been doped by Si⁺ ion implantation with an ion energy of 12 keV and a dose of 10¹⁶ ions/cm², leading to a Si⁺ atomic dopant fraction of about 7 at.% at a mean depth of 20 nm in SiO₂, i.e. near the interface.

After this high fluence Si⁺ ion implantation near to the interface an ion-beam mixed SiO_x buffer layer in this region is detected by means of EFTEM and EELS, demonstrated in figure 1.

This structure is due to atomic knock-on and knock-off effects and respective ion beam mixing processes during the Si⁺ ion implantation near and into the SiO₂/Si interface region. Thus the interface layer is smeared out and extended over 20 nm, even 10 nm into the previous Si substrate and consists mainly of an understoichiometric SiO_x matrix $2 < x < 0$ with gradually decreasing of x towards and into the Si substrate.

The respective cathodoluminescence (CL) spectra in the near infrared (NIR) region indicate such structural changes by appearance of an additional side-band shifting with thermal annealing from the red band R towards lower energies, very probably caused by Si nanocluster growth and respective quantum confinement effects as we had seen previously in Refs.[1] and [2].



References

1. H.-J. Fitting, L. Fitting Kourkoutis, Roushdey Salh, M. V. Zamoryanskaya, B. Schmidt, *Physica Status Solidi A* **207** (2010) 117 – 123.
2. Roushdey Salh, A. von Czarnowski, M.V. Zamoryanskaya, E.V. Kolesnikova, H.-J. Fitting, *Physica Status Solidi (a)* **203** (2006) 2049-2057.

Fluorides and Oxyfluorides with Elpasolite-Cryolite Structure: Order-Disorder Phase Transitions and Barocaloric Efficiency

I. Flerov, M. Gorev

Kirensky Institute of Physics, Russian Academy of Sciences, Krasnoyarsk, Russia

Institute of Physical Engineering and Radioelectronics, Siberian State University, Krasnoyarsk, Russia

e-mail: flerov@iph.krasn.ru

Six-coordinated species $[\text{MeO}_x\text{F}_{6-x}]$ ($x = 0, 1, 2, 3$) are the important structural elements which strongly effect on the physical properties behaviour of compounds with the general chemical formulation $\text{A}_2\text{A}'\text{MeO}_x\text{F}_{6-x}$ ($\text{A}, \text{A}' = \text{K}, \text{Rb}, \text{Cs}, \text{NH}_4$; Me : trivalent metals including Ln at $x = 0$ and $\text{W}, \text{Mo}, \text{Ti}, \text{Nb}$ at $x \neq 0$). In spite of the low local symmetry of anionic species at $x \neq 0$, the crystal structure is very often characterized by the elpasolite-like cubic symmetry ($\text{Fm-}3\text{m}, Z = 4$). A lot of compounds above undergo structural phase transitions and show interesting properties such as ferroelectricity and ferroelasticity important from the fundamental and practical points of view [1].

In the present paper we consider the effect of both internal and external pressure on structural stability of initial and distorted phases, and order-disorder as well as displacive processes followed the phase transitions of different physical nature. The models of structural ordering are considered and the role of ions with different shape and size in the mechanism of structural distortions is discussed.

One of the most promising properties of fluorides and oxyfluorides with crystal structure containing octahedral species is connected with the significant barocaloric effects associated with a heat emission or absorption at the change of external hydrostatic pressure. It is shown that both intensive and extensive caloric effects are strongly dependent on the order and entropy of structural transformation and also on the susceptibility of phase transition temperature to pressure. The comparison of some results of barocaloric effect determination with the cooling efficiency of ferroelectrics and ferromagnetics in electric and magnetic fields, respectively, show that some fluorides and oxyfluorides under study can be considered as new highly efficient solid refrigerants.

Acknowledgments

The study was supported by Russian Foundation for Basic Research (N 12-02-00056).

References

1. I. N. Flerov, M. V. Gorev, K. S. Aleksandrov, A. Tressaud, J. Grannec and M. Couzi, Mater. Sci. Eng. **R 24**, 81 (1998).

Hydrogen Sorption Behavior of Nanostructured Mg Alloys with Ni and RE

P.V. Fursikov¹, R.V. Denys^{2,3}, A.A. Poletaev¹, V.A. Yartys³, B.P. Tarasov¹

¹Institute of Problems of Chemical Physics of RAS, Chernogolovka, Russia

²Karpenko Physical-Mechanical Institute of NASU, Lviv, Ukraine

³Institute for Energy Technology, Kjeller, Norway

e-mail: fpv@icp.ac.ru

Our recent studies of hydrogen-accumulating alloys which belong to the RE-Mg-Ni system are reported. The first group comprises Mg-based alloys which are suitable for solid state accumulation of hydrogen gas: a) ECAP-ed alloys of the binary Mg-Ni and ternary Mg-La-Ni (or Mg-Mm-Ni) eutectics [1], b) rapidly solidified (RS-ed) LaMg₁₂ and LaMg₁₁Ni [2].

By varying the ECAP parameters, such as temperature and pressing number one may refine the microstructure and enlarge the area of phase boundaries. An increase in the cooling rate during RS changes the microstructure of the alloys LaMg₁₂ and LaMg₁₁Ni: starting from microcrystalline to nanocrystalline and finally to almost amorphous. It is discussed in details how the microstructure, phase composition, crystal lattice structure, and crystallite sizes of the modified magnesium alloys influence their hydrogen sorption and desorption performances. An improvement to the hydriding kinetics is provided by the modified alloys having submicro- and nanosized crystallites of Mg and by LaH_x (or MmH_x) and Mg₂Ni phases catalyzing the dissociation of H₂ molecules and facilitating the hydrogen diffusion. In particular, appropriately ECAP-ed binary eutectic Mg-Ni and annealed RS-ed LaMg₁₁Ni alloys exhibit the following hydrogen sorption characteristics: at 350°C stages of both sorption and desorption of 5 wt.% of hydrogen last about 3 min.

The second group under study encompasses Mg-containing intermetallics (La,Mg)Ni₃ and (La,Mg)₂Ni₇. The replacement of RE by light metal would increase the hydrogen storage capacity of the corresponding hydrides, which is useful for the development of novel materials for Ni-MH batteries. Recent obtained results are discussed in terms of microstructure and phase composition of the Mg-containing alloys.

Acknowledgments

The authors are grateful for the support from Russian Foundation for Basic Research and the State Fund for Fundamental Researches of Ukraine.

References

1. P.V. Fursikov, D.N. Borisov, B.P. Tarasov, Russ. Chem. Bull., Int. Ed. **60**, No.9, 1816 (2011)
2. A.A. Poletaev, Doctoral Theses at NTNU, Trondheim, **2011:197**, ISBN: **978-82-471-2947-0**, and references therein.

***Ab Initio* Thermodynamic Calculations of Oxygen Vacancies in Perovskites: the Case Study of (La,Sr)(Co,Fe)O_{3-δ} and SrTiO_{3-δ}**

D. Gryaznov^{1,2}, R. Evarestov³, E. Blokhin¹, E. Kotomin^{1,2}, J. Maier¹

¹Max Planck Institute for Solid State Research, Stuttgart, Germany

²Institute of Solid State Physics, University of Latvia, Riga, Latvia

³St. Petersburg State University, Russia

e-mail: d.gryaznov@fkf.mpg.de

The *ab initio* thermodynamic approach to calculate the point defect formation energies as a function of temperature in perovskites is discussed in detail. In order to demonstrate good quantitative agreement with the existing experimental data, two cases were chosen, namely La_{1-x}Sr_xCo_{0.25}Fe_{0.75}O_{3-δ} (LSCF) and SrTiO_{3-δ} (STO).

The content of Sr in LSCF was varied from 12.5% to 50%. The thermodynamic calculations of oxygen vacancy formation energies included the chemical potential of oxygen and phonon frequencies. We show for LSCF that the phonon contribution to the formation energy becomes important not only with the temperature increase but also with the Sr content. Thus, the defect formation energies decrease significantly with the Sr content due to two effects: charge compensation of Sr²⁺ ions and the phonon contribution. The neglect of phonon contribution to the formation energy leads to the errors as high as 0.5 eV in the formation energy of oxygen vacancy.

The formation energy of oxygen vacancy in STO was calculated for the concentrations of oxygen vacancies 6.25% and 12.5% taking into account the phonon contribution. A particularly good agreement with the experiment was obtained for the relatively low concentration of oxygen vacancies 6.25%. The formation energy decreases here considerably (by ~0.8 eV) as temperature increases from 300 K to 1000 K. The phonon contribution to the oxygen vacancy formation energy increases with temperature; being ~5% at 1000 K. We, thus, demonstrated that the method employed in this paper could be used for a wide class of defects in non-metallic solids.

One-dimensional Diffusion in Heterogeneous Medium

J.R. Kalnin¹, E. Kotomin²

¹Ventspils International Radioastronomy Center, Latvia

²Institute of Solid State Physics, University of Latvia, Latvia

e-mail: simts@latnet.lv

A closed formula for the effective diffusion coefficient in the heterogeneous media with the periodically distributed inclusions has been developed. It is shown that previously^{1,2} accepted ad-hoc assumption about concentrations on the boundary matrix-inclusion follows in a self consistent way from the effective medium approximation.

One representative element of one dimensional medium is shown in Fig.1 (A), where l_1, l_2 are mean free paths and D_1, D_2 – diffusion coefficients for matrix and inclusions, respectively. Simple, considerations (replacement (B)) give us for the effective diffusion coefficient

D_{eff} :

$$D_{eff} = \frac{D_1}{\left(1 - f + \frac{2h+b}{b} f\right)^2},$$

(f - inclusion volume fraction) which reduces to

$$D_{eff} = \frac{D_1}{\left(1 - f + \bar{c}_2 / \bar{c}_1 \cdot f\right) \left((1 - f) + D_1 \bar{c}_1 / D_2 \bar{c}_2 \cdot f \right)}$$

with the averaged concentration

ratio $\bar{c}_2 / \bar{c}_1 = 2h/b + 1$. Additional assumptions about equilibrium concentrations are not necessary.

Discussion of diffusion with trapping also included.

References

1. J. R. Kalnin, E. A. Kotomin, and J. Maier. *J. Phys. Chem. Solids.* 63, 449-456 (2002).
2. J. Jamnik, J. R. Kalnin, E. A. Kotomin and J. Maier. *Phys. Chem. Chem. Physics.* 8(11), 1310–1314 (2006).

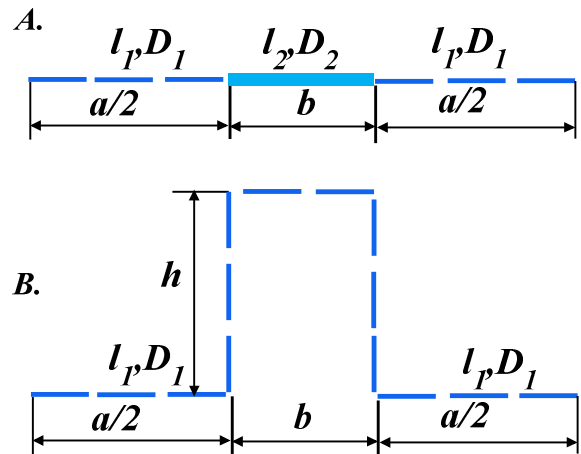


Fig.1 One dimensional heterogeneous medium (A) is replaced by simple model (B).

Recovery of Radiative Transitions of Ce³⁺ Ions in Gadolinium Gallium Garnet Crystal Using High Hydrostatic Pressure

A. Kaminska¹, M. Berkowski¹, P. Sybilski¹, C.G. Ma², M.G. Brik², A. Suchocki^{1,3}

¹Institute of Physics, Polish Academy of Sciences, Al. Lotników 32/46, 02-668 Warsaw, Poland

²Institute of Physics, University of Tartu, Riia 142, Tartu 51014, Estonia

³Institute of Physics, University of Bydgoszcz, Weysenhoffa 11, Bydgoszcz 85-072, Poland

e-mail: kaminska@ifpan.edu.pl

Studies of the spectroscopic properties of Ce³⁺ dopant in bulk gadolinium gallium garnet (GGG) crystal under pressure are presented. In spite of strong inter-shell $4f \rightarrow 5d$ absorption bands at ambient pressure the cerium luminescence in GGG is entirely quenched even at low temperature. It has been shown that applying pressure allows for recovering the $5d \rightarrow 4f$ radiative transitions. Further increase of pressure improves the emission efficiency.

This effect is analyzed in terms of two possible phenomena: (i) by pressure-induced electronic crossover of the excited $5d$ energy level of the Ce³⁺ with the conduction band bottom of host crystal, and (ii) by decrease of electron-lattice coupling with increasing pressure, resulting in reducing of Stokes shift and non-radiative transitions between the low vibrational levels of the $5d$ state and high vibrational levels of the ground $4f$ state.

The results of high-pressure absorption and luminescence measurements point out, that the ambient pressure luminescence quenching is caused by the donor-like charge transfer processes due to the resonant location of the Ce³⁺ $5d$ electronic levels with respect to the host conduction band. In such a situation the ionization of Ce³⁺ to Ce⁴⁺ occurs, accompanied by large lattice relaxation, which enables the non-radiative recombination to the Ce $4f$ state. The pressure induced crossing of the conduction band bottom of host crystal by the excited $5d$ energy level of the Ce³⁺ results in appearing of the $5d \rightarrow 4f$ radiative transitions. Using the configuration coordinate model, quantitative description of the system has been carried out. Additionally, crystal field analysis of the temperature dependence of absorption bands enabled us to determine the strength of tetragonal distortion of cube-like surrounding of cerium dopant and symmetry properties of the Ce $4f$ and $5d$ states split by the crystal field.

Acknowledgements

This work was partly supported by the projects no N N202 203838 of Polish Ministry of Science and Higher Education and by the European Union within European Regional Development Fund, through grant Innovative Economy (POIG.01.01.02-00-108/09). Bilateral project between the Polish and Estonian Academies of Sciences for the years 2010-2012 is also acknowledged.

Micro- and Nanostructured Silica Surfaces as Cell Substrates

T. Kangur¹, P. Reemann², D.T. Bennetsen³, R. Saar¹, V. Kiisk¹, A. Lõhmus¹, M. Järvekülg¹

¹Institute of Physics, University of Tartu, Estonia

²Department of Physiology, University of Tartu, Estonia

³Interdisciplinary Nanoscience Center, Aarhus University, Denmark

e-mail: triin.kangur@ut.ee

Investigation of biomaterials, including materials and technical solutions, is a relatively new and growing field of materials science and nanotechnology. The topography has important role in cell adhesion [1, 2]. It has also been shown that cells are essentially affected not only by the microstructure of the surrounding environment, but also by the nanostructure of the substrate [3, 4]. Additionally, materials electrical and mechanical properties are significant as electrical stimulation has been shown to enhance wound healing [5] and mechanical properties have been shown to affect cell growth [6].

We have studied topographic interactions between different human cell lines and silica structures, which were obtained via sol-gel technology by phase-separation between silicon alkoxide and solvent (Fig 1 and 2). Varying several parameters, micro- and nanostructures with different size, contact angle and density have prepared. Fluorescence and scanning electron microscopy analysis have applied to evaluate cell viability, adhesion, migration and spreading on prepared surfaces.

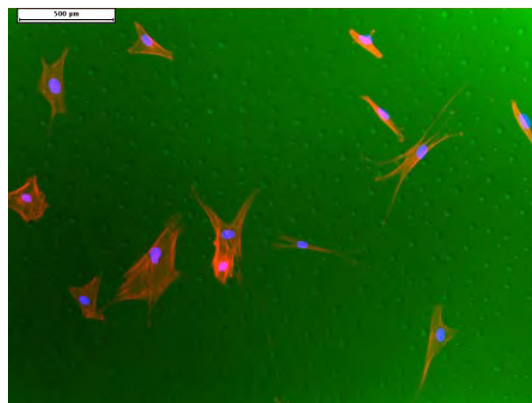


Fig1. Human dental pulp stem cells on microstructured silica substrate.

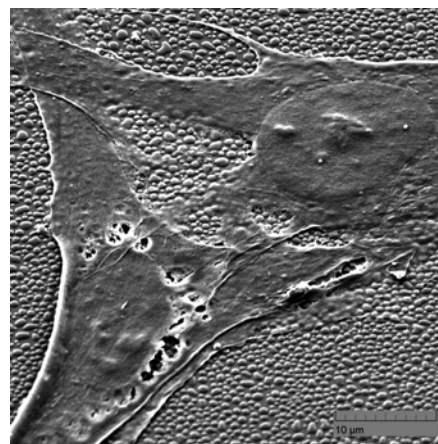


Fig2. Human dermal fibroblasts on microstructured silica substrate.

References

1. A. Curtis, C. Wilkinson, *Biomater* 18 (1997) 1573–1583.
2. M. Tirrel, E. Kokkoli, M. Biesalski, *Surf Sci* 500 (2002) 61–83.
3. Y. Yang and K. W. Leong, *WIREs Nanomed Nanobiotechnol* 2 (2010) 478–495.
4. S. Verma, A. J. Domb and N. Kumar, *Nanomed* 6 (2011) 157–181.
5. A. Sebastian et al., *Wound Rep Reg* 19 (2011) 693–708.
6. L.A. Hidalgo-Bastida et al. *Acta Biomaterialia* 3 (2007) 457–462.

First Principles Calculations of Structural Stability for Complex Perovskites

E.A. Kotomin^{1,2}, Yu. Mastrikov², J. Maier¹, M.M. Kuklja³, A. Weizman⁴, D. Fuks⁴

¹Max Planck Institute for Solid State Research, Heisenbergstr. 1, Stuttgart, Germany

²Institute for Solid State Physics, University of Latvia, Kengaraga str. 8, Riga, Latvia,

³Mater. Sci. and Engineering Department, University of Maryland, College Park, USA

⁴Dept Materials Engineering, Ben Gurion University of the Negev, Beer Sheva, Israel

The flexibility of the perovskite structure provides significant technological advantages for making fuels cell cathodes and permeation membranes. The perovskite ABO_3 lattice allows for a large variety of chemical elements to be used in designing the material and hence crafts a playground for achieving targeted mass and charge transport properties by manipulating chemical compositions. However, understanding the interplay between the chemical composition, structural order/disorder, and crystalline stability in most perovskites is extraordinarily complex and essentially unexplored.

Among novel advanced materials for clean energy, $Ba_xSr_{1-x}Co_{1-y}Fe_yO_{3-\delta}$ (BSCF) are considered as promising materials for cathodes in solid oxide fuel cells (SOFC) and oxygen permeation membranes. BSCF exhibits a good oxygen exchange performance, mixed ionic and electronic conductivity, high oxygen vacancy concentration, and low diffusion activation barrier, which largely define the oxygen reduction kinetics.

We present first principles calculations of an ideal BSCF crystal, the crystal containing basic point defects, and a set of relevant solid-solid solutions. Our DFT modeling of defects (Frenkel, Schottky and cation exchange) and disordering in the BSCF perovskites reveals that the material tends to decompose at low temperatures into a mixture of new perovskite and oxide phases, including grain boundaries and surfaces. This instability is predicted to negate advantages of fast oxygen transport chemistry and impede the applicability of BSCF-based SOFC and ceramic membranes. We discuss possible mechanisms of defect-induced (in)stability in the context of available experiments.

The DFT calculations were used to develop thermodynamics of perovskite solid solutions under realistic operational conditions, and in particular, to draw BSCF phase diagram.

The energy parameters determining the relative stability of different BSCF phases are extracted from DFT calculations. It is demonstrated that these parameters are concentration-dependent which results in asymmetric (with respect to stoichiometric compositions) regions of the homogeneity of phases on T-c phase diagram

References

M.M. Kuklja, Yu.A. Mastrikov, S.N. Rashkeev, E.A. Kotomin. - Electrochem. Soc. Transactions, 2011, **35**, p. 2077-2084.

Ab Initio Modeling of the Benzene Molecule Adsorption on Graphene

V. Krasnenko, J. Kikas, M.G. Brik

Institute of Physics, University of Tartu, Riia 1 142, Tartu 51014, Estonia

e-mail: veera.krasnenko@ut.ee

Recently, enormous research efforts are placed into graphene and its interaction with various chemical substances. Understanding of behavior of graphene under different conditions is of paramount importance for gaining a deeper insight into the physical properties of the carbon nanotubes, graphite and fullerene as other allotropic modifications of carbon.

In the present work we report on our recent results of *ab initio* modeling of the benzene molecule adsorption on a graphene sheet.

Two scenarios can be realized, depending on separation between the graphene layer and benzene molecule. The first situation is characterized by the weak van der Waals interaction between the graphene and benzene at a greater distance of about 0.33 nm. In this case, both graphene and benzene keep their planar structure. Even a finite density of such adsorbates on the graphene (regular placement with a distance of 1.05 nm) does not destroy the metallic nature of the pure graphene.

The second one is characterized by the strong covalent bonding between carbon atoms of both graphene and benzene, which is formed at a short separating distance of 1.56 Å. The geometrical shapes of graphene and benzene demonstrate a strong deviation from planarity (Fig. 1). For a regular placement of benzene molecules on the surface of graphene with the regular spacing of 1.05 nm, the gapless graphene (in the absence of benzene) is transformed into the semiconducting material with the calculated band gap of about 0.8 eV.

Formation of such controlled defects on the top of a single graphene layer can be important for application in 2D electronics and for modification of desirable electronic properties of graphene by properly chosen molecules and/or atoms attached to the graphene sheet.

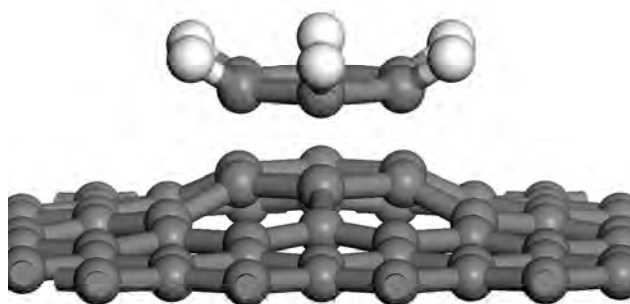


Fig.1 Optimized structure of the benzene/graphene system at the covalent bonding distance of 1.56 Å.

***Ab-Initio* Study of Metal-Zirconia Interfaces**

S. Kulkova^{1,2}, A. Bakulin², S. Hocker³, S. Schmauder³

¹Tomsk State University, Tomsk, Russia

²Institute of Strength Physics and Materials Science SB RAS, Tomsk, Russia

³Institute of Materials Testing, Materials Science and Strength of Materials, University of Stuttgart, Germany

e-mail: kulkova@ispms.tsc.ru

ZrO₂-based ceramics exhibit various interesting properties which can be used in industrial applications. Zirconia is used as refractory material and support material for catalysis, for metal coatings and composite materials, in gas sensors and fuel cells. Alloying of zirconia by MgO, CaO, CeO, Y₂O₃ allows to stabilize cubic (c) and tetragonal (t) ZrO₂ at room temperatures that influence considerably on their functional properties. Oxide doping leads to increase of oxygen vacancies in ZrO₂ and to its high ionic conductivity. Metal-zirconia interfaces are very important for producing of structural composites in which a zirconia matrix is reinforced with metal particles. Since many properties are related to the existence of strong metal-zirconia interfaces, we present a comparative study of differently oriented Me/ZrO₂ interfaces with fcc (Cu, Ni, Fe, Pd, Pt, Rh) and bcc (Mo, Ta, W, Nb, etc.) metals using *ab-initio* methods within density functional theory. Obtained results demonstrate that the high adhesion can be achieved at the O-terminated interface with bcc metals. The high adhesion at the interface is related to an ionic contribution in the chemical bonding. The structural and electronic factors which are responsible for decrease of adhesion at (110) and (111) interfaces are discussed. The influence of CaO, MgO and Y₂O₃ doping on the work of separation at Me(001)/c-ZrO₂(001) is analyzed. It is shown that appearance of oxygen vacancies in the interface layer leads to substantial decrease of the work of separation (W_{sep}) but this effect is less pronounced in the case of substitutional impurities (Ca, Mg, Y). For fully stabilized zirconia the decrease of W_{sep} is connected with decrease of hybridization between Ca(Mg) *s*-states and *Me s,d*-orbitals in comparison with yttria stabilized cubic zirconia (YSZ). In YSZ decrease of W_{sep} is mainly connected with the reduction of a number of *Me-O* bonds due to presence of O vacancies but not with weakening of *Me-O* interaction. The restore of interatomic bonds in the presence of Y in the interfacial layer in YSZ leads to decrease of critical influence of oxygen vacancies on W_{sep} . The estimation of displacement of metals and oxygen atoms near the interface as well as interatomic distances was performed. Finally we discuss a relationship between electronic, geometrical factors and mechanical properties at Zr- and O-interfaces with fully stabilized zirconia.

Microwave and THz Probing of Multi-Walled CNT / Polymer Composites *versus* CNT Oxidation Treatment, Average Outer Diameter and Number of Shells

P. Kuzhir¹, A. Paddubskaya¹, S. Maksimenko¹, J. Macutkevic², G. Valusis², J. Banys³,
V. Kuznetsov⁴

¹Institute of Nuclear Problems of Belarus State University, Bobruiskaia ave. 11, 220030, Minsk, Belarus

²Center for Physical Sciences and Technology, A. Gostauto g. 11, LT-01108, Vilnius, Lithuania

³Vilnius university, Sauletekio al. 9, LT-00122, Lithuania

⁴Boreskov Institute of Catalysis SB RAS, Lavrentiev ave. 5, 630090, Novosibirsk, Russia

Electromagnetic response properties of polymethyl methacrylate (PMMA) filled with small amounts (0.25-2 wt.%) of multi-walled carbon nanotubes (CNT) versus nanotubes diameter, number of walls and oxidation treatment have been studied in wide frequency range (26-37 GHz, 100GHz-4THz). CNT (10-20 μm length) with narrow outer diameter distribution (~ 9 nm and 12-14 nm) and known number of inner shells (estimated as 3-7 for thin CNT and 8-15 for thick ones) were produced via reaction of ethylene decomposition at 650-700 $^{\circ}\text{C}$ in standard CVD setup using Fe-Co catalysts.

It was proved experimentally that CNT oxidation treatment has a significant impact on CNT/PMMA electromagnetic behavior both in the THz and microwave frequency ranges. The constitutive parameters of CNT/PMMA composites in microwave frequencies have been also found to be strongly dependent on CNT mean diameter. In contrast to that, in THz frequency range CNT average diameter has not been denoted as an important factor influencing the EM response of composites for particular CNT geometry. The theoretical background for these experimental observations has been proposed within the nanoelectromagnetics theory [1].

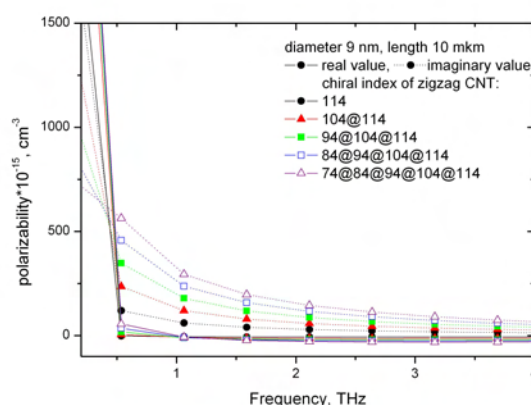


Fig.1 CNT Polarizability in microwave and THz ranges *versus* number of CNT walls.

References

1. G. Ya. Slepyan, S. A. Maksimenko, A. Lakhtakia, O. Yevtushenko, A. V. Gusakov, Phys. Rev. B **60** 17136 (1999)

Magnetic Properties of Carbon Nanoparticles

E. Lähderanta¹, A.V. Lashkul¹, K.G. Lisunov^{1,2}, D.A. Zhrebtsov³, D.M. Galimov³, A.N. Titkov⁴

¹Department of Mathematics and Physics, Lappeenranta University of Technology, PO Box 20, FIN-53851
Lappeenranta, Finland

²Institute of Applied Physics, Academy of Sciences of Moldova, Academiei Str. 5, MD-2028 Kishinev, Moldova

³South Ural State University, 454080 Chelyabinsk, Russia

⁴A.F. Ioffe Physico-Technical Institute, 194021 St. Petersburg, Russia

e-mail: erkki.lahderanta@lut.fi

Unusual magnetic properties, including ferromagnetic behavior even well above the room temperature, attracted recently considerable attention to a broad variety of carbon-based materials [1]. Here we investigate magnetization, M , of powder and glassy samples containing carbon nanoparticles in the interval of temperature $T \sim 3 - 300$ K and magnetic field B up to 5 T. Low-field magnetization exhibits large magnetic irreversibility, which is suppressed above $B \sim 1$ T. The dependence $M(B)$ demonstrates saturation already at room temperature above the field of ~ 2 T. Magnetic hysteresis is observed already at $T = 300$ K, as well. The values of the low-temperature saturation magnetization, $M_s(0) \approx 4.7 - 7.2$ Am²/g, the coercivity field, $B_c(0) \approx 36 - 52$ mT and the maximum blocking temperature $T_b^* \approx 400 - 580$ K are obtained. Analysis of the experimental data gives evidence for concentration of the magnetization close to the surface of the particles, yielding a thickness of the magnetic layer of the particle ~ 1 nm. This is consistent with the origin of magnetism in nanocarbon presumably due to intrinsic surface defects.

References

1. T. Makarova and F. Palacio (editors), *Carbon Based Materials*, North-Holland, Elsevier (2006)

Commercial and Prosthetic PMMA Surface Wettability Regulation

J. Dehtjars¹, A. Grīva¹, L. Lancere¹

¹Institute of Biomedical Engineering and Nanotechnologies, Riga Technical University, Latvia

The subject of current research is modification of surface properties in nano scale with aim to improve poly methyl metha acrylate performance for biomedical applications where interaction between material and surrounding environment is critical, e.g. contact lenses, dental applications, bone cement and many others. Charge on materials surface is strongly related to surface energy which in turn influences surface adhesion property and wettability property. Prosthetic PMMA surface properties including related biocompatibility are affected during time due to mechanical impact – wear between eye lense and eye lid; surrounding factors – wind, sand, sun. Mentioned factors lead to discomfort, inflammations for patients in case of eye lenses; to poor attachment capability in case of dental applications therefore many are trying to improve PMMA material.

It has been found previously that Ultra Violet radiation might be in use to regulate wettability properties of prosthetic PMMA [1]. Namely UV radiation affects surface level influencing surface charge which is strongly related to surface hydrophobicity/ hydrophilicity, werewith – to adhesion and biocompatibility property.

The mentioned irradiation method is new (200-400nm wavelength has been very poorly studied) and relatively to existing methods – a simple method at room conditions, with energy enough to modify properties only at surface level. Therefore in frames of current study commercial PMMA (“Nudec”) was brought under the same UV radiation influence to verify efficiency of the method. Contact angle measurements (sessile drop method) demonstrated very close effect that on prosthetic PMMA occurred (fig.1) – material properties alterate from more hydrophobic to more hydrophilic.

Results show that it might be possible to regulate surface properties also of commercial PMMA that would open new possibilities in both medical and non-medical fields.

References

1. Y. Dekhtyar, L. Lancere. *Surface wettability regulation for prosthetic applications*. 15th International Conference of Biomedical Engineering, 215-218 (2011), ISSN 2029-3380.

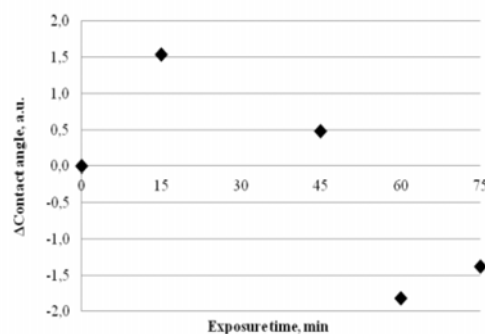


Fig.1 Contact angle increment depending UV radiation exposure time.

Microwave Solvothermal Synthesis of Highly Biocompatible Nano Hydroxyapatite

D. Smolen¹, W. Lojkowski¹, T. Chudoba¹, A. Kędzierska, E. Pietrzykowska, W. Swieszkowski²,
M. Kołodziejczyk³, M. Lewandowska-Szumieł³

¹Polish Academy of Sciences, Institute of High Pressure Physics, Warsaw, Poland

²Warsaw University of Technology, Faculty of Materials Science and Engineering, Warsaw, Poland

³Department of Histology and Embryology, Centre of Biostructure Research, Medical University of Warsaw

The most common approach for regrow of bone in case of large bone gaps is to use autografts and various hydroxyapatite (HAP) containing grafts to fill small fissures. For large bone gaps bone regrowth scaffolds are being developed.

The Institute of High Pressure Physics of the Polish Academy of Sciences (IHPP) developed the technology for synthesis of ndoped nanoparticles with narrow size distribution, using Microwave Solvothermal Synthesis (MSS) technology. The MSS technology permits synthesis of nanoparticles with precise control of the reaction time in the range of 100 seconds. The powders were pressed into dense flat pellets and tested in vitro for their biocompatibility. In collaboration with the Warsaw Medical University it was shown excellent spreading of the osteoblasts on the surface of these pellets, superior than on tests samples from renown HAP suppliers.

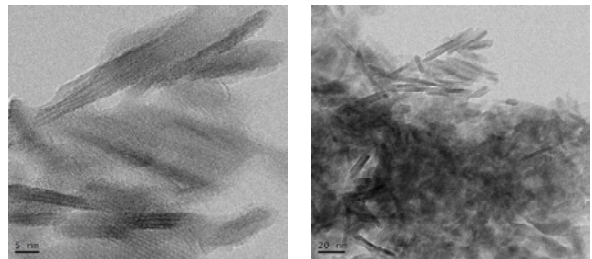


Fig 1: TEM pictures of n-HAP produced at IHPP using the MSS technology

Acknowledgements

The current project was co-supported by the projects: Bioimplant, Sonosca, and Center for Preclinical Research and Technologies.

***Ab Initio* Calculations of Structural, Elastic, Electronic and Thermodynamic Properties for Cubic Perovskites $CsMF_3$ ($M=Ca, Cd, Hg, Pb$)**

C.G. Ma, M.G. Brik

Institute of Physics, University of Tartu, Rii1 142, Tartu 51014, Estonia

e-mail: chonggeng.ma@ut.ee

The cubic perovskite crystals are extensively studied, both theoretically and experimentally, due to their remarkable properties such as ferroelectricity, high-temperature superconductivity, ionic conductivity etc. In the present work we have chosen four representatives from the fluoroperovskites' group, $CsMF_3$ ($M=Ca, Cd, Hg, Pb$). The reason for such a selection was that in spite of a simple structure of these materials, only $CsCdF_3$ has been studied previously [1].

So, we performed the *ab initio* calculations of the structural, electronic, elastic and thermodynamic properties of the selected compounds using the CRYSTAL 09 program [2]. Special attention has been paid to the pressure effects on the structural and electronic properties; in particular, pressure dependences of the band gap, lattice constant and interionic distances were obtained. Elastic anisotropy for all hosts was visualized by drawing three-dimensional dependences of the Young's moduli on the direction in the crystal. Using the calculated values of the elastic stiffness constants, the Debye temperatures and specific heat capacities (Fig. 1) were calculated. All obtained results were systematically analyzed to relate the variation of the calculated properties to the second cation changes ($Ca \rightarrow Cd \rightarrow Hg \rightarrow Pb$). We emphasize that for three perovskites ($CsCaF_3$, $CsHgF_3$, and $CsPbF_3$) the obtained results are reported for the first time, to the best of the authors' knowledge.

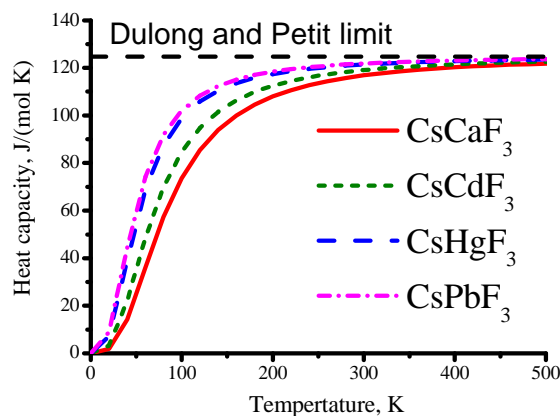


Fig.1 Calculated specific heat capacities for $CsXF_3$ ($X=Ca, Cd, Hg, Pb$) crystals.

References

1. B. Ghebouli, M.A. Ghebouli, M. Fatmi, Eur. Phys. J. Appl. Phys. **53**, 30101 (2011), and ref. therein.
2. R. Dovesi *et al*, CRYSTAL09 User's Manual, University of Torino, 2009

Influence of Deformation of Carbon Nanotube Based Polymer Composites on Their Electromagnetic Properties

S.A. Maksimenko¹, D.S. Bychanok¹, M.V. Shuba¹, A.G. Paddubskaya¹, A.O. Plushch¹,
P.P. Kuzhir¹, M.A. Kanygin², A.V. Okotrub²

¹Research Institute for Nuclear Problems of Belarusian State University, Minsk, Belarus

²Nikolaev Institute of Inorganic Chemistry SB RAS, Novosibirsk, Russian Federation

e-mail: sergey.maksimenko@gmail.com

Experimental measurements and theoretical model of the deformation influence on electromagnetic response of carbon nanotube (CNT) based polymer composites is presented. Anisotropy of dielectric permittivity was observed and theoretically modeled in frequency range 26-37 GHz (Ka-band).

Cylindrical structure of carbon nanotubes (CNT) causes anisotropy of their electromagnetic and mechanical properties. For instance, polarizability of isolated CNT in axial direction is much greater than polarizability in perpendicular to nanotube axis direction. Therefore in the case, when CNT are oriented in composite, it is possible to observe the

anisotropy of electromagnetic properties. Stretching deformation was used for orientation of CNT in polymer matrix (PMMA). In this case electromagnetic response of composite depends on direction of electric-field vector of scattered electromagnetic wave. The change of nanotube orientation during stretch deformation of composite was simulated. The distribution function of carbon nanotubes in deformed composite material was analytically derived (see Fig.) and used for calculation of complex dielectric permittivity tensor of composite material. Obtained theoretical results are in good agreement with experimental measurements of electromagnetic response in microwave frequency range.

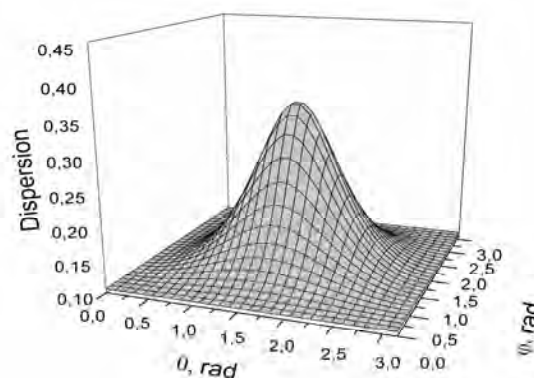


Fig.1 Dispersion function of stretched composite (relative deformation $\chi=1.5$).

Acknowledgements

This research was partially supported by the RFBR Project No. 11-03-90905-mob-sng-st, the BRFR Projects No. F10R-002 and No. F10CO-020, EU FP7 under Project FP7-266529 BY-NanoERA, and ISTC Project No. B-1708.

XPS Analysis of Carbon Nanostructures

M. Mannsberger, T. Nunney

Thermo Fisher Scientific, East Grinstead UK

XPS enables us to do a semi-quantitative analysis of the sp^2/sp^3 hybridization ratios on various carbon nanostructures. This is demonstrated on Reduced Graphene Oxide (RGO), a material which – when doped with TiO_2 – is used for photocatalysis, i. e. for the decomposition of organic compounds. High performance sputter depth profiling in combination with principal component analysis (PCA) allows us to identify two distinct graphene oxide layers.

X-ray photoelectron spectroscopy (XPS, also known as ESCA) is commercially available since about 40 years. However, it is particularly the latest generation of instruments which has developed it into a highly demanded technique. It allows the researcher to identify the local chemical environment of the topmost 5 - 10 nm of material. The key benefit of ESCA (electron spectroscopy for chemical analysis) is the ability to quantify individual chemical states.

First Principles Study of Oxygen Vacancies in Perovskite Solid Solutions

Yu.A. Mastrikov¹, D. Gryaznov^{1,2}, E.A. Kotomin^{1,2}, R. Merkle², M.M. Kuklja³, J. Maier²

¹Institute for Solid State Physics, University of Latvia, Kengaraga str. 8, Riga, Latvia

²Max Planck Institute for Solid State Research, Heisenbergstr.1, Stuttgart, Germany

³Materials Science and Engineering Dept., University of Maryland, College Park, USA

Complex ABO_3 -type perovskite solid solutions with oxygen deficiency exhibit a perceptible ionic conductivity, leading to their use as electrolytes $((La,Sr)(Ga,Mg)O_{3-\delta})$ or materials for oxygen permeation membranes and solid oxide fuel cell cathodes $((La,Sr,Ba)(Mn,Fe,Co)O_{3-\delta})$. The oxygen migration in these materials occurs by the vacancy mechanism with the migration through "critical triangle" of one B site cation and two A cations as the bottleneck [1].

Based on first principles DFT calculations for supercells containing 40 atoms, we analyze the formation and migration of oxygen vacancies in a series of complex $(La,Sr)(Co,Fe)O_{3-\delta}$ (LSCF) perovskites, which are two major factors determining oxygen reduction rate. The atomic relaxation, charge redistribution and energies of the transition states for oxygen ion migration are obtained and compared to those of $(Ba_{1-x}Sr_x)(Co_{1-y}Fe_y)O_{3-\delta}$ (BSCF) perovskites [2] (which exhibit considerably lower migration barriers).

Used in LSCF calculations, oxygen deficiency value $\delta=1/8$ is comparable to the experimental values under SOFC operation conditions. Some compositions (SCF) of the material exhibit even larger deficiencies of $\delta \approx 0.4$ at 800°C in air.

Acknowledgements

This work was partly supported by the EC FP7 NASA-OTM project, GIF research project # 1-1025-5-10/2009 and National Science Foundation

References

1. R.Merkle et al, Solid State Ionics, 188, 1 (2011)
2. R.Merkle et al, J Electrochem.Soc. 159, B 219 (2012).

Caloric Effects and Phase Transitions in Ferroelectric-Ferromagnetic Composites (x)La_{0.7}Pb_{0.3}MnO₃ - (1-x)PbTiO₃

E. Mikhaleva, A. Kartashev, M. Gorev, A. Cherepakhin, K. Sablina, N. Mihashenok, I. Flerov

Kirensky Institute of Physics, Krasnoyarsk 660036, Russia

e-mail: katerina@iph.krasn.ru

Electro- (ECE), magneto- (MCE) and barocaloric (BCE) effects in ferroics attract a great attention thanks to their importance from the fundamental and applied points of view. Of particular interest is the study of different caloric effects in the same material.

In this paper we present the results of ECE, MCE and BCE studies in ferroelectric PbTiO₃, ferromagnetic La_{0.7}Pb_{0.3}MnO₃ and composites (x)La_{0.7}Pb_{0.3}MnO₃ - (1-x)PbTiO₃.

Analyzing in the framework of phenomenological theory of phase transitions the results of heat capacity $C_p(T)$ and thermal dilatation $\beta(T)$ measurements we determined the coefficients in electric equation of state: $E=2A(T-T_C)P+4BP^3+6CP^5$. From the polarization-temperature-electric field surfaces using equation $\Delta T_{AD}^{ECE} = -(T/C_{p,E})(\partial P/\partial T)_{p,E} \Delta E$, the temperature dependence of intensive ECE ΔT_{AD}^{ECE} for PbTiO₃ was evaluated.

Direct measurements of intensive MCE in La_{0.7}Pb_{0.3}MnO₃ performed by adiabatic calorimeter have revealed significant temperature change at $S=\text{const}$ even under low magnetic field due to rather large phase transition entropy $\Delta S \approx 0.5 R$.

Using the data on $C_p(T)$ and $\beta(T)$ and Pippard relation we determined the baric coefficients dT/dp for both ferroics. Assuming a negligible effect of low pressure on lattice entropy S_L the total entropy $S(p,T)$ can be considered as the sum of pressure independent $S_L = \int (C_p/T)dT$ part and anomalous $\Delta S = \int (\Delta C_p/T)dT$ contribution determined at $p = 0$ and shifted along temperature scale in accordance with dT/dp value. The values of intensive BCE was evaluated as the difference $\Delta T_{AD}^{BCE}(S, p) = T(S, p \neq 0) - T(S, p=0)$ at constant entropy.

It was found that the equal effects $|\Delta T_{AD}^{ECE}| = |\Delta T_{AD}^{BCE}| \approx 1.6 K$ in PbTiO₃ can be realized at low values of electric field $E = 1.5 kV/cm$ as well as pressure $p = 0.16 kbar$. To get the same temperature change ΔT_{AD}^{MCE} associated with MCE near ferromagnetic phase transition in La_{0.7}Pb_{0.3}MnO₃ it is necessary to use rather strong magnetic field $\sim 20 kOe$.

The study of composites (x)La_{0.7}Pb_{0.3}MnO₃ - (1-x)PbTiO₃ allowed us to obtain information about the effect of magnetic and electric fields as well as hydrostatic pressure and temperature on the caloric efficiency of different physical nature in the same material.

Crystal Field Analysis of Energy Levels for the Off-center Ni²⁺ Ions in MgO

N. Mironova-Ulmane¹, I. Sildos², M.G. Brik²

¹Institute of Solid State Physics, University of Latvia, Kengaraga street 8, LV-1063, Riga, Latvia

²Institute of Physics, University of Tartu, Riia 142, Tartu 51014, Estonia

e-mail: brik@fi.tartu.ee

The magnesium oxide MgO can be easily doped with the transition metal ions, which occupy the substitutional octahedral Mg sites. Doping with Ni²⁺ ions is of special interest, since no charge compensation is needed and for any concentration of dopant the Mg_{1-x}Ni_xO system forms a continuous series of solid solutions without any composition-induced phase transitions [1]. This circumstance suggests that the Ni²⁺ ions are always six-fold coordinated by the oxygen ions. The difference in the ionic radii of the Mg²⁺ and Ni²⁺ ions may induce appearance of a low-symmetry component of crystal field, which, in its turn, may lead to the splitting of the Ni²⁺ orbital triplets. This idea has been suggested in Ref. [2] (see Fig. 1 for the corresponding absorption spectrum), and in the present work we quantify it by performing consistent crystal field calculations of the Ni²⁺ energy levels in the trigonal crystal field. The exchange charge model of crystal field [3] has been employed in all calculations. We have shown that the off-center displacement of Ni²⁺ by 0.2

Å along the (111) direction in a crystal splits the ³T_{2g} state into two sublevels located at 8008 cm⁻¹ and 8177 cm⁻¹, which agrees very well with the corresponding experimental peaks presented in Fig. 1 (8005 cm⁻¹ and 8182 cm⁻¹, [2]). We also note that this result is very close to the values reported for Ni²⁺ in SrO (0.26 Å, [4]) and for Fe³⁺ in SrO (0.22 Å, [5]).

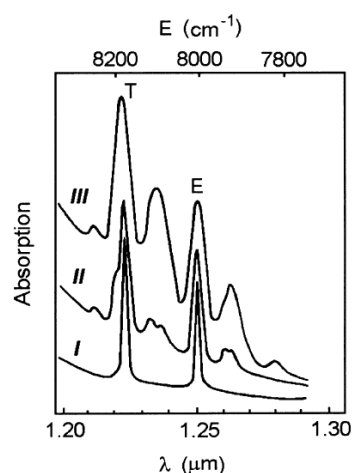


Fig.1. Experimental absorption spectra of Mg_{1-x}Ni_xO system for x=0.01 (I), 0.05 (II), 0.1 (III). The split components of the ³T_{2g} state are denoted by T and E.

Å along the (111) direction in a crystal splits the ³T_{2g} state into two sublevels located at 8008 cm⁻¹

and 8177 cm⁻¹, which agrees very well with the corresponding experimental peaks presented in Fig. 1 (8005 cm⁻¹ and 8182 cm⁻¹, [2]). We also note that this result is very close to the values reported for Ni²⁺ in SrO (0.26 Å, [4]) and for Fe³⁺ in SrO (0.22 Å, [5]).

References

1. N.A. Mironova, U.A. Ulmanis, Radiation Defects and Metal Ions of Iron Group in Oxides, Zinatne, Riga, 1988 (in Russian).
2. N. Mironova, A. Kuzmin, J. Purans, A. Rodionov, SPIE Proc. J. Phys. Chem. Solids **2706**, 168 (1995).
3. B.Z. Malkin, in: A.A.Kaplyanskii, B.M. Macfarlane (Eds.), Spectroscopy of solids containing rare-earth ions, North-Holland, Amsterdam, 1987, p. 33.
4. M. J. L. Sangster, A. M. Stoneham, Phil. Mag. B **43**, 597 (1981).
5. A.F.M.Y. Heider, A. Edgar, J. Phys. C: Solid State Phys. **15**, L41 (1982).

Stability of mesoporous silicas under acidic conditions

S.E. Mourabit¹, M. Guillot¹, F. Goettmann², A. Grandjean¹

¹Marcoule Institute for Separative Chemistry (ICSM), Bagnols-sur-Cèze, France

²CEA/DEN/DTCD/LCFI

e-mail: sabah.el-mourabit@cea.fr

Ordered mesoporous silicas, which are already widely found in applications such as catalysis, sensing, drug delivery and optics, are also promising materials for applications in the field of ion separation, be it for environmental remediation or metallurgical purposes. Up to now, numerous (hybrid) mesoporous solids have been investigated as solid ligands especially for extracting heavy metal cations from waste fluxes [1].

The application of these mesoporous solids for the above mentioned purposes are heavily relying on the chemical and mechanical stability of these matrices in, usually, acidic to strongly acidic media. Consequently, it is necessary to carry out stability studies of these materials under the conditions in which they are going to be employed.

To the best of our knowledge such stability data were not yet recorded. We thus investigated the behaviour of different mesoporous silicas under strongly acidic conditions. In particular, we intended to establish the incidence of various synthesis parameters, such as the nature of the surfactant, the pH of the synthesis or the presence of catalysts, on the chemical stability of our matrices.

These materials were characterized by N₂ adsorption-desorption, by X-ray scattering (SAXS) and by NMR ²⁹Si solid state. Our results evidence that all types of mesoporous silicas are altered very rapidly (within 24h) under such acidic conditions, but also that silicas synthesized under acidic conditions and featuring interconnected porosity were the most stable (losing no more than 20% of the specific surface area within 24 hours).

References

1. Liu et al. Chem. Commun., 1145-1146 (2000)

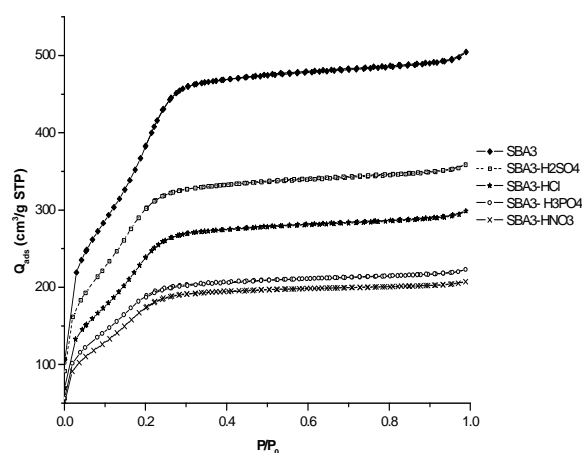


Fig.1 N₂ adsorption-desorption isotherms of SBA-3 silica contacting with different acids.

The Luminescence of Pr³⁺-Doped LiBaAlF₆ Crystals

S.I. Omelkov^{1,2}, V. Nagirnyi¹, V.A. Pustovarov², M. Kirm¹, L.I. Isaenko³, S.I. Lobanov³

¹Institute of Physics, University of Tartu, Estonia

²Ural Federal University, Russia

³Institute of Geology and Mineralogy SB RAS, Russia

e-mail: omelkovs@gmail.com

In recent years, great attention has been paid to the investigation of photon cascade emission (PCE) in different luminophores. PCE is a subsequent emission of two and more photons under UV or VUV excitation. This mechanism is promising for enhancing the efficiency of mercury-free luminescent lamps, solar cells and for other applications [1]. Pr³⁺ ion is one of the most studied cascade photon emitters, because of its suitable energy level scheme and intraconfigurational 4f transitions in the visible spectral region. The main criterion for the observation of the PCE in Pr³⁺ activated compounds is given by the following relation: the higher excited ¹S₀ level of the 4f-configuration should lie at lower energies than the 5d levels [2]. The position of the latter is heavily affected by the strength of crystal field. Therefore, the search of new efficient PCE-active materials should begin with the spectroscopic investigation of novel hosts. The promising hosts for Pr³⁺, enabling PCE process, include binary and ternary fluorides with low-symmetry and weak crystal field at the activator positions, such as LiBaAlF₆ [3].

In the present work, the PCE of Pr³⁺ ions and host-related luminescent phenomena in LiBaAlF₆:Pr³⁺ are studied. The lowest 4f¹5d¹ state of isolated Pr³⁺ ions is located approximately 0.13 eV higher than the (4f²)¹S₀ state, providing a possibility for emitting two photons in two stages of Pr³⁺ relaxation. At least part of the Pr³⁺ ions is accompanied by the defects, responsible for excess charge compensation of dopant ions. A broad emission band peaking at 3 eV and two fast emission decay components ($\tau_1=2.0$ ns, $\tau_2=8.5$ ns) can be ascribed to the transitions occurring in the defect centers. Energy transfer from the defects to the ³P₀ state of the Pr³⁺ ions is also observed. A configuration diagram of the complex luminescence center explaining consistently the observed experimental facts will be discussed.

References

1. Q. Zhang and X. Huang, Progress in Materials Science **55**, 353 (2010)
2. P. Rodnyi, A. Mishin and A. Potapov, Optics and Spectroscopy **93**, 714 (2002)
3. S. I. Omelkov, M. Kirm, E. Feldbach, V.A. Pustovarov, S. O. Cholakh and L. I. Isaenko, J. Phys.: Condensed Matter **22**, 295504 (2010)

Synthesis and Characterization of Magnetic Nanodiamond Films

A.C. Peterlevitz¹, H.G. Zanin¹, R.F. Teófilo², H.J. Ceragioli¹, V. Baranauskas¹

¹Faculdade de Engenharia Elétrica e de Computação, Departamento de Semicondutores, Instrumentos e Fotônica –
Universidade Estadual de Campinas, Brazil

²Departamento de Química – Universidade Federal de Viçosa, Brazil
e-mail: alfredo@dsif.fee.unicamp.br

Magnetic semiconductors are promising materials for electronic applications. While traditional (non-magnetic) electronic devices operation is based on the control of charge carriers in n-type or p-type semiconductor, in magnetic semiconductors it is also possible to control the quantum state of the electron spin (up or down), providing almost total spin polarization.

We present nanocrystalline diamond boron doped samples with magnetic properties prepared by Chemical Vapor Deposition (CVD) process. Ferromagnetic elements were incorporated into the diamond films by diffusion from stainless steel substrates, during film growth. The CVD process allows the incorporation of magnetic particles concomitantly to boron incorporation, forming p-type magnetic semiconductor materials. We believe that this process, compared with ion beam implantation, produces better samples since there is no need of annealing to reconstruct the damaged path caused by implantation.

The material characterization was performed by Energy Dispersive X-ray Spectroscopy (EDS), Raman Spectroscopy, Scanning Electron Microscopy (SEM), X-ray Photoelectron Spectroscopy (XPS) and Superconducting Quantum Interference Device (SQUID).

PbS Nanodots in ZrO₂ Thin-film Matrix as a Possible Material for Microdosimetry of Ionizing Radiation

Y. Dekhtyar¹, A. Katashev¹, R. Reisfeld², M. Romanova¹, T. Saraidarov², K. Stalidzane¹

¹Institute of Biological Engineering and Nanotechnology, Riga Technical University, Latvia

²Hebrew University of Jerusalem, Israel

e-mail: marina.romanova@inbox.lv

Lead sulfide (PbS) nanodots embedded in a thin layer of zirconia (ZrO₂) (ZrO₂:PbS thin films) can be a promising material for radiation dosimetry purposes [1]. Application of the ZrO₂:PbS thin films for microdosimetry of ionizing electron radiation was studied in this research. Spatial resolution of the radiation dosimeter is important in microdosimetry. This means it is important to define the smallest sensitive area of the dosimeter that can respond to radiation. To estimate the detection resolution of the ZrO₂:PbS films, the samples were irradiated with 6 MeV electron beam using medical linear accelerator. One half of each sample was covered with radiation attenuating material (2.3 mm thick aluminium plate). This resulted in scattering of the electrons on the border between the irradiated and covered parts of the samples. It was hypothesized that electron scattering distance limited the resolution of the potential dosimeter. Electron scattering distance was estimated by scanning surface electrical potential of the films in the direction from the covered to the irradiated part perpendicularly to the border line. Measurements were done using Kelvin mode of atomic force microscopy. The film surface right and left to the border line had an increased value of the electrical potential in comparison with the other parts of the films.

It was found that the electron scattering distance depended on the concentration of the PbS nanodots in the ZrO₂ matrix. The estimated electron scattering distance was: in the ZrO₂:20%PbS films ~ 1.5 mm; in the ZrO₂:10%PbS films ~ 0.6 mm; in the ZrO₂ matrix ~ 0.4 mm. It was supposed that increase in the concentration of the PbS nanodots might have resulted in possible deterioration of the ZrO₂:PbS dosimeter spatial resolution. Perhaps this was due to the electron scattering on PbS nanodots.

References

1. Yu. Dekhtyar, M. Romanova, A. Anischenko, A. Sudnikovich, N. Polyaka, R. Reisfeld, T. Saraidarov, B. Polyakov, 15th NBC on Biomedical Engineering & Medical Physics, IFMBE Proceedings **34**, 133 (2011)

Thermal Behaviour and Hydration Dynamics of Layered Double Hydroxide Zn-Al Pyrovanadate

A.N. Salak¹, J. Tedim¹, A.I. Kuznetsova¹, J.L. Ribeiro², L.G. Vieira², M.L. Zheludkevich¹,
M.G.S. Ferreira¹

¹Department of Ceramics and Glass Engineering/CICECO, University of Aveiro, Portugal

²Physics Centre, University of Minho, Braga, Portugal

e-mail: salak@ua.pt

Polycrystalline Zn-Al layered double hydroxide (LDH) intercalated with pyrovanadate ($V_2O_7^{4-}$) anion is promising as a (nano) container-inhibitor system in self-healing coatings for corrosion protection of aluminium alloys. Because of the extremely complex chemistry of vanadium anions in aqueous solution, variety of polytypes and their dependence on pH and other factors, preparation of this LDH is not straightforward. The best crystallized Zn(2)Al-pyrovanadate (Zn/Al=2:1) is prepared by anion exchange from the parent composition Zn(2)Al-nitrate at pH~8. It was found, however, that even for the properly prepared LDH-pyrovanadate, some variations in drying/storage conditions can result in noticeable change of its crystal structure.

TG, in situ XRD and IR spectroscopy methods were used in order to investigate the thermal behaviour of Zn(2)Al- V_2O_7 in comparison with relative LDH compositions. In Zn(2)Al-pyrovanadate, the calcination was found to lead to an irreversible decomposition of the LDH phase. Only samples that were heat-treated up to temperatures not exceeded 100⁰C were able to retrieve the initial crystal structure and crystallinity on rehydration. The pyrovanadate polytype of the intercalated anion was found to remain stable until the collapse of the layered structure, which were observed at about 300⁰C. Two structural modifications of the LDH corresponding to different arrangements of the pyrovanadate anions were observed, depending on the relative content of the crystal water in interlayer. The observed dehydration path of Zn(2)Al- V_2O_7 differs from those observed in Zn-Al LDHs intercalated with either different vanadate polytypes or volatile species (nitrate, carbonate etc.).

Luminescent Protection Against Defect Creation in $\text{Lu}_3\text{Al}_5\text{O}_{12}:\text{Ce}$

A. Shugai¹, A. Lushchik¹, M. Nikl², F. Savikhin¹, K. Schwartz³, E. Vasil'chenko¹

¹Institute of Physics, University of Tartu, Estonia

²Institute of Physics AS CR, Prague, Czech Republic

³Gesellschaft für Schwerionenforschung (GSI), Darmstadt, German

e-mail: annasu@ut.ee

The resistance of various metals, semiconductors, dielectrics and superconductors against irradiation with X- and γ -rays, fast electrons, neutrons, protons, light and heavy swift ions is one of the "hottest" problems of modern technology and energetics. It is generally recognized that Frenkel defects (FD) in solids can be formed due to the universal impact (knock-out) mechanism connected with elastic collisions of high-energy incident particles with the atoms/ions of a crystal causing the creation of separated vacancies (v) and interstitials (i). This rapid creation mechanism of $v-i$ pairs is especially essential for metals as well as for dielectrics, where the formation energy of a pair of FD exceeds the energy gap, $E_{\text{FD}} > E_{\text{g}}$. In metal halides with $E_{\text{FD}} < E_{\text{g}}$, FD can be efficiently formed at the recombination of relaxed conduction electrons (e) and valence holes (h) or at the decay of excitons (the so-called nonimpact mechanisms). In the present study, the nonimpact processes of defect creation are investigated on the example of $\text{Lu}_3\text{Al}_5\text{O}_{12}$ single crystals (LuAG, 160 atoms per unit cell). The possibility to suppress these processes by doping LuAG with Ce^{3+} ions, which are able to transform partly the energy of hot $e-h$ pairs into impurity luminescence or phonon package are analysed as well. LuAG samples have been irradiated with fast electrons (Institute of Physics) or 2.2-GeV ^{238}U and ^{198}Au ions (GSI, Darmstadt; ion range is $\sim 46 \mu\text{m}$). At fluences of 10^{11} – 10^{12} ions/ cm^2 , the average distance between ion cylindrical tracks varies from 30 to 10 nm. More than 99% of $\sim\text{GeV}$ -ion energy is spent to the formation of electronic excitations. The applied methods of VUV (6–35 eV) and thermoactivation (5–800 K) spectroscopy allowed to estimate the contribution of excitons, cold and hot $e-h$ pairs to the creation of FD.

References

1. M. Nikl, E. Mihokova, J. Pejchal, et al., IEEE trans. Nucl. Sci. **55**, 1035 (2008)

Electromagnetic Properties in CNT and Graphene Based Nanostructures

Y. Shunin^{1,2}, Yu. Zhukovskii¹, V. Gopeyenko², N. Burlutskaya², S. Bellucci³

¹Institute of Solid State Physics, University of Latvia, Latvia

²Information Systems Management Institute, Latvia

³INFN-Laboratori Nazionali Di Frascati, Frascati, Italy

e-mail: shunin@isma.lv

CNT and graphene nanostructures constitute the basis of effective high-speed nanoelectronics and nanosensors. Special attention has been paid to fundamental properties of various CNT-Me, GNR-Me and CNT-graphene interconnects. The cluster approach based on the multiple scattering theory formalism as well as effective medium approximation (EMA-CPA) can be efficiently used for nano-sized systems modeling. This allows calculating the dispersion law $E(\mathbf{k})$, the electronic density of states, the conductivity, *etc.* The multiple scattering problems are stated for radial (*e.g.*, quantum dots) and axial (*e.g.*, nanowires, nanotubes) symmetry approaches [1].

Technological interest to contacts of CNTs or (GNRs) with other conducting elements in a nanocircuit has been the major reason for making calculations of C-Me *interconnect resistances* taking into account the influence of chirality effects in interconnects of single-wall (SW) and multi-wall (MW) CNTs, single-layer (SL) and multi-layer (ML) GNRs with the fitting metals (Me = Ni, Cu, Ag, Pd, Pt, Au) for the predefined carbon system geometry [1, 2].

Wide-scale simulation results on *interconnect electromagnetic properties* (interconnect resistances, interconnect frequency (GHz, THz) and temperature properties) have been presented. Parametric calculations of CNT conductivities for various chiralities have been carried out. The model of CNT growth with the predefined chiralities in a magnetically managed CVD process with the use of magnetically anisotropic $\text{Fe}_x\text{Pt}_{1-x}$ nanoparticles with various substitutional disorders has been developed. A special attention is paid to the unique property of interconnects such as the presence of *dangling atomic bonds* that make interconnects chemically, electrically and magnetically sensitive. This property allows considering interconnects as perspective nanosensor structures.

References

1. Yu.N.Shunin, Yu.F.Zhukovskii, N.Burlutskaya, S. Bellucci, Central Eur. J. Phys **9** (2), 519 (2011).
2. Yu. N. Shunin, Yu. F. Zhukovskii, V. I. Gopejenko, N. Burlutskaya, S. Bellucci, Nanosci. Nanotechnol. Lett. **3** (6), 1 (2011).

Converse Magnetoelectric Effect in CoFe₂O₄/BaTiO₃ Core-Shell Composites

V.V. Shvartsman, M. Etier, D.C. Lupascu

Institut für Materialwissenschaft, Universität Duisburg-Essen, Universitätsstr. 15, 45141, Essen, Germany

e-mail: vladimir.shvartsman@uni-due.de

The magnetoelectric (ME) effect, which enables to control the magnetic state by applying an electric field and vice versa, opens attractive possibilities to invent novel types of sensors, actuators, and memory devices.¹ The largest effect was observed in so-called composite multiferroics: compounds consisted of separate electric and magnetostrictive phases. In these materials the ME coupling is artificially engineered between the polarization and magnetization of two phases via a mechanical strain arising at the phase interfaces under an external electric or magnetic field. The magnitude of the ME effect depends not only on the properties of the constituents, but also on the type of connectivity. In particular, an enhanced ME coupling is expected in composites with a core-shell structure having relatively large, well-defined interface areas.

We report on ME characterization of cobalt ferrite/barium titanate core-shell ceramic composites prepared by covering cobalt ferrite nanoparticles by a barium titanate layer using a sol-gel route. Scanning probe microscopy studies confirm formation of the core-shell structures with a magnetic core and a piezoelectric shell. The converse ME effect, $M(E)$, was measured using a modified SQUID ac susceptometer. The ME coefficient reaches 22 ps/m surpassing values reported previously for similar structures. A change of the sign of the ME coefficient was observed at the increasing magnetic bias field.² This effect is related to the non-monotonic field dependence of magnetostriction in polycrystalline CoFe₂O₄.

References

1. C. A. F. Vaz, J. Hoffman, C. H. Ahn, and R. Ramesh, *Adv. Mater.* **22**, 2900 (2010).
2. V. V. Shvartsman, F. Alawneh, P. Borisov, D. Kozodaev, and D. C. Lupascu, *Smart Mater. Struct.* **20**, 075006 (2011).

Production of Metal Oxide Nanopowders Using Pulsed Electron Beam in Low Pressure Gas

S.Yu. Sokovnin^{1, 2}, V.G. Il'ves¹

¹Institute of Electrophysics, Ural Branch RAS, 106 Amundsen St., Yekaterinburg, Russia; 620216

²Ural Federal University named after First President of Russia B.N. Yeltsin, 19, ul. Mira, Yekaterinburg,

e-mail: sokovnin@iep.uran.ru

The installation for production of metal oxide nanopowders was created. The method involves evaporation of the target by a pulsed electron beam, condensation of the vapors of the material in low-pressure gas, and deposition of nanopowders on a cold large area crystallizer [1]. In new installation, a higher power electron gun with hollow cathode, which ensures the formation of the current pulse of the electron beam with an amplitude up to 1A and duration of 100 μ s, and crystallizer of larger diameter (0.3 m) and length (0.5 m), which makes it possible to decrease the agglomeration of nanoparticles, were used.

The results of the evaporation of YSZ, CeGdOx, Al₂O₃ and ZnO targets were presented.

Room-temperature ferromagnetism has been observed in YSZ [2], Zn-ZnO and Cu,Al-doped Al₂O₃. The proposed method makes it possible to obtain nanopowders of oxides with a characteristic particle size of 3–5 nm and agglomerates consisting of them 20–600 nm in size, specific surfaces of up to 338 m²/g, productivity of up to 12 g/h, and a specific power consumption ≥ 112 (W h)/g.

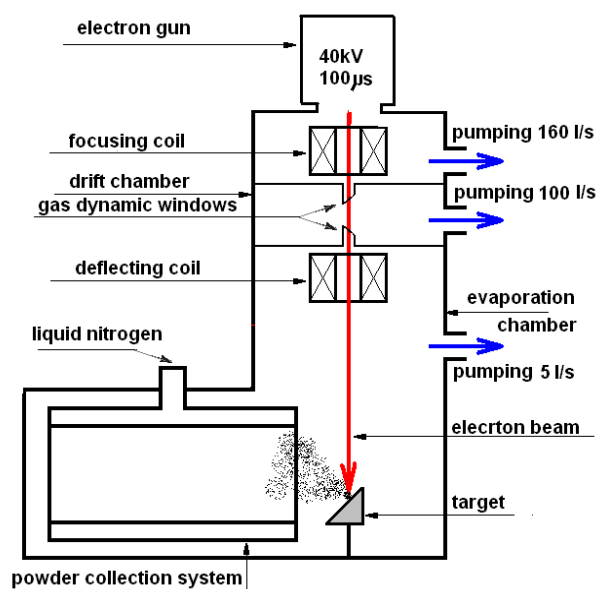


Fig. 1 Installation diagram of the «Nanobeam-2»

References

1. V.G. Il'ves, Yu.A. Kotov, S.Yu. Sokovnin, C.K. Rhee, Russian nanotechnologies. **2**, 96 (2007).
2. S.Yu. Sokovnin, V.G. Il'ves, Technical Physics Letters. **35**, 1026 (2009).

Modern Raman Techniques– Probing the Nanoworld

A. Sozańska¹

¹Renishaw Sp. z o.o., ul Szyszkowa 34, 02-285 Warszawa

e-mail: agnieszka.sozanska@renishaw.com

Confocal micro-Raman spectroscopy is a powerful tool for chemical characterization of nanomaterials like carbon nanotubes, graphene flakes, thin layers, semiconductors and composite materials. The unique confocal and spatial resolution of micro-Raman systems enables optical far field resolution to be pushed to its limits with often sub-micron (to 100nm) resolution achievable for chemical imaging of small structures.

When micro-Raman is combined with Scanning Electron Microscope (SEM), chemical information from Raman spectra is supplemented with structural characterization obtained from SEM.

The combination of SEM and Raman provides high spatial resolution, large depth of field and good contrast, whilst Raman, photoluminescence (PL) and cathodoluminescence (CL) allows determine chemical, physical, electronic and structural information from the sample.

We present the results of SEM-SCA analysis on single nanotubes (Fig.1.), and ultra high resolution imaging at nm scale of SWNT samples, graphene and defects investigation in semiconductors. The ability to create chemical and compositional images by acquiring Raman spectra from an

array of positions and then processing them to reveal the parameters of interest is a powerful technique. Raman signal from graphene is proportional to layer thickness. Using Streamline Plus technique for Raman analysis we can identify graphene thicknesses including mono- and bi-layer regions (Fig 2.) and other nanomaterials.

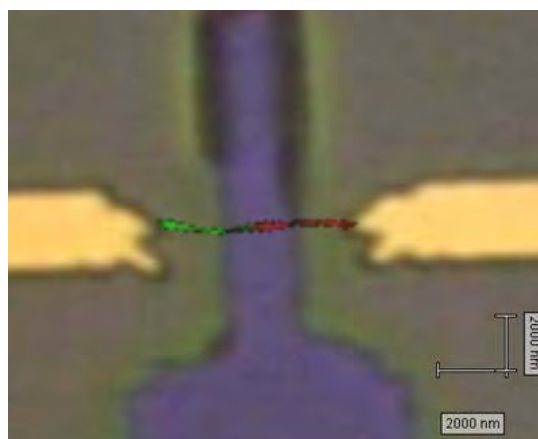


Fig.1. Zoomed view of SWNT Raman image overlaid on white light image. Green part of image shows where G band is strongest, and red part where RBM band is strongest (265.2 cm⁻¹)

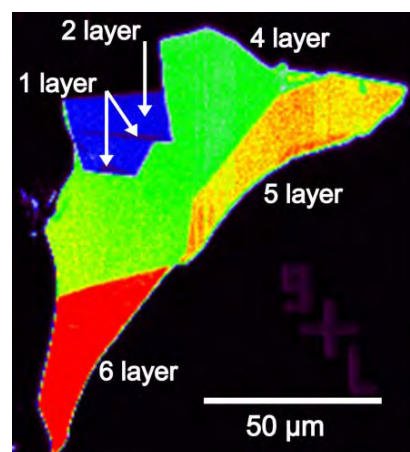


Fig. 2. Analysis of a multilayered graphene flakes

Hydrogen Influence on ITO Layer Sputtering on Polymeric Film Using HIPIMS

I. Strazdina¹, J. Kazuss¹, E. Macevskis², V. Kozlovs²

¹Institute of Mechanical Engineering, Riga Technical University, Latvia

²SIDRABE Inc., Latvia

e-mail: inguna.strazdina@rtu.lv

Indium Tin oxide is the most widely used material for transparent conductive oxide coatings [1]. However, concern about increasing price and depleting resources leads to two alternative directions: to find alternative materials to substitute the ITO; or to look for technological development how to deposit the ITO coating more effective [1]. The focus of this research is on the second one, where ITO sputtering process is analyzed using HIPIMS power supply and adding Hydrogen gas during the deposition.

ITO was deposited using magnetron sputtering roll-to-roll laboratory coater. The substrate width was 80 cm and it was treated by glow discharge before the deposition. During the deposition different oxygen gas flow amount with and without the Hydrogen was studied. The best result were achieved using Hydrogen gas

(5sccm) during the deposition process when sheet resistance $44\Omega/\square$ was reached with the thickness of 142nm and transmittance 83% in visible range. The influence of Oxygen flow on resistivity and transmission with and without Hydrogen gas supply during the deposition process is presented in Figure 1 and discussed more detailed in the paper.

The advantages and drawbacks of HIPIMS power supply as a tool for improved ITO coating are analyzed.

References

1. M.Fahland, T.Vogt and A.Schoenberger, 53rd Annual Technical Conference Proceeding of the Society of Vacuum Coaters, 531 (2010)

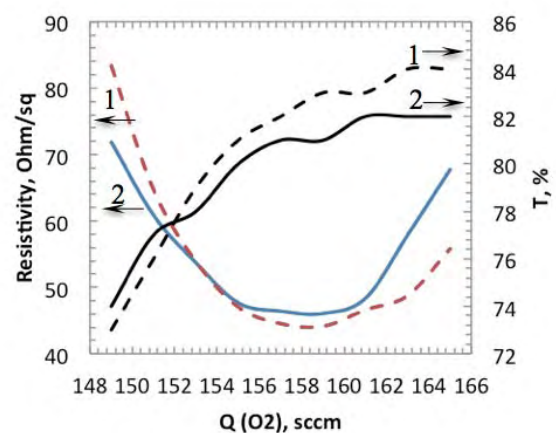


Fig.1 Resistivity and transmission dependence on amount of oxygen flow during deposition. Sample 1 with the H₂ supply, sample 2 without.

The High-Pressure Studies of Structural and Optical Properties of ZnO Bulk and Nano-Crystals

A. Duzynska¹, R. Hrubia², V. Drozd², H. Teisseyre^{1,3}, W. Paszkowicz¹, A. Reszka¹,
A. Kaminska¹, S. Saxena², J.D. Fidelus^{1,3}, J. Grabis⁴, C.J Monty⁵, A. Suchocki^{1,6}

¹Institute of Physics, Polish Academy of Sciences, Lotników 32/46, 02-668 Warsaw, Poland

²CeSMEC, Florida International University, University Park, Miami, FL 33199, USA

³Institute of High Pressure Physics, Polish Academy of Science, Sokolowska 29/37, 01-142 Warsaw, Poland

⁴Institute of Inorganic Chemistry, Riga Technical University, 34 Miera, LV-2169 Salaspils, Latvia

⁵CNRS Laboratoire Procédés, Matériaux et Énergie Solaire (PROMES), Odeillo, 66120 Font-Romeu, France

⁶Institute of Physics, Kazimierz Wielki University, Plac Weysenhoffa 11, 85 - 072 Bydgoszcz, Poland

e-mail: suchy@ifpan.edu.pl

Nowadays zinc oxide (ZnO) is promising wide-band-gap semiconductor for optoelectronic applications, especially in the blue and ultraviolet spectral ranges. An important factor affecting mechanical, electric and optical properties of ZnO are methods/conditions of growth as well as its crystal form.

In this project we have studied pressure dependence of the near band gap photoluminescence (using the diamond anvil cell technique) of various samples:

- **bulk ZnO crystal grown by vapor-phase deposition during industrial process of production of zinc white,**
- **two samples of hexagonal ZnO nano-powders (size of crystallite: 1 μm and 65 nm) grown by plasma technique.**

We also investigated the stability and the volume behaviour under hydrostatic pressure by X-ray powder-diffraction of bulk crystal using synchrotron radiation. The values the bulk moduli (B_0), and their pressure derivative (B_0'), before and after phase transition from wurtzite (B_4) to rock salt (B_1) structure were obtained from these measurements for very good quality ZnO crystals. We found that for wurtzite structure B_0 is equal to (156 ± 13) GPa and for rock salt phase $B_0 = (180 \pm 18)$ GPa. In zinc oxide the B_4 - B_1 transition has been earlier reported at ~ 10 GPa. The change of nanoscale grain size has a strong influence on the characteristic of phase transition. However, we did not find any signs of existence of a tetragonal (iT) or a hexagonal intermediate phases (iH) at the B_4/B_1 transition, predicted theoretically in earlier publications. The experimental data of pressure dependence of the energy gap E_g ($\approx E_{PL}$), has been studied in our samples. The band gap pressure coefficients for bulk crystal, films grown on sapphire are about 20 meV/GPa, but for nano-powders are lower, equal to about 15 meV/GPa. This effect will be discussed.

The photoluminescence is quenched at about 10 GPa for ZnO bulk materials as results of transition from direct to indirect gap in the rock salt structure. Nonetheless for smaller size nano-powder the photoluminescence vanishes at 20 GPa. ***The origin of this phenomenon will be analysed in this work.***

Acknowledgements

This work was partly supported by the European Union within European Regional Development Fund, through the Innovative Economy grant POIG.01.01.02-00-108/2009/4) and by the project "Nanomaterials for renewable energy applications" (RENANOS, 2010) within the framework of the EU-DG RTD's "Solar Facilities for the European Research Area (SFERA)".

Lattice Dynamics and Structural Disorder in Rhenium Trioxide: Reverse Monte Carlo Study

J. Timoshenko¹, A. Kuzmin¹, J. Purans¹

¹Institute of Solid State Physics, University of Latvia, Latvia

e-mail: janis.timoshenko@gmail.com

Reverse Monte Carlo (RMC) method is a simulation technique, which allows one to determine a 3D model of the material atomic structure by minimizing the difference between its structure related experimental and calculated properties. Mostly it is used to analyze diffraction data, but in our recent paper [1] we have demonstrated that it can be also applied to the analysis of the extended fine structure of X-ray absorption spectra (**EXAFS**) of crystalline materials.

We present the application of the method to study EXAFS signals from Re L_3 -edge in **perovskite-type oxide ReO_3** . The study of the structure and lattice dynamics of ReO_3 using conventional EXAFS analysis is a challenging task due to strong influence of the so-called multiple scattering (MS) contributions. In this work we show that the RMC method can successfully be used to treat the MS contributions. Moreover, the presence of the MS effects allows us to obtain the information not only about interatomic distances, but also about bond angles, anisotropy of atomic oscillations and even bond strength (Fig. 1).

In this work we present the RMC analysis of thermal disorder effect on the temperature-dependent Re L_3 -edge EXAFS data [2] in ReO_3 as well as of the hydrogen intercalation effect [3] on the local structure in H_xReO_3 .

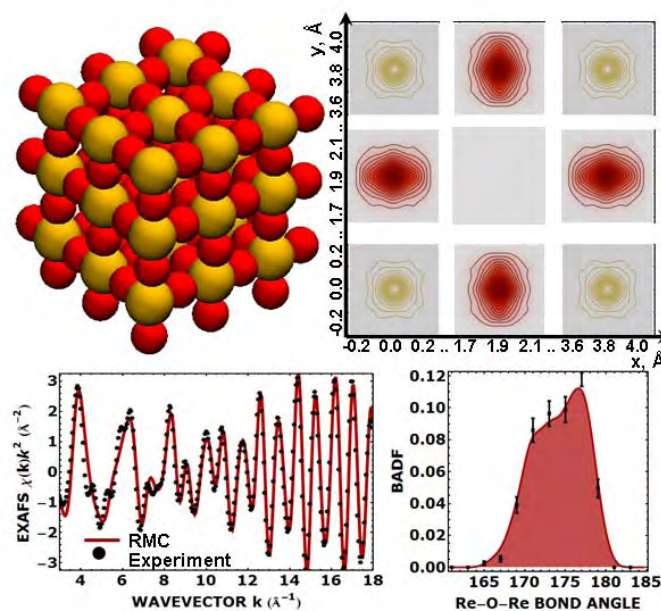


Fig.1 RMC modeling for ReO_3 ($T = 100$ K): the atomic configuration, obtained in the simulations (*top left panel*); experimental and simulated Re L_3 -edge EXAFS spectra (*bottom left panel*), thermal ellipsoids for Re and O (*top right panel*) and the obtained distribution of the Re-O-Re bond angle (*bottom right panel*).

References

1. J. Timoshenko, A. Kuzmin, J. Purans, *Comp. Phys. Commun.* **183**, 1237 (2012).
2. J. Purans, G. Dalba, P. Fornasini, A. Kuzmin, S. De Panfilis, F. Rocca, *AIP Conf. Proc.* **882**, 422 (2007).
3. M. Castriota et al., *Mol. Cryst. Liq. Cryst.* **474**, 1 (2007).

First Principles Molecular Dynamics Studies of Proton Transport Mechanisms in Phosphorus Oxoacids

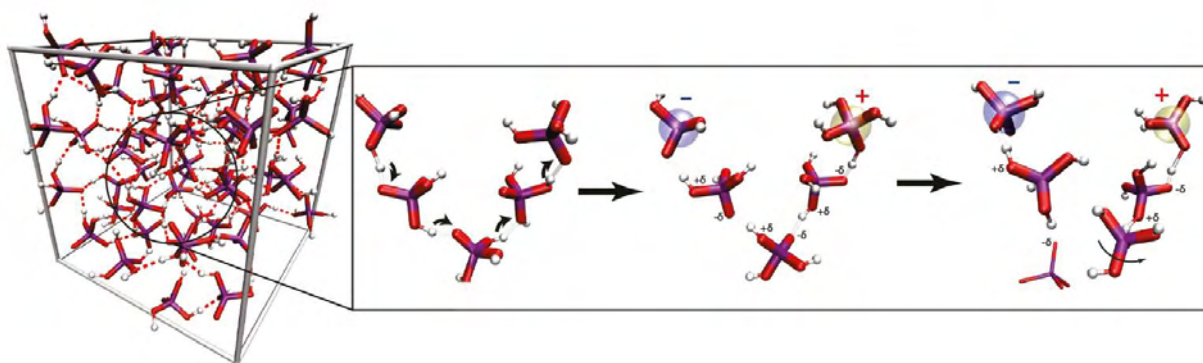
L. Vilčiauskas¹, M.E. Tuckerman², G. Bester¹, K.D. Kreuer¹

¹Max-Planck-Institut für Festkörperforschung, Heisenbergstr. 1, D-70569 Stuttgart, Germany

²Dept. of Chemistry and Courant Institute of Mathematical Sciences, New York University, NY 10003, USA

e-mail: l.vilciauskas@fkf.mpg.de

Pure molten phosphoric acid (H_3PO_4) has the highest intrinsic proton conductivity of any known substance.[1] Our results from *ab initio* molecular dynamics simulations, for the first time, reveal the microscopic mechanism of this phenomenon. [2] We observe that strong, polarizable H-bonds are involved in coupled proton motion and a pronounced protic dielectric response of the H_3PO_4 medium. This leads to the formation of *extended*, polarized H-bonded (Grotthuss) chains, and it is the interplay between these chains and a frustrated H-bond network that is found to lead to extremely high proton conductivity in phosphoric acid. [2] This mechanism stands in stark contrast to water, which cannot form *extended*, polarized chains and has negligible intrinsic proton conductivity. Aqueous media transport excess charge defects at anomalously high rates, however this primarily occurs not through *extended* chains but rather through *local* H-bond rearrangements that drive individual proton transfer reactions. [3]



References

1. T. Dippel, K. D. Kreuer, J. C. Lassegues, D. Rodriguez, Solid State Ionics **61**, 41 (1993).
2. L. Vilčiauskas, M. E. Tuckerman, G. Bester, S. J. Paddison, K. D. Kreuer, Nature Chemistry (in press).
3. M. E. Tuckerman, D. Marx, M. L. Klein, M. Parrinello, Science **275**, 817 (1997).

First Principles Calculations on Properties of the Rutile-Based TiO₂ Nanowires with Ti-atom Centered Symmetry Axes

R.A. Evarestov¹, Yu.F. Zhukovskii²

¹Department of Quantum Chemistry, St. Petersburg State University, Petrodvorets, Russia

²Institute of Solid State Physics, University of Latvia, Riga, Latvia

e-mail: quantzh@latnet.lv

Due to a variety of promising applications, single-crystalline titania nanowires (TiO₂ NWs) attract enhanced attention in modern nanotechnology [1]. Rutile-based TiO₂ NWs are modeled as monophasic (1D) structures cut from 3D crystal along [001] and [110] crystallographic axes (Fig. 1). These nanowires in the case of Ti-atom centered symmetry axes can be described using the same rod group $Pmmm$ (D_{2h} point symmetry).

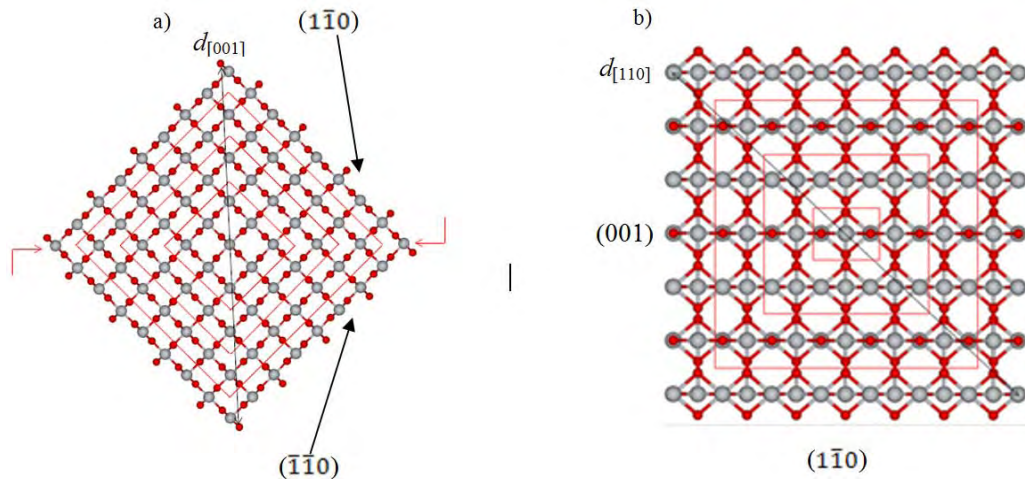


Fig. 1. Cross sectional images of rutile-based TiO₂ [001]-oriented NW (a) and [110]-oriented NW (b) containing 81 vs. 105 formula units *per* large NW unit cells, respectively. Quasi-square rectangles show borders for prism models of middle, small and smallest TiO₂ NWs (containing 49 vs. 55, 25 vs. 21 and 9 vs. 3 formula units *per* unit cells, respectively). Figure indicates indices of lateral facets and diameters (d) of both NW types.

We have performed systematic large-scale calculations on structural and electronic properties of both types of nanowires using DFT-LCAO-PBE method as implemented in *CRYSTAL-09* code [2]. We have found that nanowire with [001] orientation and lateral {110} facets is energetically more favorable than that with [110] orientation containing {001} facets.

Acknowledgement

All the calculations have been performed using facilities of Computer Center at St. Petersburg State University.

References

1. B. Liu, J.E. Boercker and E.S. Aydil, *Nanotechnology*, 2008, 19, 505604.
2. R. Dovesi, V.R. Saunders, C. Roetti, R. Orlando, C.M. Zicovich-Wilson, F. Pascale, B. Civalleri, K. Doll, N.M. Harrison, I.J. Bush, Ph. D'Arco, *et al.*, *CRYSTAL-2009 User's Manual* (University of Torino, 2009).

Microscopic Approach to the Kinetics of Pattern Formation of Charged Molecules on Surfaces

G. Zvejnieks¹, V.N. Kuzovkov¹, E.A. Kotomin¹, M.O. de la Cruz²

¹Institute of Solid State Physics, University of Latvia, Latvia

²Department of Materials Science and Engineering, Northwestern University, Evanston, USA

e-mail: guntars@latnet.lv

A microscopic formalism based on computing many-particle densities is applied to the pattern formation analysis in the diffusion-controlled kinetics of oppositely charged molecules (i) on surfaces or (ii) adsorbed at interfaces with competing long-range Coulomb and short-range Lennard-Jones interactions. Particular attention is paid to the proper molecular treatment of energetic interactions that drive pattern formation in inhomogeneous systems. The reverse Monte Carlo method is used to visualize the spatial molecular distribution based on the calculated radial distribution functions (joint correlation functions). We show the formation of charge domains for certain combinations of temperature and dynamical interaction parameters. The charge segregation evolves into quasicrystalline charge clusters, due to the competing long- and short-range interactions. The clusters initially co-exist with a gas phase of charges that eventually attach to the clusters, thus generating "fingers" or lines of charges of the same sign, Fig.1. This differs from the nanopatterns expected in molecular dynamic simulations in systems with competing (such as strain or dipolar versus van der Waals) interactions in two dimensions.

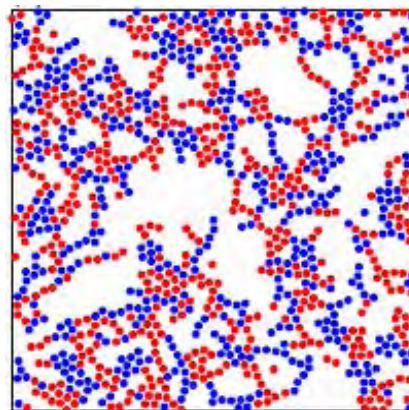


Fig.1 Calculated "finger"-like structures (Reverse Monte Carlo snapshot) formed by oppositely charged particles A (red) and B (blue).

References

1. V.N. Kuzovkov, E.A. Kotomin, G. Zvejnieks, M. Olvera de la Cruz, Phys. Rev. E **82**, 021602 (2010)

**Abstracts of the invited presentations in the sessions devoted
to Inta Muzikante**

In Search for Efficient Blue-Light Emitters

S. Jursenas¹, S. Krotkus¹, K. Kazlauskas¹, A. Miasojedovas¹, A. Gruodis², A. Tomkeviciene³,
J.V. Grazulevicius³

¹Institute of Applied Research, Vilnius University, Vilnius, Lithuania

²Department of General Physics and Spectroscopy, Vilnius University, Vilnius, Lithuania

³Department of Organic Technology, Kaunas University of Technology, Kaunas, Lithuania

e-mail: saulius.jursenas@ff.vu.lt

Stability of phosphorescent blue emitters is a major challenge for both organic light-emitting diode (OLED) display and OLED-based general lighting technologies. An alternative to phosphorescence emitters is fluorescent blue emitting compounds that can provide high emission efficiency, longer lifetime and pure blue color.

In the present work a series of pyrene-functionalized soluble 9-alkyl-carbazole and 9-alkyl-fluorene compounds have been designed, synthesized and investigated. Aiming for high efficiency emitting compounds, 2,- and 2,7- positions of the carbazole and fluorene moieties were utilized, which, particularly in the case of the pyrenyl di-substituted compounds, resulted in an elongated molecular shape favorable for controlling molecule orientation in layers, and consequently, for enhancing their emission efficiency. Introduction of the different alkyl chains, ethylhexyl and dioxyl, into carbazole and fluorene moieties, respectively, permitted to investigate their effect on the glass-forming and emission properties of the wet-casted films.

To reveal the emission properties of the compounds they were thoroughly studied by measuring fluorescence spectra, fluorescence quantum yields, fluorescence decay times in dilute solutions, polymer (polystyrene) matrixes at different chromophore concentrations and wet-casted neat films. The photophysical properties of the compounds were also assessed by density functional theory. Theoretical analysis of electronic transitions was addressed by emphasizing intramolecular twisting. The advantages of the emission properties of the pyrenyl di-substituted fluorene and carbazole compounds against mono-substituted compounds were rationalized in terms of differently twisted conformers. Intermolecular coupling peculiarities were disclosed by thorough investigations of emission concentration quenching of the compounds in a solid state. The possibility of using the mono- and di-substituted compounds as efficient blue emitters as well as optical gain media for lasing applications was explored.

Reduced Langevin Recombination in Organic Solar Cells

G. Juška

Department of Solid State Electronics, Vilnius University, Lithuania

e-mail: gytis.juska@ff.vu.lt

In the organic solar cells due to low charge carriers mobilities a bimolecular Langevin recombination is usually observed, which causes reduction of the energy conversion efficiency. Recently, the reduced Langevin recombination was observed in the high efficiency solar cells [1].

In this work we will discuss different models of the Langevin recombination's reduction: the influence of the random potential [2], the intrinsic electric field [3], the influence of the mobility of the slower charge carriers in the bulk heterostructures [4] and the morphology of the structure [5]. For the determination of the origin of the reduction we used three methods: the extraction of the photogenerated charge carriers by the linearly increasing voltage (photo-CELIV), the double injection current transients (DoI) and time of flight (TOF).

The experimental results of the reduced Langevin recombination in the regioregular poly(3-hexylthiophene) with [6,6]-phenyl-C61-butyric acid methyl ester (RRP3HT/PCBM) organic solar cells proof that this reduction is caused by two-dimensional Langevin recombination when the lamellar structure is formed [5]. In this case the relaxation of the density of the photogenerated charge carriers follows $n \sim t^{-2/3}$ and the bimolecular recombination coefficient depends on the density of the charge carriers $\beta \sim n^{1/2}$. The spacing between the lamellas evaluated from the experimental results is close to one determined from the X-ray studies.

References

1. A. Pivrikas, G. Juška, A.J. Mozer, M. Scharber, K. Arlauskas, N.S. Sariciftci, H. Stubb, R. Österbacka, Phys. Rev. Lett. 94,176806 (2005).
2. G. J. Adriaenssens and V. I. Arkhipov, Solid State Commun. 103, 541(1997).
3. C.Deibel, A.Wagenpfahl, V.Dyakonov. Phys.Rev. B 80, 075203 (2009).
4. L. J. A. Koster, V. D. Mihaletchi, P. W. M. Blom, Appl. Phys. Lett. 88, 052104 (2006).
5. G. Juška, K. Genevičius, G. Sliaužys, N. Nekrašas, phys.stat.sol. C7, 980-983 (2010).

Plasmonic Organic Electronic Devices

F. Liu¹, J.M. Nunzi^{1,2}

¹Department of Chemistry, Queen's University, Kingston, ON

²Department of Physics, Queen's University, Kingston, ON

e-mail: nunzijm@queensu.ca

Surface plasmons are known as collective oscillations of the conduction electrons at a metallic interface. The phenomenon has been extensively studied in the fields of surface enhanced Raman spectroscopy, metal enhanced fluorescence, and non-linear optics.¹⁻² However, only limited research has been dedicated to its application in organic light emitting diode (OLED). Here we have fabricated a plasmonic OLED by incorporating silica coated silver nanoparticles (NPs) into the emitting layer of a phosphorescent organic light emitting diode (PHOLED), as shown in the schematic diagram Fig. 1. As a result, the luminescence efficiency of the PHOLED is significantly improved under low charge carrier injection level due to surface plasmon enhanced exciton formation probability. In contrast, the incorporation of uncoated bare silver NPs greatly suppresses luminescence of the PHOLED due to metal NPs induced luminescence quenching. A silica shell

with thickness 13 nm or above coated on Ag NPs surface can avoid the luminescence quenching of the emitting molecules caused by Ag NPs.

So far metal nanoparticles (NPs) have been used in thin film silicon solar cell research successfully as the substitute of traditional inverted pyramid surface texture for light trapping. However, the application of metal NPs in organic solar cell research is not as successful as that in silicon solar cell. Although many works have been dedicated to organic solar cells incorporating NPs, none explicitly isolates the optical function of NP from its electronic function in organic solar cells due to the multiple roles played.

We designed a polymer solar cell with configuration shown in Fig. 2 from which we can investigate solely the optical functions of metal NPs in the solar cell. The incorporation of NPs underneath the active layer results in degraded performance due to massive light loss caused by Ag NPs scattering and absorption. In contrast, the incorporation of Ag NPs above active layers can harvest more sun light due to the fact that the surface plasmon of Ag NPs enhances the extinction coefficient of the active polymer layer and the back-scattering from Ag NPs improves the optical absorption path length in the active layer, thus solar cell power conversion efficiency (PCE) is improved. However, a direct contact of Ag NPs with active polymer results in exciton quenching, which compromises its enhancement effect on PCE. The best position to incorporate Ag NPs into the solar cell appears to be above the active layer, with a spacer layer, which is PEDOT in our prototype device.

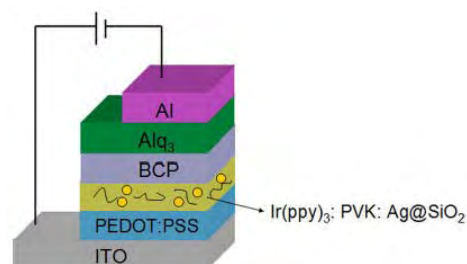


Fig. 1. Configuration of PHOLED doped with silica coated Ag NPs

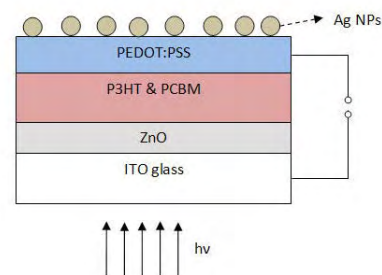


Fig. 2. Schematic diagram of inverted plasmonic solar cell.

References

1. F. Liu, G. Aldea, and J. M. Nunzi, *J. Lumin.* 130, 56 (2010).
2. J. M. Nunzi and D. Ricard, *Appl. Phys. B* 35, 209 (1984).

Coherent Dynamics and Dissipative Relaxation of Excitations in Molecular Aggregates

L. Valkunas

Department of Theoretical Physics, Faculty of Physics, Vilnius University, Sauletekio av. 9, build. 3, Vilnius LT-10222
Lithuania

Institute of Physics, Center for Physical Sciences and Technology, A. Gostauto 9, Vilnius LT-01108 Lithuania

To efficiently harvest solar light, photosynthetic organisms are equipped with pigment-protein antenna complexes. These complexes are responsible for the absorption of light energy, which is subsequently transferred to the reaction center (RC), where this energy is stabilized as a chemical potential. As a result of the structural arrangement and spectral composition of the pigment molecules, at low excitation intensities the efficiency of this process is close to unity. In addition to the light-harvesting function, the light-harvesting complexes have also another – regulation function, which is a physiologically significant strategy evolved by plants [1]. Rapid excitation density control in photosystem II (PSII), termed as non-photochemical quenching (NPQ), ensures high efficiency and robustness of plant photosynthesis under fluctuating light, even at very high intensities. For a reasonable effect to be achieved, the mechanism responsible for NPQ should be competitive with the excitation trapping by an open RC [2]. The NPQ phenomenon is usually attributed to some activated quenching species which allow the excitation to undergo a rapid non-radiative decay. The exact location of these quenching species within the antenna and its precise nature are a matter of on-going debate, with both chlorophylls (Chl) and carotenoids (Car) being put forward as essential components of the quenching mechanism, while the regulation function is usually attributed to the external conditions. For this purpose the exciton dynamics in a molecular heterodimer is studied as a function of differences in excitation and reorganization energies, asymmetry in transition dipole moments and excited state lifetimes. It is demonstrated that the system-bath interaction rather than the excitonic effect determines the excitation quenching ability of such a dimer. The dynamics are simulated using nonperturbative density matrix theory, which allows us to describe the spectral and temporal signatures of various system-bath coupling regimes [3]. Electronic excitations in molecular aggregates embedded in protein environment experience a complex multistep relaxation, which could be traced using various time-resolved spectroscopy techniques. To understand the regulation abilities a diffusion-controlled model describing the fluorescence blinking of single photosynthetic light-harvesting complexes (LHCII) is developed and discussed [4].

References

1. A. V. Ruban, M. P. Johnson, C. D. P. Duffy, *Biochim. Biophys. Acta* 1817: 167-181 (2012).
2. L. Valkunas, G. Trinkunas, J. Chmeliov, A. V. Ruban, *Phys. Chem. Chem. Phys.* 11:7576-7584 (2009).
3. A. Gelzinis, D. Abramavicius, L. Valkunas, *Phys. Rev. B* 84: 245430 (2011).
4. T. P. J. Krüger, C. Ilioaia, L. Valkunas, R. van Grondelle, *J. Phys. Chem. B* 115: 5083-5095 (2011).

**Abstracts of the oral presentations in the sessions devoted to
Inta Muzikante**

Excited State Dynamics of PPI Dendrimers Functionalized with 4-(4'-ethoxybenzoyloxy)salicylaldehyde Chromophores

M. Franckevičius¹, R. Vaišnoras², M. Marcos³, J.L. Serrano³, V. Gulbinas¹

¹Center for Physical Sciences and Technology, Savanorių Ave 231, LT-02300 Vilnius, Lithuania

²Liquid Crystals Laboratory, Lithuanian Educological University, Studentų st. 39, LT-08106, Vilnius, Lithuania

³Facultad de Ciencias de Materiales de Aragon, Universidad de Zaragoza, Pedro Cerbuna 12, E-50009, Zaragoza, Spain.

In this study we present ultrafast dynamics investigations of different generations (G1 and G5) poly(propylene-imine) (PPI) dendrimers functionalized with 4-(4'-ethoxybenzoyloxy)salicylaldehyde (SA) chromophore moieties (PPI-SA). Structures of the first and fifth generations PPI dendrimers containing SA type terminal groups are shown in Figure 1. Reaction of a primary amine-terminated dendrimers with aldehyde (composite part of 4-(4'-ethoxybenzoyloxy)salicylaldehyde (SA)) yields imine functional group – responsible for the keto-enol tautomerization reaction. Keto-enol tautomerism of the salicylideneimine functional group may take place due to the intramolecular proton shifts between the phenol–oxygen and the imine–nitrogen via intramolecular hydrogen bonds O–H...N or O...H–N determining their excited state dynamic properties.

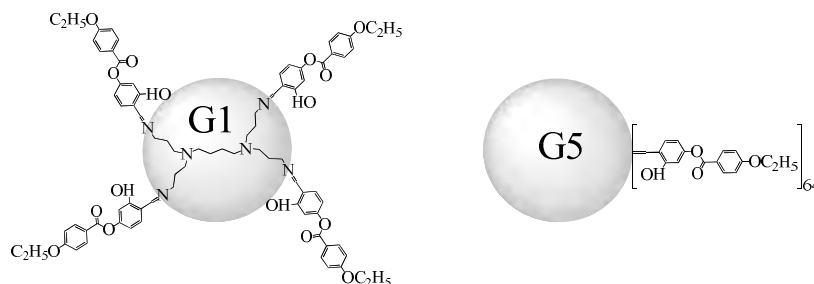


Fig. 1. Structures of the first and fifth generations PPI dendrimers functionalized with 4-(4'-ethoxybenzoyloxy) salicylaldehyde terminal groups.

Based on the analysis of the

absorption spectra and quantum chemistry calculation results, we attribute different absorption bands to the enol closed *trans*-keto and *cis*-keto tautomers and to $n\pi^*$ transitions of keto tautomers, which gain intensity under their geometrical distortion. Relative concentration of keto tautomers in solutions increases with the dendrimer generation. We attribute this dependence to the interaction between dendrimer chains, in particular to formation of interchromophore hydrogen bonds stabilizing the *trans*-keto form.

Transient absorption investigations revealed different relaxation dynamics of different tautomeric forms. Excited *cis*-keto tautomers decay to the weakly fluorescent excited state during about 10 ps and form conformationally distorted photoproduct states absorbing in the blue spectral region. Excited enol-closed tautomers relax to photoproduct states on a subpicosecond time scale, however they form different photoproducts than excited *cis*-keto tautomers. Only a small fraction of terminating groups forms fluorescent states, which are identical for all tautomeric forms, however formation yields are different.

Acknowledgements

This research was funded by the European Social Fund under the Global Grant measure.

Influence of Specific and Non-Specific Solvent Effects on Frontal MO of DMABI System

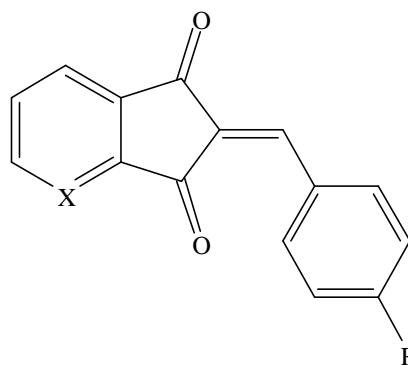
V. Kampars, P.J. Pastors, G. Ornicane

Institute of Applied Chemistry, Riga Technical University, Latvia

e-mail: valdis.kampars@rtu.lv

Carbonyl group containing molecules are popular nonlinear optical chromophores and components of electro-optical devices, but derivatives of 2-(4'-dimethylaminobenzylidene)-1,3-indandione (DMABI) within this field are traditional objects of investigation. Electro-optical device is build up from thin films, containing active chromophore. Medium (polymer or molecular glass) alter the electronic energy levels of the individual, isolated chromophore molecule. The effect of the medium depends on the strength of local electric fields inside the electro-optic material and the effect of specific interaction with medium and is analogue of liquid solvation effect. It is known that the solvents with different polarity and weak H-bond interaction can change the energies of frontal MO of DMABI within 1300 cm^{-1} what is more than one order below the influence of substituents with strong electron donating or withdrawing effect on the frontal MO energies. In order to obtain information about more powerful medium influence on the frontal MO energies of DMABI system in this work we have studied the electronic spectra of derivatives of 2-benzylidene-1,3-indandiones (I) and 4-aza-2-benzylidene-1,3-indandiones (II) in an ethanol/hydrochloric acid media.

Strong acidic medium alter the electronic energy levels of 1,3-indandione dyes and cause a remarkable bathochromic shift of the long wave absorption band. The bathochromic shift as result of strong H-bond formation with carbonyl groups is about 800-900, as a result of protonation of 4-N atom 2200-2600 and as a result of protonation of carbonyl groups about 6500 cm^{-1} .



- I X=CH; R= CH₃ (Ia); OCH₃ (Ib); N(CH₃)₂ (Ic)
II X=N; R= CH₃ (IIa); OCH₃ (IIb); N(CH₃)₂ (IIc)

Holographic Studies of Photoinduced Anisotropy in Molecular Glassy Films Containing Diphenylamine Based Azochromophores

A. Ozols, V. Kokars, P. Augustovs, K. Traskovskis, D. Saharov

Faculty of Material Science and Applied Chemistry, Riga Technical University, Latvia

e-mail: aozols@latnet.lv

Photoinduced anisotropy (PA) is experimentally studied in three molecular glassy films synthesized in our Faculty and containing diphenylamine based azochromophores {4-((4-nitrophenyl)diazenyl)-N-(4-((4-nitrophenyl)diazenyl)phenyl)-N-(2-trityloxy)ethyl) benzeneamine (shortly K-D-24), 4-((2-chloro-4-tritylphenyl)diazenyl)-N-(4-((2-chloro-4-tritylphenyl)diazenyl)phenyl)-N-(2-(trityloxy)ethyl)benzenamine (shortly K-D-25) , 4,4'-(2-(trityloxy)ethylazanediy)bis(4,1-phenylene)bis(diazene-2,1-diyl)dibenzonitrile (shortly K-D-32) } and, for comparison, in an a-As₂S₃ film. Holographic method enabling simultaneous measurements of *s*- and *p*-polarized diffracted light powers proposed in Ref.[1] was applied in both transmission and reflection modes. Holographic grating recording with the period of 2 μm was made by two equally strong 532 nm *p*- polarized laser beams with total light intensity of 0.81 W/cm². The readout was made by 633 nm circularly polarized beam, and the *s*- and *p*-polarized components of diffracted light were separated by Glan-Thompson prism.

PA was characterized by diffraction efficiency difference (DED), $\eta_s - \eta_p$, and by anisotropy contrast $A = (\eta_s - \eta_p)/(\eta_s + \eta_p)$. Corrections of the results were made taking into account the inherent anisotropy of HG and the anisotropy of Fresnel reflection losses [2]. DED exhibited markedly different kinetic behavior in transmission and reflection modes. There was a deep negative minimum in transmission mode in all samples, and a growth with oscillations up to saturation in reflection mode. Small initial DED maxima were specific to a-As₂S₃ film. The highest PA was found in K-D-24 film in transmission mode ($A=-0.23$) and in K-D-25 film ($A=0.49$).The photoinduced refractive index difference, $|n_s - n_p|$ absolute values of the studied samples were estimated to vary in the 0-0.24 range. The obtained results can be explained in terms of *trans-cis* photoisomerisation (K-D films) and photooriented bond switching (a-As₂S₃) accompanied by other processes.

References

1. A.Ogiwara, H.Kakiuchida, M.Tazawa, and H.Ono, Jap.J.Appl.Phys. **11**, 7341 (2007).
2. A.Ozols and M.Reinfelde, Proc.SPIE **5123**, 133 (2003).

Assessment of Quantum Chemical and Experimental Methods for Ionization Energy and Electron Affinity Evaluation of Organic Thin Films

I. Muzikante¹, M. Rutkis¹, V. Kampars², P.J. Pastors², B. Turovska³, A. Jurģis¹, J. Sīpols¹,
R. Gržibovskis¹

¹Institute of Solid State Physics, University of Latvia, Latvia

²Institute of Applied Chemistry, Riga Technical University, Latvia

³Latvian Institute of Organic Synthesis, Latvia

e-mail: martins.rutkis@cfi.lu.lv

Organic molecular thin films have attracted remarkable attention due to their great potential for different practical applications, such as organic light emitting devices (OLED), organic solar cells, organic thin film transistors, sensors and optoelectronic devices. Performance of organic films employed in devices is defined by energy levels. Depending of them films can work as a transporters or barriers of electrons, holes and excitons. Energy level engineering quite often is done on basis of quantum chemical (QC) HOMO and LUMO eigenvalues *in vacuo*. This approach could lead to significant ambiguities and errors due to fact that molecular orbitals are an abstraction from molecular orbital theories and environment surrounding is not taken into account. Therefore direct calculation scheme of solid state ionization energy (IE) and electron affinity (EA) should be developed. One of possibilities is based on single point energy calculation of neutral molecule and corresponding charged ions in “self-solute” environment by DFT and polarizable continuum model.

Solid state IE and EA of the material can be measured directly by ultraviolet photoemission spectroscopy (UPS) and inverse photoelectron spectroscopy (IPES). Unfortunately, realizations of those methods are expensive and connected with experimental problems. Therefore investigators are looking for alternative methods to evaluate energy levels. One of possibilities is based on correlation of solid state IE and EA levels with oxidation and reduction potentials obtained in solution by cyclic voltammetry (CV). Another possibility could be measurements of the molecule IE in solid state by Kelvin probe (KP) technique in combination with the energy gap obtained by photoelectrical (PE) methods.

Assessment of QC, CV and KP+PE methods will be done on the basis of the investigation results of fourteen 4'-substituted 2-benzyl-1,3-indandiones. These structurally equal dyes allow us to cover wide range of IE and EA and at same time to minimize unwanted side effects in correlation analysis of results obtained by above mentioned methods.

Optical Field-Induced Surface Relief Formation on Chalcogenide and Azo-Benzene Polymer Films

J. Teteris

Institute of Solid State Physics, University of Latvia, Latvia

teteris@latnet.lv

An interaction between laser light beam with high intensity gradient and soft materials (amorphous chalcogenide and organic polymer films) was studied. The single light beam focusing and two coherent beam interference were used for high light intensity gradient formation. Under intensive illumination the formation of relief structures on the surface of amorphous films due to lateral mass transport regarding the light propagation direction has been observed.

The amorphous films of chalcogenides (As-S, As-S-Se, As-Se and Ge-Se systems) and azo-dye doped organic polymers were used for studies. The influence of the amorphous film thickness, recording laser wavelength (532 nm, 632.8 nm and 671 nm), grating period, light intensity and polarization state on the relief formation process in amorphous inorganic and organic films was studied. It was shown that the efficiency of the surface-relief formation strongly depends on the recording light polarization state [1]. The best gratings were obtained with (+45⁰, -45⁰) and (RCP, LCP) combinations, which involve primarily variation in polarization state across the film. The relief grating profile on amorphous films was analyzed by means of atomic force microscope (AFM).

A strong relationship between surface relief grating (SRG) and polarization holographic grating formation was observed and studied. The study of the phase relationship between the exciting light field and the resulting surface deformation is crucial in understanding the mechanism of SRG formation. It was observed that the peak of the SRG on chalcogenide films was formed at the position of p-polarization state in the polarization modulation pattern. The peak formation of the surface relief on organic azobenzene doped polymers was observed at the position of s-polarization state.

The mechanism of the direct recording of surface-relief on amorphous films based on the photo-induced softening of the matrix, formation of defects with enhanced polarizability, and their drift under the optical field gradient force has been discussed.

References

1. J. Teteris, U. Gertners, M. Reinfelds, *Phys.St.Sol.(c)*, **8**, 2780 (2011)

Abstracts of the poster presentations

INTERREG project “Technet_nano” – National Network of Clean Rooms and Research Facilities in Nanotechnology Making Accessible Innovation Resources and Services to SMEs in the BSR

D. Erts¹, A. Sternbergs², M. Rutkis²

¹Institute of Chemical Physics, University of Latvia, Raina blvd. 19, Riga, Latvia

²Institute of Solid State Physics, University of Latvia, Kengaraga 8, Riga, Latvia

e-mail: donats.erts@lu.lv

Technet_nano project aims to join innovation resources of clean rooms and research institutions around the Baltic Sea in the field of micro- and nanotechnology. The purpose of this network is to make these innovation facilities and high quality services accessible across the borders to regional SMEs.

Universities with clean rooms, R&D institutions in the field of micro- and nanotechnology and technology transfer organisations and business development agencies are involved in the project.

Lead partner of the project is University of Southern Denmark, partners are Royal Institute of Technology (Sweden), Christian Albrechts University Kiel (Germany), Flensburg University of Applied Sciences (Germany), Business Development and Technology Transfer Corporation of Schleswig Holstein (Germany), University of Latvia, Kaunas University of Technology (Lithuania), Applied Research Institute for Prospective Technologies (Lithuania), Center of Physical and Technology Science (Lithuania), Silesian Science and Technology Centre of Aviation Industry Ltd. (Poland), Acreo AB (Sweden), University of Tartu (Estonia).

During the project the validation of regional demands will be finalised. Specialization of the partners, clean room facilities, and R&D services will be analyzed. R&D potentials between SMEs and Technet_nano partners will be identified. High quality services for SMEs fostering innovations through micro- and nanotechnology will be developed as well as concept of transnational services for SMEs.

Rules for the access to the research facilities, demonstrations and services for industrial partners will be discussed. In the presentation, special attention will be devoted to the local industrial demands and R&D accessibility.

A New Approach to the Engineering of *Ab Initio* Materials Simulations on an Example of CRYSTAL, VASP and WIEN2K Packages

E. Blokhin¹, D. Gryaznov^{1,2}, R. Evarestov³, J. Maier¹

¹Max-Planck Institute for Solid State Research, Stuttgart, Germany

²Institute of Solid State Physics, University of Latvia, Latvia

³Department of Quantum Chemistry, St. Petersburg State University, Peterhof, Russia

e-mail: e.blokhin@fkf.mpg.de

Nowadays no common methodology exists to organize computer simulation data in material science produced by the popular simulation packages for molecules and solids. The traditional way is to process needed data manually and exchange and review them via the peer reviewed journal publications, which however suffers due to high time costs, much non-automated computer work and lack of interoperability standards between software packages and, additionally, within scientific community [1]. Several attempts have been made so far in the last years to collect and organize raw calculations results and to present them using World Wide Web (WWW) [2-5].

A new approach [6] is to utilize a free operating-system-independent graphical user interface (GUI) in a web browser to solve the above-mentioned tasks. The popular programming languages Python, PHP and JavaScript have been employed for this purpose. The resulted software allows users to store, visualize and manipulate complex input or output results derived from modeling via only a web browser (though minimal installation of additional software is recommended). This solution dramatically speeds up both the results processing and bugs fixing, with the several usage scenarios being supported: (1) crystalline structures rendering, (2) visualization of geometry optimization and phonon calculations, (3) organizing the data depending on modeling methods, employed techniques and resulted physicochemical properties. Among the range of simulation software, the focus is currently on CRYSTAL, VASP and WIEN2K packages.

References

1. O'Boyle et al. J. Chem. Inf. 2011 3:37 <http://dx.doi.org/10.1186/1758-2946-3-37>
2. EDS: Uppsala Electron Density Server: <http://eds.bmc.uu.se/>
3. CDF: Computational Database Framework: <http://kitchingroup.cheme.cmu.edu/cdf>
4. CMR: Computational Materials Repository: <https://wiki.fysik.dtu.dk/cmr/>
5. J-ICE: A Jmol Interface for Crystallographic and Electronic Properties: <http://j-ice.sourceforge.net/>
6. Tilde: Cheminformatics Database and Calculations Manager: <http://code.google.com/p/wwwtilda/>

Joint Theoretical-Experimental Study of Iron Impurities and Oxygen Vacancies in SrTiO₃

E. Blokhin¹, A. Kuzmin², J. Purans², E. Kotomin^{1,2}, R. Evarestov³, J. Maier¹

¹Max-Planck Institute for Solid State Research, Stuttgart, Germany

²Institute of Solid State Physics, University of Latvia, Latvia

³Department of Quantum Chemistry, St. Petersburg State University, Peterhof, Russia

e-mail: e.blokhin@fkf.mpg.de

Fe-doped SrTiO₃ represents a wide group of materials promising for non-volatile resistive random access memory devices [1]. In the presented work the novel structural information on iron impurity and oxygen vacancy complexes in SrTiO₃ is provided by *ab initio* and XANES simulations. The relation of Fe–O bond length, doping level and Fe oxidation state in SrTi_{1-x}Fe_xO_{3-d} systems is discussed. A combination of the experiment methods (EXAFS, XANES, EPR and Raman spectroscopy) [1] and state-of-the-art *ab initio* simulations [2] is used, to give new insights into the local structure and oxidation state of Fe in SrTi_{1-x}Fe_xO_{3-d}.

For both defects considered separately [2], the Jahn-Teller effect occurs thus reducing the cubic symmetry of a perfect SrTiO₃ crystal and leading to the asymmetric structural relaxation around the defect. In its turn, this results in appearance of the observable Raman modes in the phonon spectrum of SrTiO₃. On the other hand, for these two defects considered in a complex [1], no Jahn-Teller effect fingerprints are detected. The phonon spectrum remains insensitive to the defects introduction. This phenomenon is addressed in a presented study. It is shown that simulated XANES spectra based on the *ab initio* calculated defect geometry are in a good agreement with the real experiments. Additional focus is on insulator-to-metal transitions, which take place at the very low defect content in SrTiO₃.

References

1. C. Lenser, A. Kalinko, A. Kuzmin, D. Berzins, J. Purans, K. Szot, R. Waser and R. Dittmann, Phys.Chem.Chem.Phys., 2011, 13, 20779
2. R. Evarestov, E. Blokhin, D. Gryaznov, E. A. Kotomin, R. Merkle and J. Maier, Phys.Rev.B, 2012, accepted

A Comparative Study of Structural Energetics and Chemical Bonding in Ca-Based Dielectric Materials: An Integrated View from First-Principles Calculations

A. Pishtshev¹, M. Klopov²

¹Institute of Physics, University of Tartu, Tartu, Estonia

²Tallinn University of Technology, Tallinn, Estonia

e-mail: aleksandr.pishtshev@ut.ee

In this work, we demonstrate for one important class of the wide-gap compounds how the use of the first-principles calculations allows one not only to look at the underlying dynamical processes associated with bonding arrangements, but also to assess specific features of alkaline earth metal cations in terms of the overall bonding picture. By taking Ca²⁺ ions as a test case, we have carried out *ab initio* electronic structure calculations on eight representative members of Ca-based crystalline systems: CaF₂, CaCl₂, CaFCl, CaHCl, CaH₂, Ca(OH)₂, CaSO₄, and Ca₁₀(PO₄)₆(OH)₂. The investigation employed both GGA and hybrid functional schemes, as well as semi-empirical dispersion corrections. Local charge geometries, the bonding properties, different roles of cations and anions, and the extent of cation-anion electron transfer were studied for these systems in terms of effective charges and the electron localization function. In the context of the cation-anion interactions, the obtained results were used to perform a comparative analysis of relative strengths and weaknesses of ionic bonding and covalent effects associated with presence versus absence of the certain structural and compositional features. Our investigation indicates that for most members of the given class of compounds, the relevant bonding arrangement involves an admixture of the dynamic covalency effects related to the calcium cations. The work demonstrates how the interplay between the lattice and electronic degrees of freedom provides a delicate covalent linkage of the Ca²⁺ cations to anion groups and how this leads to a certain optimization of an ionic bonding picture typical for the crystal structures like CaF₂. For the given series of Ca-based dielectric materials we also considered why the coupling of the lattice and electronic degrees of freedom may never play the same fundamental role which it plays in lattice dynamics of displacive ferroelectrics.

Acknowledgements

This work was supported by the European Union through the European Regional Development Fund (Centre of Excellence "Mesosystems: Theory and Applications", TK114). It was also supported by the Estonian Science Foundation grant No 8991.

Treatment of Excitons by Discrete Variable Representation

E. Klotins, G. Zvejnieks

Institute of Solid State Physics, University of Latvia, Latvia

e-mail: klotins@cfi.lu.lv

The properties of excitons, a variety of particle-like excitations in solids, is a long standing problem and so far no appropriate solution has been obtained. A conventional approach to this problem is the effective- mass (Wannier-Mott) approximation, a hydrogen-like bound state of an electron and a hole interacting through their Coulomb attraction. Corrections to the hydrogen-like properties are of special importance for excitons with radius, comparable with the lattice spacing and are accounted for by implementing fermionic operators for electron and hole. These conceptual developments tremendously enlarges the computing resource consumption and provides motivation for methods going beyond the conventional matrix diagonalization techniques.

The present work is addressed to the matrix eigenvalue problem on a lattice distinguished by an electron – hole Hamiltonian with anharmonic terms [1]. The discrete variable representation (DVR) [2] treatment includes orthonormality, completeness, variational principle preserving and the error propagation tests for basis functions providing both periodic and nonperiodic boundary conditions. A distinguishable advancement to the standard DVR is adapting of the original DVR in a form in which the matrix elements of the potential energy operator are diagonal.

The survey of DVR calculations for the simplest models include estimates of the exciton energies and the exciton Bohr radius corresponding to the minimum energy with potential extensions toward realistic band structures from *ab initio* LDA and GW calculations.

References

1. A. Alvermann, P. B. Littlewood and H. Fehske, Phys. Rev. B, **84**, 035126 (2011)
2. Yi Liu, D. A Yarne, M. E. Tuckerman, Phys. Rev. B, 68, 125110 (2003)

Modelling of Turbulent Silicon Melt Flow in Purifying Process with Electron Beam

K. Bergfelds¹, G. Chikvaidze¹, A. Muiznieks², A. Krauze²

¹Institute of Solid State Physics, University of Latvia, Latvia

²University of Latvia, Faculty of Physics and Mathematics, Latvia

e-mail: kristaps.bergfelds@lu.lv

Photovoltaic power industry requires economical mass production methods for producing solar-grade silicon from metallurgical-grade silicon. One of such methods, currently under development, is melting and purifying silicon by using electron beam technology [1, 2]. Polycrystalline silicon in a water cooled crucible is melted and overheated by an electron beam in a system depicted in Fig. 1. High overheating temperatures ($\Delta T \sim 1000$ K) ensure effective evaporation of some impurities from the melt due to differences in the evaporation rates of silicon and these impurities. Due to extremely high temperature gradients in the silicon, melt motion is strong enough to be turbulent and to be an important aspect of the melting process.

In the present work, a system of axially-symmetric mathematical models is proposed for the modeling of the turbulent silicon melt flow in the crucible. Turbulent heat transfer in the melt is studied by solver based on *OpenFOAM* library (see Fig. 1 and 2).

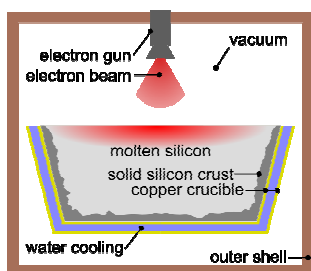


Fig.1 System schematics

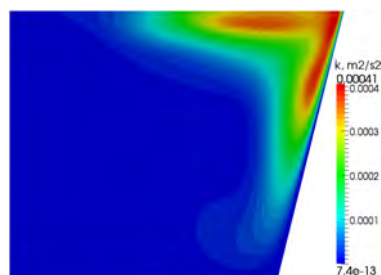


Fig.2 Turbulence kinetic energy

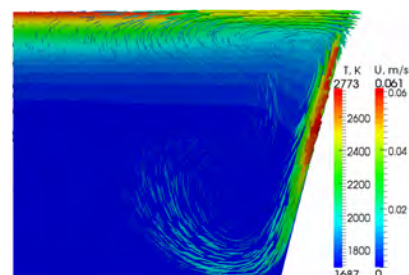


Fig.3 Velocity and temperature

Acknowledgements

Work has been supported by the European Social Fund, project contract No. 2009/0223/1DP/1.1.1.2.0/09/APIA/VIAA/008, and by the European Regional Development Fund No. 2011/0002/2DP/2.1.1.1.0/10/APIA/VIAA/085 and No. 2010/0245/2DP/2.1.1.1.0/10/APIA/VIAA/114.

References

1. Kazuhiro Hanazawa, Noriyoshi Yuge, Yoshiei Kato. Evaporation of Phosphorus in Molten Silicon by an Electron Beam Irradiation Method. *Materials Transactions*, Vol. 45, No. 3 (2004), p. 844 to 849.
2. A. Krauze, A. Muiznieks, K. Bergfelds, K. Janisels, G. Chikvaidze. Reduction of silicon crust on the crucible walls in silicon melt purifying processes with electron beam technology by low-frequency travelling magnetic fields, *Magnetohydrodynamics*, Vol. 47, No. 4 (2011), p. 369 to 383.

Phase Shapes and Melt Motion 3D Modeling for FZ Silicon Single Crystal Growth Process

K. Janisels¹, A. Muiznieks¹, A. Krauze¹, A. Sabanskis¹, K. Lācis²

¹Faculty of Physics and Mathematics, University of Latvia, Latvia

²Inc. Sidrabe, Latvia

e-mail: karlisjanisels@gmail.com

Floating zone (FZ) growth process with high frequency (HF) inductor is mainly used for silicon single crystal production for power-electronics needs due to high purity of the FZ material. The industrial development of FZ process is continuously supported by mathematical modeling of the process [1].

Modeling of FZ process contains 3 main components: 1) 2D axis-symmetric solid silicon phase boundary calculation; 2) coupled 3D calculation of the melt free surface and HF EM field (both components implemented in self-developed program *FZZone* [1]); 3) unsteady 3D calculations of melt motion and dopant transport inside the molten zone by self-developed solver based on open source code library *OpenFOAM* [2]. Calculation results for FZ 4" crystal growth system from Institute for Crystal Growth (Berlin) are illustrated in Fig. 1.

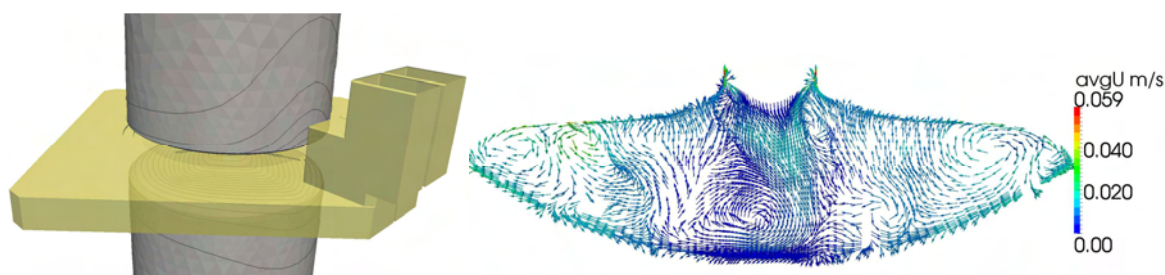


Fig.1 Induced 3D HF current lines on silicon (poly feed rod, melt and single crystal) surfaces (left) and 3D calculated flow in the molten zone (right)

Acknowledgements

The present work is carried out at the University of Latvia and has been supported by the European Regional Development Fund, project contract No. 2011/0002/2DP/2.1.1.1.0/10/APIA/VIAA/085; European Social Fund, project contract No. 2009/0223/1DP/1.1.1.2.0/09/ APIAA/VIAA/008 and within the project „Support for Doctoral Studies at University of Latvia”.

References

1. G. Ratnieks, A. Muiznieks, A. Muhlbauer. Modelling of phase boundaries for large industrial FZ silicon crystal growth with the needle-eye technique. *J. Crystal Growth* **255**, 227-240 (2003)
2. K. Lācis, A. Muiznieks, A. Rudevics, A. Sabanskis. Influence of DC and AC magnetic fields on melt motion in FZ large Si crystal growth. *Magnetohydrodynamics* **46**(2), 199-218 (2010)

Lattice Dynamics of WOCl_4

J. Gabrusenoks

Institute of Solid State Physics, University of Latvia, Latvia

e-mail: gabrusen@latnet.lv

The WOCl_4 structure consists of pyramidal WOCl_4 units which are linked by linear asymmetric O - - - W----O bridges to polymeric $(\text{WOCl}_4)_n$ chains. The vibrational modes of WOCl_4 have been investigated. Calculations have been performed by using hybrid exchange density functional theory to determine equilibrium geometries and phonon frequencies. The Grimme dispersion correction for energy and gradient has been used in combination with B3LYP functional. The CRYSTAL09 computer code was used.

Hydroxyapatite OH-Channels for Proton Transferring Aimed to Surface Charging

A. Bystrova^{1,3}, V. Bystrov^{2,4}, Y. Dekhtyar³, E. Maevsky¹, E. Paramonova², N. Polyaka³

¹Institute of Theoretical and Experimental Biophysics RAS, Russia

²Institute of Mathematical Problems of Biology RAS, Russia

³Inst. of Biomedical Eng.&Nanotechnology, Riga Technical University, Latvia

⁴Dept.Cer.&Glass Eng.&CICECO, University of Aveiro, Portugal

e-mail: bystrova@physics.msu.ru

HAP is one of the most widely used materials in contemporary nanobiomedicine and nanotechnology. The interaction between HAP based biomaterials and living cells is improved, if the HAP surface is charged electrically [1]. The charge is inducible on HAP structures by the proton transport along the OH chains in columnar channels. These chains are formed by OH ions along c-axis and are surrounded by calcium triangles.

The results of computing simulation and studying of hydroxyapatite (HAP) properties and its hydrogen bonds and proton transfer peculiarities, surface and polarization properties [1] are presented. The reported data presents as *ab initio* quantum-chemical calculations (with Gaussian98 code, HF, 6-31G(d)), as well semi-empirical (PM3) and DFT by HyperChem 8.0, which clarify the double-well asymmetric potential energy profile and were held to investigate the energy barriers for proton transport along the columnar channel. The calculated values of barriers can explain long storage of polarization charge, which is observed in experiments, as electrets effect. A possibility to transfer proton via the barrier is supported due to the experiment. High pressure of hydrogen and followed electromagnetic stimulation induced transfer of the proton. In fact, the electron work function was altered for different kind of ceramics.

References

1. V.S. Bystrov, E. Paramonova, Yu. Dekhtyar, A. Katashev, A. Karlov, N. Polyaka, A.V. Bystrova, A. Patmalnieks and A.L. Kholkin. J.Phys.: Condens. Matter. **23**, 065302 (2011)
2. Yu. Dekhtyar, V. Bystrov, I. Khlusov, N. Polyaka, R. Sammons and F.Tyulkin.- In: The Society for Biomaterials 2011 Annual Meeting.-April 13-16, 2011, Orlando, Florida, USA.

The Investigation of Chemical Bonding at Metal-Ceramic Interfaces

A. Bakulin^{1,2}, S. Hocker³, S. Schmauder³, S. Kulkova^{1,2}

¹Tomsk State University, Tomsk, Russia

²Institute of Strength Physics and Materials Science SB RAS, Tomsk, Russia

³Institute of Materials Testing, Materials Science and Strength of Materials, University of Stuttgart, Germany

e-mail: alex@phys.tsu.ru

Metal-ceramic interfaces play very important role for modern technologies. They are in a focus of both experimental and theoretical studies in the last decade. The first principles calculations can provide a deep insight into microscopic nature of the metal-ceramic interfaces. We present a comparative *ab-initio* study for some metal/metal carbide (Me/TiC, Me/VC, Me/NbC, etc.) and metal/metal nitride (Me/TiN, Me/VN) interfaces performed by the projector-augmented-wave method. The structural and electronic properties, surface and interface energies were calculated. It was shown that elastic deformation influences significantly on the metal carbide (nitride) surface stability. The change in the binding energy and magnetic moments of metal atoms was studied in dependence on a number of metal layers at the interface. The chemical bonding of metals (Al, Fe, Ni, Co, Mo, Rh, etc.) at the polar and non polar metal/ceramic interfaces are analyzed. The study of the adhesion at the Me(001)/TiC(001), Me(001)/VC(001) interfaces showed that the work of separation is less in the case of Me-Ti(V)-top configuration in comparison with Me-C(N)-top one. The values of 0.66 and 2.49 J/m² were obtained for Al/VC(001) as well as 0.76 and 1.99 J/m² for Al/TiC(001) system, respectively. The same trends were obtained for Al/TiN and Al/VN systems. The analysis of the local densities of states and charge density distribution confirm a more stronger interaction in the case of Al-metalloid component-top position that indicates the dominant role of the covalent contribution in the chemical bonding at these interfaces. The influence of metal and carbon or nitrogen vacancies on the adhesion is discussed. It was shown that in the case of metal vacancy in substrate the diffusion of aluminum inside substrate is observed alongside with the change of the metal film configuration from metal-top to metalloid-top that results in the increase of the adhesion. In general, the performed investigations allow us to reveal a relationship between electronic, geometrical factors and mechanical properties of considered metal-ceramic interfaces.

Acknowledgements

Financial support was provided by the Russian Foundation for Basic Research under grant No. 09-03-00523-a.

***Ab Initio* Calculations of SrTiO₃, BaTiO₃, PbTiO₃, CaTiO₃, BaZrO₃, SrZrO₃ and PbZrO₃ (001), (011) and (111) Surfaces as Well as Nb Impurity Segregation Towards the SrTiO₃ Surface**

R.I. Eglitis¹

¹Institute of Solid State Physics, University of Latvia, Latvia

e-mail: reglitis@yahoo.com

While the (001) surfaces of ABO₃ perovskites, such as SrTiO₃, BaTiO₃, PbTiO₃, CaTiO₃, SrZrO₃, PbZrO₃ and BaZrO₃ have been extensively studied [1-5], much less is known about the (011) and (111) surfaces. On the (001) surfaces, I consider both AO (A=Sr, Ba, Pb or Ca) and BO₂ (B=Ti or Zr) terminations. The (001) surface AO layer is found to relax inward for all seven materials with the sole exception of SrO-terminated SrTiO₃ (001) surface first layer O atom. My calculated surface rumplings of 6.77 % for the SrO-terminated SrZrO₃ (001) and 3.32 % for the PbO-terminated PbZrO₃ (001) surfaces are almost ten times larger than those of the corresponding ZrO₂-terminated SrZrO₃ and PbZrO₃ (001) surfaces [5].

As for the (011) surfaces, I consider three types of surfaces, terminating on a BO layer, A layer and O layer. Turning now to the surface energies, I find that both the AO and BO₂-terminated (001) surfaces are about equally energetically favorable and may co-exist. In contrast, I see very large differences in the surface energies on the ABO₃ (011) surfaces. The calculated surface energies for ABO₃ perovskite (111) surfaces is even larger than for the (011) surfaces [6]. I demonstrate that Nb is shallow donor in SrTiO₃ and discuss also its segregation towards the SrTiO₃ surface [7].

References

1. R. I. Eglitis, J. Phys.: Condens. Matter **19**, 356004 (2007)
2. R. I. Eglitis and D. Vanderbilt, Phys. Rev. B **76**, 155439 (2007)
3. R. I. Eglitis and D. Vanderbilt, Phys. Rev. B **77**, 195408 (2008)
4. R. I. Eglitis and D. Vanderbilt, Phys. Rev. B **78**, 155420 (2008)
5. R. I. Eglitis and M. Rohlfing, J. Phys.: Condens. Matter **22**, 415901 (2010)
6. R. I. Eglitis, Ferroelectrics **424**, 1 (2011)
7. R. I. Eglitis and E. A. Kotomin, Physica B **405**, 3164 (2010)

Electronic Structure and Lattice Dynamics of ScF₃ from *Ab Initio* LCAO Calculations

P. Zhgun¹, D. Bocharov^{1, 2, 3}, S. Piskunov^{1, 2, 3}, A. Kuzmin³, J. Purans³

¹Faculty of Physics and Mathematics, University of Latvia

²Faculty of Computing, University of Latvia

³Institute of Solid State Physics, University of Latvia

e-mail: pjotr.zgun@gmail.com

ScF₃ is a peculiar compound having simple ReO₃-type cubic structure. Recent discovery of strong negative thermal expansion (NTE) coefficient in ScF₃ over a wide range of temperatures, from 10 to 1100 K [1], makes its investigation challenging. In spite of a number of attempts has been made to explain the NTE in ScF₃ by estimating anharmonicity of certain phonon modes within the framework of Rigid Unit Modes model, the origin of the NTE is still under debate [2].

In our study we have performed *ab initio* LCAO calculations of ScF₃ using hybrid HF-DFT approach as implemented in CRYSTAL09 total energy program [3]. The use of hybrid HF-DFT computational scheme allowed us to reproduce the experimentally observed lattice constant ($a_0 = 4.026 \text{ \AA}$ [1]) and to obtain the values of the band gap and bulk modulus, which to the best of our knowledge are not known experimentally at low temperatures.

The calculation of phonon modes in high symmetry k -points (Γ , M, X, R) across the Brillouin zone allowed us to access the thermodynamic properties of ScF₃. The analysis of different phonon modes and their variation upon lattice contraction/expansion gives us the ground for the prediction of the phonons impact on uncommon thermal properties of ScF₃.

Finally, the *ab initio* calculated parameters for ScF₃ were used in the construction of the force field model, which provides an access towards its temperature dependent dynamics *via* classical molecular dynamics simulation.

References

1. B. K. Greve et al., J. Am. Chem. Soc. **132**, 15496 (2010).
2. C. W. Li et al., Phys. Rev. Lett. **107**, 195504 (2011).
3. R. Dovesi et al., CRYSTAL09 User's Manual (University of Torino, Torino, 2009).

First Principles Calculations of Defective ZnO Crystals: The Role of Symmetry and Phonons

A.V. Sorokin¹, D. Gryaznov², Yu.F. Zhukovskii², E.A. Kotomin², J. Purans²

¹Faculty of Physics and Mathematics, University of Latvia, Latvia

²Institute of Solid State Physics, University of Latvia, Latvia

e-mail: as08504@lu.lv

Zinc oxide is considered as a suitable material for manufacturing of transparent conducting films, which can be used in production of *e.g.* solar cells and LCD screens. Properties of ZnO vary with the concentration and the type of defects that are present in the lattice of monocrystals. The main point defects usually considered for practical applications are substitutions of Zn with other metal atoms (Al, Ga, *etc.*) and hydrogen interstitials [1].

The technological process of manufacturing of doped ZnO is connected with formation of intrinsic defects, such as Zn and O vacancies. These defects can influence the conductivity rather strongly, and so they are to be considered both in experiments and when making theoretical predictions of electronic properties of ZnO. In this work we investigate the way in which such properties are affected by zinc vacancies.

In this study *ab initio* calculations employing density functional theory with a basis set of the linear combination of atomic orbitals were used [2]. The hybrid exchange-correlation functional PBE0 was chosen for wide-band gap ZnO ($E_g = 3.44$ eV). The concentration of V_{Zn} was sufficiently low, 2 %. Moreover, the vacancies were treated using the so-called ‘ghost’ functions replacing a missing atom. A particular emphasis in our study is given to 1) Basis set optimization of both Zn and O for pure ZnO; 2) The symmetry changes related to the formation of vacancies; 3) Incorporation of Al(Ga) into vacancies. The resulting electronic structure is analysed in detail. We calculated the defect formation energies with respect to chemical potentials of species and estimated the phonon contribution.

References

1. L. Schmidt-Mende, J. L. MacManus-Driscoll, *Mater. Today* (2007), **10**(5), 40–48
2. R. Dovesi, V.R. Saunders, C. Roetti, *et al.* *CRYSTAL-2009 User Manual*. Turin:University of Torino (2009)

Ab Initio Calculations of Hydrogen Impurities in ZnO

A. Useinov¹, A. Sorokin², Yu.F. Zhukovskii², E.A. Kotomin², A.T. Akilbekov¹, J. Purans²

¹L.N. Gumilyov Eurasian National University, Astana, Kazakhstan

²Institute of Solid State Physics, University of Latvia, Latvia

e-mail: useinov_85@mail.ru

The atomic and electronic structure of zinc oxide continues to attract great attention due to a number of promising technological applications. For example, successful development was achieved in the growth of perfect ZnO single crystals (with the band gap $E_{\text{gap}} = 3.44$ eV) [1]. After special treatment these crystalline samples transformed to a suitable material for synthesis of transparent conducting films. This is due to a fact that a variety of intrinsic and extrinsic defects considerably modify physical and optical properties of ZnO.

In this study, we analyze the influence of neutral H impurity defects on the redistribution of the electronic charge, the band structure and optical properties of ZnO. Special attention is paid to an interstitial hydrogen atom (H_i) (Fig. 1). To solve the problems of the relaxation of zinc oxide lattice around point defect, the transformation of electronic structure and the charge density redistribution, we have performed large-scale *ab initio* calculations within the formalism of linear combination of localized atomic functions (LCAO), including optimized atomic basis sets, combined with the *PBE0* hybrid exchange-correlation functional as implemented into the *CRYSTAL-09* code [2]. Hybrid exchange-correlation functionals provide much better correlation of calculated band structures with experiment, including width of band gap and position of defect levels. As in earlier studies [3, 4], we confirm that the impurity hydrogen H_i give rise to shallow levels, close to the conduction band minimum of ZnO, which can explain the increase of the electrical conductivity.

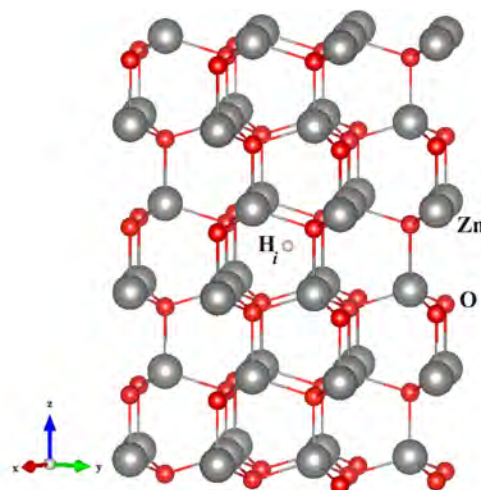


Fig. 1. Arrangement of the interstitial hydrogen atom H_i in the $3 \times 3 \times 3$ supercell of ZnO

References

1. D.C. Reynolds, D.C. Look, B. Jogai, C.W. Litton, G. Gantwell, W.C. Harsch, Phys. Rev. B 60, 2340 (1999).
2. R. Dovesi, V.R. Saunders, C. Roetti, *et al.* *CRYSTAL-2009 User's Manual* (University of Torino, 2009).
3. Mao-Hua Du and Koushik Biswas, Phys. Rev. Letters, PRL 106, 115502 (2011).
4. Federico Gallino, Gianfranco Pacchioni, and Cristiana Di Valentin, J. Chem. Phys., 133, 144512 (2010).

The Role of Nanopowder Particle Surfaces and Grain Boundary Defects in the Sintering of ZnO Ceramics

F. Muktepavela¹, V. Sursajeva², L. Grigorjeva¹, K. Kundzins¹, E. Tamanis³

¹Institute of Solid State Physics, University of Latvia

²Institute of Solid State Physics, Russian Academy of Sciences, Chernogolovka

³University of Daugavpils, Latvia

e-mail:famuk@latnet.lv

It is well-known that individual nanoparticles in the nanopowder compacts tend to agglomerate and form strong inter-particle bonds associated with their high surface-to-volume ratio. That is why in recent years energy-intensive compaction technologies have been widely applied. In the meanwhile, improving the structure and properties of ceramic obtained by simple high temperature sintering remains a live problem. ZnO has a variety of 1D and 3D nanostructures: such as tetrapods, nanowires, etc., which have extended free surfaces with minimum energy, surface-to-volume ratio is low and, we can assume they will not cling together. In our work the obtained grained ($d=50-100$ nm) and tetrapod-like ($d=50-100$ nm, $l=3-10$ μm) ZnO powders have been sintered at 1200°C and the role of free surface and grain boundary (GB) defects (pores, facets, triple junctions) are considered. Results showed that ceramics sintered from the grained powder have high (8%) porosity at GB as well as inside grains that causes brittleness. At 12 K temperature the photoluminescence (PL) spectrum of this ceramics besides excitonic peak exhibited broad green band attributed to defect states. The structure of ceramics obtained from the tetrapod-like powder contains small individual micropores in the vicinity of triple junctions (TJ), porosity was $<2\%$. PL at 12 K revealed a narrow excitonic band with a satellite peaks (LO_Ex states) and an almost non-existent green luminescent band that is an evidence of high quality of this ceramic. Experiments on the bi-and three crystals have shown that motion of GB in the stages of grain growth is controlled by TJ mobility. The influence of TJ is very high for spherically shaped particle powders and depends on temperature. The obtained results from the point of view of thermally activated adhesion and evolution of GB microstructure processes at different sintering stages are discussed.

Shear Banding Mechanism of Plastic Deformation in LiF Irradiated With Swift Heavy Ions

R. Zabels, J. Maniks, I. Manika

Institute of Solid State Physics, University of Latvia, Latvia

e-mail: rzabels@gmail.com

The deformation behavior of LiF crystals after irradiation with high energy ions has been investigated. The irradiation was performed using different ions (U, Pb, Au, Ni, S) with energy in the range from 3 MeV to 2 GeV at fluences up to 10^{14} ions/cm². For the study of deformation mechanisms the microindentation and instrumented nanoindentation were applied. In unirradiated LiF, the deformation occurs by dislocation glide on the {110} planes along the <100> and <110> directions. The ion irradiation leads to decrease of dislocation mobility and increase of hardness due to impeding of dislocations by radiation defects [1].

The obtained results show that at high-fluence irradiation the resource of the dislocation mechanism is depleted and the deformation develops by means of shear banding. The evolution of shear banding follows the stress distribution in the indentation zone and shows no preferable crystallographic directions. The formation of localized shear bands was more pronounced in the case of heavy ions exhibiting track core damage. The initiation of shear banding, which develops without work hardening, intermits the ion-induced increase of hardness at a definite comparatively high limit (around 4 GPa), which surpasses the hardness of the unirradiated LiF by 170%.

The deformation by shear banding at indentation is known to occur in nanocrystalline materials exhibiting grain boundary sliding and in amorphous materials, in which the formation of deformation bands is facilitated by a free volume [2]. We suggest that the grain boundary sliding, which becomes possible due to nanostructuring in heavily irradiated LiF [3], and localization of deformation, facilitated by swelling-induced formation of free volume, are the main mechanisms of shear banding in ion-irradiated LiF.

References

1. I.Manika, J.Maniks and K.Schwartz. J.Phys.D: Appl Phys.**41**, art No.65961f (2008).
2. A. S Argon. Acta metall. **27**, 47(1979)
3. J.Maniks, I.Manika, R.Grants, R.Zabels, K.Schwartz, M.Sorokin, R.M.Papaleo. Applied Phys.A 104, 1121 (2011).

Effects of Deuterium Ion Implantation on the Hardness TiN-based Nanocrystalline Films

V.A. Belous, A.S. Kuprin, N.S. Lomino, V.D. Ovcharenko, E.N. Reshetnyak, O.M. Morozov,
V.I. Zhurba, G.N. Tolmachova

National Science Center “Kharkov Institute of Physics and Technology”, Kharkov, Ukraine

e-mail: kuprin@kipt.kharkov.ua; morozov@kipt.kharkov.ua

Multicomponent nanostructural coatings basis on titanium nitride with additives Zr, Al, Si, B, Cr, Y possess high hardness, corrosion resistance and thermal stability [1]. Investigation properties stability of nitride coatings at various kinds of an irradiation is represented an actual problem [2, 3]. In this study the influence of ion-implanted deuterium on changes of the mechanical properties TiZrN, TiAlSiN, TiAlYN films were investigated. Films with thickness $\sim 3 \mu\text{m}$ were deposited by filtered vacuum arc plasma flux [4]. Composition of the coatings was determined by X-ray fluorescence method. According to X-ray diffraction analysis of the films is detected a single crystalline phase – cubic nitride based on TiN (structural type NaCl). Nanohardness measured on Nanoindenter G200. In the table the composition, characteristics of the substructure and hardness of the films are shown.

The irradiation was performed at room temperature with 12 keV D^+ ions to dose $\sim 1 \cdot 10^{18} \text{D}/\text{cm}^2$. For all irradiated films nanohardness are decreased. The lowest changes occurred in the coatings $\text{Ti}_{99}\text{Zr}_1\text{N}$ and $\text{Ti}_{75}\text{Al}_{21}\text{Si}_4\text{N}$ in which columnar structure are dominated.

Coating composition, at%	Texture axis	crystallite size, nm	H, GPa as deposited	H, GPa Irradiated $\sim 1 \times 10^{18} \text{D}/\text{cm}^2$
$\text{Ti}_{99}\text{Zr}_1\text{N}$	[111]	22	30	26
$\text{Ti}_{59}\text{Al}_{37}\text{Si}_4\text{N}$	[110]	10	40	15
$\text{Ti}_{75}\text{Al}_{21}\text{Si}_4\text{N}$	—	10	25	23
$\text{Ti}_{31}\text{Al}_{68}\text{Y}_1\text{N}$	amorphous		23	15
$\text{Ti}_{50}\text{Al}_{48}\text{Y}_2\text{N}$	—	7	26	11

References

1. S. PalDey, S.C. Deevi, Mater. Sci. Eng. **A 342** 58 (2003).
2. H. Wang, R. Araujo, J.G. Swadener et al, Nucl. Instr. and Meth. **B 261** 1162 (2007).
3. V.V. Uglov, D.P. Rusalski, S.V. Zlotski, A.V. Sevriuk, G. Abadias, S.B. Kislitsin, K.K. Kadyrzhanov, I.D. Gorlachev, S.N. Dub, Surf. Coat. Technol. **204** 2095 (2010).
4. I.I. Aksenov, V.M. Khoroshikh, N.S. Lomino, V.D. Ovcharenko, Y.A. Zadneprovskiy, IEEE Transactions on Plasma Science. **27** 1026 (1999).

Electron Beam Charging of Semi-Insulating Samples

H.J. Fitting¹, M. Touzin²

¹Institute of Physics, University of Rostock, Universitätsplatz 3, D-18051 Rostock, Germany

²Unité Matériaux, UMR CNRS 8207, Université de Lille 1, F-59655 Villeneuve d'Ascq, France

e-mail: hans-joachim.fitting@uni-rostock.de

The former flight-drift model (FDM) of charge carriers in pure insulating materials of the authors, [1, 2], has been extended by an intrinsic field conductivity $j = cF$ to a flight-drift-conduction model (FDCM), [3] and describes the selfconsistent charge transport and storage in full insulators ($c=0$), semi-insulators and/or wide-gap semiconductors up to an intrinsic conductivities of $c = 10^{-6}$ S/m. It reflects a more realistic simulation of charging processes in dielectric semiconducting, semi-insulating, and insulating materials.

Thus, the electron-hole creation, their ballistic flight, followed by field-drift transport, superposed by a variable but small and limited intrinsic conduction cF , together with trapping in localized states and/or electron-hole recombination are taken into account. The experimentally accessible quantities of field assisted secondary electron emission $\sigma(t)$ as well as the resulting surface potential $V_0(t)$ (see Fig.1) due to internal currents $j(x,t)$, charges $\rho(x,t)$, field $F(x,t)$, and potential $V(x,t)$ distributions are obtained. The detailed results for semi-insulating materials are described in Ref. [3].

The surface potential V_0 can be measured directly in real time by the x-ray bremsstrahlung (BS) high energy edge, where the landing energy E_0^* of the electron beam is diminished by a negative surface potential: $E_0^* = E_0 + eV_0$, as demonstrated in Fig.1. The intrinsic electrical conduction current I_C is measured by the sample current mode

$I_{SC} = I_P + I_C$ where I_P presents the short-time dynamical displacements (polarization) current during charging and I_C the real steady-state dc-current due to an intrinsic electrical conductivity c . Thus the given Al_2O_3 ceramic samples approach an intrinsic electrical conductivity of $c \approx (10^{-10} - 10^{-8})$ S/m.

References

1. M. Touzin, D. Goeriot, C. Guerret-Piécourt, D. Juvé, D. Tréheux, and H.-J. Fitting, J. Appl. Phys. **99** (2006), 114110.
2. N. Cornet, D. Goeriot, C. Guerret-Piécourt, D. Juvé, D. Tréheux, M. Touzin, and H.-J. Fitting, J. Appl. Phys. **103** (2008), 064110.
3. H.-J. Fitting and M. Touzin, J. Appl. Phys. **110** (2011) 044111-1-10.

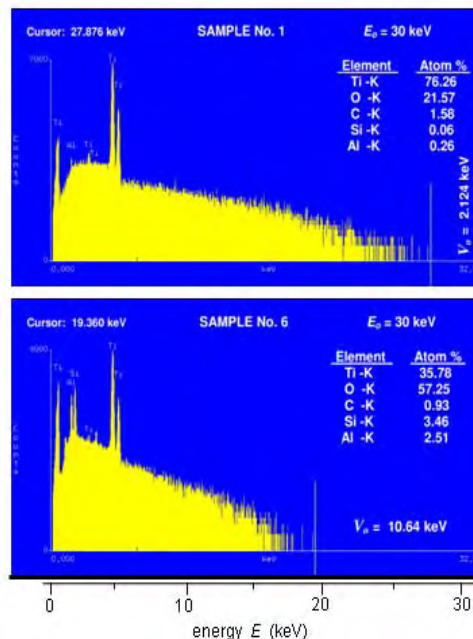


Fig. 1. Bremsstrahlung (BS) high energy edge measurements at $E_0 = 30$ keV showing the actual electron landing energies $E_0^* = E_0 + eV_0$ with the respective surface potentials $V_0 \approx -2.12$ kV (top) and -10.64 kV (bottom) for two Al_2O_3 ceramics of different compositions and with decreasing electrical conductivity c (higher internal resistance) of the second sample below.

New Materials for Neutron Shielding Based on Boron Enriched Unfired Phosphate Ceramics

S. Bellucci¹, P.P. Kuzhir², S.A. Maksimenko², K.N. Lapko³, V.A. Lomonosov³, O.A. Ivashkevich³,
A.I. Lesnikovich³, P.V. Sedyshev⁴, V.N. Shvetsov⁴, A.S. Kurilin⁴, L. Sartinska⁵, P. Silenko⁵,
G. Frolov⁵, Yu. Solonin⁵

¹INFN-Laboratori Nazionali di Frascati, Via E. Fermi 40, 00044 Frascati, Italy

²Research Institute for Nuclear Problems of Belarusian State University, 11, Bobruiskaya, Minsk 220030, Belarus

³Belarusian State University, 14, Leningradskaya, 220030Minsk, Belarus

⁴Joint Institute for Nuclear Research, 6 Joliot-Curie, 141980 Dubna, Moscow region, Russia

⁵Frantsevich Institute for Problems of Materials Science, NAS of Ukraine, 3 Krzhyzhanivsky Str., 03680 Kyiv, Ukraine

New multifunctional coatings with advanced performance and functional properties, combining neutron shielding properties of boron compounds with the outstanding heat resistance and mechanical strength of thermally stable phosphate composites produced at room temperatures, are discussed for nuclear physics applications.

Mechanical Properties of Nb₂O₅ and Ta₂O₅ Ceramics

M. Palatnikov¹, O. Shcherbina¹, V. Efremov¹, N. Sidorov¹, K. Bormanis²

¹Institute of Chemistry, Kola Science Centre RAS, Russia

²Institute of Solid State Physics, University of Latvia, Latvia

e-mail: palat_mn@chemy.kolasc.net.ru

Studies of mechanical characteristics of niobium and tantalum pentoxide ceramics obtained by conventional ceramics technology and exposed to concentrated light flow (CLF) in an optical furnace are reported. As a rule, ceramics of Nb₂O₅ and Ta₂O₅ refractory oxides obtained by conventional techniques are of macro-crystalline structure, extremely brittle and feeble, of weak plasticity and crack resistance limiting practical applications. Mechanical characteristics of the ceramics can be improved by advanced methods of treatment (for instance, by exposure to CLF) to obtain a material of the smallest scale (micro- and nano-meter) structure. Ceramic niobium and tantalum pentoxides subjected to CLF in an optical furnace are demonstrated to increase micro-hardness and mechanical characteristics such as strength, crack resistance and brittle hardness.

The strength of Nb₂O₅ and Ta₂O₅ ceramics is found increasing with the intensity of the CLF, reducing the size of the structures forming under the CLF. Mechanical characteristics of ceramics treated in optical furnace are likely due to the smaller size of forming structures increasing the volume fraction of the boundaries between the nano-structures (nano-cracks).

The Effect of Feed Charge Grain Size on the Electrical Characteristics of the $\text{Li}_{0.03}\text{Na}_{0.97}\text{Ta}_{0.05}\text{Nb}_{0.95}\text{O}_3$ Perovskite Ceramics

M. Palatnikov¹, V. Efremov¹, I. Efremov¹, O. Shcherbina¹, N. Sidorov¹, K. Bormanis²

¹Institute of Chemistry, Kola Science Centre RAS, Russia

²Institute of Solid State Physics, University of Latvia, Latvia

e-mail: palat_mn@chemy.kolasc.net.ru

A comparative evaluation of the microstructure and electrical characteristics of two ceramic samples of the ferroelectric $\text{Li}_{0.03}\text{Na}_{0.97}\text{Ta}_{0.05}\text{Nb}_{0.95}\text{O}_3$ ceramic solid solution obtained by conventional ceramic technology using feed charges preliminary ground in a ball mill to different grain sizes is presented. Analysis of the microstructure has revealed that the sample prepared from a charge with grain sizes of $d \leq 28 \mu\text{m}$ has the mean grain diameter of $\sim 6.53 \mu\text{m}$. The average grain size of ceramics from charge of particle sizes $28 \mu\text{m} \leq d \leq 63 \mu\text{m}$, is slightly larger, viz. $\sim 8.58 \mu\text{m}$. The electrical properties of the samples are strongly dependent on the grain size of the initial charge, regardless of identical chemical composition and regimes of synthesis. Thus, the dielectric permittivity of a sample obtained from charge of $d \leq 28 \mu\text{m}$ is lower over a wide range than compared with the sample obtained from particles of the size $28 \mu\text{m} \leq d \leq 63 \mu\text{m}$. The high-frequency dielectric permittivity ϵ_∞ reflecting the lattice contribution to dielectric response representing one of fundamental characteristics of the system is provided as a function of temperature $\epsilon_\infty(T)$.

The diagrams of admittance and impedance reveal two relaxation processes: a high-frequency one and a low-frequency. Within the ferroelectric phase, specific conductivity for both relaxation processes in the samples is quantitatively the same and has identical enthalpies of activation: 0.5 and 0.67 eV, respectively, for each of the contributions to the general pattern of conductivity. Upon passing the Curie point, within the paraelectric phase, the conductivity of the ferroelectric solid solution (FE SS) from feed charge particles of up to $28 \mu\text{m}$ increases a little in comparison with the FE SS from charge of particle sizes between 28 and $63 \mu\text{m}$. Simultaneously, the activation enthalpy of conductivity increases for both the relaxation processes. Actually, the difference of properties of the FE SS does not depend directly on the particle size of the feed charge but is rather due to possible emergence of component gradients at the diffusion stage and some difference in the composition in grains of different size likely significantly altering the structure and physical characteristics of a solid solution, especially the $\text{Li}_{0.03}\text{Na}_{0.97}\text{Ta}_{0.05}\text{Nb}_{0.95}\text{O}_3$ SS belonging to the region of the morphotropic ferroelectric-antiferroelectric phase transition.

Conoscopic Microscopy Studies of Optical Homogeneity of the LiNbO₃:Mg Crystals

M. Palatnikov¹, O. Pikuly², N. Sidorov¹, O. Makarova¹, K. Bormanis³

¹Institute of Chemistry, Kola Science Centre RAS, Russia

²Far-East State University of the Means of Communication, Khabarovsk, Russia

³Institute of Solid State Physics, University of Latvia, Riga, Latvia

e-mail: palat_mn@chemy.kolasc.net.ru

The current interest in methods improving measuring and control of the optical parameters of crystals is due to the importance of the quality of crystalline materials used in laser physics, recording systems, processing of optical data, and optical communication. The conoscopic technique since long is applied to analyse the optical properties determining the functional capabilities of crystals.

An essential modification of conoscopy is proposed in the presented study to observe figures on a larger scale by using a system wherein a diverging wide-aperture beam provided by a diffuser enters the crystal. The system, consisting of a polarizer, a diffuser, the crystal, and an analyzer, projects the conoscopic figures to the size of up to 0.5 m on a semi-transparent screen to be recorded by a digital camera. The large size of the image enables to analyze the fine features in both the centre and periphery of the visual field. The results of conoscopic examination of Mg-doped lithium niobate crystals: 0.01; 0.1; 0.25; 0.5; 1.0; and 1.5 mole% reveal a fairly high optical homogeneity of weakly doped samples containing 0.01 – 1.5 mole % of Mg, even from different crystals grown under different conditions. The scale of the conoscopic figure, intensity distribution, the shape and size of the Maltese cross, and the isochromatic lines of LiNbO₃:Mg crystals are found to be not changed upon the dopant concentration (Mg) between 0,01 and 1,5 mole % in samples with similar geometric parameters. At higher Mg contents (3.0 – 5.5 mole %) in lithium niobate samples basically remaining uniaxial local inclusions of double refraction are recorded as extra interfering figures on the background of the main conoscopic figure (both in the centre and periphery of the visual field). The largest limited anomalous bi-axial region is recorded in the case of 3.0 mole%, as proved by a rupture and blooming of the Maltese cross in the centre of the conoscopic figure of the crystal. Both defectiveness and degree of distortion of the conoscopic image of the crystal tend to diminish with increasing the dopant concentration from 3.0 to 5.5 mole% suggesting the applicability of the proposed technique of conoscopic examination to reveal even the minor changes in optical characteristics of crystals.

Influence of Lithium Substitution on Structure, Electric and Pyroelectric Properties of Sodium Niobate Ceramic

W. Śmiga¹, B. Garbarz-Glos¹, M. Livinsh², I. Smeltere²

¹Institute of Physics, Pedagogical University, Podchorążych 2, 30-084 Kraków, Poland

²Institute of Solid State Physics, University of Latvia, Kengeraga 8, LV-1063, Riga, Latvia

e-mail: mlivins@cfi.lu.lv

Ferroelectrics and antiferroelectrics are the materials most frequently used in practice. Among a number of well-known ferroelectric materials the perovskite-type structure ferroelectrics are most interesting. One of examples is a sodium niobate $Na^{+1}Nb^{+5}O_3$. Some solid solutions based on sodium niobate have very good piezoelectric properties, moreover, they contain no lead so they fulfil a very important demand of high technology industry concerning the reduction of environmental pollution. One of the most interesting and extensively studied systems is a sodium niobate-lithium niobate solid solution ($NaNbO_3$ - $LiNbO_3$). The $Li_{0.02}Na_{0.98}NbO_3$ ceramic sample was prepared by a conventional method in the Institute of Solid State Physics at University of Latvia in Riga. The X-ray measurements were made by means of Seifert equipment XRD-7. It was shown by XRD at room temperature that the structure of $Li_{0.02}Na_{0.98}NbO_3$ is of perovskite type, with a single phase of orthorhombic symmetry. From the analysis of the structural rentgenographic investigation the values of lattice parameters a , b , c and the volume of unit cell V were determined. The microstructure and EDS measurements were performed by means of a scanning electron microscope with field emission Hitachi S4700 and a microanalyses system Noran-Vantage. They revealed that the $Li_{0.02}Na_{0.98}NbO_3$ sample was perfectly sintered. It contained a little glassy phase and its grains were well shaped. The electric measurements were performed in heating and cooling processes at temperature ranging from 300K to 750K and frequency from 0.1kHz to 200kHz. It was shown that the dielectric behaviour of the investigated sample was sensitive to the frequency of the applied electric field. On the Arrhenius plot the local minima of electrical conductivity σ which are associated with a polaronic transport mechanism can be observed. The minimum values of this electrical conductivity are the result of the change in the nature of the conduction mechanism: from a tunnel into a hopping mechanism, from a short-range into a long-range mechanism. These measurements revealed that the a.c. conductivity changed with frequency according to the formula: $\sigma(\omega) = \sigma_{dc} + A\omega^n$ where $n < 1$. These results were discussed considering the conduction mechanism as a type of polaron hopping.

Ultrasonication as a Method of Investigation of the Mechanical Properties of Doped Hafnium Barium Titanate

B. Garbarz-Glos¹, W. Piekarczyk², W. Śmiga¹, M. Antonova³, I. Smeltere³

¹Institute of Physics, Pedagogical University, Podchorążych 2, Kraków

²Faculty of Materials Science and Ceramics, University of Science and Technology, Mickiewicza 30, Kraków

³Institute of Solid State Physics, University of Latvia, Kengeraga 8, LV-1063, Riga

e-mail: ilze.smeltere@cfi.lu.lv

The barium zirconium titanate samples $BaHf_xTi_{1-x}O_3$ ($0 \leq x \leq 35$) were prepared by a conventional ceramic technology. The room temperature X-ray powder diffraction profiles show a single phase with perovskite structure. The performed SEM and EDS studies reveal that the samples are perfectly sintered and the material is chemically homogeneous. The examined samples are of good quality, the grains are well shaped and there is a very small amount of a glassy phase. To determine the elastic constants (the Young's modulus E , the shear modulus G and the Poisson's ratio ν) of $BaHf_xTi_{1-x}O_3$ a method of measurement of the longitudinal (V_L) and transverse (V_T) ultrasonic wave velocities for this type of material was developed, as well as the selection of a suitable apparatus and ultrasonic heads was executed. The ultrasonic method is based on the measurement of a propagation velocity of ultrasonic waves in elastic media, where the velocity is a function of microstructure, elastic constants, density as well as the geometrical dimensions of the investigated material. The ultrasonic tests are repeatable and they can be taken on the samples of different shapes, sizes and compositions (phase and volume) in the different directions and places of the studied object. The ultrasonic measurements were performed on 11 samples of the following dimensions: the height (h) ranging from 4 to 6 mm and the diameter (Φ) from 14 to 15 mm. With the increase in hafnium content in the BHT the values of the velocity of the longitudinal and transverse ultrasonic waves increase. The largest average velocities 5758.3 m/s and 5472.5 m/s for UZP-1 and MT-541 apparatus respectively were obtained for the $BaHf_{0.30}Ti_{0.70}O_3$ sample. The values of both the Young's modulus and the shear modulus are the highest for BHT30 sample ($E = 147.7$ GPa and $G = 57.72$ GPa for both devices UZP-1 and MT-541). The measurements of the longitudinal wave velocity in the direction of the samples formation and in the perpendicular direction indicated a small anisotropy in $BaHf_xTi_{1-x}O_3$ solid solutions but its value did not exceed 3.8%. The tested samples should be treated as isotropic.

The Effect of BaTiO₃ on Dielectric and Ferroelectric Properties of Lead-Free Ceramics Based on KNN

I. Smeltere^{1,2}, M. Antonova¹, M. Livinsh¹, A. Kalvane¹, B. Garbarz-Glos³

¹Institute of Solid State Physics University of Latvia, Riga, Latvia

¹Biomaterials Innovation and development centre, Riga Technical University, Riga, Latvia

³Institute of Physics, Pedagogical University, Krakov, Poland

e-mail: ilze.smeltere@cfi.lu.lv

Alkali niobates are promising material for replacing lead containing piezoelectric ceramics. In the present work dielectric and ferroelectric properties of lead free KNN based ceramics have been studied. Compositions with a stoichiometric formula $(1-x)(K_{0.5}Na_{0.5})Nb_{1-y}Sb_yO_3-xBaTiO_3$ ($x=0.01, 0.015, 0.02, 0.04$; $y=0.04, 0.07$) were produced by solid state sintering method. Manganese oxide MnO₂ was used as a sintering aid. Presence of MnO₂ in the composition lowers the optimal sintering temperatures. The influence of BaTiO₃ on the density, microstructure, dielectric and ferroelectrical properties was investigated. X-ray diffraction analysis confirmed pure perovskite structure with no traces of secondary phase. However with increasing content of BaTiO₃ the cell changed from monoclinic to tetragonal at room temperature. The density of modified ceramic samples exceeds 4.5g/cm³ in comparison to 4.2g/cm³ for pure KNN. Microstructural investigation reveals that ceramic samples have homogenous structure with cubical grain shape and grain sizes of 0.4-2 μm. Phase transition point T_c is shifted to lower temperatures with increasing BaTiO₃ content in the composition. Phase transition peak at T_c is broad indicating the diffuse phase transition. The highest value of dielectric permittivity and Pr had the samples with 1 wt% of BaTiO₃. Mechanical properties determined by ultrasonic method revealed that the highest value of Young's modulus is for the sample with a formula 0.985NKNb_{0.96}Sb_{0.04}O₃-0.015BaTiO₃+0.5%MnO₂.

Phase Transitions in Li, K and Ag Modified $\text{Na}_{1/2}\text{Bi}_{1/2}\text{TiO}_3\text{-SrTiO}_3\text{-PbTiO}_3$ Solid Solutions

M. Dunce, E. Birks, M. Antonova, A. Sternberg
 Institute of Solid State Physics, University of Latvia, Latvia
 e-mail: marija.dunce@cfi.lu.lv

$\text{Na}_{1/2}\text{Bi}_{1/2}\text{TiO}_3\text{-SrTiO}_3$ is a well-known relaxor ferroelectric. The transfer from relaxor to normal ferroelectric state, passing various intermediate states, characteristic for relaxor ferroelectrics, was found in $\text{Na}_{1/2}\text{Bi}_{1/2}\text{TiO}_3\text{-SrTiO}_3\text{-PbTiO}_3$ solid solutions, if Pb content is increased. Particularly for $0.4\text{Na}_{1/2}\text{Bi}_{1/2}\text{TiO}_3\text{-0.4SrTiO}_3\text{-0.2PbTiO}_3$ the spontaneous transfer between relaxor and ferroelectric state at temperature T_1 is approaching the relaxing maximum of temperature dependence of dielectric permittivity at temperature T_m . As a result the relaxing state almost disappears.

In the present work the influence of monovalent metals (Me^{1+} : Li, K, Ag) on the properties of $0.4(\text{Na}_{1-x}\text{Me}^{1+}_x)_{1/2}\text{Bi}_{1/2}\text{TiO}_3\text{-0.4SrTiO}_3\text{-0.2PbTiO}_3$ solid solutions is studied in the concentration range till $x=0.25$. The x-ray diffraction results show that all obtained compositions are single-phase solid solutions with tetragonal symmetry. The concentration dependences of the unit cell parameters indicate that Me^{1+} ions in all cases substitute Na^{1+} ions in the A-site of the perovskite structure. The obtained compositions can be characterized by phase transition and dielectric properties, qualitatively similar to those of $0.4\text{Na}_{1/2}\text{Bi}_{1/2}\text{TiO}_3\text{-0.4SrTiO}_3\text{-0.2PbTiO}_3$. However their concentration dependences are mostly not monotonous. Na substitution by Li increases, while substitution with Ag decreases the temperatures of the dielectric permittivity maximum (T_m) and of the ferroelectric phase transition (T_1). The stability of the relaxor state, which can be characterized by the temperature $T_m\text{-}T_1$ difference, increases in case of substitution of Na by Li and decreases in case of substitution by Ag. Influence of K is weak in comparison with Li and Ag. The obtained results show rather small role of Me^{1+} in formation of ferroelectric properties in $0.4\text{Na}_{1/2}\text{Bi}_{1/2}\text{TiO}_3\text{-0.4SrTiO}_3\text{-0.2PbTiO}_3$.

Dynamics of Phase Transition in $0.4\text{Na}_{0.5}\text{Bi}_{0.5}\text{TiO}_3\text{-(}0.6\text{-X)}\text{SrTiO}_3\text{-xPbTiO}_3$ Solid Solutions

Š. Svirskas¹, M. Ivanov¹, Š. Bagdzevičius¹, J. Banys¹, M. Dunce², M. Antonova², E. Birks²,
A. Sternberg²

¹Vilnius University, Faculty of physics, Saulėtekio av. 9, III b., LT-10222 Vilnius, Lithuania

²Institute of Solid State Physics, University of Latvia, Kengaraga street 8, LV-1063 Riga, Latvia

e-mail: sarunas.svirskas@ff.stud.vu.lt

$\text{Na}_{1/2}\text{Bi}_{1/2}\text{TiO}_3$ (NBT) containing solid solutions is one of the most studied family of ferroelectric materials. It is well known that SrTiO_3 (ST) and PbTiO_3 (PT) act differently upon the NBT [1]. Strontium titanate enhances relaxor properties, while lead titanate increases characteristics of the 1st order phase transition.

Compositions of ternary solid solutions $0.4\text{NBT}\text{-(}0.6\text{-x)}\text{ST}\text{-xPT}$ represent various stages of the relaxor state, allowing to follow changes of physical properties depending on stability of the relaxor state.

Results of dielectric measurements, made for $x = 0\text{-}0.25$ in $35\text{-}500\text{K}$ temperature range and $0.01\text{ Hz}\text{--}40\text{ GHz}$ frequency range, are used to construct a distribution function of relaxation times and calculate the parameters of Vogel-Fulcher law. It is found that these parameters follow a simple trend depending on stability of the relaxor state.

The obtained phase diagram for $0.4\text{NBT}\text{-(}0.6\text{-x)}\text{ST}\text{-xPT}$ system of solid solutions is shown in Fig. 1.

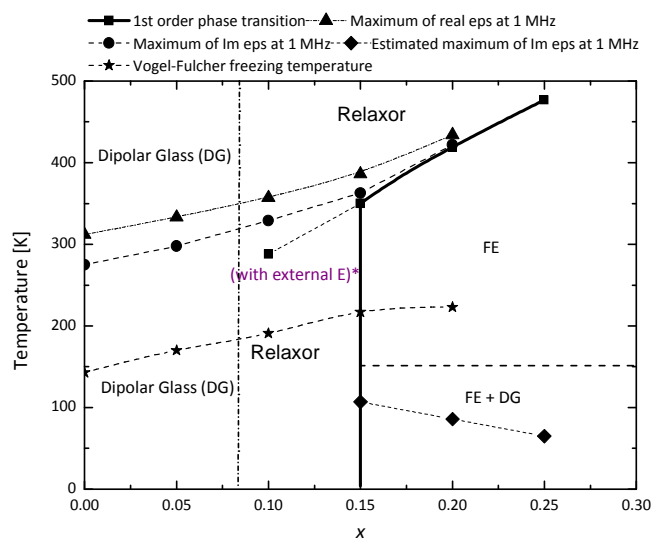


Fig. 1 Phase diagram of $0.4\text{NBT}\text{-(}0.6\text{-x)}\text{ST}\text{-xPT}$.

*indicates results taken from [2]

References

- Lee, J.-K.; Hong, K. S.; Kim, C. K.; Park, S.-E.; Phase transitions and dielectric properties in A-site ion substituted $(\text{Na}_{1/2}\text{Bi}_{1/2})\text{TiO}_3$ ceramics (A=Pb and Sr), *J. Appl. Phys.* 91 (7) (2002)
- Birks, E., Dunce, M., Antonova, M. and Sternberg, A., Phase transitions in modified $\text{Na}_{1/2}\text{Bi}_{1/2}\text{TiO}_3\text{-SrTiO}_3$ solid solutions, *Physica Status Solidi C*, 6 (12) (2009)

Investigation of Ferroelectric Phase Transition in $\text{Ba}_2\text{Nd}_{(1-x)}\text{Pr}_{(x)}\text{FeNb}_4\text{O}_{15}$ Ceramics Using Ultrasonic Spectroscopy

M. Kinka¹, V. Samulionis¹, M. Albino², E. Castel², M. Josse², S. Bagdzevicius¹, R. Grigalaitis¹,
J. Banys¹, M. Maglione²

¹Faculty of physics, Vilnius university, Lithuania

²CNRS, Université de Bordeaux, ICMCB-CNRS, France

e-mail: martynas.kinka@delfi.lt

Tetragonal Tungsten Bronze (TTB) structure allows solid state chemists to perform a wide range of substitutions triggering various ferroic properties. Recently, the family of $\text{Ba}_2\text{LnFeNb}_4\text{O}_{15}$ (Ln = La, Pr, Nd, Sm, Eu, Gd) TTB niobates has been identified as a unique room temperature multiferroic composite system in which ferroelectric and magnetic properties evolve with respect to a unique crystal-chemical parameter [1]. Besides the multiferroic aspect, unexpected dielectric behaviours were also discovered in this family of TTBs. In the $\text{Ba}_2\text{Pr}_x\text{Nd}_{1-x}\text{FeNb}_4\text{O}_{15}$ solid solution, while for the unsubstituted Nd and Pr compounds, purely ferroelectric and relaxor behaviours were observed, a coexistence of ferroelectric and relaxor behaviours was found in all the substituted samples [2]. The associated phase transition sequence “paraelectric–ferroelectric–relaxor states” upon cooling, already observed in perovskite systems, is still controversial in the literature [3].

We have investigated elastic properties of $\text{Ba}_2\text{Pr}_x\text{Nd}_{1-x}\text{FeNb}_4\text{O}_{15}$ solid solution family using ultrasonic spectroscopy. This method is a non-destructive technique and is very useful for identification of the phase diagram, as it can characterize all kinds of phase transitions - magnetic, ferroelectric, ferroelastic and etc. We have studied the temperature dependence of the longitudinal ultrasonic velocity and ultrasonic attenuation. In addition our ultrasonic method allowed us to investigate piezoelectric sensitivity of these TTB ceramics. The experiments showed small anomalies of ultrasonic velocity and attenuation with heating-cooling temperature hysteresis, dependent on the thermal history of samples. The piezoelectric sensitivity which was observed in low temperature phase confirmed the existence of the polar phase e.g the ferroelectric phase transition in $\text{Ba}_2\text{NdFeNb}_4\text{O}_{15}$ material and their solid solutions with $\text{Ba}_2\text{PrFeNb}_4\text{O}_{15}$.

References

1. M. Josse, O. Bidault, F. Roulland, E. Castel, A. Simon, D. Michau, R. Von der Muhll, O. Nguyen and M. Maglione, *Solid State Sci.* **11**, 1118 (2009)
2. E. Castel, M. Josse, D. Michau and M. Maglione, *J. Phys.:Condens. Matter*, **21**, 452201 (2009)
3. V.A. Stephanovitch, *J. Phys. Condens. Matter.*, **22**(23), 235902 (2010)

Dielectric Properties of CoFe_2O_4 and NiFe_2O_4 Ceramics

M. Kinka¹, K. Bormanis², A. Kalvane², V. Samulionis¹

¹Faculty of physics, Vilnius university, Lithuania

²Institute of Solid State Physics, University of Latvia, Riga, Latvia

e-mail: martynas.kinka@delfi.lt

Spinel ferrites CoFe_2O_4 and NiFe_2O_4 are magnetic oxides, possessing high magnetic ordering temperatures and large saturation magnetizations, which make them very attractive for a wide range of applications. Recently, special interest has been paid to the possible use of spinel ferrites as magnetic components in the design of artificial multiferroic heterostructures and composite materials [1]. Furthermore, they have been shown to exhibit interesting magnetic properties in the nanocrystalline form compared with those of the micrometre-size grains [2]. Despite the growing number of publications addressing the properties of small size ferrite structures (thin films, nanoparticles, etc.), few reports are available in the literature on the electrical conductivity and dielectric properties of bulk CoFe_2O_4 and NiFe_2O_4 . The dielectric properties of these ferrites are dependent on several factors, such as the method of preparation, sintering temperature, sintering time and chemical composition.

We have investigated CoFe_2O_4 and NiFe_2O_4 ceramics prepared by conventional ceramic technology. Powders of CoFe_2O_4 and NiFe_2O_4 were synthesized from the corresponding oxides by solid phase thermal chemical reactions. Dielectric properties were measured in the 20 Hz – 1 MHz frequency range starting from 120 K and reaching temperatures above magnetic phase transitions. Dielectric responses of characteristic shape, caused by electrical conductivity, common for both investigated materials were obtained. Two conductivity processes were distinguished with Arrhenius behaviors of σ_{DC} and possible underlying mechanisms of charge transport are discussed.

References

1. J. Ryu, S. Priya, K. Uchino and H. Kim, Journal of Electroceramics, **8**, 107 (2002)
2. I. P. Suzdalev, Russian Chemical Reviews **78** (3), 249 - 282 (2009)

Dielectric Properties of $0.98\text{Pb}(\text{Mg}_{1/3}\text{Nb}_{2/3})\text{O}_3 - 0.02\text{La}(\text{Mg}_{2/3}\text{Nb}_{1/3})\text{O}_3$ Crystal

D. Jablonskas¹, R. Grigalaitis¹, J. Banys¹, Z.G. Ye², A.A. Bokov²

¹Vilnius University, Faculty of Physics, Lithuania

²Department of Chemistry, Simon Fraser University, Burnaby, British Columbia, Canada

e-mail: dziugas.jablonskas@ff.stud.vu.lt

A-site La^{3+} -doping has been found to be an effective way to enhance B-site cation order in PMN ABO_3 perovskite structure [1]. However, it is not clear how the chemically ordered regions affect the dynamics of polar nano regions (PNRs). Thus the investigations of broadband dielectric properties of $0.98\text{Pb}(\text{Mg}_{1/3}\text{Nb}_{2/3})\text{O}_3 - 0.02\text{La}(\text{Mg}_{2/3}\text{Nb}_{1/3})\text{O}_3$ (PLMN) crystal promotes the deeper understanding of the mechanisms of relaxor behavior and PNRs dynamics.

The dielectric properties of PLMN crystal were observed in frequency range of 100 Hz – 48 GHz and in temperature range of 110 K – 500 K. The sample was heated to 500 K temperature in order to eliminate “memory effects” – disarrange “frozen” PNRs. The measurements of dielectric permittivity took part in freezing cycle with 1 K/min temperature drop rate. Fig. 1 shows the temperature dependency of complex dielectric permittivity.

The peak of $\varepsilon'(T)$ goes towards higher temperatures with increase of frequency. This is common behavior of FR and is caused by the broad distribution of PNR relaxation times. The dispersion of complex dielectric permittivity $\varepsilon^*(f)$ was fitted with Cole – Cole formula, which describes the conventional relaxation process rather well. Although, another dispersion was found in frequencies $f < 1$ kHz, which requires further investigations. The temperature dependency of mean relaxation time τ can be described with Vogel – Fulcher formula, which showed that the dynamic of the system slow down critically at temperature $T_f = 191$ K.

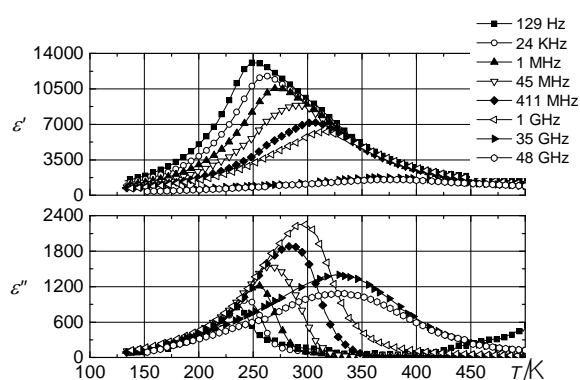


Fig.1 Temperature dependency of complex dielectric permittivity of PLMN single crystal

References

1. X. Long, A. A. Bokov, Z-G. Ye, W. Qu, X. Tan, J. Phys.: Condens. Matter **20** 015210 (2008)

Dielectric properties of $\text{Pb}(\text{Fe}_{2/3}\text{W}_{1/3})\text{O}_3 + 1\% \text{MnO}_2$ ceramics

R. Mackeviciute¹, J. Banys¹, J.A. Eiras²

¹Vilnius University, Faculty of physics, Saulėtekio av. 9, III b., LT-10222 Vilnius, Lithuania

²Grupo de Cerâmicas Ferroelétricas, Departamento de física, Universidade Federal de São Carlos, Brazil

e-mail: Rūta.Mackevičiūtė@ff.stud.vu.lt

Recently, there is a great interest in multiferroics – materials which in certain temperature range are ferroelectrics and ferromagnetics. One of the most popular multiferroics are lead – iron tungsten $\text{Pb}(\text{Fe}_{2/3}\text{W}_{1/3})\text{O}_3$ and bismuth ferrite BiFeO_3 . These multiferroics could be used in microelectronics, for example, producing MERAM memories.

In order to produce high quality samples, a modified B-site precursor method was proposed as an effective method to obtain a pure perovskite phase in lead-based ceramics [1]. $\text{Pb}(\text{Fe}_{2/3}\text{W}_{1/3})$ ceramic was prepared using this method. Dielectric measurements were performed at (110 – 500) K temperature range and in 20 Hz – 40 GHz frequency band. Measurements were performed during cooling cycle with temperature variation rate of about 1 K/min.

Figure 1 shows the temperature dependence of the real and imaginary parts of dielectric permittivity of PFW+1%MnO₂ ceramic. We observe the anomaly of dielectric permittivity which is typical for ferroelectric relaxors at temperatures below 300 K: peaks of dielectric permittivity move to higher temperature with increasing frequency with frequency independent losses observed at temperatures below 120 K.

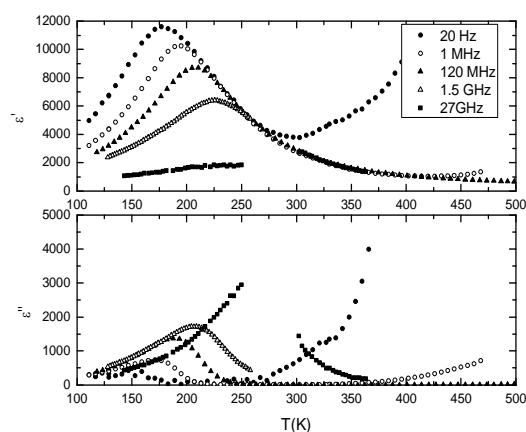


Fig.1 Temperature dependence of the real and imaginary parts of dielectric permittivity of PFW+1%MnO₂ ceramic.

References

1. J. A. Eiras, B. M. Fraygola, D. Garcia, Structural and Dielectrics Properties of $(1-x)\text{Pb}(\text{Fe}_{2/3}\text{W}_{1/3})\text{O}_3-x\text{PbTiO}_3$ Ceramics, *Key Engineering Materials* **434-435**, 307-310 (2010).

Dielectric Spectra of Relaxor PMN-PT Ceramics

R. Grigalaitis¹, J. Banys¹, A. Brilingas¹, K. Bormanis², A. Sternberg²

¹Faculty of Physics, Vilnius University, 9 Sauletekio str., 10222 Vilnius, Lithuania

²Institute of Solid State Physics, University of Latvia, 8 Kengaraga str., 1063 Riga, Latvia

e-mail: robertas.grigalaitis@ff.vu.lt

Relaxor ferroelectric (RFE) single crystals and ceramics $(1-x)\text{Pb}(\text{Mg}_{1/3}\text{Nb}_{2/3})\text{O}_3-x\text{PbTiO}_3$ (PMN-PT) have attracted a huge amount of attention over the last years. Properly manufactured and oriented, they have piezoelectric coefficients which are the highest yet reported, with electromechanical deformations one order of-magnitude larger than those of conventional high piezoelectric $\text{PbZrO}_3\text{-PbTiO}_3$ PZT materials [1]. Such properties make them very attractive for next generation sensors and actuators and much work is currently being done to implement PMN-PT solid solutions in underwater hydrophones, ultrasonic transducers, etc. These materials are also important from the fundamental point of view. Four characteristic regions having different crystallographic symmetry and accordingly different physical properties can be distinguished in PMN-PT family solid solutions [2]. While the region near the morphotropic phase boundary is under active research, $(1-x)\text{Pb}(\text{Mg}_{1/3}\text{Nb}_{2/3})\text{O}_3-x\text{PbTiO}_3$ with small x content still lacks a comparable interest. Thus, the aim of this work was the broadband dielectric spectroscopy of small x PMN-PT compounds.

Dielectric permittivity measurements of $(1-x)\text{Pb}(\text{Mg}_{1/3}\text{Nb}_{2/3})\text{O}_3-x\text{PbTiO}_3$ ($x \leq 0.1$) ceramics were performed at frequencies ranging from Hz to GHz range by several techniques: HP4284 impedance analyzer, AGILENT 8718ET network analyzer and by a set of some built rectangular waveguide transmission lines. Obtained results showed broad frequency dispersion below 400 K. The anomaly of dielectric permittivity shifts to the region of lower temperatures with decreasing the frequency of measurement. The frequency dependencies have shown behaviour, typical for RFE. Calculated distributions of relaxation times are composed from two overlapped peaks at short and much longer relaxation times. The peaks at short relaxation times can be attributed to the contribution of individual dipoles and these at long relaxation times to the contribution of polar nano regions.

References

1. S.-E. Park and T.R. Shrout, *J. Appl. Phys.* **82**, 1804 (1997)
2. B. Noheda, D. E. Cox, G. Shirane, Z.-G. Ye, and J. Gao, *Phys.Rev. B* **66**, 054104 _2002_.

Dopant (Mn, Co, Fe) Effects on the Structure and Dielectric Properties in (Ba, Pb)TiO₃ Ceramics

A. Plaude, K. Kundzins, A. Kalvane, V. Dimza

Institute of Solid State Physics, University of Latvia

e-mail: vilnis.dimza@cfi.lu.lv

The most popular ferroelectrics under consideration for the technical applications are perovskite oxides represented by AB₃ structure. They are very sensitive to electric fields, temperature, defects, and dopants.

Regardless of a lot of studies having been made, the microscopic nature of the dopants (as 3d elements: Mn, Fe, Co) effects is still unclear.

In this work the structural and dielectric properties of (Ba_{1-x}, Pb_x)TiO₃ + Me (x=0; 0,05; 0,2 and Me=0,001; 0,01; 0,1 wt. % of Mn, Fe, Co) ceramics were investigated by:

- 1) dielectric spectroscopy ($\epsilon(f,T)$ in temperature ($T=20-400^\circ\text{C}$) and frequency ($f=10^2-10^6\text{ Hz}$) range),
- 2) room temperature scanning electron microscopy (SEM), XRD analysis, electron paramagnetic resonance (EPR), Raman spectroscopy.

A doping causes following changes in dielectric behaviour of (Ba, Pb)TiO₃ + Me:

- 1) decreasing of ϵ_{max} value, which is due to decreasing of contribution of high frequency mechanisms, simultaneously increasing the role of low frequency mechanisms
- 2) increasing of diffuseness of $\epsilon(T)$;
- 3) increasing of the $T_{\text{max}\epsilon}$ only for Mn, Co, but for Fe - even decreasing of the $T_{\text{max}\epsilon}$;

XRD patterns show following changes:

- 1) increasing of ratio of diffraction maxima 210/211;
- 2) asymmetric broadening of diffraction maxima.

The micromechanisms of doping effects are discussed.

The Changes of Relaxor Behaviour of PLZT8/65/35 Ceramics at Doping with 3d Elements

L. Kundzina, M. Kundzins, K. Kundzins, A. Plaude, M. Livins, M. Antonova, V. Dimza

Institute of Solid State Physics, University of Latvia

e-mail: marisk@latnet.lv

The PLZT 8/65/35 compound, commonly known for relaxor behaviour, doped with 3d elements (Cr, Mn, Fe, Co, Ni, Cu) is being studied.

A number of different techniques being used:

- 1) measure of complex dielectric permittivity $\epsilon^* = \epsilon' - i\epsilon''$ in temperature ($T=20-400^\circ\text{C}$) and frequency ($f=10^2-10^6\text{Hz}$) range;
- 2) x-ray diffraction (XRD), Raman scattering, EPR and Electron Microscopy Studies (Fracture Mode Behaviour).

At doping were found changes in $\epsilon(f, T)$ behavior:

- 1) increasing the $T_{\max\epsilon}$ of $\epsilon(T)$;
- 2) ϵ_{\max} value: decreasing for Mn doping, increasing for Fe, Co doping;
- 3) diffuseness of $\epsilon(T)$: broadening for Mn doping, sharpening for Co, Fe doping;
- 4) depth of dispersion (relaxation effect),

and in XRD:

- 1) decreasing of unit cell volume;
- 2) increasing of ratio of diffraction maxima 210/211;
- 3) appearance of likely monoclinic distortion.

According to our studies, the magnitude of most of the dopant-induced effects follows the sequence $\text{Mn} > \text{Fe} > \sim \text{Co}$ or $\text{Co} > \sim \text{Fe} > \text{Mn}$.

The micromechanisms of doping are being discussed now.

Physical Properties of $Ba_{0.95}Pb_{0.05}TiO_3+0.1\%Co_2O_3$ Ceramic

R. Bujakiewicz-Korońska¹, A. Kalvane², B. Garbarz-Głos¹, A. Suchocki³ Y. Zhydachevsky³,

W. Śmiga¹, L. Vasylechko⁴, A. Kamińska³, D. Sitko¹

¹Institute of Physics, Pedagogical University, Podchorążych 2, 30-084 Kraków, Poland

²Institute of Solid State Physics, University of Latvia, Kengeraga 8, LV-1063, Riga, Latvia

³Institute of Physics, Polish Academy of Sciences, Lotników 32/46, 02-668 Warszawa, Poland

⁴Max Planck Institute, Dresden

e-mail: anna.kalvane@cfi.lu.lv

The $Ba_{0.95}Pb_{0.05}TiO_3+0.1\%Co_2O_3$ ceramic were prepared by a conventional ceramic technology. A single-phase perovskite structure of the investigated ceramic was identified by the X-ray diffraction method. The performed SEM, EDS and EPMA studies reveal that the samples are perfectly sintered and the material was chemically homogeneous. The examined samples are of good quality, the grains are well shaped without a glassy phase. For the measurements of dielectric properties a computerised automatic system based on LCR 821 meter was used. The investigations were made in the frequency range from 1 kHz to 200 kHz with amplitude 2 kV/m as a function of temperature. A differential scanning calorimetry (DSC) measurement was carried out using a DSC 200 F3 Netsch apparatus. The results for the tested sample were compared to the DSC outcomes obtained for the original $BaTiO_3$ sample. All obtained results pointed out the diffused character of a phase transition. The reflectance spectroscopy made on UV-VIS-NIR Cary 5000 spectrophotometer was helpful in the determination of the energy gap. The performed measurements showed that the addition of lead (Pb) and cobalt (Co) strongly influences the physical properties of pure barium titanate particularly the phase transition.

Magnetic Properties and Microstructure of Modified Lead Ferrotantalate Ceramics

O. Malyshkina¹, R. Grechishkin¹, E. Kaplunova¹, A. Ivanova¹, K. Bormanis², A. Kalvane²

¹Tver State University, Russia

²Institute of Solid State Physics, University of Latvia, Latvia

e-mail: Olga.Malyshkina@mail.ru

The coexistence of ferroelectric and magnetic orders is pushing a number of research fronts in the area of multiferroic materials because of their promise in the realization of new types of electronic devices. Of special interest are some unusual perovskite-type oxide materials including magnetic elements (Feibig M., J. Phys. D, 2005). Lead ferrotantalate $\text{PbFe}_{0.5}\text{Ta}_{0.5}\text{O}_3$ (PFT), being one of the group, is a ferroelectric exhibiting a diffuse phase transition and antiferromagnetic ordering occurring at low temperatures. In the present study we examine the effect of aliovalent substitutions with lead titanate PbTiO_3 (PTO) on the microstructure and electromagnetic properties of PFT / PTO compounds. Standard ceramics technology (sintering, firing) were used for the sample preparation.

Shown in Fig. 1 are secondary electron SEM images of single phase PFT and 0.8 PFT/0.2 PTO ceramics demonstrating polycrystalline microstructure of both samples. Modification by PTO significantly decreases the grain size. X-ray microanalysis confirmed the assumed chemical composition. Specific saturation magnetization measurements in a field of 1.2 T gave a negligible value of $\sigma_s < 1$ emu/g typical of antiferromagnetic, weak ferromagnetic or paramagnetic ordering of pure PFT, while unexpectedly high $\sigma_s = 16$ emu/g values characteristic of ferro- or ferrimagnetic ordering were measured for 0.8 PFT/0.2 PTO. The extra observed moment may be explained by the ferrimagnetic arrangement of Fe^{2+} and Fe^{3+} ions in the modified PFT compounds.

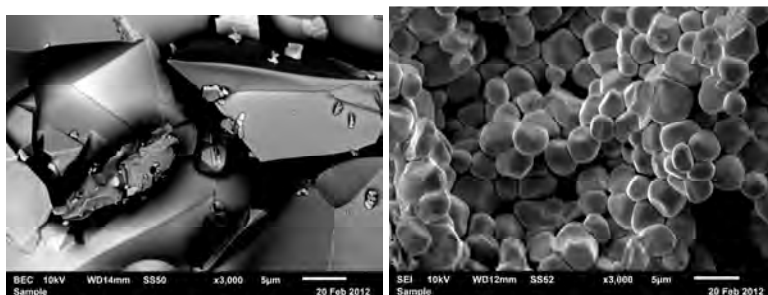


Fig.1 SEM images of the fracture surface of PFT (left) and 0.8 PFT/0.2 PTO (right) ceramic samples

Acknowledgements

This work was performed within the Federal Target Program "Research and Research-Pedagogical Personnel of Innovation Russia for 2009-2013" and was supported by the Shared Service Centre of Tver State University.

Static Analysis of Piezoelectric Composite Structure Based on Thermal Analogy Method

A. Kovalovs, S. Rucevskis, E. Barkanov

Institute of Materials and Structures, Riga Technical University, Latvia

e-mail: sandris_r@bf.rtu.lv

The thermal analogy is presented to predict the static behaviour of composite rotor blade with distributed piezoelectric Macro-Fiber Composite actuators. Based on the analogy between the converse piezoelectric effect and thermoelastic effect, an applied electric field is modelled as a thermal load and piezoelectric coefficients characterizing an actuator are introduced as thermal expansion coefficients.

The application of this method is discussed using a cantilever composite rotor blade with surface bonded Macro-Fiber composite actuators. The results in terms of static response obtained from the model based on thermal analogy are compared with the results of experiment by German Aerospace Centre (DLR). DLR developed a demonstrator blade with a rotor radius 2 m. The helicopter rotor blade consists of C-spar made of unidirectional glass-fiber reinforced plastic (UD GFRP), skin made of $\pm 45^{\circ}$ GFRP, foam core and MFC actuators.

The experimental twist deformation of blade is obtained using MFC embedded in the composite blade construction. These actuators are situated at the top and bottoms of helicopter rotor blades and oriented at $\pm 45^{\circ}$ to the spanwise axis of the rotor blade. Electric field activates the piezoelectric effect in the piezoceramic fibers of MFC, which elongate along the length of fibers and thus distribute a twisting movement along the blade.

Modelling a voltage actuation with a piezoelectric Macro-Fiber Composite actuators based on the thermal analogy was performed in ANSYS finite element program. The finite element model of rotor blade was built using ANSYS two different types of elements: linear layered structural shell elements SHELL 99 and structural solid elements SOLID 186, which was used to model the different components of blade. The rotor blade skins and MFC are modelled by shell elements (SHELL99) and foam with 3D 20-node structural solid elements (SOLID186). The spar is modelled by shell and solid elements.

Excellent agreement is observed and it is concluded that the use of thermal analogy to simulate the static behaviour of piezoelectric structures leads to promising results.

Extractive-Pyrolytic Method for FePt Alloy Production

V. Serga¹, L. Kulikova¹, M. Maiorov², A. Krumina¹, A. Cvetkov¹

¹Institute of Inorganic Chemistry, Riga Technical University, Latvia

²Institute of Physics, University of Latvia

e-mail: vera_serga@inbox.lv

Synthesis based on decomposition of iron pentacarbonyl $\text{Fe}(\text{CO})_5$ and reduction of platinum acetylacetonate $\text{Pt}(\text{acac})_2$ is widely used to produce FePt nanoparticles[1]. To transfer FePt nanoparticles from the low-anisotropy face-center-cubic (FCC) phase to the high-anisotropy face-center-tetragonal (FCT) phase, thermal treatments above 600 °C are necessary [2]. To prevent oxidation, it is necessary to rapidly anneal in Ar.

In the present work, possibilities of the extractive-pyrolytic method to produce FePt with the FCT phase were studied. The performed investigations show that if an equimolar mixture of solutions of iron caproate $\text{Fe}(\text{C}_6\text{H}_{11}\text{O}_2)_2$ in caproic acid and tri-n-octylammonium hexachloroplatinate $[(\text{C}_8\text{H}_{17})_3\text{NH}]_2\text{PtCl}_6$ in toluene (Fe:Pt = 1:1) produced preliminary by metal extraction from aqueous solutions, is used as a precursor, then due to XRD phase analysis data, as a result of pyrolysis in air ($T_{\text{pyr}} = 500$ °C, $t_{\text{annil}} = 5$ min), no formation of FePt alloy takes place. The obtained sample contains pure Pt with the FCC phase and hematite $\alpha\text{-Fe}_2\text{O}_3$.

If a fine-disperse powder of carbonyl iron is used in the initial mixture instead of the solution of iron caproate, the thermal treatment ($T_{\text{pyr}} = 600$ °C, $t_{\text{annil}} = 30$ min) results in the formation of FePt with the FCT phase ($a = 3.857$, $c = 3.726$). The final product contains admixture phases as well. The composition of these phases is determined by the content of metals (mol%) in the precursor: Fe50%Pt50% composition - hematite, $\text{Fe}_{0.14}\text{Pt}_{0.86}$ and $\text{Pt}_x\text{Fe}_{1-x}$ with $x = 0.25\text{-}0.55$; Fe60%Pt40% composition – FePt_3 , maghemite $\gamma\text{-Fe}_2\text{O}_3$ and hematite; Fe80%Pt20% composition – hematite and wustite FeO . If the content of Fe is more than 50%, the FeCl_2 phase appears in the final products. If the content of Fe is 40 mol%, then, along with FePt with the FCT phase ($a = 3.853$, $c = 3.713$), the formation of FePt with the FCC phase ($a = 3.816$) occurs as well as Fe_3Pt and $\text{Fe}_{0.65}\text{Pt}_{0.35}$. The magnetic measurements show (Fig. 1) that the coercivity decreases with the increasing Fe concentration from 50 to 80 mol%.

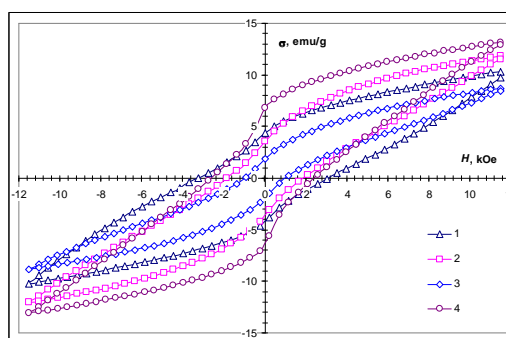


Fig. 1. Hysteresis loops of the FePt compositions: 1- Fe50%Pt50%; 2 - Fe60%Pt40%; 3- Fe80%Pt20%; 4 - Fe40%Pt60%.

References

1. S. Sun, C.B. Murray, D. Weller, L. Folks, A. Moser, Science, 289, 1989 (2000)
2. D. Li, N. Poudyal, V. Nandwana, Z. Jin, K. Elkin, J.P. Li, J. Appl. Phys., 99, 08E911 (2006)

Relaxing Polar Nanoregions and Creeping Domain Walls in the Strontium-Barium Niobate Uniaxial Relaxor Crystal

J. Dec¹, W. Kleemann², V.V. Shvartsman³, T. Łukasiewicz⁴

¹Institute of Materials Science, University of Silesia, PL-40-007 Katowice, Poland

²Applied Physics, Duisburg-Essen University, D-47048 Duisburg, Germany

³Institute of Materials Science, Duisburg-Essen, D-45141 Essen, Germany

⁴Institute of Electronic Materials Technology, PL-01-919 Warsaw, Poland

The lead free, environmentally friendly tungsten-bronze type uniaxial ferroelectric material strontium barium niobate, $\text{Sr}_x\text{Ba}_{1-x}\text{Nb}_2\text{O}_6$ (SBN100 x) bears a high potential for a variety of applications, particularly in the fields of pyroelectricity, piezoelectricity, electro-optics, photorefractive and nonlinear optics. These compounds take a particular place among the ferroelectrics, since by changing the ratio between the strontium and barium components one may tune the system from conventional ferroelectric ($x < 0.5$) to relaxor behavior ($x > 0.6$) while keeping the structure unchanged.

Investigations of the linear dielectric response measured in the frequency range $10^{-2} \leq f \leq 10^5$ Hz along the polar c -axis of eleven single crystalline SBN compounds with nominal concentration $0.26 \leq x \leq 0.80$ reveal a gradual crossover from ferroelectric (SBN26) to relaxor (SBN80) behavior. Analysis of these data within the framework of activated dynamic scaling shows that the Curie points of the ferroelectric compounds lie on a linear extrapolation of the "estimated" phase transition temperatures determined for the other SBN crystals. Correspondingly, a change from "normal" compact domains (SBN40) to the smaller ones with jagged (fractal-like) boundaries was revealed by piezoresponse force microscopy.

In the case of the composition SBN80, which reveals utmost relaxor behavior, the relaxation of polar nanoregions (PNRs) reveals a distinct anisotropic breathing mode when approaching the structural phase transition, $T_C \approx 290$ K, on cooling. Two distinct dispersion steps and peaks, respectively, of the complex susceptibility components in the milli- and megahertz frequency range reflect their large length-to-width aspect ratio.

Acknowledgements

Thanks are due to the Polish Ministry of Science for financial support under grant No. N N507 455034.

Influence of Laser Radiation on Electrical Properties of CdZnTe Crystal

A. Medvid¹, A. Mychko¹, E. Dauksta¹, E. Dieguez², H. Bensalah²

¹Riga Technical University, Riga, Latvia

²Universidad Autónoma de Madrid, Madrid, Spain

e-mail: edvins.dauksta@gmail.com

Cadmium telluride (CdTe) and cadmium zinc telluride (CdZnTe) compound semiconductor crystal has been shown to be the most promising materials for X-ray and gamma ray detectors [1, 2]. It is due to possibility to use this material at room temperature. However, the yield of high-quality crystals is still limited due to presence of Te inclusions, crystal twins, dislocations, grain boundaries and other defects.

Several researchers have shown a possibility to improve crystal quality by CO₂ laser irradiation [3, 4]. The disadvantages of this method are long processing time - about 100 h and damage of crystal the surface.

We have studied the influence of weakly absorbed laser radiation on CdZnTe crystal electrical properties and radiation detector parameters.

CdZnTe crystal was grown by vertical gradient freezing method using high-purity Cd, Zn and Te. Grown crystal had high concentration of non-controllable impurities and Te inclusion. Infrared microscopy was used to characterize concentration of Te inclusions. CdZnTe samples where irradiated by Nd:YAG laser and afterwards current voltage (I-V) characteristic measurements were performed. I-V characteristic showed that the sample resistivity increased after irradiation by 700 laser pulses at intensity 6.6 MW/cm². Treatment by higher intensity laser radiation leads to damage of the opposite side of the crystal. This effect is more pronounced with higher Te inclusion concentration. Moreover, scanning electron microscopy did not show any changes of chemical composition.

CdZnTe samples performed as a better radiation detector after laser treatment due to reduction of leakage current by 30% and improved spectral energy resolution, especially at low quantum energies.

References

1. T. E. Schlesinger, J. E. Toney, H. Yoon, YE. Lee, B. A. Brunett, L. Franks, R. B. James, *Mat. sci. eng. R*, **32**, 103 (2001)
2. F. Lebrun. *Nucl. instrum. meth.*, A. **563**, 200 (2006)
3. M. Meier, M. J. Harrison, S. Spalsbury, D. S. McGregor, *J. cryst. growth*. **311**, 4247 (2009)
4. S. V. Plyatsko, L. V. Rashkovetskyi, *Semiconductors+*, **40**, 287 (2006)

Microstructure and Mechanical Properties of High-Pressure $\text{Li}_x\text{Na}_{1-x}\text{Ta}_y\text{Nb}_{1-y}\text{O}_3$ Solid Solution Perovskite Ceramics

K. Bormanis¹, M.N. Palatnikov², O.B. Scherbina², V.V. Efremov², N.V. Sidorov², I.N. Efremov²

¹Institute of Solid State Physics, University of Latvia, Riga, Latvia,

²I.V. Tananaev Institute of Chemistry, Kola Science Centre RAS, Apatity, Russia

e-mail: bormanis@cfi.lu.lv

The perovskite structure of $\text{Li}_x\text{Na}_{1-x}\text{Ta}_y\text{Nb}_{1-y}\text{O}_3$ solid solutions (SS) allows for different deformations inducing complex and diverse of properties, a number of concentration-induced phase transitions including ferroelectric and anti-ferroelectric, and determining existence of morphotropic regions. All of it generates internal strain, particularly in ceramics, affecting elastic properties of polycrystalline samples.

The presented study concerns effects of the temperature of synthesis and proportions of the components on microstructure of high-pressure $\text{Li}_x\text{Na}_{1-x}\text{Ta}_y\text{Nb}_{1-y}\text{O}_3$ solid solution perovskite ceramics ($x = 0.12, 0.17$; $y = 0$; $y \geq 0.5$). Original results on elastic properties of high-pressure $\text{Li}_x\text{Na}_{1-x}\text{Ta}_y\text{Nb}_{1-y}\text{O}_3$ ($x = 0.17$; $0 \leq y \leq 0.5$) solid solutions measured by contact probe techniques are reported. The high-pressure $\text{Li}_x\text{Na}_{1-x}\text{Ta}_y\text{Nb}_{1-y}\text{O}_3$ SS ceramics is mainly composed of isomorphic grains the shape of which is characteristic to perovskite structure compliant with rhombic unit cell symmetry. Increasing the temperature at which the $\text{Li}_{0.17}\text{Na}_{0.83}\text{Ta}_y\text{Nb}_{1-y}\text{O}_3$ ceramics is synthesised under high pressure reduces the elasticity modulus, obviously being related to re-crystallisation of disordered SS at synthesis under high pressure and, consequently, to emergence of microscopic fractions weakening adhesion along the grain boundaries. The decrease of the modulus of elasticity with increasing the baking temperature observed in high-pressure $\text{Li}_{0.17}\text{Na}_{0.83}\text{Ta}_y\text{Nb}_{1-y}\text{O}_3$ is assumed to be related to conditions of re-crystallisation of disordered solid solutions at high pressure synthesis.

The modulus of elasticity of $\text{Li}_{0.17}\text{Na}_{0.83}\text{Ta}_y\text{Nb}_{1-y}\text{O}_3$ ($0 \leq y \leq 0.5$) high-pressure ceramics has a complex behaviour with concentration. A considerable anomaly of the modulus of elasticity is observed in the region of Ta concentrations $y \sim 0.1$ which is close to the singular concentration point $y = 0.125$ (Ta:Nb = 1:7) and likely related to a concentration-induced structural transition.

Heat Capacity and Dielectric Properties of the PNN-PT Ferroelectric Ceramics

K. Bormanis¹, S.N. Kallaev², Z.V. Omarov², A.R. Bilalov², A. Kalvane¹

¹Institute of Solid State Physics, University of Latvia, Riga, Latvia

²Institute of Physics, Dagestan Science Centre, RAS, Makhachkala, Russia

e-mail: bormanis@cfi.lu.lv

The multi-component mixed perovskites of extraordinary crystal structure and unique properties, an enormous dielectric permeability, strong piezoelectricity and electrostriction in particular, for decades have been of increasing interest. The $(1-x)\text{PbNi}_{1/3}\text{Nb}_{2/3}\text{O}_3 - x\text{PbTiO}_3$ ((1-x)PNN-xPT) solid solution system is one of mixed ferroelectric relaxors.

The presented study is focused on heat capacity and dielectric permittivity of the (1-x)PNN-xPT ($x = 0.5, 0.4$, and 0.3) ferroelectric ceramics within the 150 – 750 K range of temperature. The PNN-PT samples were obtained by conventional ceramics technology.

Results of dielectric measurements reveal decreasing of the temperature T_m of the maximum of dielectric permittivity ϵ of the (1-x)PNN-xPT system with the increase of the PNN component while the maximum value of the dielectric permittivity increases and the region of phase transition broadens. Dispersion of the dielectric permittivity peak value ϵ_m specific to ferroelectric relaxors is observed in case of the $0.7\text{PbNi}_{1/3}\text{Nb}_{2/3}\text{O}_3-0.3\text{PbTiO}_3$ compound.

Two thermal anomalies on the heat capacity C_p curve characteristic to phase transitions are observed in compounds of $x = 0.5$ and $x = 0.4$, four – in case of $x = 0.3$. The high-temperature anomaly around 520 K on the $C_p(T)$ curves of all the compounds has never before been observed. In the latter case a broad irregularity of heat capacity $C_p(T)$ characteristic to relaxors is observed in the 250 – 450 K range. The anomalous component of heat capacity in the range of phase transition was found as the difference between the measured value and calculated phonon heat capacity.

According to the obtained data of the (1-x)PNN-xPT measurements the “temperature-composition” phase diagram is linear indicating to regular thermodynamic type of solid solutions. The experimental results are discussed with respect to the structure of the ceramics.

Relaxation of Polarisation at the Broad Phase Transition in Doped PMN Ferroelectric Ceramics

K. Bormanis¹, A.I. Burkhanov², I.E. Tumanov², A. Kalvane¹

¹Institute of Solid State Physics, University of Latvia, Riga, Latvia; E-mail: bormanis@cfi.lu.lv

²Volgograd State Architectural and Engineering University, Volgograd, Russia

The dielectric nonlinearity of the lead-magnesium niobate $\text{Pb}(\text{Mg}_{1/3}\text{Nb}_{2/3})\text{O}_3$ (PMN) with admixture of lithium is studied in the thermal range of the low-frequency dielectric permittivity maximum (at 1 Hz frequency and weak measuring field intensities the maximum is reached at temperature $T_m \approx -16$ °C, at frequency of 1000 Hz – at $T_m \approx -3$ °C [1]). A Sawyer-Tower circuit was used to detect the dielectric response at frequencies from 0.1 to 10 Hz. The $\text{Pb}(\text{Mg}_{1/3}\text{Nb}_{2/3})\text{O}_3 + 2\text{wt.}\%$ Li_2O samples were prepared by conventional ceramics technology.

The features of the behaviour of the effective dielectric permittivity are revealed from polarisation loops in accordance to $\varepsilon'_{\text{eff}} = P/(\varepsilon_0 \cdot E)$. Dependence on the amplitude of field intensity $\varepsilon'_{\text{eff}}(E)$ at temperatures above and near the T_m is illustrated by Fig. 1. As seen from Fig. 1, at some E_i the effective dielectric permittivity $\varepsilon'_{\text{eff}}$ becomes independent of temperature the value of E_i substantially depending on the frequency of the measuring field: the lower the frequency, the lower is E_i . The feature is the result of a significant contribution of conductivity to relaxation of polarisation at $T > T_m$ and, at approaching T_m and growing E – of a gradually increasing contribution of polar clusters and phase (domain) boundaries of widely scattered relaxation constants.

References

1. A.I. Burkhanov, I.E. Tumanov, K. Bormanis, and A. Kalvane. Physics Solid State **54**, 5 (2012).

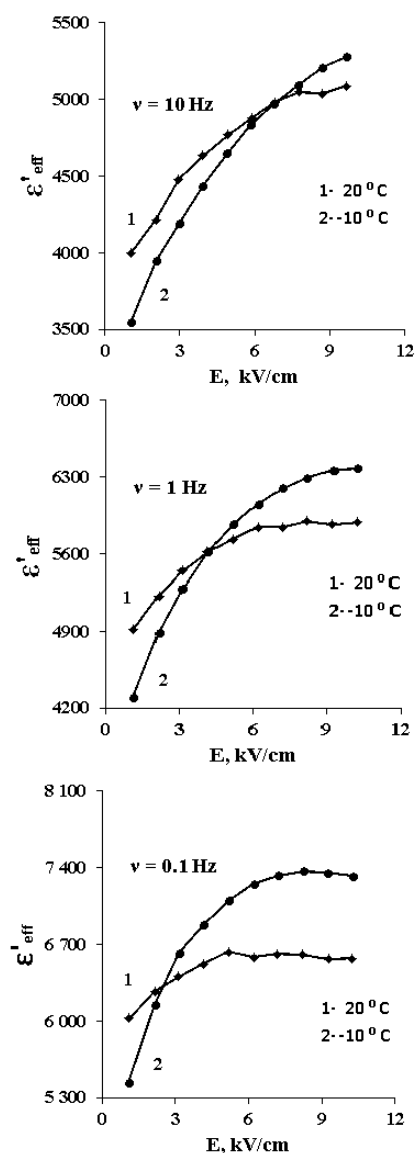


Fig. 1. Effective dielectric permittivity as a function of bias field at frequencies of 0.1, 1, and 10 Hz.

The Ferroelectric Polarization Effects in the Surface Superconductivity

P. Konsin¹, B. Sorkin¹

¹Institute of Physics, University of Tartu, Riia 142, 51014 Tartu, Estonia

e-mail: sorkin@fi.tartu.ee; konsin@fi.tartu.ee

The electric field effects in high- T_c superconductors are studied in [1-7]. The theory of the surface and bulk superconductivity in ferroelectric-superconducting film structures are developed. The modified Ginzburg-Landau (GL) equations are derived for these structures within the two-band model. We obtained new de Gennes boundary conditions for the GL equations. The ferroelectric polarization essentially determines the dependence of the de Gennes boundary condition for the GL equations through the electric induction. In a general case this dependence can be a nonlinear one. The dielectric constant of the quantum paraelectrics and their temperature dependence can lead to an additional shift of the superconducting transition temperature. The small coherence lengths (in the two-band model there are two correlation lengths ξ_1 and ξ_2). The length ξ_1 depends critically on the temperature in the high- T_c superconducting films. The smallness of the coherence length ($\xi_1(0) \sim 5-15 \text{ \AA}$) and the Thomas-Fermi radius lead to the appearance of electric field effects. A boundary condition for the GL wave function of a one-band superconductor on surfaces biased by a strong static transverse electric field is derived with the de Gennes approach. This boundary condition is applied to the metal-dielectric-superconductor structure. The dependence of the T_c shift with the electric field in thin and thick cuprate films is calculated. The positive transverse electrostatic field leads to the increase of the critical temperature, which does not depend on the width of the sample and saturates in thick films. The dependences of ΔT_c for negative fields are also obtained.

Acknowledgment

The research was supported by the Estonian Ministry of Education and Research (SF0180013s07), Estonian Science Foundation (ETF7389) and by the European Union through the European Regional Development Fund (TK114, SF0180013s07AP).

References

1. R.E.Glover and M.D.Sherill, Phys. Rev. Lett. **5**, 248 (1960)
2. J.Mannhart, J.G.Bednorz, K.A.Müller, and D.G.Schlom, Z. Phys. B **83**, 307 (1991)
3. T.Frey, J.Mannhart, J.G.Bednorz, and E.J.Williams, Phys. Rev. B **51**, 3257 (1995)
4. P.Konsin, Physica C **235-240**, 1437 (1994)
5. P.Konsin and B.Sorkin, Phys. Rev. B **58**, 5795 (1998)
6. P.Konsin and B.Sorkin, Journ. of Non-crystalline Sol. **356**, 2656 (2010)
7. J.Mannhart, Supercond. Sci. Technol. **9**, 49-67 (1996)

Active Vibration Control of Structure with an Optimum Placement of Macro-Fiber Composite Actuators

A. Kovalovs, E. Barkanov

Institute of Materials and Structures, Riga Technical University, Latvia

e-mail: kovalovs@bf.rtu.lv

The present methodology of active vibration control has been developed for an optimum placement of actuators in the rectangular plate. The main aim of this work is modelling and analyze of smart structures under harmonic loading and influence of the Macro-Fiber actuators placement and size on the response of this structures.

The development of smart structure technology offers great potential in the field of active vibration control and noise control of structures in different fields of application, such as aerospace, civil, and mechanical engineering.

During the past few years, piezoelectric materials have been extensively used as actuators and sensors for noise and vibration control. This new structural concept requires the use of sensors and actuators for controlling the mechanical behavior of structural systems when using the converse piezoelectric effect to induce control forces and moments.

Due to increasing interest in the design of complex smart structures with piezoelectric actuators and the need for fast and simple implementation of piezoelectric control systems, technology developers are beginning to provide more convenient tools to model smart structures.

In this work, MFC actuators are used for the modeling of piezoelectric actuators, as an innovative actuator that offers high performance and flexibility in a cost-competitive device.

Simulation and numerical computations of smart structures are performed in ANSYS 11.0 environment. The applied voltage is modelled as a thermal load according to thermal analogy for MFC actuator. According to numerical researches of smart structures, maximal reduce of vibration was achievement by the placement and direction of MFC actuators depended of mode shapes. Finally numerical results in terms of the harmonic response of smart structures with surface bonded MFC actuator demonstrates the validity of this method, which can be used for implementation of piezoelectric control system.

Non-destructive Technique for Determination of Material Properties

A. Kovalovs, P. Akishin, E. Barkanov

Institute of Materials and Structures, Riga Technical University, Latvia

e-mail: kovalovs@bf.rtu.lv

It is well known that material properties determined from the standard tests of small specimens, which are made by cutting samples, may differ from the actual material properties in structure. Therefore, the determination of realized material properties using non-destructive evaluation techniques has become actual problem. The determination of stiffness parameters for complex materials is much more complicated than for isotropic materials. A number of various non-destructive evaluation techniques have been proposed for determining the material properties of materials.

In the present study, attention is focused on the identification of the material properties using vibration test data. The problem associated with vibration testing is converting the measured modal frequencies to elastic constants. A standard method for solving this problem is the use of a numerical-experimental model and optimization techniques. The numerical-experimental method proposed in the present investigation consists of the experimental set-up, numerical model, and material identification procedure.

The work comprises two main experimental parts. The first part, deals with the identification of material properties of composite plate. Elastic constants of laminated composite plates are identified via modal frequencies by using a mixed numerical-experimental technique. The presented method derives the properties from the measured modal frequencies of unidirectional as well as multidirectional reinforced laminated composite plates and is able to identify four out of five major elastic constants of a transversally isotropic material.

In the second part, identification technique is applied for determination of elastic material properties of aluminium alloys with different Carbon nanotubes (CNT) volume content. Nowadays CNT-reinforced aluminium alloys have promising perspectives for an application in many industrial sectors such as aerospace, automotive and electronics industries.

Dimensional Effects of Microstructure and Sample Geometry of NiZn-Ferrites

J. Jankovskis¹, N. Ponomarenko¹, N. Mironova-Ulmane², D. Jakovlevs¹

¹Riga Technical University, Latvia, Riga, Kalku Str. 1, LV-1048

²Institute of Solid State Physics, Latvia, Riga, Kengaraga Str.8, LV-1063

In the general case the effects of dimensions within polycrystalline ferrites (PF) may manifest themselves through at least two attributes of a sample: its microstructure (adequately characterized by polycrystal grain size distribution, the average grain size and defects) and geometrical dimensions (typically toroidal cores with different outer/inner diameters, OD/ID , and cross section areas, A). The effects of these attributes there are investigated as to the one of most important characteristic of PF for their applications at high frequencies: the magnetic spectrum (MS) – the frequency dependence of complex initial permeability (CIP): $\tilde{\mu}(f) = \mu'(f) - j\mu''(f)$ where $\mu'(f)$ and $\mu''(f)$ stands for the real and imaginary parts.

Experiments have been performed on toroidal samples of NiZn-ferrites. The cores with different sizes were specifically cut out from sintered PF tile of *Ferroxcube 4S60* with the goal to have the samples with similar microstructure. The Raman spectra of PF were recorded on “Nanofinder-S” using the $532nm$ excitation line; the elemental composition was assessed by energy dispersive X-ray spectrometry (EDS, Oxford instruments 7378) performed on the scanning electron microscope. Microstructural characteristics of samples were obtained by analysis of differently oriented micrographs. They reveal that probability distribution function $f(D)$ of grain sizes D actually is log-normal:

$$f(D) = (\sqrt{2\pi} \sigma D)^{-1} \exp [-(\ln D - \ln D_{med})^2 / 2\sigma^2]$$

where D_{med} is the median of distribution and σ is the standard deviation of $\ln D$ correspondingly. The micrographs allow to determine the parameters and show that within numerous of grains there are clearly observable defects. Measurements of CIP were performed within typical frequency range of large amplitude dispersion of $\tilde{\mu}(f)$ for these ferrites (50kHz...50MHz; the quality of measured spectra were verified by their compatibility to Kramers-Kronig relations). The graphical display of MS demonstrates that there is combination both of relaxation features (dispersion of CIP within broad range of frequency) and resonance ones (overshoot and backswing). Such a combination in spectrum is possible to explain only on the basis of grain size distribution effects. The obtained MS for the samples with similar microstructure show almost no difference as to the changes of size of cores; thus it is possible to conclude that no size-dependent electrodynamic effects manifest themselves at least in the samples of NiZn-ferrites up to their moderate size ($OD < 40mm, A < 50mm^2$).

DC Magnetron Sputter Deposition of Zinc Oxide Based n- and p-Type Transparent Conductor Thin Films

M. Zubkins, K. Vilnis, A. Ecis, R. Kalendarev, A. Azens, J. Purans

Institute of Solid State Physics, University of Latvia, Riga, Latvia

e-mail: purans@cfi.lu.lv

Zinc oxide (ZnO) is a wide band gap semiconductor with potential applications in multifunctional transparent electronic devices. Depending on the dopant, the films may exhibit either n- or p- type conductivity. The aim of the present work was to investigate the process of DC magnetron deposition of n-type conducting thin films of Al:ZnO (AZO) and p-type conducting thin films of Ir:ZnO (IZO).

AZO films were deposited by reactive sputtering from metallic (Zn=98%, Al=2%) target in an Ar+O₂ and Ar+O₂+H₂ atmosphere. IZO films were deposited by reactive sputtering from metallic mosaic targets made of Zn and Ir pieces, with Zn 92-96%, Ir=4-8% surface area. In both cases, the substrate was glass kept at ≈310°C temperature, the sputtering was conducted at 3 mTorr working pressure and 100W sputtering power.

The process was controlled by plasma optical emission spectroscopy. To achieve the highest conductivity in AZO films, and to reproduce the process conditions from run to run, the behavior of zinc emission line at 480.05 nm was investigated as a function of oxygen flow. For IZO films, the process control was based on zinc emission line at 480.05 nm and iridium emission line at 390.2 nm.

Synthesis and Electrochemical Performance of $\text{Li}_2\text{FeSiO}_4$ Cathode Material for Lithium Ion Batteries

G. Kucinskis¹, G. Bajars¹, J. Kleperis¹, A. Dindune², Z. Kanepe², J. Ronis²

¹Institute of Solid State Physics, University of Latvia, Latvia

²Institute of Inorganic Chemistry, Riga Technical University, Latvia

e-mail: gints.kucinskis@gmail.com

$\text{Li}_2\text{FeSiO}_4$ has recently received much attention from scientific community as a promising cathode material for lithium ion batteries. Its main advantages are its relatively high charge capacity (166 mAh/g theoretically, up to 162 mAh/g experimentally^[1]), high stability and potentially low cost of production. It is also environmentally friendly, especially when compared to most of the widely used cathode materials in lithium ion batteries, such as LiCoO_2 and LiMn_2O_4 . $\text{Li}_2\text{FeSiO}_4$ has been used in combination with other Li_2MSiO_4 type materials (M – metal), yielding a higher charge capacity. Such cathode materials, however, often have significantly higher charge capacity loss during first few cycles due to structural instabilities.

$\text{Li}_2\text{FeSiO}_4$ has been synthesized via solid state synthesis. Its structure and morphology have been studied via x-ray diffraction and scanning electron microscopy. Voltammetry, chronopotentiometry and EIS (electrochemical impedance spectroscopy) have been performed in order to determine the electrochemical performance of the obtained material.

Cyclic voltammetry shows peaks characteristic to charge and discharge processes of $\text{Li}_2\text{FeSiO}_4$, which descend to lower voltages during cycling, suggesting structural changes in the material itself. Discharge capacity of the material has been determined at various discharge rates. Lithium ion diffusion coefficient in $\text{Li}_2\text{FeSiO}_4$ has been determined by using cyclic voltammetry and EIS.

References

1. T. Kojima, A.Kojima, T.Miyuki, Y.Okuyama, T.Sakai, J. Electrochem. Soc. **158**, 1340 (2011)

Characterization of LiFePO₄/C Composite Thin Films Using Electrochemical Impedance Spectroscopy

G. Bajars, J. Smits, G. Kucinskis, J. Kleperis, A. Lūsis

Institute of Solid State Physics, University of Latvia, Latvia

e-mail: gints.kucinskis@gmail.com

LiFePO₄ has been considered as one of the most promising cathode material for lithium-ion batteries. In spite of such attractive features as low cost, environmental benignity and thermal stability, LiFePO₄ requires further modifications to overcome limitations involving low electronic conductivity and slow lithium-ion diffusion. One way to solve these problems is to increase the surface area of the cathode by the use of thin film technology. In addition, the use of thin film electrodes enables to investigate electrochemical properties of active material in detail. This is especially useful for poorly conductive materials because the thickness can be reduced to an extent which does not significantly affect the electrochemical behaviour. In this study, LiFePO₄/C composite thin films prepared by RF magnetron sputtering were investigated by electrochemical impedance spectroscopy (EIS), which is a very powerful method to determine the rate of individual electrode kinetic steps.

Three element equivalent circuit which contains charge transfer resistance R_{ct} , Warburg impedance Z_w and constant phase element CPE was constructed to analyse the EIS results of LiFePO₄/C thin film. The dependence of charge transfer resistance, double layer capacitance C_{dl} and lithium ion diffusion coefficients on applied electrode potential were calculated from EIS data. The charge transfer resistance increases in relation with an appearance of the FePO₄ phase. The minimum value of charge transfer resistance is acquired in discharged state which corresponds to maximum concentration of Li⁺ ions in lithium iron phosphate. Contrary to R_{ct} , values of double layer capacitance decrease with the lithium ions extraction from the thin film material. Obtained values of lithium diffusion coefficient were in the range from $8.3 \cdot 10^{-13} \text{ cm}^2 \text{ s}^{-1}$ to $1.2 \cdot 10^{-13} \text{ cm}^2 \text{ s}^{-1}$ at 3.4 V and 3.7 V, respectively, and show a similar dependence on applied voltage as C_{dl} .

Acknowledgements

The authors acknowledge Taiwan – Latvia – Lithuania cooperation project “Materials and processing development for advanced Li ion batteries” and National Program in Energetic for financial support. The technical assistance and consultations of AS Sidrabe, Juris Katkevics and Arturs Viksna are acknowledged.

Influence of Moisture on the Functional Properties of Physically and Chemically Modified Technical Textiles

R. Janeliukštis, L. Veļķere, J. Zandersons, E. Pentjuss, A. Lūsis

Institute of Solid State Physics, University of Latvia

Kengaraga Street 8, Riga, LV-1063, Latvia

e-mail: luisis@latnet.lv

Textiles have wide technical applications. The different kinds of physical and chemical treatments and metal coatings are widely used for functionalization of textiles (woven and nonwoven) for different technical applications. Our research work is devoted to study the influence of moisture on the functional properties of the fabrics based on glass, hemp and flax fibers. The interaction of metal particles with fiber as well as the influence of environment moisture on physical and chemical properties is topics for research functionality of technical textiles.

There are used leaching, etching and coating technologies to modify properties of the fabrics based on glass, hemp and flax fibers. The fabrics and yarns have been modified in the technological processes in vacuum: etching with argon plasma and deposition of particles (Al, Ni, Cu, Cu₂O and CuO) in magnetron process. The electrical and thermo-mechanical properties for such fabrics have been studied. The electrical properties have been studied by impedance analyzers HP 4194A (100 HZ – 15 MHz) and Solartron FRA 1250/ECI 1287 (0.01Hz -50 kHz) with Dielectric Test Fixture for solids HP 16451B and Liquid Test Fixture HP16452A. The impedance characteristics of fabrics analyzed at different moisture content.

All samples of glass fabrics below the equilibrium moisture content (about 2 mg/cm²) behave as insulators with dielectric constant of the corresponding substances in the sample in the range from 100 Hz to 15 MHz. The increase of moisture above of its equilibrium values, leads to increase of dielectric constant of fabric. The increase of dielectric constant is much higher at the lowest frequencies (100 Hz) and exceed the value of 100 000 at moisture level of 10 mg/cm². The complex impedance $Z^* - Z''$ plane shows diffusion of ions and percolation threshold in dielectric constants and losses dependency of water content.

The thermo-mechanical strength of unmodified and modified hemp yarns at fixed temperatures in the range of 25-500 OC depending on the humidity and density of deposited mass of active of particles have been studied. TGA shows two weight loss temperature areas of 30-110 OC (moisture retention) and 200-300 OC (hemp fiber carbonization). Modified yarn strength decreases by 30%, which correlated with the moisture content (6-12 % wt). Relative strength at 280 OC yarn with active particles respect to unmodified increased in the direction Cu, Cu₂O and CuO.

Electrochemical Impedance and Moisture Contents of Glass Fabric

E. Pentjuss, A. Lūsis, G. Bajars, J. Gabrusenoks, L. Jekabsone

Institute of Solid State Physics, University of Latvia, Latvia

e-mail: pentjuss@cfi.lu.lv

The electrochemical impedance characteristics of sodium aluminosilicate glass fabric are analyzed at different its moisture content. The elements of threads have the pores containing oxides of alkali metals that may be partly eluted by water or acids. As measurement capacitor there was used HP 16451B dielectric test fixture with contacting plates coated by sputtered Ni (or other metal).

All samples of fabric below equilibrium moisture content (around 2 mg/cm^2) behave similar to dielectrics having dielectric constants values that may be prospective from its materials values in range of 100Hz-15MHz. The increase of moisture usually above its equilibrium values leads to the increase of dielectric constant of fabric. The increase of dielectric constant is much higher at the lowest frequencies (100 Hz) and usually exceed the value of 100 000 at moisture level of 10 mg/cm^2 . In contrary at frequencies of 15 MHz the increase is small and may be associated with the increase of water content. The increase of oxide content in sample and metal deposition on the surface of fabric leads to the increase in dielectric constant. The results mentioned above indicate that water serves as continuous media of ions transportation. The Randles-circuit type characteristic in $Z' - Z''$ plane is indicative of ions diffusion to metallic surface and formation of the charge layer if there are continuous water paths in fabric and low enough frequency (sufficient time). The role of water in pores and in space between the elements of threads and threads is discussed.

Cotton Fabric Surface Modification by Sol-Gel Deposition of ZnO Thin Films

S. Vihodceva¹, S. Kukle¹

¹Institute of Textile Materials Technology and Design, Riga Technical University, Latvia

e-mail: Svetlana.Vihodceva@rtu.lv

Zinc oxide show high absorption in the ultraviolet (UV) region of the light spectrum, while absorption of visible light is quite low. In comparison with organic absorbers conventionally used in the textile industry, inorganic materials show no significant degradation and are therefore extremely stable and the oxides are classified as non-toxic materials. [1] Sols were prepared using sol-gel technology. Ethanol, tetraetoxysilane, distilled water and hydrochloric acid was stirred for 30 minutes, after stirring was added Zn acetate and for second variant $ZnSO_4$. The fabric samples were immersed in the prepared sols, after samples was dried at 50°C and cured in an oven at 120°C. Experiment results show that a moderate thermal treatment at 120°C after the sol is applied to the cotton textile is appropriate. In this work comparison of coatings of samples prepared using Zn acetate or $ZnSO_4$ was made (Fig.1.).

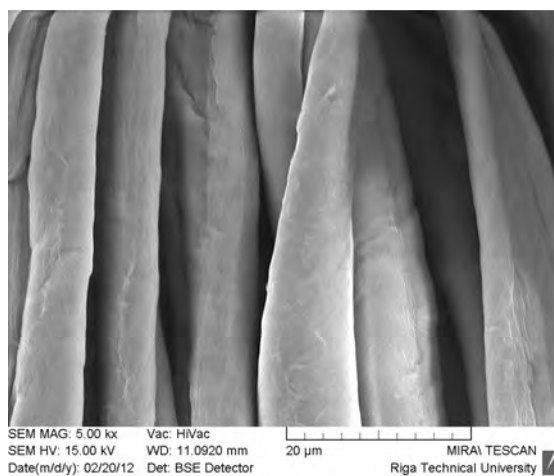


Fig.1 SEM image of transparent ZnO coating on natural cotton textile fibers received with sol-gel technology used $ZnSO_4$

SEM and laser laboratory complex were used to examine the nature of the surface modification with ZnO coating by the sol-gel technique as also after exploitation of samples; energy dispersive X-ray spectroscopy was used for the analysis of chemical composition of coated fabric samples.

Acknowledgments

This work has been supported by the European Social Fund within the project «Support for the implementation of doctoral studies at Riga Technical University».

References

1. Q. Weu, Surface modification of textiles. Woodhead Publ. in Textiles. **97** (2009)

Elaboration of High Performance Electro-Optical Films by Sol-Gel Method

A. Salundi, M. Timusk, M. Järvekülg, R. Lõhmus, I. Kink, K. Saal

Institute of Physics, University of Tartu, Riia 142, 51014 Tartu, Estonia

aigi.salundi@ut.ee

GDLC (Gel-Glass Dispersed Liquid Crystal) materials were first reported in 1991 [1]. GDLCs are, in their nature sol-gel analogs to polymer dispersed liquid crystal materials (PDLCs) composing of organically modified silica [1-3] or mixed oxide [4] dispersed liquid crystal. GDLC material strongly scatters light in its normal state and changes its optical transmittance when electric field is applied, becoming more transparent. In order to achieve high performance, refractive index of the matrix must match the ordinary refractive index of the liquid crystal and the film thickness must be in order of 10 μ m. Achieving these conditions has been very difficult until now.

GDLC has several potential advantages over PDLC: smaller solubility of LC inside the matrix (smaller amount of LC needed in preparation of unit volume of the film material), better resistance to ultraviolet radiation, easier to control LC director field configuration through droplet shape and surface anchoring forces, determined by the chemical composition. Also, refractive index of the matrix is more easily tunable due to the availability of large amount of suitable precursors. The main potential applications of GDLC materials is “smart glass” (window with variable transmittance).

In this work we report the significant improvement compared to our previously reported results [3]. GDLC film preparation process was elaborated to incorporate titanium alkoxides in synthesis process. This enabled the adjustment of the refractive index of silica glass matrix without having destructive influence on macroscopic liquid crystal phase separation at the same time. A high-performance xerogel-liquid crystal composite electro-optical film that exhibits a 75.9 % change in its transmittance as an electric field is applied was prepared. Field-dependent scattering behaviour of a refractive index matched GDLC film over a broad spectral (from visible to near-IR) and temperature range was investigated. Transmittance vs. applied voltage measurements at different temperatures demonstrate electro-optical effects at least down to -13 °C which means that liquid crystal must be in molten (liquid crystal) state at these temperatures in the microscopic volume confined in xerogel matrix. That is remarkable since it is known that the used liquid crystal 4-cyano-4'-pentylbiphenyl crystallizes in macroscopic volume at 24.5 °C. The largest electro-optical effect was observed at 25.2 °C.

References

1. D. Levy, C. J. Serna, J. M. Otón, *Mat. Lett.* 10, 470-476, (1991).
2. M. Zayat, D. Levy, *Chem. Mater.*, 15, 2122-2128, (2003).
3. M. Timusk, M. Järvekülg, R. Lõhmus, I. Kink, K. Saal, *Mater. Sci. Eng. B.*, 172, 1-5, (2010).
4. M. Timusk, M. Järvekülg, A. Salundi, R. Lõhmus, S. Leinberg, I. Kink, K Saal, *J. Mater. Res.*, (2012), accepted

Novel Methods in Synthesis of Microtubes and Composite Materials via Sol-Gel Route

M. Part¹, T. Tätte¹, K. Riikjärv¹, K. Hanschmidt¹, K. Saal¹, M. Timusk¹, M. Järvekülg¹, A. Salundi¹,
A. Lõhmus¹

¹Institute of Physics, University of Tartu, Estonia

e-mail: markopa@ut.ee

Sol-gel chemistry is versatile route for preparation of ceramic materials with different defined geometries (fibers, tubes, powders, films, monoliths etc.) at relatively low temperatures. Gelation of sols enables to prepare highly homogenous nanocrystalline materials.

Much attention has been devoted to the microtubes and coatings obtained via sol-gel route [1]. Although methods for preparation of materials with mentioned geometries exist, the gaps have still left. For example, it is very difficult to prepare high enough quality metal oxide ceramic microtubes. The methods also are too expensive and complicated in order to apply for real production.

We have elaborated sol-gel composite material: glass dispersed liquid crystal (GDLC). Its transparency can be controlled by electric field [2]. Microdroplets of liquid crystal are obtained into ORMOSIL matrix by phase separation. We have achieved 74% transparency difference (between transparent and opaque state), which marks superior performance of our GDLC based devices, compared to these reported in papers by other groups.

We have also developed new technique to obtain microtubes and fibers from metal alkoxide-based precursors and provided theoretical background for explaining the phenomena behind the formation process [3, 4]. Like GDLC, microtubes form as a results of phase separation processes from initial jet. Obtained YSZ microtubes exhibit highly unique physical and chemical properties e.g. mechanical and chemical stability in wide temperature range and high ionic conductivity. The tubes can be used in applications like ionic membranes in microfluidic systems operating at high pressure and temperature [4], gas or fluid carriers in microfluidic devices, nozzles in spray heads and reactors for plasma environment.

References

1. T. Peng, H. Yang, K. Dai, K. Nakanishi, K. Hirao, *Advanced Engineering Materials*, 2004, 6, 4.
2. M. Timusk, M. Järvekülg, R. Lõhmus, I. Kink, K. Saal, *Materials Science and Engineering B*, 172(1) (2010), 1 - 5.
3. K. Saal, T. Tätte, M. Paalo, R. Talviste, S. Vlassov, I. Kink, *Mater. Res. Soc. Symp. Proc.* Vol. 1017, 2007.
4. T. Tatte, M. Hussainov, M. Paalo, M. Part, R. Talviste, V. Kiisk, H. Mändar, K. Pohako, T. Pehk, K. Reivelt, M. Natali, J. Gorauskis, A. Lohmus, U. Maeorg, *Science and Technology of Advanced Materials* 2011, 12(3), 1-12.

Synthesis of Polymeric Titanium and Zirconium Precursors to Preparation of Fine Binary Carbide Systems

M. Umalas¹, V. Reedo¹, A. Lõhmus¹, I. Hussainova²

¹Institute of Physics, University of Tartu, Estonia, Estonian Nanotechnology Competence Centre

²Department of Materials Engineering, Tallinn University of Technology, Estonia

e-mail: madis.umalas@gmail.com

The binary systems of metal carbide fine powders have a great potential in technological applications as the precursors for preparation of highly homogeneous nanocomposites.

In our work we use combination of sol-gel method and carbothermal reduction for preparation of homogeneous metal carbide fine powder mixtures [1-3].

The goal of our work is elaboration of a novel way for synthesis of ZrC–TiC mixture using Zr and Ti alkoxides as starting materials. The main advantage of the used sol-gel process is the reduction of the kinetic barriers between the formed metal oxide and the carbon particles created in pyrolysis of

metal alkoxide polymer due to the homogeneous dispersion of reactants in the precursor material. Titanium and zirconium carbides were synthesized by carbothermal reduction from of metal alkoxide polymer at 1500 °C in an argon the resulting products had crystallite size (~40 nm). However, these products contained little amorphous carbon.

The structural transformations of the polymeric materials into the carbides were characterized by SEM and by X-ray diffraction analysis in Fig.1., energy dispersive X-ray spectroscopy and Raman spectroscopy method.

References

1. Haijun Zhang, Faliang Li, Quanli Jia, Guotian Ye, Sol-Gel Sci Technol 46:217–222 (2008)
2. Pierson HO. Handbook of refractory carbides and nitrides. Park Ridge, NJ: Noyes; (1996)
3. Yongjie Yan, Zhengren Huang, Xuejian Liu, Dongliang, Sol-Gel Sci Technol 44:81–85 (2007)

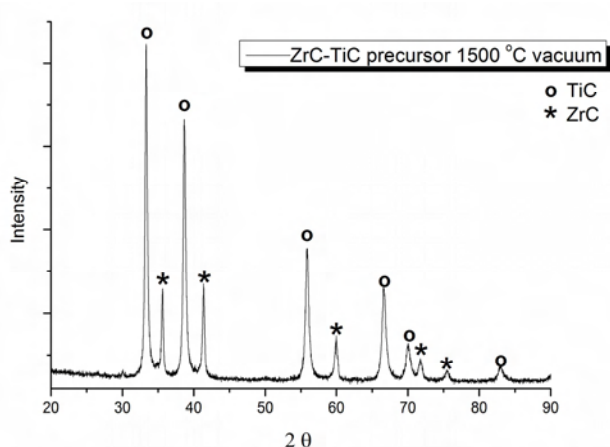


Fig.1. X-ray diffraction patterns of fine ZrC-TiC mixture

Preparation and Characterization of Transparent Fiber Electrodes Based on CNT-s Metal Oxides

M. Paalo¹, T. Tätte¹, M. Hussainov¹, K. Hanschmidt¹, M. Lobjakas¹, A. Lõhmus¹, U. Mäeorg²,
I. Kink¹

¹Institute of Physics, University of Tartu, Estonia,

²Institute of Chemistry, University of Tartu, Estonia

e-mail: madis.paalo@fi.tartu.ee

During the past decade, significant efforts have been made to convert extraordinary and unique properties of carbon nanotubes (CNT-s) for bulk materials in order to give them some novel functionality. To take advantage of the unique properties of CNT-s, numerous studies have carried out on reinforcing different materials. Resulting composites combine the properties of CNT-s and the matrix material. CNT doping is widely acknowledged as a means of improving tensile strength and electrical properties of organic polymers [1]. Aforementioned materials may still not be suitable for applications under harsh conditions. Contrary to organic polymers, high corrosion resistance and thermal stability makes metal oxide ceramics very attractive candidates to be alternatively used as CNT composite matrices. A wide selection of papers have published in recent years, reporting nanotubes in ceramic matrices like SiO₂, Al₂O₃, MgO, SiC, TiN, BaTiO₃ etc. [2].

In the current paper we describe our studies of the preparation and characterization of CNT doped ceramic composites obtained by sol-gel chemistry. Fiber-shape electrodes were prepared by pulling jets from polymerized CNT-alkoxide mass. SEM and FIB analysis revealed that fiber-pulling process orients CNT-s in host matrix. The electrical properties of the materials were measured by 4-point method using In-Ga alloy contacts. The best electrical conductance, 2000 S/m, was achieved with SnO₂ fibers heated up to 450 °C and containing 0,1% MWCNT-s.

References

1. Spitalskya Z., Tasisb D., Papagelis K., Galiotis C., *Prog. Polym. Sci.*, 2010, **35**, 357–401
2. Cho J., Boccaccini A. R., Shaffer M. S. P., *J Mater Sci*, 2009, **44**, 1934-1951
3. Ham H. T., Choi Y. S., Chung I. J. , *J. Colloid. Interf. Sci.*, 2005,**286**, 216-223.

Color Representation Dependence on Printing Technology

K. Luse¹, M. Ozolins^{1,2}, S. Fomins^{1,2}

¹University of Latvia, Latvia

²Institute of Solid State Physics, University of Latvia, Latvia

e-mail: kaiva.luse@gmail.com

Color deficiency tests are widely used to diagnose the type and severity of color vision deficiencies. Among the most frequently used are pseudoisochromatic test plates.

Previous studies have shown that the printing technology impacts the color display accuracy of the test plates, resulting in a wide distribution of color coordinates along the desired points on the confusion lines in CIE color space diagrams [1].

The aim of the research is to study availability of different color print technologies (three layer photographic process, tint printing) for creation of color vision test plates, for an accurate diagnosis and grading of color vision anomaly.

The study incorporates (1) evaluating the adequacy of commercially available color vision deficiency test plates, (2) modeling the vision perception in terms of cone signals and thus predicting the outcome perception in case of deficiency and (3) evaluating the impact of non-standard illuminating conditions on the manifestation of color vision deficiency.

For final assessment of printed tests six (four color deficient, 2 unaffected) subjects to be tested using both: commercially available tests and generated color sets, and their color discrimination thresholds to be acquired. The threshold increases with severity of color vision anomaly [2].

References

1. S. Fomins, M. Ozolins, Multispectral Analysis of Color Vision Deficiency Tests, MATERIALS SCIENCE (MEDŽIAGOTYRA), 2011, Vol. 17, No. 1.
2. E. Konstantakopoulou, M. Rodriguez-Carmona, J. L. Barbur, Processing of color signals in female carriers of color vision deficiency, Journal of Vision, 2012, Vol. 12, No. 2.

Print Materials Colorimetric Changes Due To Illumination

S. Fomins¹, M. Ozoliņš^{1,2}

¹Institute of Solid State Physics, University of Latvia, Latvia

²University of Latvia, Optometry and Vision Science Dept., Latvia

e-mail: sergejs.fomins@gmail.com

Halftone print ink composition of CMYK devices could be well characterized using Neugebauer and Demichel equations [1], and is a necessary procedure for specific (color vision tests) and precise color reproduction. Colorimetry of reflected objects could be represented as the combination of illumination spectra, reflectance and human color matching functions (CMFs) [2]. ASTM E308 (2008) standard provide CMFs adapted for different standardized illuminations and is a standard procedure for CIE colorimetry [3]. However, growing in popularity LED illumination was not included in ASTM standard.

We analyze the spectral composition of printed color vision tests and chromatic samples to obtain illumination introduced colorimetric changes, according to E308. Alternatively, color appearance model (CAM) [4], which takes into account adaptation illumination properties and viewing conditions, is applied. More thorough analysis of fluorescent and LED lamps produced spectral and colorimetric changes is provided.

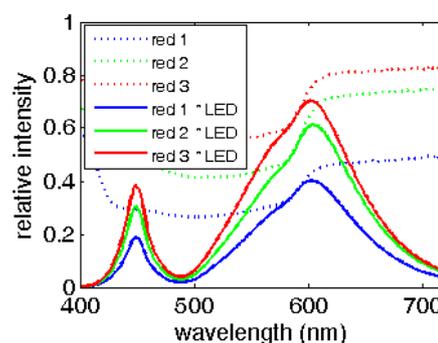


Fig.1 Reflection spectra of red ink of three intensities (dots) and same reds spectra under LED (3000K) illumination (solid).

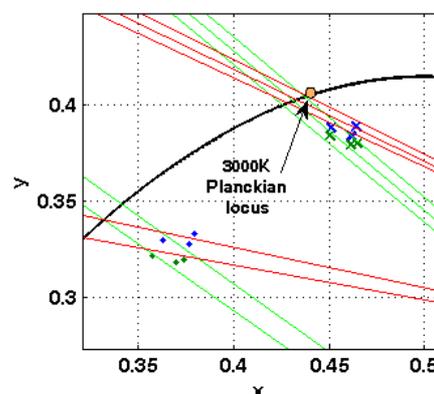


Fig.2. Pigment colorimetric coordinate shifts due to LED illumination in CIE 1931 x,y diagram. Reflection plotted by points and reflection under LED 3000K is plotted by crosses. Red and green lines are protanope and deuteranope color confusion lines.

References

1. S. Westland, C. Ripamonti. Computational Color Science using Matlab. John Wiley & Sons. 145-155 (2004)
2. Berns, R.S. Principles of Color Technology. John Wiley & Sons, 56 (2000)
3. ASTM E308 - 08 Standard Practice for Computing the Colors of Objects by Using the CIE System. Subcommittee: E12.04, Standards Volume: 06.01 (2008)
4. Fairchild, M.D. and Reniff, L. JOSA A, **12**(5), 824-833 (1995)

The Minimum Motion Techniques to Determine Lutein and Zeaxanthin Macular Pigment Optical Density Using CRT and Different Spectral Emission Light Emission Diode Light Sources

M. Ozolinsh^{1,2}, P. Paulins¹

¹University of Latvia, Latvia

²Institute of Solid State Physics, University of Latvia, Latvia

e-mail: ozoma@latnet.lv

The decrease of density and consequentially optical density of macular pigment (MPOD) serves as a diagnostic mean for a number of ophthalmological pathologies. Macular pigment absorbs light in short wavelength blue spectral range. Thus MPOD can be detected by various optical – both objective and subjective psychophysical techniques. Latter techniques use eye and brain visual pathways as spectral sensitive optical detector and decision maker, and exploit perception facility to process information flow in a unique manner to create various perception illusions. The psychophysical methods of detection of MDOD include heterochromatic flicker photometry and minimum illusory motion photometry [1-3].

The minimum motion technique is applied to determine effective red-blue isoluminance affected by MPOD in central retina areas. Test stimuli are consecutively presented on CRT screen in concentric arcs with central fixation, thus allowing to measure MPOD in different retinal eccentricity.

We employ a similar motion nulling grating method as proposed by Cavanagh and Anstis [1]. A chromatic CRT generated red-blue grating is displayed sequentially with a neutral luminance grating. The perceptual left-right direction of grating drift is dependent on the relative perceived luminance of the red and blue components. The same principles are used in a method developed by us where LED are used as stimuli light emitted elements. LED emission maximum wavelengths in blue spectrum region can choose in range 445-460 nm, that corresponds to maxima of light absorption for two types of macula pigments – lutein and zeaxanthin [4]. Thus replacement of planar CRT screen with a modular LED compound consisting of controllable red, neutral and two types of blue LEDs allows to realize a separate detection of lutein and zeaxanthin macular pigment densities.

Acknowledgements

Research was supported by Latvian project ERAF 2.1.1.1.0/10/APIA/VIAA/137.

References

1. S.Anstis and P.Cavanagh. A minimum motion technique for judging equiluminance. In: Colour vision: Psychophysics and physiology, London: Academic Press, 155–166 (1983)
2. J.Mellerio, S.Ahmadi-Lari, F.J.G.M.van Kuijk, D.Pauleikhoff, A.C.Bird, and J.Marshall. A portable instrument for measuring macular pigment with central fixation. *Cur.Eye Res.* **25**, 37–47 (2002)
3. J.D.Moreland. Macular pigment assessment by motion photometry. *Arch.of Biochem.and Biophys.* **430**, 143–148 (2004)
4. J.van de Kraats, M.J.Kanis, S.W.Genders, and D.van Norren. Lutein and Zeaxanthin Measured Separately in the Living Human Retina with Fundus Reflectometry. *Invest. Ophthalmol. Vis. Sci.* **49**, 5568–5573 (2008)

Leds Brightness Modulation Application in Anomaloscope and Heterochromatic Flicker Tests

R. Trukša¹, S. Fomins², M. Ozoliņš^{1, 2}

¹University of Latvia, Optometry and Vision Science Department, Kengaraga 8, Rīga, LV-1063

²Institute of Solid State Physics, Kengaraga 8, Rīga, LV-1063

e-mail: reenaars@inbox.lv

In previous research [1] we developed LED based anomaloscope [2]. Pulse width modulation technique was used to control LEDs brightness with computer controlled microcontroller. We were able to correctly classify [3] persons with color vision deficiencies. Developed device prototype identified color matching range for trichromatic vision is 103 to 171 units on red-green scale. Normal color vision patients make consistent matches in specified region.

Further our aim is to built multifunctional device that contain anomaloscope and heterochromatic flicker (HCF) with extra possibility to modulate LEDs brightness in real time which will be use to form stimulus for previously mention devices. Our hypothesis is that there is light intensity distribution in time what we would perceive with greater sensitivity which would allow increasing the specificity of anomaloscope match and linking color vision phenotype with existing genetic model. There is plausible information that sensitivity on OFF – sawtooth stimuli are greater than ON- sawtooth stimuli [4]. HCF originally is designed to determine overall and specific cone type sensitivity, which could serve an additional tool in color vision diagnostics in ambiguous cases, as well as independent method for other color vision and photometry related research. Possibilities of temporal light intensity modulations enable us to modify HCF to investigate visual system nonlinearities [5].

References

1. Trukša, R., Fomins, S., Ozoliņš, M. Rayleigh Equation Anomaloscope from Commercially Available LEDs. In press.
2. Woods, R. L., Rashed, A. L., Benavides, J. M., Webb, R. H. A Low-power, LED-based, High-brightness Anomaloscope. *Vision Research*, 46, 2005: pp. 3775 – 3781.
3. Birch, J. Diagnosis of Defective Colour Vision. Oxford University Press, 1993: pp. 58 – 59.
4. P.J., Demarco, V.C., Smith, J., Pokorny. Effects of sawtooth polarity on chromatic and luminance detection. *Visual Neuroscience*. Vol. 11. 1993: pp.491-499.
5. A., Stocman, D.J., Plummer. Color from invisible flicker: a failure of the Talbot –Plateau law caused by an early „hard” saturating nonlinearity used to partition the human short-wave cone pathway. *Vision Research* 38. 1998: pp. 3703–3728.

Expression of Interleukins and Defensins in the Experimental Rabbit Bone Tissue after Implantation of Different Biomaterials

J. Vamze¹, M. Pilmane¹, A. Skagers²

¹Riga Stradins University, Institute of Anatomy and Anthropology, Latvia

²Riga Stradins University, Department of Oral and Maxillofacial Surgery, Latvia

e-mail: j.vamze@inbox.lv

Bone loss is one of the complications after implantation of biomaterial into the hard tissue and inflammation is the main reason of it. Cytokine Interleukin-1 (IL-1) is suggested to increase the bone loss [1]. hBD-2 (human β defensin-2), hBD-3 and hBD-4 expression is different in patients with periodontal disease [2]. There is no complete data about expression of cytokines and defensins into the bone around the different implants. The aim of this work was to investigate the distribution and appearance of proinflammatory cytokines and anti-inflammatory proteins in the lower jaw and tibial bones of experimental rabbits in three months after implantation of different biomaterial. Material was obtained from lower jaw and tibial bone of 4 Californian rabbits after implantation of each pure and covered by polycaprolactone hydroxyapatite (HAp) tablets, unburned and burned under 1150⁰C HAp granules, commercial and uncommercial polymethylmethacrylate (PMMA) bone cement, α -Tricalcium phosphate cement with pH6 and pH7. Tissue was processed for immunohistochemical detection of IL-1, IL-6, IL-8, IL-10 and hBD-2, hBD-3, hBD-4. Bone developing zones and signs of bone-implant contact were detected in experimental tissue. Activity of cytokines and defensins in experimental material was different. The most weak activity of IL-1, IL-6 and IL-10 was presented by bone tissue with HAp granule implant, while reaction of hBD-2, hBD-3 and hBD-4 in this experiment was variable. Bone developing zones, signs of bone-implant contact and low expression of proinflammatory and anti-inflammatory cytokines in tissue with HAp granules possibly indicate better biocompatibility with this material than others used in our study.

References

1. K. Polzer, L. Joosten, J.Gasser, J. H. Distler, G. Ruiz, W. Baum, K. Redlich, K. Bobacz, J. S. Smolen, W. Van den Berg, G. Schett, J. Zwerina, Ann. Rheum. Dis. 69, 284 (2010)
2. J. Bissell, S. Joly, G.K. Johnson, C.C. Organ, D. Dawson, P.B. McCray, J.M. Guthmiller, J. Oral. Pathol. Med. 33, 278 (2004).

The Impact of Light Polarization on the Direct Relief Forming Processes in As_2S_3 Thin Films

U. Gertners, J. Teteris

Institute of Solid State Physics, University of Latvia, Latvia

e-mail: gertners@gmail.com

In this report direct photo-induced formation of surface relief gratings (SRG) in thin layers of arsenic sulfide (As_2S_3) are shown. This anisotropic light-induced mass transfer phenomenon has been discussed with the special attention focused on the polarization and intensity of the corresponding light. The experimental setup for the SRG recording is straight-forward consisting of $\sim 10\mu\text{m}$ optical slit through which an unfocused beam of light is projected on the surface of sample. The verified sets of experimental parameters (light intensity, polarization and slit opening) were chosen in accordance to the theoretical model which provided the highest recording efficiency. Additionally the evolution of surface relief in dependence from the recording time and polarization has been investigated in detail. The processes of SRG formation and mass transfer which are based on the photo-induced plasticity in As_2S_3 have been discussed.

UV Optical Record and Electron Beam Lithography in Polymer Films

A. Gerbreders¹, O. Shimane², V. Kolobjonoks², J. Teteris¹

¹Institute of Solid State Physics, University of Latvia, Latvia

²Daugavpils University, Latvia

e-mail: andrejmah@gmail.com

Possibility of UV optical record and electron beam lithography in different type of polymeric films was studied. Mechanisms of molecular structure changes: photoisomerization, destruction, cross-linking and oxidation have been discussed. The results of UV illumination of polyurethanes, polyacrilates, and some block-copolymers were described. The element analysis of polybutadien block copolymer was performed before and after UV illumination, and the changes in transmission spectra of the polymer film were measured. The resolution of electron beam lithography on polymeric films also was studied.

Photoinduced Phenomena in Azo-Dyed Gelatin Films

J. Aleksejeva, J. Teteris

Institute of Solid State Physics, University of Latvia, Latvia

e-mail: aleksejeva.jelena@gmail.com

In this work a photoinduced properties of azo-dye doped gelatin films was studied. Gelatin is the oldest polymeric matrix, which is used in holography and photography. Preparation of these films is simple and cheap, but ingredients aren't toxic. Films were synthesized using gelatin and several azo-dyes – Disperse Red 1, Disperse Red13, methylene blue and Chromotrope FB. Non-aqueous solvents - dimethyl sulfoxide and acetic acid, were used [1]. Films were coated on glass plates using applicator with layer thickness 30, 60, 90 μm then were heated in vacuum chamber.

Azo-dyed gelatin films were studied by 532nm laser radiation. Photoinduced birefringence and photoinduced dichroism dependence on films ingredients ratio, laser light intensity and sample treatment temperature were investigated [2]. Holographic recording on these films was performed in dependence on recording beam intensity and polarization. Volume polarization gratings and direct surface relief formation were studied by measuring diffraction efficiency with 660nm diode laser radiation. The obtained surface relief was investigated by AFM.

References

1. T. Balau Mindru, I. Balau Mindru, T. Malutan, V. Tura, JAOM, Vol. **9**, No. 11, p. 3633 – 3638, (2007).
2. B. Markova, B. Hristov, T.Todorov, L. Nikolova, G.. Stoilov, J. Opt. A: Pure Appl. Opt. **11**, 065403 (2009).

Thermosetting Materials of Radiation Modified High Density Polyethylene/Iron Ferrite Nanocomposites

V. Kalkis¹, I. Reinholds¹, G. Muizzemnieks¹, J. Zicans², R. Merijs Meri²

¹Faculty of Chemistry, University of Latvia, Latvia

²Institute of Polymer Materials, Riga Technical University, Latvia

e-mail: Valdis.Kalkis@lu.lv

Reinforcement of polymer matrices to develop multifunctional nanocomposites, has experienced increasing interest among researchers during the past decade. That is mainly attributed to several shape-memory effects upon the application of heat, electricity, magnetic field and other external stimulus [1]. This study is a continuation of our research of thermosetting properties of radiation cross-linked polyolefin composite materials [2]. Binary blends of high density polyethylene (HDPE) 0-10 wt.% iron ferrite content have been made. The blends have been irradiated with accelerated electrons up to irradiation absorbed doses 150-300 kGy. Thermomechanical properties – thermorelaxation stresses formed in thermal heating and the thermo residual stresses resulting in the process full seating and cooling of materials have been investigated for orientated ($\varepsilon = 100\%$) specimens. Stress-strain and stress relaxation characteristics have been also investigated (Fig. 1) at different temperatures. An increase of mechanical stiffness, thermoresidual stresses have been found.

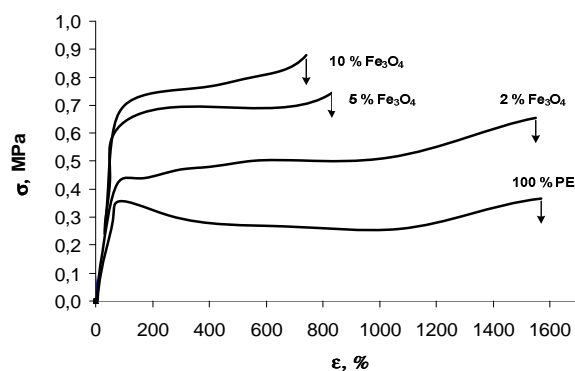


Fig.1 Stress-strain curves of HDPE and HDPE/Fe₃O₄ composites at 150°C temperature and the absorbed radiation dose equal to D = 300kGy.

Acknowledgements

This work has been supported by the European Social Fund with the project «Support for Doctoral Studies at University of Latvia».

References

1. J. Leng, X. Lan, Y. Liu, Prog. Mat. Sci. **56**, 1077-1135 (2011)
2. V. Kalkis, R. D. Maksimov, M. Kalnins, J. Zicans, T. Bocoka, O. Revjakin, Mech. Comp. Mat. **36**, 223-232 (2000)

Non-Planar Phthalocyanine for Improved Optical Coverage in Bulk Heterojunction Solar Cell

I. Kaulachs¹, G. Shlihta¹, L. Gerca², P. Shipkovs¹, V. Grehovs¹, A. Murashov¹, J. Kalnachs¹,
A. Cielavs¹, A. Ivanova¹

¹Institute of Physical Energetics, Aizkraukles 21, Riga

²Institute of Solid State Physics, Univ. of Latvia, Kengaraga str.8, Riga

e-mail: kaulacs@edi.lv

The hydroxygallium phthalocyanine (GaOHPc) and soluble fullerene derivative (PCBM) bulk heterojunction layer [1] have been used as additional layer for bulk heterojunction solar cell of poly-3-hexylthiophene (P3HT) and PCBM to increase its spectral range up to 850 nm as seen in Fig.1. Large Ga atom connected with OH group in the centre of phthalocyanine molecule provides its non-planarity and provokes strong intermolecular interaction between GaOHPc molecules in nanoclusters of GaOHPc molecules. Due to this interaction strong intermolecular charge transfer (CT) band in optical absorption spectra is observed in infrared region around 830-850 nm (see curve 5 in Fig.1). So practically uniform and strong optical absorption has been obtained for our built bi-layer bulk heterojunction system GaOHPc:PCBM/P3HT:PCBM as shown by curve 4 Fig.1. To increase internal electric field in the cell as top electrode material Ytterbium (Yb) was used having work function ~ 2.6 eV covered with Al and Se protective layer [2]. Cell thermal annealing in vacuum $10^{-6} - 10^{-5}$ mbar at 100°C for 24 hours significantly increases photocurrent external quantum efficiency (EQE) as shown in Fig. 1.

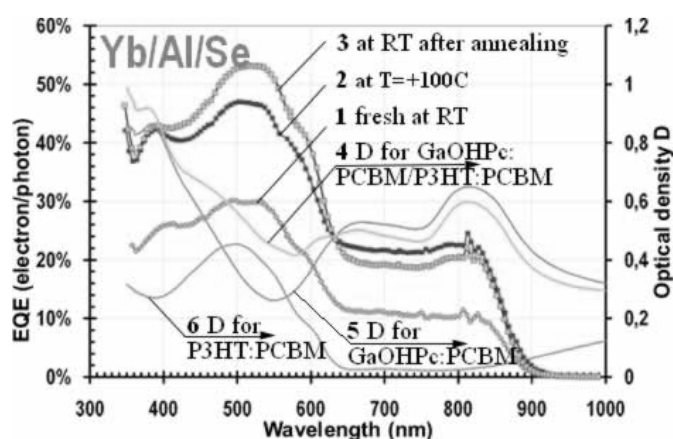


Fig.1. Spectral dependences of short circuit photocurrent EQE and optical density for ITO/PEDOT:PSS/GaOHPc:PCBM/P3HT:PCBM/Yb/Al/Se cell at light intensity $10^{12} - 10^{13}$ phot/($\text{cm}^2 \cdot \text{s}$).

References

1. I.Kaulachs, I.Muzikante, L.Gerca, G.Shlihta, P.Shipkovs, G. Kashkarova, M.Roze, J.Kalnachs, .Murashov, J.Latvels, G.Rozite., 26th EU PVSEC proceedings on DVD, pp 601- 604, (2011)
2. N. Karst, J.C.Bernede, Phys.Stat.Sol. **203** 10, R70-R72. (2006) DOI 10.1002/pssa.200622215

Iron Complexes Embedding Influence on PMAA Hydrogel Cross-Linking

L. Khenkin¹, A. Novakova¹, T. Baluyan¹

¹M.V.Lomonosov MSU, physics department, Moscow, Russia

e-mail: levkhenkin@gmail.com

The study of metal complexes incorporated into a polymer gel matrix has recently attracted considerable interest because polymer gels may react with metals to form metalorganic hybrids with unusual properties. Such systems find many applications in medicine, nonlinear optics, fluorescence, and photochromic and photorefractive systems.

In our work polymethacrylic acid (PMAA) gel was incubated in different media: the aqueous solutions of iron(II) and iron(III) chloride, the aqueous solution of ferriox (Fe²⁺–phenanthroline complex). The interaction of weakly crosslinked PMAA gel with iron complexes results in their absorption and gel collapse. This collapse occurs due to iron ions/polymer functional groups bonds that form additional cross-links contracting gel network. Internal structure of the samples was well distinguished on the images obtained by means of SEM.

The aim of present work is study of molecular lattice dynamics and metal-polymer bonds strength in PMAA gel/iron complexes systems by means of Mossbauer spectroscopy.

Mossbauer spectroscopy data for all incubated PMAA gels and for used solutions were obtained in the temperature interval from 120K till the Mossbauer effect disappear temperature. Mossbauer parameters (isomer shift and quadrupole splitting) after gel immersion kept unchanged. It means that iron ions are incorporated in gel matrix with unchanged nearest neighborhood.

Mossbauer lattice temperatures θ_M and effective vibrating mass M_{eff} were estimated from temperature dependences of recoilless fraction and second order Doppler shift d_{SOD} . All obtained data allow us to conclude that the complexes incorporate in PMAA gel matrix without destruction and forms inside the gel strong additional cross-links which have influence on gel structure.

References

1. L.V. Khenkin, A.I. Shishakov, A.A. Novakova, E.Yu. Kozhunova, E.E. Makhaeva, *Inorganic Materials* **47**, 1271 (2011)

Preparation of R-Methyl Imidazolium-Sodium Hexafluorosilicate Complex Crystals

R. Välbe¹, V. Reedo¹, U. Mäeorg², A. Hoop³, A. Lõhmus¹

¹Institute of Physics, University of Tartu, Riia 142, 51014 Tartu, Estonia

²Institute of Chemistry, University of Tartu, Ravila 14A, 50411 Tartu, Estonia

³Haine Paelavabrik OÜ, Tehase 21, Tartu, Estonia

e-mail: raul005@ut.ee

The regular complex crystals of Na_2SiF_6 have been obtained in the aqueous solutions of different methylalkylimidazolium (ethyl-, butyl- and decyl-) tetrafluoroborate ionic liquids. It is demonstrated that sodium hexafluorosilicate crystalline compounds with good regularity and narrow size distribution containing dialkyl imidazolium ions between the hexagonal crystalline clusters interconnected to each other to a whole hexagonal aggregate can be obtained in large quantities. This characteristic phenomenon of crystallization of ionic liquids containing BF_4^- ions is reported for the first time. The mechanism of formation of various $[\text{RMIm}]\text{BF}_4\text{-Na}_2\text{SiF}_6$ microcrystalline morphologies and the influence of temperature on growth kinetics are discussed. Crystallographic studies of the product were carried out by X-ray diffractometer (XRD), characterization by scanning electron microscopy (SEM) and optical microscopy; also infrared spectra (IR) were recorded. Thermal analyses were performed by differential scanning calorimetry-thermogravimetric analyser (TGA-DSC). Presence of ionic liquid cations was confirmed by high resolution mass spectrometry (HRMS).

Structural and Surface Properties of SBA-15 and SBA-16 Mesoporous Materials Functionalized With Different Groups

M. Barczak

Faculty of Chemistry, Maria Curie-Skłodowska University, Maria Curie-Skłodowska Sq. 5, 20-031 Lublin, Poland

e-mail: mbarczak@umcs.pl

Ordered mesoporous organosilicas are very attractive materials due to their high surface areas, large volumes of ordered mesopores and diverse morphology what makes them attractive potential catalysts and adsorbents. From the other hand the possibility of introduction of the organic groups into the ordered structure of the final material during the synthesis is an invaluable advantage of the sol-gel processing of organosilicas. In the present work mesoporous SBA-15 and SBA-16 organosilicas were synthesized via co-condensation of tetraethyl orthosilicate (TEOS) with alkoxysilanes bearing terminal functionalities.

Obtained materials were characterized by broad range of instrumental techniques including infrared spectroscopy, powder X-ray diffraction, thermogravimetry, nitrogen sorption measurements, elemental analysis, scanning electron spectroscopy, and transmission electron microscopy. The resulted materials exhibit well-ordered mesoporous structure, high values of specific surface areas and pore volumes and a high content of functional groups introduced during co-condensation. It was establish that even small amount of alkoxysilanes substantially changes the properties of the final materials so co-condensation can be used not only to introduce the surface functional groups but also to modify the structural-adsorption characteristics of the resulted materials.

Acknowledgements

This work has been supported by Polish Ministry of Higher Education and Science under Grant No. N N204 111135.

Molecular Dynamics of Amylin 10-29 Amyloid Formation

D. Lapidus¹, S. Ventura², C. Czaplewski³, A. Liwo³, I. Liepina¹

¹Latvian Institute of Organic Synthesis, Latvia

²Institut de Biotecnologia i de Biomedicina, Universitat Autònoma de Barcelona, Spain

³University of Gdansk, Poland

e-mail: Dmitrijs.Lapidus@gmail.com; inta@osi.lv

Amyloid formation mechanism is investigated both to find amyloid inhibitors as potential medical drugs, and to use amyloids as potential self-assembling biomaterials [1]. Amylin is one of the most amyloidogenic peptides. Amylin amyloid fibrils cause type II diabetes. Amyloid formation of amylin 10-29, its reverse and designed analogue beta-sheets and beta-sheet stacks was studied by molecular dynamics (MD), Amber 9.0, f99 force field. MD revealed that for amylin 10-29 and its reverse analogue both the parallel (Fig.1) and antiparallel beta-sheet and beta-sheet stack structures are stable suggesting that this could explain the high tendency of amylin to form amyloid fibrils. Parallel amylin beta-sheet stacks are kept together by two hydrophobic cores (Fig.1.b), while for the antiparallel system the dominating is the backbone hydrogen bonding between neighbor strands.

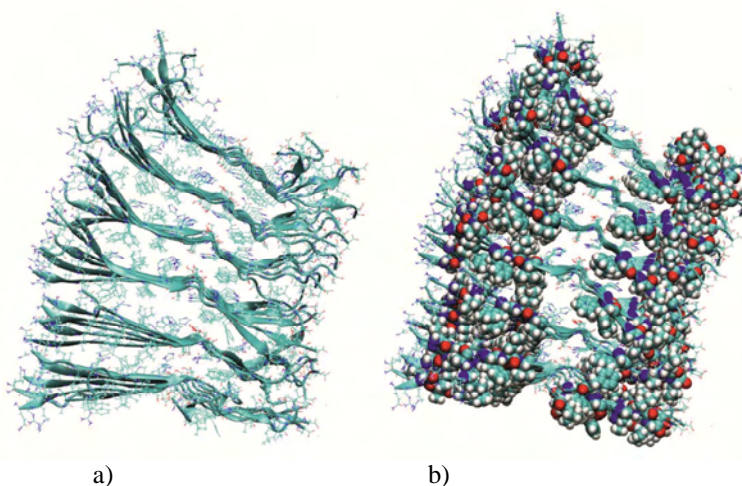


Fig.1 Amylin 10-29 parallel beta-sheet stack after 110 ns of MD run: a) cartoon representation displaying secondary structure – beta structure, b) hydrophobic residues (in VdW representation) keeping together the beta-sheet stack.

Acknowledgments

Supported by ESF project 2009/0197/1DP /1.1.1.2.0/09/ APIA/VIAA/014, Gdansk Academic Computer Center TASK.

References

1. Juan José Valle-Delgado, Inta Liepina, Dmitrijs Lapidus, Raimon Sabaté, Salvador Ventura, Josep Samitier, Xavier Fernández-Busquets. Self-Assembly of Human Amylin-Derived Peptides Studied by Atomic Force Microscopy and Single Molecule Force Spectroscopy. *Soft Matter*, 2012, 8, 1234-1242.

Molecular Dynamics of Amyloid Formation of Two Abl-SH3 Domain Peptides

D. Lapidus¹, V. Duka¹, V. Stonkus¹, S. Ventura², C. Czaplewski³, A. Liwo³, I. Liepina¹

¹Latvian Institute of Organic Synthesis, Latvia

²Institut de Biotecnologia i de Biomedicina, Universitat Autònoma de Barcelona, Spain

³University of Gdansk, Poland

e-mail: inta@osi.lv

Molecular dynamics (MD) of two peptides **DLSFMKGE (MK)** and **DLSFKKGE (KK)** not related to any known disease was run to investigate the mechanism of the amyloid formation. The beta-sheet stacks built from sixteen stranded antiparallel beta-sheets of MK- and KK-peptides: 10x6xMK and 10x6xKK, were subjected to MD, Amber 9.0, f99 force field. It was found that the MK-system, 10x6xMK, is strongly kept together due to hydrophobic core built from methionine, phenylalanine and leucine, but KK-system, 10x6xKK, which differs only by one mutation dissolves already at 20 ns of MD run (Fig.1). The hydrophobic core of the MK-system consists of hydrophobic units centered on the phenylalanine-methionine hydrophobic interactions, and two leucines from the both sides stabilize the unit. This mechanism could be used in amyloid based biomaterials.

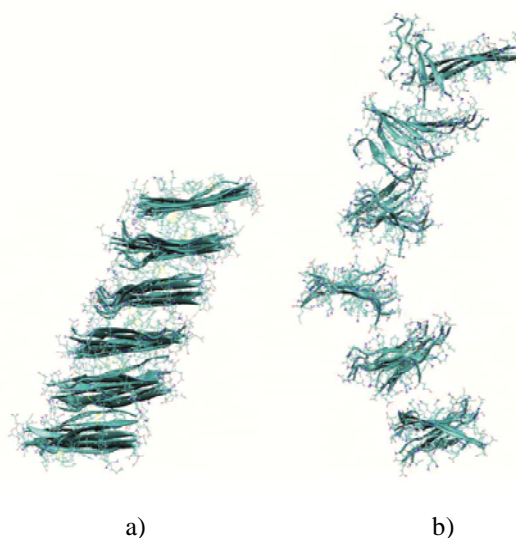


Fig.1 MK beta-sheet stack after 74ns of MD run strongly keeps together because of Met-Phe-Leu hydrophobic core, b) KK-beta-sheet stack after 20ns of MD run dissolves.

Acknowledgments

Supported by ESF project 2009/0197/1DP /1.1.1.2.0/09/ APIA/VIAA/014, Gdansk Academic Computer Center TASK.

References

1. Dmitrijs Lapidus, Vita Duka, Cezary Czaplewski, Adam Liwo, Salvador Ventura, and Inta Liepina. Multiple beta-sheet molecular dynamics of amyloid formation of two Abl-SH3 domain peptides. (*submitted*)
2. Inta Liepina, Salvador Ventura, Cezary Czaplewski, Adam Liwo. Molecular dynamics study of amyloid formation of two Abl-SH3 domain peptides. *Journal of Peptide Science*, 2006, 12, 780-789.

Influence of Laser Radiation on Electrical Resistivity of Polyisoprene/Nanostructured Carbon Composites

K. Ozols, M. Knite

Riga Technical University, Institute of Technical Physics, Latvia

e-mail: kozols@ktf.rtu.lv

It is known that polymer/carbon nanotube composites are being tested for their potential use in optoelectronic devices [1]. It is also known that polyisoprene/nanostructured carbon (PNC) composites have a pronounced resistance change under the influence of mechanical strain and vapour of volatile organic compounds [2,3]. The goal of this study was to test PNC composites for their potential use as optoelectronic materials. Measurements of relative resistance change of polyisoprene/nanostructured carbon black composites irradiated by semiconductor laser beam were conducted. One illustration of composites photoresistivity measurements at different intensities of laser radiation is given in Fig.1. Two competing mechanisms of composites resistivity change, induced by laser radiation, have been proposed: 1) photoconductivity of carbon nanostructures and 2) exponential reduction of tunnelling currents between carbon nanostructures in composite caused by thermo-optically induced matrix expansion. Further photoresistivity and optical studies of PNC composites are in progress.

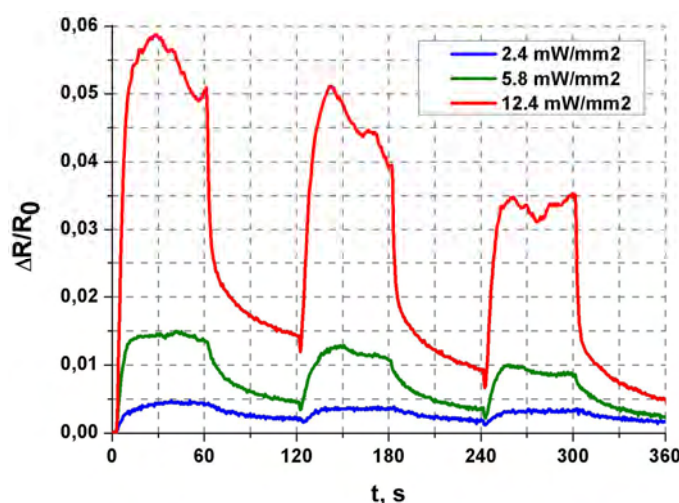


Fig.1 Relative resistance change of polyisoprene/nanostructured carbon composite with 8 m.p. of carbon black irradiated by 532 nm laser beam of different intensity.

References

1. B. Pradhan, R. R. Kohlmeyer, K. Setyowati, H. A. Owen and J. Chen. Carbon 47 (2009) 1686-1692
2. J. Zavickis, M. Knite, K. Ozols, G. Malefan, Materials Science & Engineering C, 31 (2011) 472-476
3. M. Knite, K. Ozols, G. Shakale, V. Teteris, Sensors and Actuators B Chemical, 126 (2007) 209-213

Electrical Properties and Morphology of Pentacene Thin Films Evaporated on Different Temperature Substrate

K. Pudzs, J. Latvels, A. Vembris, I. Muzikante

Institute of Solid State Physics, University of Latvia

e-mail: Kaspars.Pudzs@cfi.lu.lv

Organic molecules mostly form polycrystalline films in the evaporation process when substrate is at room temperature. The grain boundaries may act as trap states for charge carriers which negatively affect the electrical properties. This problem could be avoided in amorphous films. Cooled substrate during the evaporation could assist formation of amorphous films from organic molecules.

In this work we have investigated electrical properties (charge carriers mobility, energy structure and current-voltage characteristics) of thin pentacene films which were evaporated on substrates with different temperatures. We used “sandwich” type samples consisting of pentacene film as an active layer sandwiched between aluminium as top and gold as bottom electrode. The thickness of pentacene layer was 1 μm which allows us to use space charge limited current regime to characterise charge carrier injection and energy distribution of traps in the samples [1]. Energetical structure of local trapping states was obtained from activation energy dependence on voltage which was measured by thermally modulated space charge limited current method [2]. Charge carrier mobility was determined using charge extraction by linear increasing voltage (CELIV) method [3]. Thin film morphology was investigated by optical microscope.

The dependence of charge carrier mobility, local trapping state distribution and film morphology on substrate temperature during evaporation process will be discussed.

Acknowledgements

This work is supported by the ERAF Project No. 2010/0252/2DP/2.1.1.1.0/10/APIA/VIAA/009

References

1. E.A.Silins, *Organic Molecular Crystals. Their Electronic States* (Springer-Verlag, Berlin-Heidelberg-New-York, 1980)
2. S.Nešpůrek, O.Zmeškal, J.Sworakowski, *Thin Solid Films* **516**, 8949 (2008)
3. G.Juška, K.Arlauskas, M.Viliunas, J.Kocka, *Physical Review Letters*, **84**, 4946 (2000)

Mechanical and Structural Properties of Polyolefin/Iron Ferrite Magnetic Nanocomposites

I. Reinholds¹, V. Kalkis¹, J. Zicans², R. Merijs Meri², A. Grigalovica²

¹Faculty of Chemistry, University of Latvia, Latvia

²Institute of Polymer Materials, Riga Technical University, Latvia

e-mail: Valdis.Kalkis@lu.lv

Polymer nanocomposites of high density polyethylene (HDPE) and polypropylene (PP) with different content (2-10 wt.%) of iron ferrite Fe_3O_4 nanofiller have been made. It is known that photo, radiation or thermally initiated grafting of acrylate monomers can improve the properties of polyolefin based polymers [1]. For such a purpose the 2,2'-bis-[4-(2-methylprop-2-enoyloxy)phenyl]-propane (BAD) has been added to polymers during the thermoplastic mixing to improve compatibility of the filler and polymer matrix in composite materials. The mechanical properties of have been estimated, showing increase of stiffness as reinforcement effect of nano filler [2], an increment of plasticity for composites modified with BAD (Fig 1.) was found.

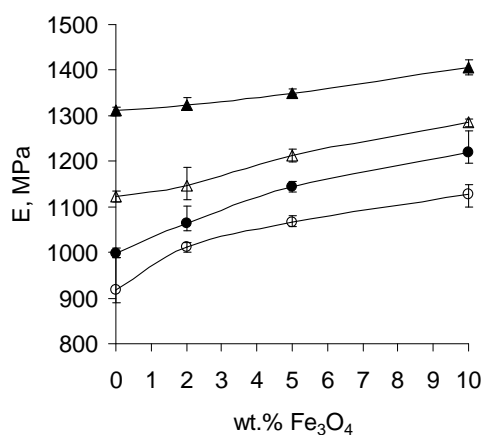


Fig.1 The effect of filler content on the elastic modulus of HDPE (1), HDPE-BAD (2), PP (3) and PP-BAD (4) based composite materials.

The methods of XRD, DSC and TGA have been used to investigate the effect of filler dispersion in the polymers on the crystallinity and the calorimetric properties, showing increase of thermal stability of composites in comparison to that of pure polymers.

Acknowledgements

This work has been supported by the European Social Fund with the project «Support for Doctoral Studies at University of Latvia».

References

1. F. Carosio, A. Fina, M. Coisson, Polym. Bull. Phys. **65**, 681-689 (2010)
2. G. Gomes de Barros, F. Galembeck, Polym. Bull. **16**, 499-505 (1986)

Synthesis and Use of Methacrylic and Styrenic Monoliths as Stationary Phases in HPLC

R. Fedorovskis¹, Z. Zanriba¹, K. Kucins¹, R. Poplauskis², D. Erts², I. Susinskis³, K. Kuprevics³,
J. Hmelnickis³, S. Ābele¹

¹The Faculty of Chemistry, University of Latvia, Riga, Latvia

²The Institute of Chemical physics, University of Latvia, Riga, Latvia

³ISC"Grindeks", Riga, Latvia

e-mail: silvija.abele@lu.lv

Research of new progressive and more efficient methods for detection and quantification of various substances in different samples is one of the objectives of analytical chemistry. In HPLC there are several aspects that can be still optimised, one of them being the research of new alternative stationary phases. In early 1990's F. Svec and Fréchet suggested methacrylic organic monoliths as stationary phase in HPLC [1-2], this column was used to separate proteins [3].

Organic monoliths are continuous cross linked polymers with porous structure and large surface area synthesized *in situ* in fused silica capillary or other molds (Fig 1.).

In the present work separation of a mixture of uracil and tegafur was done using obtained capillary column of poly(styrene – *co* – divinylbenzene) monolith. The best results were obtained using 95 % water with 5 % methanol as mobile phase. Retention time was 1.65 min for uracil and 3.61 min for tegafur. Poly(glycidyl methacrylate – *co* – ethylene dimethacrylate) monolithic capillary column was used for separation of imatinib base, imatinib mesilate and aminophenyl pyrimidine. Retention times were 9.40 min for imatinib base and imatinib mesilate and 8.20 min for aminophenyl pyrimidine. Both monolithic columns showed a potential in separations of pharmaceutical compounds and their byproducts.

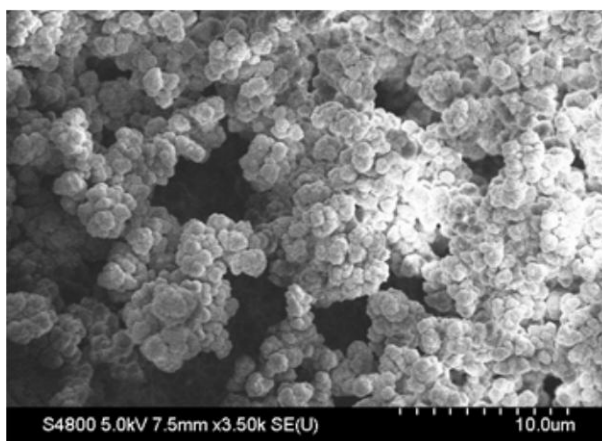


Fig.1 Structure of poly(glycidyl methacrylate - *co* - dimethacrylate) monolith, image obtained by SEM, magnification 3,5 K

References

1. F. Svec, J. M. J. Fréchet, *Science*, **273**, 205 – 211 (1996)
2. F. Svec, J. M. J. Fréchet, *Anal. Chem.*, **64**, 820 – 822 (1992)
3. D. Lee, F. Svec, J. M. J. Fréchet, *Journal of Chromatography A*, **1051**, 53 – 60 (2004)

Synthesis Tri-Metallic Platinum Group Metal Electrocatalysts Using Organometallic Chemical Vapour Deposition Technique for Methanol Oxidation

Q. Naidoo¹, S. Naidoo^{2,3}, A. Nechaev¹, P. Ndungu⁴, L. Petrik¹, G. Vaivars⁵

¹Environmental and Nanosciences Research Group, Department of Chemistry, University of the Western Cape, Bellville, South Africa

²Environmental and Process Systems Engineering, Department of Chemical Engineering, University of Cape Town, South Africa

³Centre for Occupational and Environmental Health Research, Department of Occupational Health and Family Medicine, University of Cape Town, South Africa

⁴School of Chemistry, University of KwaZulu-Natal, Westville Campus, Durban, South Africa

⁵Institute of Solid State Physics University of Latvia 8 Kengaraga iela LV-1063, Riga, Latvia
e-mail: qiling.naidoo@uct.ac.za

A series high active tri-metallic platinum group metal nanocatalyst was successfully synthesized by a simple but effective solvent free, organometallic chemical vapour deposition method (OMCVD). The electrocatalysts were characterized by ICP, XRD, HRTEM. The catalytic activity was determined by cyclic voltammetry (CV). In the investigation of platinum alloy electrocatalysts, the results of the tri-metallic catalysts showed that the additional metals of platinum alloys could reduce the metal particle sizes and resulted in a larger chemical-active surface area and higher methanol oxidation activity of the catalysts. A significantly higher electrocatalytic activity for PtRuV/CNT catalyst was also found in this study.

Formation of Nanosized Strontium Substituted Hydroxyapatites

A. Jershova¹, K.A. Gross², D. Grossin³, C. Rey³, A. Vīksna¹

¹Department of Analytical Chemistry, University of Latvia, Latvia

²Institute of Biomaterials and Biomechanics, Riga Technical University, Latvia

³Université de Toulouse, CIRIMAT, France

e-mail: anastasija.jershova@gmail.com

Hydroxyapatite (HAp) is a widely used biomaterial for bone regeneration and provides a surface for bone attachment to implants. The crystal lattice of hydroxyapatite $[\text{Ca}_{10}(\text{PO}_4)_6(\text{OH})_2]$ can accommodate many divalent cation substitutions such as strontium (Sr), magnesium (Mg), barium (Ba) and zinc (Zn). These influence the processability of hydroxyapatite and impact the biological properties. The osteoconductive properties of Sr make it a very interesting candidate for inclusion in the lattice for the preparation of nanosized apatite. The inclusion of the larger strontium ion may decrease the diffusion within the lattice and thus enable easier formation of nanosized Sr enriched hydroxyapatite.

In the current work atomic assemblies were produced to a chemistry of hydroxyapatite and different degrees of calcium substitution with Sr (0%, 25%, 75% and 100%). These were heated using differential thermal analysis and thermogravimetry (DTA/TGA) to follow the evolution of the apatite phase upon heating. A larger concentration of Sr produces a less

stable assembly that provides crystallization at a lower temperature. The transition does not have a large driving force, and this provides control of both the crystallinity and nanocharacteristics of the strontium enriched phase. The phases were investigated with X-ray diffraction (XDR) both before and after heat treatment at 900°C and confirmed apatite phase purity. Quantitative analysis of calcium, strontium and phosphorus was performed using wavelength dispersive X-ray fluorescence.

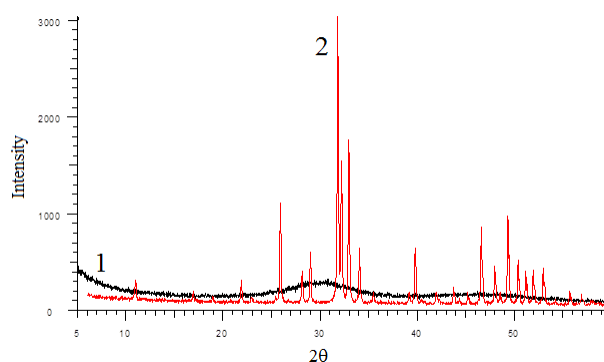


Fig.1 25% Sr substituted hydroxyapatite X-ray diffraction before (1) and after (2) heating.

Two Thin Polymer Sheets Identification of Flexural Modulus

S. Gluhihs, A. Kovalovs, A. Chate

Institute of Materials and Structures, Riga Technical University, Latvia

e-mail: s_gluhihs@inbox.lv

The purpose of the present investigation is to elaborate a method for determining the flexural modulus of a polymer material based on the solution of compression problem by using the finite-element method in the finite element program ANSYS.

The cylindrical shell consists of two layers with different elastic modulus. The inner layer (bandage) of the cylindrical shell is made from a rigid polymeric material with relatively high Young's modulus. The outer layer is unknown and made from a softer polymer. Layers are considered homogeneous and isotropic.

For the identification of the elastic modulus of the outer layer the *TWCS method* (Method for the Identification of the Elastic Properties of Polymer Materials by Using Thin-Walled Cylindrical Specimens) is considered.

The contact problem is solved by using the Finite Element Method. The deformation of a thin polymer shell is characterised by great displacements and relatively low elastic deformations in a large range of movement of parallel planes.

According to the above mentioned method at first the so-called reduced elastic modulus E_{priv} (modulus of inelastic buckling) is determined from the compression experiment of a cylindrical shell. The cylindrical shell is assumed to be single-layered with thickness $t=t_1+t_2$. Then the step-down ratio for the elastic modulus $K=E_1/E_{priv}$ is introduced. Further a Finite Element model for the problem of compression of a two-layer cylindrical shell is built by using software package ANSYS.

The series of calculations of the cylindrical shell with different elastic modulus of the outer layer are carried out. Obtained results are tabulated and then on the basis of these tables the graph of the dependence of the relative Young's modulus E_1/E_{priv} from the logarithm of the ratio of the elastic modulus of layers $lg(E_1/E_2)$ is constructed.

Determination of Cerium Oxidation State in Cerium Substituted Hydroxyapatites

L. Bauermeistere¹, A. Viksna¹, A. Kareiva², K.A. Gross³

¹Faculty of Chemistry, University of Latvia, Latvia

²Faculty of Chemistry, Vilnius University, Lithuania

³Institute of Biomaterials and Biomechanics, Riga Technical University, Latvia

e-mail: lauma.bauer@gmail.com

Hydroxyapatite (HAp) is chemically similar to the mineral component of bones and hard tissues in mammals. It is one of few materials that are classed as bioactive, but it shows insufficient antibacterial properties. The antibacterial properties can be improved by substituting calcium with cerium in the HAp structure [1]. This research investigates the quantitative determination of cerium content in each oxidation state by using potentiometric titration with iron ions in an acidic media.

Cerium substituted HAp (Ce-HAp) were synthesized in the Faculty of Chemistry, Vilnius University with the sol-gel method. Ce-HAp samples with total theoretical amount of 1, 3, 5 and 10 Ce wt% were produced. The actual amount of Ce⁴⁺ ions was obtained by titrating solutions of Ce-HAp with a Fe²⁺ standard solution. Meanwhile, the Ce³⁺ ion content was obtained by titrating with a Fe³⁺ solution. The samples were prepared for titration by dissolving Ce-HAp powders in 0.1M hydrochloric acid at atmospheric pressure and in 0.08M nitric acid at increased pressure and temperature. Total amount of cerium was determined using the ICP-MS method.

The results of total amount of cerium in Ce-HAp determined by ICP-MS, show that all of the added cerium incorporates in the HAp structure using the sol-gel route. Potentiometric titration is applicable for determination of cerium oxidation states in Ce-HAp. However, the limiting factor is the low solubility of Ce-HAp, which decreases at increasing concentrations of cerium. The solubility could be encouraged by heat treatment at optimal temperature, thus facilitating dissolution for the analysis of the cerium content. By optimizing the titration conditions (temperature, solution media) successful determination of cerium in different oxidation states in Ce-HAp is possible.

References

1. Y.G. Lin et al (2007) Antibacterial property of cerium substituted hydroxyapatite nanoparticles, *J. Rare Earths* **25**: 452-456

Role of Paramagnetic Polyconjugated Clusters In Lignin Antioxidant Activity

T. Dizhbite¹, J. Ponomarenko¹, A. Andersone¹, G. Dobele¹, M. Lauberts¹, J. Krasilnikova^{1,2},
N. Mironova-Ulmane³, G. Telysheva¹

¹Latvian State Institute of Wood Chemistry, Latvia

²Riga Stradins University, Latvia

³Institute of Solid State Physics, University of Latvia, Latvia

e-mail: ligno@edi.lv

In the last years, instead of the synthetic antioxidants usually employed, natural ones are being investigated to reduce the ecological problems. Lignin (Fig.1) is the second after cellulose most abundant natural polymer. Lignin *in situ* serves to protect plants against chemical, biological and mechanical stresses. Technical lignins are multi-tonnage by-products of pulp and paper industry. The well documented antioxidant properties of technical lignins open variety of fields for their application as multifunctional products. Due to molecular complexity of lignins, it is difficult to assign their antioxidant activity to specific structural elements and further search of the relationship “structure-activity” is needed to determine directions for goal-oriented tuning of lignin structure, in order to use these naturally originated products successfully. In the present work, the lignins isolated by alkaline delignification from deciduous wood species and lignin fractions of pyrolytic oil produced from the same wood species, were characterized using EPR spectroscopy, size exclusion chromatography, analytical pyrolysis and wet chemical analysis. The data obtained were considered together with the results of DPPH[•], ABTS^{•+} and superoxide radical anion (O₂^{•-}) antioxidant assays. It was found that, besides OH_{phen} and molecular weight, paramagnetic clusters formed by π -polyconjugation systems play a crucial role in lignin antioxidant activity. The positive Pearson correlation of antioxidant capacity and size of lignin paramagnetic clusters was found and explained by the high ability of the π -polyconjugation systems to form donor-acceptor auto-complexes. In the experiment *in vitro* it was shown that the relationship found was in compliance with the decreasing indices of lipids peroxidation (malondialdehyde content, MDA) and proteins oxidation (Protein carbonyl content, PCC) in blood as the result of its incubation with lignin.

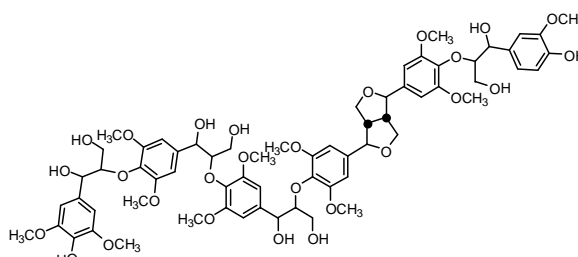


Fig.1. Potential structure of a repeated unit in hardwood lignin

Temperature Induced Color Changes in Photoluminescent Polymer/Dye Blends

R. Karpicz¹, N. Ryškevič², S. Jursenas², I. Muzikante³

¹Center for Physical Sciences and Technology, Savanoriu Av. 231, LT-02300 Vilnius, Lithuania; Vilnius, Lithuania

²Institute of Materials Science and Applied Research, Vilnius University, Sauletekio 9, LT-10222

³Institute of Solid State Physics, University of Latvia, Kengaraga 8, Riga, LV-10363, Latvia

e-mail: renata@ar.fi.lt

In recent years, the incorporation of excimer-forming luminescent molecules in transparent polymers has been extensively investigated as materials which could be used for sensors. Such materials are attractive due to the abundance of potential commercial applications. Significant interest has been directed towards the investigation of systems, in which the application of stimuli has to induce the formation or breakup of excimer-forming dye aggregates in the dye-polymer blend. Sensors based on fluorescent dye/polymer system could exhibit a change of their fluorescence characteristics (fluorescence enhancement or quenching) in response to external stimuli as heat, deformation, light.

In the present work the characterization of blend films of different polymers and excimer-forming, photoluminescent N,N-dimethylaminobenzylidene indan-1,3-dione (DMABI), which function as threshold temperature sensors are described. The impact of aggregate states on optical and morphological properties of blend films doped by DMABI molecules was studied. Formation of DMABI nanocrystallites (up to micrometer size) after annealing above polymer glass transition temperature was shown to have impact on the extent of molecular aggregation and emission properties of the films. The annealing of films leads to variation of contributions of the DMABI monomer and the self-trapped excitation crystallite emission. This results in pronounced change in the emission color of the DMABI/polymer films from orange (before annealing) to green (after annealing). We report on reversible colour change effect upon annealing (from excimer-like to molecular-like luminescence), which is attributed to diffusion induced crystallisation.

Nonlinear Optical Properties of Low Molecular Organic Glasses Formed by Triphenyl Modified Chromophores

A. Tokmakovs¹, M. Rutkis¹, K. Traskovskis², E. Zarins², L. Laipniece², V. Kokars², V. Kampars²

¹Institute of Solid State Physics, University of Latvia, Latvia

²Institute of Applied Chemistry, Riga Technical University, Latvia

e-mail: andrey.tokmakov@gmail.com

Coupling of bulky triphenyl molecular fragments, as anti-crystallization agents, with chromophores allows us to obtain amorphous materials for nonlinear optic (NLO) applications. Potential perspective of such materials we would like to proof on a basis of compounds with three types of core chromophores (see fig.1 A, B, C) in combination with different triphenyl fragments (S2 – S8). For all these materials, by spin coating from chloroform or chlorobenzene solution we are capable to obtain glassy optical quality thin films. To produce NLO active media thermo assisted electrical field poling procedure was applied via custom build corona triode setup. NLO efficiency and polar order (PO) thermal stability was evaluated by

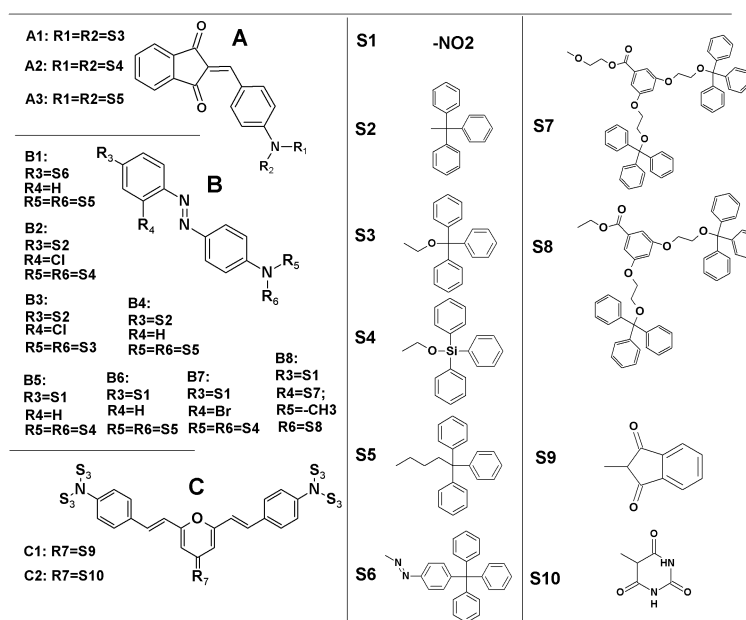


Fig.1 Structures of investigated low molecular glasses forming compounds.

Maker fringe technique and SHG efficiency with temperature scans. Relation of these properties with structure of chromophore and triphenyl fragment containing substitutes will be discussed. The highest NLO efficiency $d_{33}(0) = 22$ pm/V was archived in case of structure **A3** involving an indadione chromophore. A relatively high for molecular glasses PO stability (50% SHG decay at 71°C) was characteristic for this compound.

Hyper-Rayleigh Scattering and Two-Photon Luminescence of Phenylamine–Indandione Chromophores

I. Mihailovs^{1,2}, J. Kreicberga², V. Kampars², S. Miasojedovas³, S. Juršēnas³, L. Skuja¹, M. Rutkis¹

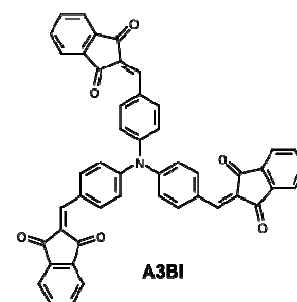
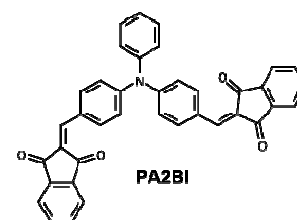
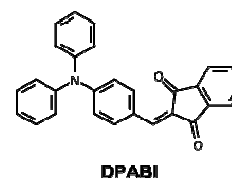
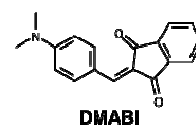
¹Institute of Solid State Physics, University of Latvia, Riga, Latvia

²Institute of Applied Chemistry, Riga Technical University, Latvia

³Institute of Applied Research, Vilnius University, Vilnius, Lithuania

e-mail: igors.mihailovs_2@rtu.lv

Since remarkable NLO properties of 4-dimethylamino-benzylidene-1,3-indandione (DMABI) were reported we have promoted indane-1,3-dione derivatives as chromophores for NLO application. Based on results of quantum chemical (QC) screening, we have synthesized phenylamine indane-1,3-dione derivatives including octupolar NLO chromophore A3BI. According to these calculations, molecular first hyperpolarizability (β) should be enhanced upon replacement of methyl substituents with phenyl groups. Surprisingly, β values obtained in our measurements by hyper-Rayleigh scattering (HRS) are much higher than one could expect from QC. Acquired β values (relative to standard compound DANS) was 1.17 (QC 0.87), 2.58 (1.04), 5.44 (1.07) and 7.89 (1.10) for DMABI, DPABI, PA2BI and A3BI, accordingly. Bearing in mind that two-photon luminescence (TPL) is usual cause for overestimation of β in HRS measurements, we have accomplished investigations of TPL properties of these compounds. All triphenylamine derivatives exhibit strong TPL. At similar excitation conditions the highest TPL intensity was recorded for PA2BI (relative TPL intensities of DMABI, DPABI, A3BI and PA2BI are 1, 10, 50 and 100). At same time TPL spectra showed comparatively low emission intensity at 532 nm, where the HRS signal should occur. Due to this only small overestimation of β by HRS could be expected. Nevertheless, to clarify our β measurements, we decided to make an attempt to record TPL spectra and HRS signal simultaneously. In case of DMABI, both signals are clearly resolved, and TPL free β value can be defined. For all triphenylamino compounds, due to fairly intensive TPL, the HRS signal was rather indistinguishable and therefore correct β values could not be extracted.



Multiscale Approach to the Structure and Spectra of Nile Red Adsorbed on Polystyrene Nanoparticles

A. Freidzon, V. Tikhomirov, A. Odinokov, A. Bagaturyants

¹Photochemistry Center, Russian Academy of Sciences, Moscow, Russia

e-mail: freidzon.sanya@gmail.com

The structure and absorption spectra of Nile Red (NR) dye adsorbed on the surface of polystyrene (PS) nanoparticles is studied by DFT.

Polystyrene nanoparticle with an adsorbed NR molecule was simulated by a large cluster consisting of PS chains using molecular dynamics in the OPLS-aa force field in the NVT ensemble at 298 K. Different surface models were tried: a surface of a single-chain coil (up to 1000 monomeric units) and of a periodic box. Next, the surface was truncated so that only the nearest-neighboring phenyl rings surrounding the chromophore (bold lines in the figure) were treated either explicitly by DFT or as effective fragment potentials (EFP). The structure of the dye from MD calculation

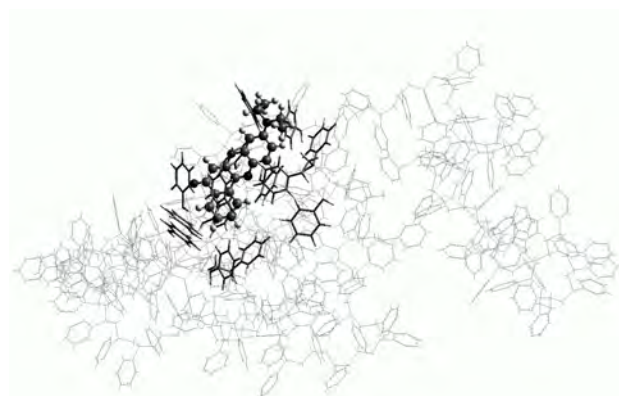


Fig.1 Polystyrene cluster with adsorbed Nile Red dye considered at different level of theory: thin lines, molecular dynamics; bold lines, effective fragment potentials; balls-and-sticks, quantum mechanics

was re-optimized by DFT in the frozen environment, and its absorption and emission spectra of were calculated by TDDFT in this environment and compared with those in vacuo and in toluene (simulated through polarizable continuum model). It is shown that the transition energies calculated in an explicit environment and in EFP are almost the same, but EFP makes the calculation cheaper. The positions of the absorption, locally excited (LE) and twisted intramolecular charge transfer state fluorescence bands are in good agreement with the experiment.

Luminescence and Structural Properties of Thermally Evaporated Benzanthrone Dyes Thin Films

A. Bulanovs¹, G. Kirilov¹, I. Mihailova¹, E. Kirilova²

¹Innovative Microscopy Center, Daugavpils University, Daugavpils, Latvia

²Department of Chemistry, Daugavpils University, Daugavpils, Latvia

e-mail: bulanov@inbox.lv

We report luminescence and structural properties of 3-N, N-diacetylaminobenzanthrone thin films deposited on glass substrate by thermal evaporation. The structural and optical properties of organic thin films were studied by means of the confocal microscope with an input of femtosecond laser radiation, X-ray diffractometer, and scanning electron microscope (SEM). Intense luminescence with the maximum at 530 nm was observed when excited by laser radiation with the wavelengths 458-514 nm. In addition, the luminescence caused by two-photon absorption of infrared femtosecond (fs) laser radiation has been investigated. The study of the structure of benzanthrone derivative thin films, created by X-ray diffraction (XRD) methods, indicate the distance between molecular layers and ordered molecular fragments.

Near-Band Luminescence of CdZnTe Detector Crystals

L. Grigorjeva¹, V. Ivanov², L. Alekseeva², D. Millers¹

¹Institute of Solid State Physics, University of Latvia, Latvia

²ZRF RITEC SIA, Riga, Latvia

e-mail: lgrig@latnet.lv

Cadmium zinc telluride, $\text{Cd}_{1-x}\text{Zn}_x\text{Te}$ (CZT) is a promising material for the room temperature X- and γ -ray detectors as well as for electro-optic modulators, solar cells and other devices. The CZT is direct band gap semiconductor with efficient exciton transitions at low temperature [1,2]. Therefore, the near-band luminescence is due to neutral donor bound exciton (D^0Ex), to neutral acceptor bound exciton (A^0Ex) and its phonon replicas (LO phonon energy is 22 meV). The luminescence of donor-acceptor pair (DAP) and deep energy level due to undefined defect state (A band) are typical for CZT crystals [1,3]. Since the luminescence centers involves the donor, acceptor and defect states we assume that the near band luminescence correlate with detectors quality and the luminescence studies could be used for nondestructive detector material selection. The luminescence spectra and decay kinetics were measured at 15K under pulsed YAG:Nd laser excitation (266 nm, 2 ns), spectral energy resolution better than 0.25 meV over the measuring range.

The samples were taken from different ingots. From the same samples the γ -ray detectors were prepared and tested. The luminescence bands were identified and the correlation with detector characteristics and the near band luminescence (Fig.1) was established and discussed.

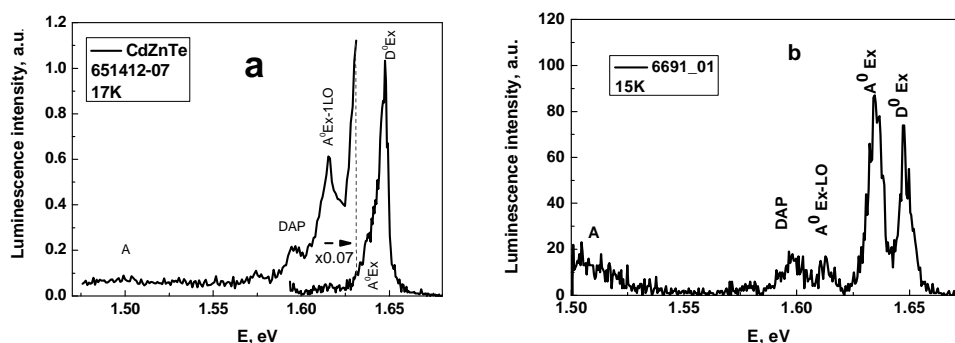


Fig.1. Photoluminescence spectra of CZT crystals. The crystal shows a good (a) and bad (b) detector spectrometric characteristics.

References

1. K.Hjelt, M.Juvonen, T.Tuomi, S.Nenonen, E.E. Eissler and M.Bavdaz. Phys.stat.sol. (a) **162**, 747 (1997)
2. T.E.Schlesiger, J.Toney, H.Yoon, et al. Material Sci. and Eng. **32**, 103, (2001).
3. P.Yu, W.Jiw, T.Wang. NIM **A643**, 53 (2011)

Induced Short-lived Absorption in PLZT Electrooptical Ceramics

V. Dimza, D. Millers, M. Antonova, L. Grigorjeva, M. Livins, K. Smits

Institute of Solid State Physics University of Latvia

e-mail: dmillers@latnet.lv

The study of induced short-lived absorption in PLZT 8/65/35 compound, commonly known for relaxor behaviour, was carried out.

The used equipment for short-lived absorption registration contain a pulsed electron beam (source operated at 270 kV accelerating voltage, pulse length 10 ns) source for excitation, a xenon flash (pulse had flat top within 10 μ s) for probing light. The probing light enter in the sample from one side, was totally reflected from the irradiated surface of sample and come out from sample other side. This configuration used allows longer optical path of probing light through the sample and therefore the more sensitive registration of absorption changes.

The induced short-lived absorption was observed within 1.10 – 2.85 eV. The spectrum reveals poor resolved bands at \sim 1.3; 1.7 and 2.3 eV. The absorption spectrum depends on recording time – the growth of absorption starts simultaneously with excitation pulse, continues after excitation pulse and this growth was followed by absorption decay. The absorption decay rate is different over spectrum. Therefore the induced short-lived absorption kinetics details were studied. It was found the time for short lived absorption maximum value reaching is approximately the same within 1.25 – 2.05 eV range, whereas within 2.25 – 2.65 eV the absorption growth time is significant longer; therefore the short-lived absorption growth time showed step like dependence over spectrum.

The induced short-lived absorption (optical density D) decay can be approximated with the stretched exponent $D = D_0 \exp\{-(t/\tau)^\beta\}$, the value of β being close to the 0.6 for all kinetics, however the τ is different and thus the absorption spectrum changes during short-lived absorption decay.

The possible mechanisms responsible for short-lived absorption induction by electron beam pulse as well as some details of this absorption decay will be discussed on bases of results obtained in experiments.

Oxygen Vacancies and RE Ion Agglomeration Caused Up-Conversion Luminescence Quenching Prevention in Zirconia

K. Smits¹, A. Sarakovskis¹, D. Millers¹, D. Jankovica^{1,2}, L. Grigorjeva¹

¹Institute of Solid State Physics, University of Latvia, Latvia

²Institute of Inorganic Chemistry, Riga Technical University, Latvia

e-mail: smits@cfi.lu.lv

Zirconia is one of the most promising oxides to be used as an up-conversion host material, because of the high chemical and physical stability well as due to relatively low phonon energy of the matrix especially among oxides (about 470 cm^{-1}) which is an important factor for the overall efficiency of the up-conversion processes in a material.

As up-conversion luminescence center we chose Er, the additional doping with Yb enhances up-conversion process efficiency due to Yb ion large cross-section for optical absorption and effective energy transfer to Er. Both Er and Yb incorporate in Zr^{4+} sites as RE^{3+} , therefore for charge compensation oxygen vacancies appear. Oxygen vacancies stabilizes tetragonal or even cubic zirconia phase, but oxygen vacancies disturb energy transfer from one RE ion to another RE ion. Therefore, to prevent the formation of oxygen vacancies additional doping of Me^{5+} ions was performed

$\text{ZrO}_2:\text{Er}:\text{Yb}$ samples with and without Nb codoping were prepared by sol-gel method. Both types of the samples were annealed at different temperatures to study the phase transition impact on up-conversion luminescence. The study of stationary and time-resolved luminescence was carried out to study the energy transfer process and an impact of intrinsic defects on the luminescence. X-ray diffraction measurements were used to determine phase composition and grain sizes. The Nb doping significantly increased up-conversion luminescence intensity.

Concentration Impact on Er³⁺ Green Luminescence Decay Kinetics in NaLaF₄

J. Grube¹, G. Doke¹, M. Voss¹, A. Sarakovskis¹, M. Springis¹

¹Institute of Solid State Physics, University of Latvia, Latvia

e-mail: jurgis.grube@cfi.lu.lv

For the materials doped with Er³⁺ ions intensive luminescence bands are often observed in wide spectral region (500 – 1000nm). Our previous studies have showed that NaLaF₄ could be promising host material for practical application due to low phonon energy [1].

In this work Er³⁺ doped NaLaF₄ at different Er³⁺ ion concentrations (0.2 – 10mol%) were synthesized. Intensive green luminescence band (origin from ⁴S_{3/2} to ⁴I_{15/2} transition) was observed for all Er³⁺ content. Studies of Er³⁺ green luminescence decay kinetics at different Er³⁺ ion concentration, which could not be fitted by a simple exponent, reveals that energy transfer process appears. Several energy transfer processes, like direct relaxation, fast migration and migration-limited relaxation, have been proposed to describe luminescence decay kinetics.

Based on the experimental results peculiarities of energy transfer processes in NaLaF₄ and their variation at different Er³⁺ content will be discussed.

Acknowledgements

The financial support of State Research Program IMIS (project 1) and ESF project 2009/0202/1DP/1.1.1.2.0/09/APIA/VIAA/141 is highly appreciated.

References

1. A. Sarakovskis, J. Grube, A. Mishnev, M. Springis, *Optical Materials* **31**, 1517-1524 (2009)

Photoluminescence and Energy Transfer in Nd³⁺ and Er³⁺ Doped NaLaF₄ Material

G. Doke, M. Voss, J. Grube, A. Sarakovskis, M. Springis

Institute of Solid State Physics, University of Latvia, Latvia

e-mail: guna.doke@gmail.com

Due to very promising optical applications rare-earth doped fluorides have been intensively studied for several decades. In past few years as one of the best host material for rare-earth ions NaLaF₄ is mentioned [1].

In this work NaLaF₄:Er³⁺, NaLaF₄:Nd³⁺ and NaLaF₄:Er³⁺,Nd³⁺ at different Er³⁺ and Nd³⁺ concentrations were synthesized. For these samples photoluminescence and excitation spectra as well as photoluminescence kinetics were measured.

From the analysis of the experimental data it is concluded that there are energy transfer from Nd³⁺ to Er³⁺ (Fig. 1). The most likely transfers are ²H_{11/2} (Nd³⁺) → ⁴F_{9/2} (Er³⁺) and ⁴G_{7/2} (Nd³⁺) → ²H_{11/2}; ⁴S_{3/2} (Er³⁺) followed by ⁴S_{3/2} (Er³⁺) → ⁴F_{9/2} (Er³⁺). Electronic transition within Er³⁺ from ²H_{11/2}, ⁴S_{3/2} and ⁴F_{9/2} to ground state ⁴I_{15/2} results in emission of “green” (540 nm, 520 nm) and “red” (660 nm) luminescence.

Based on obtained results the activator concentration impact to energy transfer mechanisms and photoluminescence spectra are discussed.

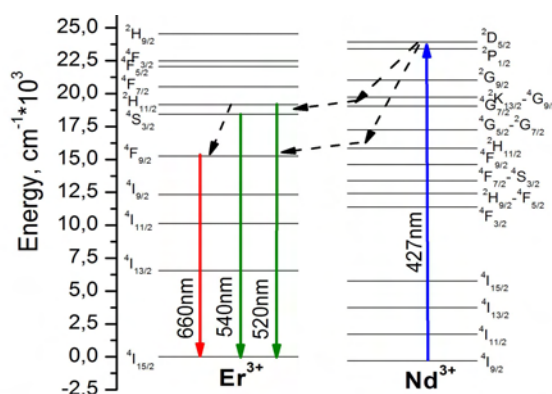


Fig.1 Energy level schemes of Er³⁺ - Nd³⁺ and possible energy transfer mechanisms. Full and dashed arrows stands for radiative and nonradiative transitions, respectively

Acknowledgments

The financial support of State Research Program IMIS (project 1) as well as ESF project 2009/0202/1DP/1.1.1.2.0/09/APIA/VIAA/141, ESF project 2009/0162/1DP/1.1.2.1.1/09/IPIA/VIAA/004 is greatly acknowledged.

References

1. A. Sarakovskis, J. Grube, A. Mishnev, M. Springis, Optical Materials 31, 1517-1524 (2009).

Up-Conversion Luminescence in Erbium Doped Cubic and Hexagonal NaYF₄

A. Sarakovskis¹, M. Voss¹, G. Doke¹, D. Jankovica², J. Grube¹, M. Springis¹

¹Institute of Solid State Physics, University of Latvia, Latvia

²Institute of Inorganic Chemistry, Riga Technical University, Latvia

e-mail: anatolijs.sarakovskis@cfi.lu.lv

Up-conversion luminescence process, which is related to absorption of several light photons (usually infrared) followed by emission of light in the visible or even ultraviolet spectral regions, has attracted interest of scientists due to its potential practical use in various applications including biolabels, temperature sensors, light sources etc. Although observable in d- and f-ions doped materials, the highest efficiency of up-conversion luminescence is usually attained in lanthanides doped hosts. Among huge variety of materials suitable as up-conversion hosts the most prominent is considered to be NaYF₄, both due to its low phonon energy and multisite nature of the crystalline lattice.

In the present report erbium doped NaYF₄ nanomaterial has been synthesized by molten salt method. Depending on the synthesis temperature the structure of the material varied from solely cubic to exclusively hexagonal. Up-conversion luminescence spectra and luminescence kinetics for the samples having different phase compositions have been measured. It was found that the shapes of the up-conversion luminescence spectra related to the cubic and the hexagonal phase were almost independent of the structure while the overall efficiency of the up-conversion process in hexagonal phase was at least order of magnitude higher compared to the cubic. In the report the structure impact on the up-conversion luminescence of NaYF₄:Er³⁺ will be discussed.

Acknowledgements

The financial support of State Research Program IMIS (project 1) and ESF project 2009/0202/1DP/1.1.1.2.0/09/APIA/VIAA/141 is highly appreciated.

References

1. F. Auzel, Proc. IEEE **61** (1973), p. 758.
2. D. L. Huber, D. S. Hamilton and B. Barnett, Phys. Rev. B **16**, 4642 (1977)

Absorption Spectra of Irradiated LiYF₄ Crystals at 15K

Y. Bikhert¹, V. Korepanov², L. Lisitsyna³, A. Dauletbekova¹, V. Lisitsyn², V. Reiterov⁴

¹L.N. Gumilyov Eurasian national university, Kazakhstan

²Tomsk national research polytechnic university, Russia

³Tomsk state university of architecture and civil engineering, Russia

⁴INCROM, Russia

e-mail: alma_dauletbek@mail.ru

The goal of the current work is to study the kinetics of induced optical absorption spectra in pure and doped with Nd³⁺ + (0,7; 1,5; 2 mol%) LiYF₄ crystals (INCROM, St.Petersburg, Russia) irradiate at low electron fluxes at 15 K. Samples were cut from single crystals along and perpendicular to the optical axis, and then polished. The irradiation and measurement were conducted at electron spectrometer. Average electron energy, pulse duration of high-current pulsed accelerator are 0.2 MeV and -10 ns, respectively. Energy per pulse absorbed by the crystal is 10² Gy. Bands with maximums at 2.1, 2.9, 3.6 eV were found in spectra of radiation-induced absorption at 15 K in crystals of LiYF₄ and LiYF₄-Nd. At longer wavelengths in the pure crystal the band has a maximum at 2.1 eV and in doped crystal at 2.0, 2.3 eV. The absorption at 2.1 eV in pure crystal is dominant. The introduction of Nd leads to a sharp decrease in generation efficiency of the centers that shows these spectra. Perhaps the capture of electrons in Nd³⁺ is a process competing with the formation of color centers responsible for the 2.1 eV band. Absorption spectra do not change with increasing the dose of radiation. This behavior was observed as for LiYF₄ and for LiYF₄-Nd crystals. With increasing the dose decrease there is a pronounced downward trend in the rate of increase of absorption in all bands. The ratio of the absorption bands in crystals irradiated at 15 K is clearly are mostly in favor of the long wavelength band, in contrast to the irradiation at 300K. Thermal annealing of the absorption spectra showed that up to 45K induced absorption remains almost unchanged. At temperatures above 45K sharp decline in the absorption is observed caused by destruction of the centers. The maximum rate of destruction of the centers is at 60K. Induced centers and corresponding induced absorption completely disappear at 80K.

Radiation Defects in LiF Crystals Irradiated with 56 MeV Ar Ions

A. Dauletbekova¹, A. Akilbekov¹, M. Zdorovets², A. Russakova², A. Mukhyshbaeva¹,

B. Abdukadyrov¹, A. Zhumazhanova^{1,2}

¹L.N. Gumilyov Eurasian national university, Kazakhstan

²Institute of nuclear physics, Kazakhstan

e-mail: alma_dauletbek@mail.ru

This work is devoted to studying of LiF crystals irradiated with 56 MeV ⁴⁰Ar ions, 25 nA/cm² current density (range $R = 12.21 \mu\text{m}$) at the cyclotron accelerator DC-60 (Astana), at 300K. Fluence varied from 10^{11} to 10^{13} ions/cm². Corresponding flux (ϕ) was equal to 2.6×10^{10} ions/(cm²×c). Radiation defects were studied using methods of optical absorption spectroscopy, thermostimulated luminescence (TSL), atomic force microscopy (AFM).

It was determined, that efficiency of creation single F centers under high fluences decreases and concentration of complex F_n centers increases nonlinearly due to considerable recombination losses of Frenkel primary pairs and processes of aggregation, as a result of track overlapping.

During TSL study the crystal was divided into 2 parts, the upper part's thickness amounted to 12 μm , equal to the track length of argon ion. TSL spectra for the upper part, which contained tracks, differ significantly from TSL spectrum of the lower part, which did not contain tracks. TSL of the lower part - two maximums at 460K and 525K, and in TSL of the upper part – 520K, 640K. Stepped thermal annealing with measurement of absorption spectrum showed thermostimulated aggregation of defects, and annealing at 653K showed presence of metal colloids.

The investigation of the structure of irradiated LiF crystals was performed on the cross-sections prepared by cleaving along the ion path (normal to the irradiated (100) surface). The cleavage surfaces before etching showed no elements of the microstructure besides cleavage steps. The AFM research showed the beginning of the process of nanostructuring along the ion track and dislocation in the end of the track. Monocrystallinity was preserved to the greater extent of that indicate dislocation rosettes under nanoindentation.

LiF Crystals Doped With Polyvalent Cations: Transformation of Oxygen-Containing Impurity Induced by Irradiation

L. Lisitsyna¹, V. Korepanov², L. Trefilova³, V. Lisitsyn², A. Dauletbekova⁴, R. Kassymkanova⁴,
Z. Yermekova⁴

¹Tomsk state university of architecture and civil engineering, Russia

²Tomsk national research polytechnic university, Russia

³Institute for Scintillation Materials, Ukraine

⁴L.N. Gumilyov Eurasian national university, Kazakhstan

e-mail: alma_dauletbek@mail.ru

Radiation stimulated transformations of the oxygen-containing impurity in LiF crystals under pulsed electron radiation have been researched with high time (20 ns) and spectral (2 nm) resolution measurement techniques.

The diversity of radiation energy dissipation channels can be observed in hydroxyl ions doped crystals. Firstly, the number of dissociated free hydroxyl ions is determined by the value of the absorbed dose in all the tested crystals only. Whereas, the yield of a stable defect in the form of a hydrogen atom (ion) can be observed in the process of hydroxyl ions dissociation depends on the crystal type. In LiF-OH crystals with no co-activators it is found to be the least efficient. In activated LiF crystals it depends on the type of the cation co-activator and decreases in the co-activator row: Fe, W, Ti.

Secondly, the transmission spectrum of polyvalent Me-nOH⁻ complexes formed in the process of crystal growing makes a number of narrow bands in the region of 3700 – 3500 cm⁻¹ and it is determined by the co-activator type and crystal growing modes. Radiation transformation of the structure in these types of complexes changes the number, relation and amplitude of the bands inherent in the complex, and it is caused by the change in the charge and magnetic state of its components and the distance between them as well.

Thirdly, the formation of Me-O₂⁻ complexes (where Me: Fe, W, Ti) can be observed under radiation with specific parameters. The cathodoluminescence spectrum of this type of complexes makes 11 narrow equidistant bands, the characteristic decay time of the spectrum is equal to 100 ns at 15 K for all the crystals with the spectral position of the amplitude envelope in the region of 2.7-2.8 eV according to the co-activator type.

Ultraviolet Luminescence and Creation of Defects under UV Irradiation of Lead Tungstate Crystals Doped with Trivalent Rare-Earth Ions

P. Fabeni¹, A. Krasnikov², T. Kärner², V.V. Laguta³, M. Nikl³, G.P. Pazzi¹, S. Zazubovich²

¹Institute of Applied Physics “N.Carrara” of CNR, Via Madonna del Piano 10, 50019 Sesto Fiorentino (Firenze), Italy

²Institute of Physics, University of Tartu, Riia 142, 51014 Tartu, Estonia

³Institute of Physics AS CR, Cukrovarnicka 10, 162 53 Prague, Czech Republic

e-mail: svet@fi.tartu.ee

Single crystals of lead tungstate (PbWO₄) are known as a fast and heavy scintillation material for high-energy physics experiments. Co-doping with stable trivalent rare-earth A³⁺ ions, substituting for Pb²⁺ ions in the PbWO₄ crystal lattice, suppresses the lead-deficient structure and reduces the number of single lead and oxygen vacancies [1-3]. As a result, considerable improvement of the scintillation characteristics of PbWO₄ crystals is achieved. However, the peculiarities of the luminescence and defects creation processes in these materials were not studied in detail. Therefore, the luminescence of PbWO₄ crystals doped with various A³⁺ ions (La³⁺, Lu³⁺, Y³⁺, Ce³⁺, Gd³⁺, Eu³⁺) is investigated in the 4.2-200 K temperature range by the time-resolved spectroscopy methods. Photo-thermally stimulated defects creation processes are studied under selective UV irradiation of the crystals in the 3.5-5.0 eV energy range. The optically created centers are detected by the TSL and ESR methods.

The electron (WO₄)³⁻ and {(WO₄)³⁻-A³⁺} centers are found to be created under irradiation in the defect-related 3.80±0.40 eV energy range. In this energy range, a new UV emission peaking at 3.05-3.20 eV is excited. At T>60 K, both the thermal quenching of this emission and the photo-thermally stimulated creation of {(WO₄)³⁻-A³⁺} centers take place with the same activation energy (10-25 meV). It is suggested that the UV emission arises from the radiative decay of the excitons localized near A³⁺ ions which are produced as a result of the two-step excitation process. The non-radiative decay of these excitons is responsible for both the appearance of {(WO₄)³⁻-A³⁺} centers and the thermal quenching of the UV emission.

References

1. Han Baoguo, Feng Xiqi, Hu Guanqin, Wang Pingchu and Yin Zhiwen, J. Appl. Phys. **84**, 2831 (1998).
2. V. V. Laguta, M. Martini, A. Vedda, M. Nikl, E. Mihokova, P. Bohacek, J. Rosa, A. Hofstaetter, B. K. Meyer and Y. Usuki, Phys. Rev. B **64**, 165102 (2001).
3. V. V. Laguta, M. Nikl, and S. Zazubovich, Radiat. Measur. **42**, 515 (2007).

Fluctuations in an Inorganic Glass Forming System Capable to Liquid-Liquid Phase Separation

V. Bogdanov¹, L. Maksimov², S. Nemilov³, A. Anan'ev², V. Rusan²

¹Saint Petersburg State University, Saint Petersburg, Russia

²Research and Technological Institute of Optical Material Science, Saint Petersburg, Russia

³Saint Petersburg State University of Information Technology, Mechanics, and Optics, Saint Petersburg, Russia

e-mail: maksimov@interglass.spb.su

Rayleigh and Mandel'shtam-Brillouin scattering (RMBS) spectroscopy and high temperature ultrasonic study (HTUS) are effectively used for estimation of "frozen-in" fluctuations in inorganic glasses [1]. For the first time these methods are applied to a glass forming system characterized by stable liquid immiscibility such as PbO-Al₂O₃-B₂O₃ system studied by SAXS earlier [2]. HTUS includes temperature dependencies of longitudinal velocity in melts at 550 - 1300°C taken at 1 - 5MHz frequencies [1]. Abnormal "water-like" variation of equilibrium ultrasonic velocity and compressibility in these melts with temperature was observed. From HTUS data the density fluctuations in glass melts were estimated. "Frozen-in" index fluctuations of single phase glasses were estimated on the base of Landau-Placzek ratios found from RMBS spectra of glasses at room temperature. The data was discussed in terms of Macedo-Schroeder formalism [3]. Comparison with SAXS data evidences that 30-100Å fluctuations are the origin of light scattering in the studied glass forming system.

Acknowledgements

The study was performed under partial financial support of RFBR (Grant 10-03-00323-a).

References

1. L.Maksimov, A. Anan'ev, V. Bogdanov, T. Markova, V. Rusan, O. Yanush, IOP Conf. Series: Materials Science and Engineering. **25**, 012010, 1 (2011).
2. J. Zarzycki and F. Naudin, J. Non-Cryst.Solids. **5**, 415, (1971).
3. J.Schroeder, "Light Scattering of Glass", in Treatise on Material Science and Technology. Glass 1, Academic, New York N.Y., **12**, 157 (1977).

Absorption and Luminescence in Amorphous 95%SiO₂ 5%GeO₂ Films with Fluorine Fabricated by SPCVD. If GeODC(I) exist

A.N. Trukhin¹, K.M. Golant², J. Teteris¹

¹University of Latvia, Solid State Physics Institute, LV-1063, Riga, Latvia

²Kotel'nikov Institute of Radio-engineering and Electronics of RAS, 125009 Moscow, Russia

We have studied influence of fluorine on germanium oxygen deficient luminescence center (GeODC) in films (~100 μm) produced by the surface-plasma chemical vapor deposition (SPCVD) without any consequent treatment, then corresponding to amorphous layer production at temperatures lower than temperature of glass softening. Two kinds of samples were studied: a sample with “high” concentration of fluorine and a sample with “low” concentration of fluorine. Main feature of the samples difference corresponds to difference in detection of GeODC luminescence. For the case of “high” level of fluorine a “normal” GeODC or so call GeODC(II) or twofold coordinated germanium is observable. That there is absorption band at 5 eV were luminescence of GeODC is excited. In the case of low fluorine concentration the absorption band at 5 eV is not well expressed and however luminescence of GeODC is observed there under 248 nm excimer laser (KrF) it intensity is much lower than in the case of high fluorine concentration. Most significant difference is observed for excitation with higher than 5 eV photons – that is excitation with 193 nm (ArF) and 157 nm (F2) of excimer lasers. The decay kinetics of luminescence for observed under these conditions is very different from usual GeODC, however luminescence bands positions are close to usual GeODC. Noticeable effect under both last case of excitation is luminescence intensity growth during long time excitation (half an hour and more), therefore it was concluded that GeODC are produced by this irradiation.

In the case of “high” concentration of fluorine the yield of GeODC luminescence excited with 157 nm photons (F2 excimer laser) still be high and the absorption in the range of such excitation is high. Then is was concluded that hypothetical GeODC(I) does not exist at least in the produced samples. It is known from literature that SiODC(I) of pure silica glass could be passivated with fluorine with strong diminishing of famous 7.6 eV absorption band of oxygen deficient pure silica glass.

Measurements of SiO₂ Glass Surface Parameters by Methods of Microscopy

E. Gavars¹, A. Svagere¹, A. Skudra¹, N. Zorina¹, R. Poplauskis²

¹Institute of Atomic Physics and Spectroscopy, University of Latvia

²Institute of Chemical Physics, University of Latvia

e-mail: anda.svagere@gmail.com

Our work is concerned with the preparation and investigation of high-frequency electrode-less light sources (HFELS). Such lamps are well suited for the investigation of plasma interaction with the lamp bulb, due to the absence of electrodes. During the operation of electrode-less lamp plasma interacts with the bulb wall material, causing nanoscale modifications of this material. The surface topography influences some important properties of the lamp, for example, the operating lifetime. The characteristics of surface become especially important when decreasing the dimensions of the light source. Plasma-surface interaction studies are also interesting for surface treatment technologies [1,2], as plasma could be used as alternative to chemically active substances that are used in chemical surface cleaning methods.

In this work we tested how does different types of treatment change surface of SiO₂ glass. For our experiments we used five equal high-frequency electrode-less lamps. One was without treatment, two were chemically treated - one with tequila and another with alcohol and two were treated with Ar+Se and Ar+As plasma respectively. For exploration of surface of lamps we broke them to obtain glass samples. Then acquired samples were measured by atomic force microscope and data were processed with analytical program. In the end we got results for one untreated and four differently treated SiO₂ glass surface samples. The main conclusion is that every treatment method changes SiO₂ glass surface and its characteristics. By comparing chemical and plasma treatment methods we can see that surface treated with plasma is smoother and maxima have decreased. Also SiO₂ surface modified with Ar+As plasma has irregular topography because in some places metallic coating has formed up.

Acknowledgments

The work was partly supported by European Social Fund (ESF) project #2009/0210/1DP/1.1.1.2.0/09/APIA/VIAA/100 and National Research Program in Materials Science Project #1 Multifunctional materials.

References

1. H. S. Park, S. J. Kim, Y.Q. Wu, J. K. Lee, IEEE Transactions on Plasma Science 31, (2003) 703-710
2. H. Aribart, D. Abriou, Ceramics Silikaty 44 (2000) 121-128

VUV Excited luminescence and Energy Transfer in $\text{LiGdP}_4\text{O}_{12}:\text{Eu}^{3+}$

T. Shalapska¹, A. Krasnikov¹, G. Stryganyuk², A. Voloshinovskii², S. Zazubovich¹

¹Institute of Physics, University of Tartu, Estonia

²Ivan Franko National University of Lviv, Ukraine

e-mail: tetiana.shalapska@ut.ee

The development of new quantum cutting phosphors for the efficient converting of vacuum ultraviolet photons into visible light has physical interest from phenomenological point of view and great practical importance for application in high-performance mercury-free lighting and in plasma display panels (PDP). Recently, it was shown that Gd-based phosphates doped with Eu^{3+} ions are rather promising luminescence materials for these devices due to their easy preparation and high physical and chemical stability as compared with commercial PDP phosphors [1, 2]. The present work reports on the investigation of the luminescence properties of $\text{LiGd}_{1-x}\text{Eu}_x\text{P}_4\text{O}_{12}$ ($x=0, 0.1$ and 0.5) performed with the aim to clarify the processes of the excitation energy migration and transfer, which take place between the Gd^{3+} and Eu^{3+} ions.

Under selective excitation of unoped $\text{LiGdP}_4\text{O}_{12}$ with the high-energy VUV photons, the photon cascade luminescence of Gd^{3+} ions is studied in detail. Doping with Eu^{3+} ions leads to the essential changes in the luminescence parameters. Upon VUV excitation, the $\text{LiGdP}_4\text{O}_{12}:\text{Eu}^{3+}$ shows not only the emission of Gd^{3+} , but also the intense emission of Eu^{3+} ions. In the excitation spectrum of $\text{LiGdP}_4\text{O}_{12}:\text{Eu}^{3+}$ monitored at 590 nm (${}^5\text{D}_0 \rightarrow {}^7\text{F}_1$), the absorption lines at 273 nm (${}^8\text{S}_{7/2} \rightarrow {}^6\text{I}_J$) and 311 nm (${}^8\text{S}_{7/2} \rightarrow {}^6\text{P}_J$) of Gd^{3+} ions are revealed. This indicates to the $\text{Gd}^{3+} \rightarrow \text{Eu}^{3+}$ energy transfer. The study of time-resolved emission spectra of Eu^{3+} (${}^5\text{D}_0 \rightarrow {}^7\text{F}_1$) under excitation in the Gd^{3+} absorption lines (${}^8\text{S}_{7/2} \rightarrow {}^6\text{I}_J$) as well as of the decay kinetics of Gd^{3+} - (${}^6\text{P}_J \rightarrow {}^8\text{S}_{7/2}$) and Eu^{3+} - (${}^5\text{D}_0 \rightarrow {}^7\text{F}_1$) related luminescence, carried out at 4.2-300 K, confirms the conclusion on the presence of the $\text{Gd}^{3+} \rightarrow \text{Eu}^{3+}$ energy transfer. Temperature dependence of the decay and rise times of these emissions indicates that the energy transfer is effective at $T > 160$ K. As the high-intensity charge transfer band of Eu^{3+} is overlapped with the absorption lines of Gd^{3+} ion (${}^8\text{S}_{7/2} \rightarrow {}^6\text{G}_J$), the well known quantum cutting process via downconversion in $\{\text{Gd}^{3+}-\text{Eu}^{3+}\}$ couples [3] is excluded.

References

1. B. Han, H. Liang, H. Ni, Q. Su, G. Yang, J. Shi and G. Zhang, Opt. Express 17, No 9, 7138 (2009)
2. S. Hachani, B. Moine, A. Ei-akrmi and M. Ferid, Opt. Mater. 31, 678 (2009)
3. R.T. Wegh, H. Donker, K.D. Oskam and A. Meijerink, J. Lumin. 82, 93 (1999)

Optical Properties of Irradiated Yttrium Aluminum Garnet

V. Skvortsova, N. Mironova - Ulmane

Institute of Solid State Physics, University of Latvia, Latvia

e-mail: vera@cfi.lu.lv

Yttrium aluminum garnet ($Y_3Al_5O_{12}$, YAG) based phosphors have been widely used in advanced optical technologies, solid-state laser, and fluorescent materials for luminescent applications [1-3]. Y^{3+} and Al^{3+} in YAG can be replaced by many kinds of other cations with different valency and size within a suitable range. The point defects and its associates presence in structure influence on a number of physical properties and make impossible the use of these crystals in devices. The current understanding of the role of transition metal impurities in optical absorption and photoluminescence of YAG is not yet completely established, particularly in relation to the effect of irradiation in this material. The photoluminescence (PL) and optical absorption of $Y_3Al_5O_{12}$ containing transition metal ions and defects produced by fast neutron and electron irradiation are investigated.

The 370, 500 and 830 nm bands are observed in absorption spectra of $Y_3Al_5O_{12}$ containing manganese. After neutron irradiation in absorption spectra additional bands with maxima 549.5, 595.2 and 714.3 nm appear, the 370 and 500 nm bands intensity increases but the 830 nm band intensity decreases. Photoluminescence spectra of YAG before neutron irradiation at $T=80$ K contain in orange region fine lines, ascribed to Mn^{2+} ions in octahedral position. After irradiation in the luminescence spectra of garnet crystals band broadening is observed. Electron irradiation produced broad band with a complex structure related to Mn^{4+} ions (Fig.1). Exchange interaction between radiation defect and impurity ions during neutron irradiation lead to appearance of additional lines and luminescence bands broadening in investigated crystals.

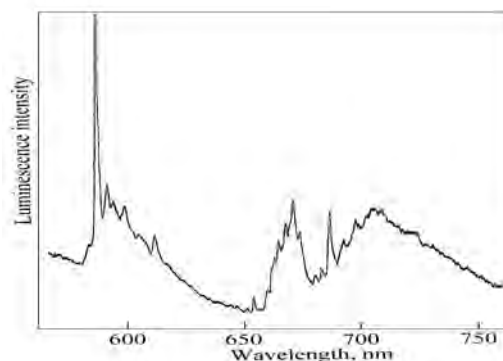


Fig.1 Photoluminescence spectra of $Y_3Al_5Mn_xO_{12}$ crystal irradiated by electron (fluence $\Phi=10^{16}$ cm $^{-2}$).

References

1. N. Ter-Gabrielyan, L.D. Merkle, E.R. Kupp, G.L. Messing, M. Dubinskii, *Opt. Lett.* **35**,922 (2010)
2. T. Tamura, T. Setomoto, T. Taguchi, *J. Luminescence* **87-89**, 1180 (2000)
3. W. Guo, Y.G. Cao, Q.F. Huang, J.T. Li, J.Q. Huang, Z. Huang, F. Tang, *J. Eur. Ceram. Soc.* **31**, 2241(2011)

Raman Scattering Study of $\text{YVO}_4:\text{Eu}^{3+}$ Nanocrystals

L. Shirmane, A. Kuzmin, A.I. Popov, V. Pankratov

Institute of Solid State Physics, University of Latvia, Latvia

e-mail: liana.shirmane@inbox.lv

Europium doped yttrium vanadate ($\text{YVO}_4:\text{Eu}$) is one of the most important phosphor materials, which currently finds a variety of applications in cathode ray tubes, fluorescent lamps and as a scintillator in radiation detectors. Nanocrystalline $\text{YVO}_4:\text{Eu}$ is relevant for these issues as well, since nanoparticles do not show any scattering effect in the visible region, being embedded in transparent matrices.

Three samples have been studied in the present work: commercial powder (from Philips), nanocrystalline powder (particle size about 12 nm) and nanocrystalline powder coated by YF_3 1-2 nm thick layer. Synthesized powders have zircon-type tetragonal structure ($I4_1/amd$) [2]. The luminescence properties of these samples were recently studied in details in [1, 2].

Characteristic Eu^{3+} radiative transitions were observed for all three samples. However, quantum yield of Eu^{3+} emission in nanosized $\text{YVO}_4:\text{Eu}$ is drastically lower compared with bulk powder, but protection of the luminescent core with YF_3 layer results in a partial recuperation of the quantum yield. Besides, significant differences were observed in excitation spectra for all three samples in UV and vacuum UV spectral ranges.

In order to understand the difference in luminescent properties, the samples were studied by Raman spectroscopy. The obtained Raman spectra agree with literature data for bulk and uncoated $\text{YVO}_4:\text{Eu}$ nanocrystals [3,4] and can be assigned to the vibrational modes of YVO_4 . However, the reduction in crystallites size below 20 nm results in the Raman bands broadening and can be significantly influenced by coating with YF_3 layer (Fig. 1).

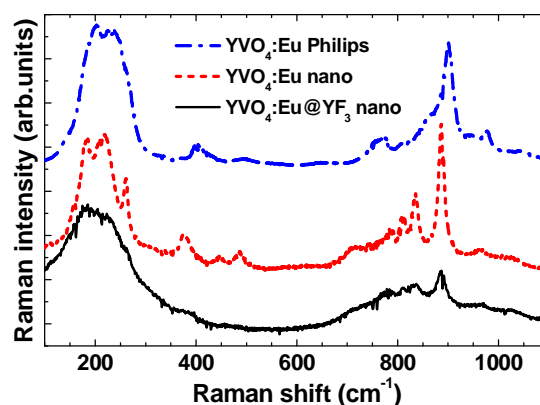


Fig. 1. Raman spectra of $\text{YVO}_4:\text{Eu}$ samples.

References

1. V. Pankratov, A. I. Popov, L. Shirmane, A. Kotlov, C. Feldmann, J. Appl. Phys. 110, 053522 (2011).
2. A. Zharkouskay, H. Lunsdorf, C. Feldmann, J. Mater. Sci. 44, 3936 (2009).
3. B.K. Grandhe, V.R. Bandi, K. Jang, S. Ramaprabhu, et al., Electr. Mater. Lett. 7, 161 (2011).
4. Yu.K. Voron'ko, A.A. Sobol', V.E. Shukshin, et al., Phys. Solid State 51, 1886 (2009).

Time-Resolved Luminescence Properties of $\text{YVO}_4:\text{Eu}^{3+}$ Nanocrystals

L. Shirmane, V. Pankratov, A. Sarakovskis

Institute of Solid State Physics, University of Latvia, 8 Kengaraga, LV-1063, Riga, Latvia

e-mail: liana.shirmane@inbox.lv

Europium doped yttrium vanadate is one of the most important phosphor materials which currently find a variety of applications in cathode ray tubes, fluorescent lamps and scintillator in image detectors. $\text{YVO}_4:\text{Eu}$ is characterized by its high energy-conversion efficiency, brightness, color purity, and high thermal stability.

Recently we demonstrated luminescence properties of $\text{YVO}_4:\text{Eu}$ in vacuum ultraviolet spectral range investigated under using synchrotron radiation [1], where a significant difference in excitation spectra was established between bulk and nanocrystalline samples. In order to clarify the origin of such difference a comparative analysis of time-resolved luminescence properties under excitation of picosecond laser was performed. Temperature dependence measurements of luminescence spectra as well as luminescence decay kinetics were carried out in 20-300 K range.

In the present study a macrocrystalline sample was commercially produced by Philips, while nanocrystalline $\text{YVO}_4:\text{Eu}$ (average particles size is about 12 nm) was produced by means of a microwave-induced synthesis in ionic liquids, which allows the efficient particle size, quality and impurity level control. In order to minimize possible surface related losses $\text{YVO}_4:\text{Eu}$ nanoparticles have been covered by non luminescent 1-2 nm thickness YF_3 layer [2].

A significant discrepancy of time-resolved luminescence characteristics (both intrinsic and Eu^{3+}) between nano and macro crystals was obtained and analyzed. The mechanisms explaining such distinctions as well as the role of surface states in luminescence quenching and energy transfer processes will be elucidated and discussed.

Acknowledgment

The work was supported by ESF Project #2009/0202/1DP/1.1.1.2.0/09/APIA/VIAA/141.

References

1. V. Pankratov, A. I. Popov, L. Shirmane, A. Kotlov, C. Feldmann, J. Appl. Phys. **110**, 053522 (2011)
2. A. Zharkouskay, H. Lünsdorf and C. Feldmann, J. Mat. Sci. **44**, 3936 (2009).

Transparent Ceramics Based on Barium Fluoride with Ultra Fast Scintillation Decay Time

E. Garibin¹, A. Smirnov¹, P. Rodnyi², K. Chernenko², V. Khanin², D. Seliverstov³

¹Joint Stock Venture “INCROM”, Russia

²St.Petersburg State Polytechnical University, Russia

³B.P.Konstantinov Petersburg Nuclear Physics Institute, Russia

e-mail: rodnyi@tuexph.stu.neva.ru

The presence of ultra-fast emission component in BaF₂ (0.9 ns) allows the creation of ionizing radiation detectors with a high (110 ps) time resolution [1]. BaF₂ single crystals are well studied; in this work ceramics based on BaF₂ have been investigated. Ceramics have several advantages compared with single crystals: the freedom in choosing the shape and size of samples; increased mechanical strength; relatively low cost.

The growth of crystals for investigations, preparation of ceramic materials, and subsequent treatment of samples (annealing, cutting, polishing, etc.) were performed at the Joint Stock Venture “INCROM” [2]. The ceramic materials were prepared by uniaxial hot pressing of the initial crystals. To control the spectral and kinetic characteristics of the samples the following conditions were varied: i) the impurity type and concentration; ii) annealing in reducing atmosphere of gaseous CF₄, and iii) the degree of sample deformation.

The main technological stages of the process of obtaining the scintillation ceramics are the following: a sample is subjected to cold pressing; press-shape with the sample is loaded into the furnace; the oven is set on a press; pressure is applied to the sample; the furnace is evacuated; mold with the sample is heated to a temperature of hot pressing; the sample is kept under pressure given time to achieve a given degree of deformation.

We obtained the following ceramics with improved scintillating characteristics: BaF₂:Tm, BaF₂:Sc, BaF₂:Ce. The ceramics show a high light yield of the ultrafast component (220 nm, 0.8 ns) and a decrease of light yield and decay time of slow component of scintillations compared with the BaF₂ single crystals.

References

1. C.L. Woody, P.W. Levy, and J.A. Kierstead, IEEE Trans. on Nucl. Sci. **36** 536. (1989)
2. A.A. Demidenko et al., Optical Materials, **32**, 1291 (2010).

Advances in Combined Atomic Force and Raman Microscopy

S. Kaemmer

Bruker Nano Surfaces Division

TERS requires the tip to be as close to the sample as possible without affecting the integrity of tip or sample. In addition, a metallic tip is necessary for the enhancement. STM provides a convenient way to combine these requirements and study the effects of various tip shapes, coupling mechanisms, and other variables. The analysis of opaque samples creates a challenge as high-NA oil immersion objectives cannot be used, as in transmission mode setups. A parabolic mirror approach would provide a high NA of 1 but puts a lot of constraints on the setup and flexibility. A good compromise and excellent way to excite the AFM tip and collect the Raman signal is to place the Raman objective at about a 60 degree angle with respect to the tip axis. It seems counter intuitive but the side illumination scheme has shown the highest enhancement factor for TERS in theoretical studies. A setup using this side-on geometry is realized in the Innova IRIS. The Innova lends itself as a platform for TERS on opaque samples due to its openness, its very stable and low-noise closed-loop feedback system, and its near-IR feedback diode. It can be operated in STM and a variety of AFM modes with easy switching.

IRIS enables TERS measurements in AFM modes and in STM. The control of both the AFM and Raman microscope is handled by a software package residing on the AFM computer. The sample used is Malachite Green, a dye for which literature data exist. Single-molecule sensitivity on Malachite Green using a side illumination scheme was previously reported by Neascu et al in 2006. Spectra like the one presented can be acquired in as little as 0.1s using just a few micro-watts of incident laser power.

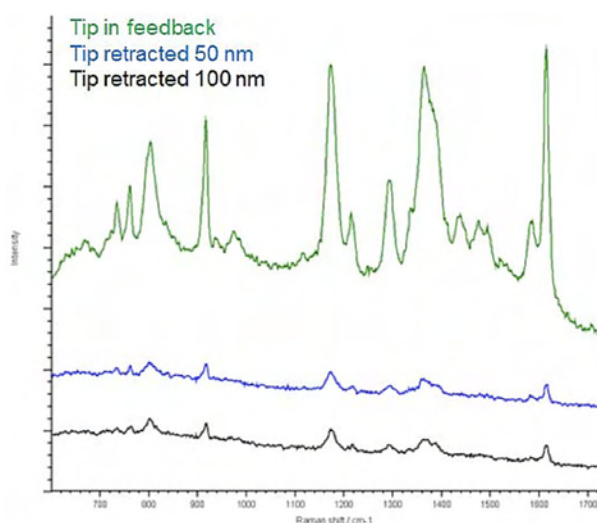


Fig. 2 TERS spectra of Malachite Green obtained using a gold tip illuminated by 633 nm light at varying distances above surface

References:

1. H. Kuzmany, Solid State Spectroscopy, 2nd edition (Springer 2009).
2. R. Stöckle, Y.D. Suh, V. Deckert, and R. Zenobi, Chem. Phys. Lett. 318, 131 (2000).
4. C.C. Neascu, S. Berweger, and M.B. Raschke, Nanobiotechnology 3, 172 (2007).

Raman Spectroscopy of Some Biogenic Carbonates

K. Salma-Ancane¹, M. Polakovs², N. Mironova-Ulmane², I. Sildos³, L. Berzina-Cimdina¹

¹Institute of General Chemical Engineering, Riga Technical University, Pulka street 3/3, LV-1007, Riga, Latvia

²Institute of Solid State Physics, University of Latvia, Kengaraga street 8, LV-1063, Riga, Latvia

³Institute of Physics, University of Tartu, Riia 142, Tartu 51014, Estonia

e-mail: kristine.salma-ancane@rtu.lv

In this work we have performed Raman spectroscopy studies of coral, pearls, eggshells, land snail shells. Also pure calcium carbonate was used for comparison. Our Raman spectra of white coral, white pearls are very similar to the spectra of pure calcium carbonate. The five fundamental bands predicted from the group theory analysis of calcite. The bands at 154 cm^{-1} and 281 cm^{-1} in the calcite spectrum have been assigned to translational and rotational modes, respectively [1]. The weak band 711 cm^{-1} and 1434 cm^{-1} modes corresponding to in-plane bending and antisymmetric stretching modes of carbonate ions. The strongest band, at 1085 cm^{-1} , is an internal mode that derives from the symmetric stretching mode of the carbonate ion. We found that the Raman spectra of white coral, white pearls are very similar to the spectra of pure calcium carbonate. But Raman spectra of eggshells, land snail shells, pink pearls have additional bands (Fig.1). The origin of these additional bands will be discussed.

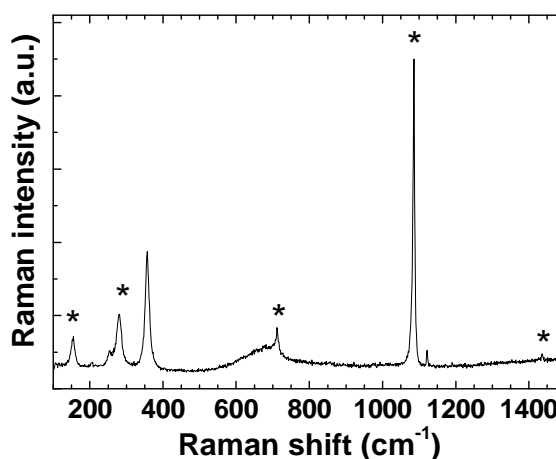


Fig.1 Raman spectra of land snail shells (the bands of calcium carbonate indicated as *).

References

1. W. D. Bischoff, S. K. Sharma and F. T. Mackenzie, Am. Mineral. 70, 581 (1985)

Effect of Aging on the Luminescence of Pure and Doped CdI₂

I. Bolesta¹, I. Karbovnyk², I. Rovetsky³, S. Velgosh, I. Kityk, V. Pankratov², A.I. Popov²

¹Department of Electronics, National University of Lviv, Ukraine

³Institute of Solid State Physics, University of Latvia, 8 Kengaraga, LV-1063, Riga, Latvia

e-mail: popov@ill.fr

Layered CdI₂ crystals can be used as prospective fast scintillators for the detection of ionizing radiation. Layered structure of these crystals allow for multiple mechanisms of the impurity localization. Thus, various ways for creating spatially confined emission and recombination centers are possible. However, efficient application of these materials require clear understanding of the electronic processes in case of high-energy excitation.

Luminescence spectra (in the 1,5–3,5 eV range) and luminescence excitation spectra (in the 3,5–45 eV range) of pure and In, Sb and Sn doped cadmium iodide crystals have been investigated using synchrotron radiation. Origin of the luminescence bands and the influence of impurities on the radiative centers formation are discussed. Luminescence spectra features in the fundamental absorption range are analyzed considering band structure data for CdI₂ [1].

Luminescence excitation and photoluminescence spectra were studied at $T = 10$ K exploiting synchrotron radiation at SUPERLUMI station (HASYLAB, DESY, Hamburg, Germany).

The effect of aging (see Fig. 1) on the luminescence from pure CdI₂ and CdI₂ doped with In, Sb and Sn has been investigated. The origin of significant difference in the emission spectra is discussed.

References

1. Coehoorn R., Sawatzky G.A., Haas C. Phys. Rev. B. **31**, 6739 (1985)

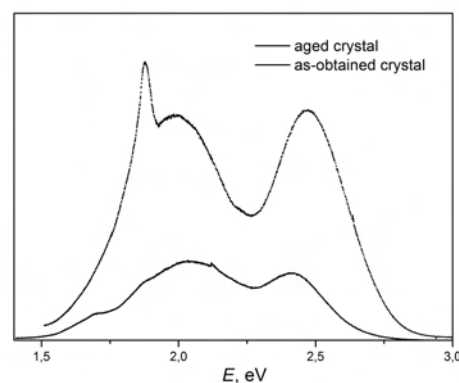


Fig.1 Example of the aging effect in case of cadmium iodide luminescence.

VUV Synchrotron Radiation Spectroscopy of PLZT Ceramics

A.I. Popov¹, V. Pankratov¹, E. Klotins¹, L. Shirmane¹, V. Dimza¹, M. Antonova¹, M. Livinsh¹,
A. Kotlov²

¹Institute of Solid State Physics, University of Latvia, 8Kengaraga, Riga, LV-1063, Latvia

²HASYLAB, DESY, Notkestrasse 85, D-22761 Hamburg, Germany

e-mail: popov@ill.fr

Lanthanum-modified lead zirconium titanate ferroelectric ceramics $\text{Pb}_{1-y}\text{La}_y(\text{Zr}_x\text{Ti}_{1-x})\text{O}_3$ (PLZT) are very interesting because of their high optical transparency in optical applications. PLZT ceramics are desirable candidates for most device applications, such as light shutters, modulators, color filters, memories and image storage devices.

In this report, for the first time the luminescence properties of PLZT 8/65/35 compounds well known for relaxor behaviour as well as Eu, Co, Cr, Ce, Mn, Ni and Fe doped PLZT were studied under vacuum ultraviolet (VUV) and ultraviolet (UV) synchrotron radiation (3.6 – 25.0 eV) emitted from DORIS III storage ring at SUPERLUMI station at HASYLAB, DESY, Hamburg, in the wide temperature range of 10–293 K.

As it is known for some PLZT, their experimentally determined band gap energy is 3.3 - 3.7 eV and thus use of synchrotron radiation provides ideal conditions for the multiplication of electronic excitations, when each absorbed photon produces two or more electronic excitations. To study this effect, we have measured the appropriate excitation spectra of the intrinsic emission (~600 nm) in the case of undoped, Ce or Eu-doped PLZT, or that of Fe-related emission (~440 nm) in the case of Fe-doped sample.

In all cases, a prominent threshold for excitation multiplication at ca. 14.0 eV (as high as (3-4) E_g) was discovered. The results obtained are compared with the appropriate reflection spectra, all measured at 10 K. The temperature dependence of the intrinsic emission band was studied in details in temperature range 10-150 K and the appropriate quenching parameters are determined.

A comparison with the results of electronic structure calculations is also presented.

Raman Spectroscopy Study of the Antiferromagnetic-Paramagnetic Phase Transition in Nickel Oxide

N. Mironova-Ulmane¹, A. Kuzmin¹, J. Grabis², I. Sildos³

¹Institute of Solid State Physics, University of Latvia, Latvia

²Institute of Inorganic Chemistry, Riga Technical University, Latvia

³Institute of Physics, University of Tartu, Tartu, Estonia

e-mail: nina@cfi.lu.lv

Bulk nickel oxide (NiO) experiences a phase transition from paramagnetic (Fm-3m) to antiferromagnetic (R-3m) phase on cooling below the Néel temperature $T_N=523$ K [1]. The magnetic ordering of nickel spins in the antiferromagnetic phase leads to a weak structural distortion due to the magnetostriction effect [1]. The lattice dynamics of NiO has been traditionally probed by Raman spectroscopy, in spite of there are no first-order Raman active modes. All available Raman data suggest the existence at 300 K of seven bands [1,4]: one-magnon band at 34 cm^{-1} ; two defect-induced one-phonon bands at 400 cm^{-1} (TO) and 560 cm^{-1} (LO); three two-phonon bands at 740 cm^{-1} (2TO), 925 cm^{-1} (TO+LO), 1100 cm^{-1} (2LO); two-magnon band at 1400 cm^{-1} .

In this work we have performed temperature dependent Raman spectroscopy studies of single-crystal (sc) and polycrystalline (nano & micro) NiO across the antiferromagnetic-to-paramagnetic phase transition. The high-quality (signal/noise ratio) of the experimental Raman data, compared to previous works [1,4], allowed us to reliably detect several effects: a new weak band at ~ 200 cm^{-1} in all samples, a weak splitting of the band at 400 cm^{-1} below 360 K in sc-NiO, and anomalous temperature dependence of some phonon bands in sc-NiO. The origin of these effects will be discussed.

References

1. W. L. Roth, Phys. Rev. 110, 1333 (1958).
2. M.T. Hutchings, E.J. Samuelsen, Phys. Rev. B 6, 3447 (1972).
3. F.U. Hillebrecht, et al., Phys. Rev. Lett. 86, 3419 (2001).
4. R.E. Dietz, G.I. Parisot, A.E. Meixner, Phys. Rev. B 4, 2302 (1971).
5. E. Cazzanelli, et al., J. Phys.: Condens. Matter 15, 2045 (2003) and references therein.

Modification of Photoluminescence and Absorption Properties of Surface Functional CdTe Single Crystal Layer under Laser Irradiation

L. Poperenko¹, T. Aoki², D. Gnatyuk¹, I. Yurgelevych¹, O. Dacenko¹

¹Faculty of Physics, Taras Shevchenko National University of Kyiv, Ukraine

²Research Institute of Electronics, Shizuoka University

e-mail: dimamid@i.ua

Effect of the chemical etching and the next laser irradiation on the (111) wafers of CdTe single crystals was studied. Chemical etching of the CdTe wafers were done in 5% bromine-methanol solution and, just after, the samples thoroughly rinsed in methanol. Concerning the laser effect, the whole surface area of the wafer was irradiated by 7 ns single pulse of the 532 nm second harmonic of a YAG:Nd laser with energy density of 45 or 80 mJ/cm², i.e., below and above the melting threshold.

Refraction n and absorption k indices were defined within of both the semi-infinite medium model and model of homogeneous absorbing surface layer upon an absorbing substrate.

Photoluminescence was excited by an LGN-402 argon-ion laser with 488 nm wavelength. The results are presented in Fig. 1, the curves are normalized by the edge band intensity. Two bands are observed at the photoluminescence spectra. The

peak of the high-energy band at 1.56 eV corresponds to the bandgap value for CdTe at the liquid nitrogen temperature. This is obviously the band of intrinsic luminescence. The another broad band peaked at 1.45 eV was slightly weakening as a result of the etching in bromine-methanol solution (curve 2). It is naturally to suggest that the band is caused by recombination at the near-surface states.

Light irradiation of CdTe sample with the energy density above the melting threshold strongly modifies the crystal surface.

References

1. S. Del Sordo, L. Abbene, E. Caroli, A. M. Mancini, A. Zappettini, P. Ubertini. "Progress in the development of CdTe and CdZnTe semiconductor radiation detectors for astrophysical and medical applications", *Sensors*, **9**(5), 3491-3526 (2009).
2. D. V. Gnatyuk, L. V. Poperenko, I. V. Yurgelevych, T. Aoki. "Characterization of the surfaces of CdTe(111) single crystals after laser processing". *Proceed. of SPIE*, 8142 81421N (2011).

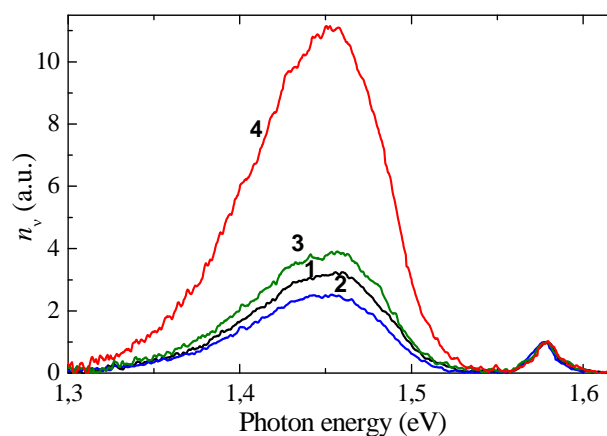


Fig. 1. Photoluminescence spectra of the CdTe samples at 80 K: initial (1), chemically etched (2) and YAG:Nd laser irradiated with energy density of 45 (3) and 80 mJ/cm² (4). The spectral density of emitted quanta is plotted as ordinate.

Preparation and Optical Properties of YSZ:Sm³⁺ Microrolls

K. Utt, T. Kangur, M. Järvekülg, V. Kiisk, I. Sildos

Institute of Physics, University of Tartu, Estonia

e-mail: kathriin.utt@ut.ee

Micro- and nanostructuring of materials can lead to novel physical properties as well as new applications. We have developed a sol-gel route leading to the formation of metal-oxide multiwall microrolls. The rolling of uniform thickness film segments is believed to be due to a gradient of gelation extent of the sol exposed to high humidity air that is introduced into the system during preparation. Initial thin gel film segments are obtained when proper solvent is added to dissolve the underlying sol layer. The obtained freestanding film segments roll spontaneously into microscopic rolls of metal-oxide alkoxide gel because gelation causes sols surface to shrink and therefore exert forces on the whole upper layer of the gelating sol [1]. However, monoclinic ZrO₂ microrolls undergo a destructive phase transformations what leads to the cracking of microrolls when annealed at high temperatures due to the formation of tetragonal and cubic phases [2]. Stabilization of desired crystallographic phase of zirconia is often problematic because the only stable phase at room temperature is the monoclinic one. Fortunately the addition of certain dopants (like yttrium) to zirconia usually helps to form stable tetragonal and cubic phases at room temperature [3].

Hereby we applied above-described method for preparation of 8 mol% of yttrium doped ZrO₂ (YSZ) microrolls, additionally co-doped with 1 mol% of samarium and annealed step by step at 500, 700 and 900°C to functionalize material for luminescence applications. Annealing is needed to induce a crystalline structure since the as-prepared microrolls were amorphous and contained hardly any crystallographic phases of zirconia.

Micro-Raman and photoluminescence measurements performed confirm formation of stable tetragonal phase for microrolls annealed from 500 to 900°C. The microrolls also remain transparent and non cracked because no destructive phase transformations occur during the annealing process due to the stabilised tetragonal phase.

References

1. V. Reedo et al., *Physica Status Solidi (a)* **205**, (2008) 1511
2. K. Utt et al., *Optical Materials* **32**, (2010) 823
3. C. Viazzi et al., *Journal of Alloys and Compounds* **452**, (2008) 377

Preparation of Persistent Strontium Aluminate Phosphor by Solar Induced Solid State Synthesis

V. Liepina¹, K. Smits¹, D. Millers¹, L. Grigorjeva¹, C. Monty²

¹Institute of Solid State Physics, University of Latvia, Latvia

²CNRS Processes, Material and Solar Energy Laboratory (PROMES), France

e-mail: virgiinija@gmail.com

Strontium aluminate phosphors activated with Eu and Dy has been reported for high brightness and long lasting afterglow [1] with wide range of applications in, for example, emergency lighting, luminous paints, optical memories etc. [2] The properties of strontium aluminates phosphors strongly depend on material preparation. The method most frequently used for this phosphor is high temperature solid state reaction; it requires high calcination temperature (~1300° C) and reducing atmosphere. Unnecessary by-products can appear as well as the incorporation of unexpected impurities is possible during material calcination. To avoid the need for high temperature treatment, other methods are used, i.e. sol-gel method, where the material is synthesized at low temperature, however the obtained materials contain a large amount of amorphous phase and its composition might be inhomogeneous.

In present investigation a different method for the synthesis was applied - the solar physical vapour deposition. This method gave the possibility for solid state reaction at high temperature in clean environment – the solar energy was concentrated on relative small area of the raw material target, the target holder was cooled and in the reactor camera the gas atmosphere and pressure was controlled. Therefore the content of non-controlled impurities is expected to be small, although it didn't prevent the origination of multiple strontium aluminate complex oxides, as it was shown by XRD analysis.

The luminescent properties of the obtained material were studied – the luminescence excitation and emission spectra, luminescence decay kinetics and thermally stimulated luminescence. The obtained results were compared with those for similar composition phosphor synthesized by conventional solid state reaction using the same raw material.

References

1. Yuanhua Lin et. al., Appl. Phys. Lett. **81**, 996 (2002)
2. Zhengwei Pan et. al., Nature Materials **11**, 58–63 (2012)

EPR Spectra of the Mn^{2+} Ion in the Oxyfluoride Glass Ceramics Containing BaF_2 Nanocrystalline Phase

Dz. Berzins, A. Fedotovs, O. Kiselova, A. Sarakovskis

Institute of Solid State Physics, University of Latvia, Latvia

e-mail: dzb@inbox.lv

In this work we continue electron paramagnetic resonance (EPR) spectroscopy studies of the oxyfluoride glass ceramics containing BaF_2 fluoride component using Mn^{2+} ion as a paramagnetic probe [1].

After successful material synthesis and specific heat treatment at temperatures above first crystallization temperature transparent glass ceramics samples were obtained. For these samples superhyperfine (SH) structure in the X-band EPR spectra taken at 77 K has been observed. Such SH structure is characteristic to fluorine hyperfine interaction observed in the fluoride crystals [2]. Obtained data allow analyzing the structure of the BaF_2 crystallites and possible location of the Mn^{2+} ion in the BaF_2 crystalline lattice.

Theoretical calculations and comparison of EPR spectra of oxyfluoride glass ceramics with the spectra of the pure $BaF_2:Mn^{2+}$ powder confirming hypothesis of Mn^{2+} ion incorporation in the BaF_2 crystalline lattice will be discussed in this presentation.

References

1. A. Fedotovs, Dz. Berzins, O. Kiselova, A. Sarakovskis, U. Rogulis, IOP Conf. Ser.: Mater. Sci. Eng. **23**, 012018 (2011)
2. W. Gehlhoff, W. Ulrici, Phys. stat. sol. (b) **102**, 11 (1980)

Characteristics of the Mn^{2+} EPR Spectra in the Oxyfluoride Glass Ceramics Containing SrF_2 Nanocrystals

A. Fedotovs, Dz. Berzins, A. Sarakovskis, O. Kiselova

Institute of Solid State Physics, University of Latvia, Latvia

e-mail: andris-f@navigator.lv

Structure sensitive spectroscopic method electron paramagnetic resonance (EPR) spectroscopy is useful for the structure studies of oxyfluoride glass ceramics which after specific heat treatment contain crystallized nanoscale fluoride components [1, 2].

In this investigation Mn^{2+} ion has been used as a paramagnetic probe in the oxyfluoride glass ceramics containing SrF_2 nanocrystals. Main characteristic in the EPR spectra of heat-treated samples is the appearance of the resolvable superhyperfine (SH) structure which indicates Mn^{2+} ion incorporation in the fluoride structure. The EPR spectra could be explained by the Mn^{2+} ion entering in the SrF_2 crystal structure. In such case it has SH interaction with the nearest fluorine atoms located at the vertices of the cube. Similar EPR spectrum has been observed also in the pure $\text{SrF}_2:\text{Mn}^{2+}$ powder which along with the theoretical modeling of the spectra supports hypothesis of the cubic structure of the SrF_2 crystallites.

References

1. R.W.A. Franco, J.F. Lima, C.J. Magona, J.P. Donoso, Y. Messaddeq, *J. Non-Cryst. Sol.*, 2006, **352**, 3414–3422.
2. A. Fedotovs, Dz. Berzins, O. Kiselova, A. Sarakovskis, U. Rogulis, *IOP Conf. Ser.: Mater. Sci. Eng.* **23**, 012018 (2011)

Gallstones Studies by EPR and EDX Spectroscopy

M. Polakovs¹, N. Mironova-Ulmane¹, V. Skvortsova¹, D. Jakovlevs², E. Reinholds³

¹Institute of Solid State Physics, University of Latvia, Kengaraga street 8, LV-1063, Riga, Latvia

²Riga Technical University, Latvia, Riga, Kalku Str. 1, LV-1048

³Nuclear Medicine Dep. P.Stradins Clinical University Hospital, Riga, Latvia

e-mail: maksims.polakovs@gmail.com

In the present work we report results of investigations of gallstones. Different types of gallstones were studied. Accordingly the paramagnetic composition gallstones could be divided on three main types: cholesterol, brown pigment and black pigment stones [1]. The samples of gallstones were received from the P.Stradins Clinical hospital of Latvia, some gallstones was donated by private persons.

The EPR spectra of gallstones were measured on a BRUKER EMX-6/1 spectrometer equipped with an Aspect 2000 data system. An ER 4102 ST Universal X-Band Resonator (TE102 mode) was used. The samples were observed in a scanning electron microscope (SEM, TESCAN Mira\LMUField-Emission-Gun) as well. The elemental composition of gallstones was assessed by energy dispersive X-ray spectrometry (EDS, Oxford instruments 7378) performed on the scanning electron microscope.

The gallstones was separated in different samples by gallstone's component color. EPR and EDX observed spectra show differences for studied components. We received information about composition of gallstones by EDX spectroscopy. EPR spectroscopy let us to receive information about electronic states of transition metal ions.

EDX spectroscopy technique let us to study the composite of gallstones and EPR spectroscopy give us information about electronic states of transition metal ions.

References

1. E.N. Chikvaidze, T.V. Gogoladze, I.N. Kirikashvili, G.I. Mamniashvili. Ternary complexes of albumin-Mn(II)-bilirubin and Electron Spin Resonance studies of gallstones. Georgian Medical News, ISSN 1512-0112, No3(168), march, 2009.

Electronic Excitations in NiWO₄ Using VUV Synchrotron Radiation

A. Kuzmin¹, V. Pankratov¹, A. Kalinko¹, A. Kotlov², L. Shirmane¹, A.I. Popov¹

¹Institute of Solid State Physics, University of Latvia, Riga, Latvia

²HASYLAB, DESY, Hamburg, Germany

e-mail: a.kuzmin@cfi.lu.lv

NiWO₄ belongs to a series of transition-metal tungstates as MnWO₄, FeWO₄, CoWO₄, and ZnWO₄, having wolframite-type structure. To our knowledge, its luminescent properties have been scarcely studied in the past. In the only work [1], it was observed that a broad blue-green (2.07-3.54 eV) photoluminescence band exists in NiWO₄ powders and sol-gel derived NiWO₄ films, calcined above 600°C.

In the present study, the low temperature photoluminescence spectra and excitation spectra of micro and nanocrystalline (crystallites size below 2 nm) NiWO₄ powders were measured exploiting ultraviolet (UV) and vacuum ultraviolet (VUV) synchrotron radiation (3.6-20 eV) emitted from DORIS III storage ring at SUPERLUMI station (HASYLAB DESY, Hamburg).

The obtained results were analyzed, based on our previous studies of nanocrystalline ZnWO₄ and solid solutions Zn_cNi_{1-c}WO₄ [2,3] as well as recent electronic structure calculations for NiWO₄ [4]. We found that the shape of the photoluminescence band at 2.5 eV, being due to radiative electron transitions within the [WO₆]⁶⁻ anions as in ZnWO₄, is strongly modulated by the optical absorption of Ni²⁺ ions (d-d transitions) as suggested in [3]. The maximum of the photoluminescence band in nano-NiWO₄ is shifted to 2.7 eV, thus located at ~0.32 eV higher energy than in nano-ZnWO₄ [2]. Such blue-shift can be explained by the difference in the relaxations of WO₆ octahedra in the two tungstates, which are directly supported by our W L₃-edge and Ni(Zn) K-edge EXAFS data. The excitation spectra of both micro and nanocrystalline NiWO₄ can be well interpreted based on the first principles band structure calculations [4].

References

1. H. He, Int. J. Mat. Res. 101, 386 (2010).
2. A. Kalinko, A. Kuzmin, J. Lumin. 129, 1144 (2009).
3. A. Kalinko, et al., Centr. Eur. J. Phys. 9, 432 (2011).
4. A. Kuzmin, A. Kalinko, R.A. Evarestov, Centr. Eur. J. Phys. 9, 502 (2011).

X-ray Absorption Spectroscopy of Cu-doped WO₃ for Use in Electrochemical Metallization Cell Memory

A. Kuzmin, A. Anspoks, A. Kalinko, J. Timoshenko, R. Kalendarev

Institute of Solid State Physics, University of Latvia, Latvia

e-mail: a.kuzmin@cfi.lu.lv

The operation of Redox Resistive Memory (ReRAM) is based on a change in resistance of a metal-insulator-metal (MIM) structure driven by ion migration combined with redox processes involving the electrode material or the insulator material, or both [1]. ReRAM can be realized utilizing electrochemical, thermochemical, and valence change phenomena [1]. Electrochemical metallization cell (EMC) device, known also as Conductive Bridging (CB) cell or Programmable Metallization Cell (PMC), is based on the electrochemical control of nanoscale quantities of metal in thin film solid electrolyte [1]. EMC devices can be, for example, realized using a thin WO₃ film sandwiched between a copper anode and an inert cathode [2-4]. One believes that under the influence of an electric field, the electron current from the cathode reduces an equivalent number of Cu-ions injected from the anode, and a Cu metal-rich electrodeposit is formed in the WO₃ electrolyte [3].

In this work we have performed first synchrotron x-ray absorption spectroscopy study of the local atomic and electronic structure around Cu and W atoms in as-prepared and annealed in air at ~135°C multilayered EMC structures WO₃/Cu/Si and WO₃/Cu/WO₃/Si.

Our analysis of the W L₃-edge EXAFS spectra indicates that the local environment around W atoms in both as-prepared and annealed samples is similar and resembles that of pure a-WO₃ thin film. On the contrary, the local environment of Cu atoms depends strongly on the type of the sample and annealing procedure. We found that as-prepared multilayers contain nanosized metallic copper, which is oxidized to Cu⁺ upon annealing. The oxidation of Cu ions in the multilayers upon annealing is also supported by the Cu K-edge shift of about 0.7 eV to higher binding energies, whereas no shift of the W L₃-edge was detected. The monovalent Cu⁺ ions having small size are able to diffuse across the multilayer and, thus, presumably participate in the formation of conducting pathways in the EMC cell.

References

1. R. Waser, R. Dittmann, G. Staikov, K. Szot, *Adv. Mater.* **21**, 2632 (2009).
2. M. N. Kozicki, et al., in *Proc. IEEE Non-Volatile Memory Technology Symp*, 2004, p. 10.
3. C. Gopalan, et al., *J. Non-Cryst. Solids* **353**, 1844 (2007).
4. Y. Li, et al., *Phys. Status Solidi RRL* **4**, 124 (2010).

First Principles LCAO Study of Copper Tungstate CuWO_4

A. Kuzmin¹, A. Kalinko¹, R.A. Evarestov²

¹Institute of Solid State Physics, University of Latvia, Latvia

²Department of Quantum Chemistry, St. Petersburg University, Russia

e-mail: a.kuzmin@cfi.lu.lv

Copper tungstate CuWO_4 belongs to the wolframite series of structurally related materials MeWO_4 (Me=Mg, Mn, Fe, Ni, Co, Cu, Zn, Cd), in which metal cations and tungsten ions occupy non-equivalent octahedral sites. However, opposite to other tungstates adopting the wolframite-type structure, the crystal structure of CuWO_4 is triclinic (space group P-1) due to a strong Jahn-Teller distortion of CuO_6 octahedra caused by the d^9 electron configuration of the Cu^{2+} ions [1]. CuWO_4 is paramagnetic at room temperature, but exhibits long-range antiferromagnetic (AFM) order below the Néel temperature of 24 K [2]. Besides its magnetic properties, during last years copper tungstate has been attracted an increasing interest because of numerous possible applications such as a photoanode material in photovoltaic electrochemical cells, in all-solid-state thin-film lithium batteries, for gas-sensitive resistors and as photocatalysts. Thus, understanding of CuWO_4 functional properties as well as their further optimization requires a precise knowledge of its electronic structure.

To the best of our knowledge, until now the band structure of CuWO_4 has been theoretically studied only using the full potential linearized augmented plane wave (FP-LAPW) method by two groups [3,4] and [5]. In the present work, the atomic, electronic, and magnetic structure as well as phonon properties of CuWO_4 have been systematically investigated using the first principles spin-polarized periodic linear combination of atomic orbitals (LCAO) method with the pure density functional (DFT) and hybrid Hartree-Fock (HF)-DFT Hamiltonians. The obtained results will be compared with previous theoretical studies and available experimental data.

References

1. B. Schwarz, et al., *Phil. Mag.* **88** (2008) 1235.
2. J. B. Forsyth, C. Wilkinson, A. I. Zvyagin, *J. Phys.: Condens. Matter* **3** (1991) 8433.
3. O. Yu. Khyzhun, V. L. Bekenev, Yu. M. Solonin, *J. Alloys Compd.* **480** (2009) 184.
4. V. V. Atuchin, et al., *Int. J. Appl. Phys. Math.* **1** (2011) 19.
5. M. V. Lalić, Z. S. Popović, F. R. Vukajlović, *Comput. Mater. Sci.* **50** (2011) 1179.

X-ray Absorption Spectroscopy Study of Local Atomic Structure and Lattice Dynamics in Copper Nitride Cu₃N

A. Kalinko, A. Kuzmin, A. Anspoks, J. Timoshenko, R. Kalendarev

¹Institute of Solid State Physics, University of Latvia, Latvia

e-mail: akalin@latnet.lv

Among perovskite-type compounds, copper nitride Cu₃N, having a cubic *anti*-ReO₃-type structure composed of the NCu₆ octahedra joined by corners [1], has been little studied, in spite of the practical interest in the fabrication of copper nitride has grown in the recent years motivated by its possible applications as a material for write-once read many (WORM) optical storage devices [2] and for the fabrication of low-resistance magnetic tunnel junctions for the use in non-volatile magnetic random access memories [3].

The dynamic properties of Cu₃N lattice are driven by the anisotropic thermal vibrations of Cu atoms, whose thermal ellipsoids are flattened perpendicular to the N-Cu-N bonds [4]. The thermal displacement parameters indicate that there could be some degree of positional disorder at the Cu site [4]. Therefore, it is possible that this disorder and the resulting local lattice distortion are one of the reasons for the structural instability of Cu₃N under pressure of ~5 GPa [5]. The anisotropy of the copper atoms thermal vibrations could also lead to the negative thermal expansion of Cu₃N at low temperatures.

In this work we have performed first temperature dependent (10-300 K) synchrotron x-ray absorption spectroscopy study of the local atomic structure and lattice dynamics around copper atoms in polycrystalline and nanocrystalline thin film Cu₃N.

The comparative analysis of the first coordination shell for polycrystalline and nanocrystalline thin film Cu₃N will be given and discussed. The advanced MD-EXAFS analysis technique was applied to the EXAFS spectra of polycrystalline Cu₃N at 300K, allowing the analysis beyond the first coordination shell to obtain the information on the N-Cu-N angle distribution.

References

1. R. Juza, H. Hahn, Z. Anorg. Allg. Chem. **239**, 282 (1938).
2. M. Asano, K. Umeda, A. Tasaki, Jpn. J. Appl. Phys. **29**, 1985 (1990).
3. D.M. Borsa, S. Grachev, C. Presura, D.O. Boerma, Appl. Phys. Lett. **80**, 1823 (2002).
4. G. Paniconi, et al., Solid State Sciences **9**, 907 (2007).
5. J.G. Zhao, et al., Phys. Status Solidi B **243**, 573 (2006).

X-ray Absorption Spectroscopy of Local Structure and Lattice Dynamics in Multiferroic MnWO_4 and $\text{Mn}_{1-c}\text{Co}_c\text{WO}_4$

A. Anspoks, A. Kalinko, A. Kuzmin, J. Timoshenko

Institute of Solid State Physics, University of Latvia, Latvia

e-mail: andris.anspoks@cfi.lu.lv

MnWO_4 is recently discovered multiferroic material, which contains formally only one magnetic ion (Mn) [1, 2]. At ambient pressure and in absence of magnetic field multiferroic material MnWO_4 undergoes three magnetic phase transitions to antiferromagnetically (AF) ordered states: paramagnet \rightarrow AF3 ($T_N=13.5$ K), AF3 \rightarrow AF2 ($T_2=12.3$ K), and AF2 \rightarrow AF1 ($T_1=8.0$ K) [3]. Ferroelectric polarization appears only in the AF2 phase: it can be explained by the loss of inversion symmetry due to the helical magnetic order and a strong spin-lattice coupling. The magnetic properties of MnWO_4 can be influenced by replacing Mn^{2+} with Fe^{2+} or Co^{2+} ions. The c-T phase diagram of $\text{Mn}_{1-c}\text{Co}_c\text{WO}_4$ ($c<0.3$) has been established recently using the temperature-dependent magnetic susceptibility and neutron powder diffraction studies [4]. It was found that Co doping at $c>\sim 0.05$ suppresses the commensurate AF1 phase and stabilizes the incommensurate spiral AF2 phase down to the lowest temperature [4]. The lattice parameters as well as the unit-cell volume decrease linearly with cobalt doping, reflecting the smaller radii of Co^{2+} ions. However, the temperature coefficients of the lattice parameters a and b show non-linear behavior with cobalt concentration suggesting that complex magnetism and transitions in $\text{Mn}_{1-c}\text{Co}_c\text{WO}_4$ are closely tied to the temperature-dependent changes in the lattice [4].

In this work we have performed the first x-ray absorption spectroscopy study of the local atomic structure and lattice dynamics around W, Mn and Co ions in pure MnWO_4 and CoWO_4 as well as in the solid solution $\text{Mn}_{0.7}\text{Co}_{0.3}\text{WO}_4$. The obtained results give direct evidence of that cobalt doping influences significantly the distortion of the MnO_6 octahedra and, thus, confirm the stabilizing role of cobalt doping in solid solutions $\text{Mn}_{1-c}\text{Co}_c\text{WO}_4$, suggested recently in [4, 5].

References

1. O. Heyer et al., J. Phys.: Condens. Matter 18, L471 (2006)
2. K. Taniguchi, et al., Phys. Rev. Lett. 97, 0972003 (2006).
3. G.Lautenschlager, et al., Phys. Rev. B **48**, 6087 (1993).
4. Y.-S. Song, J.-H. Chung, J. M. S. Park, Y.-N. Choi, Phys. Rev. B **79**, 224415 (2009).
5. M. Maczka, et al., Phys. Rev. B **83**, 174439 (2011).

X-ray Absorption Spectroscopy of the Local Atomic Structure in PbS Quantum Dots

A. Anspoks, A. Kalinko, P. Kulis, A. Kuzmin, B. Polakov, J. Timoshenko

Institute of Solid State Physics, University of Latvia, Latvia

e-mail: andris.anspoks@cfi.lu.lv

PbS is an IV-VI semiconductor with the sodium chloride type of structure and rather small bandgap ($E_g = 0.42$ eV at $T=300$ K [1]). It is a classical material for quantum dots based devices, where quantum confinement leads to an increase of effective E_g to values beyond 1eV. Therefore PbS quantum dots are a promising material for harvesting visible and infrared radiation [2].

In this work we have performed the Pb L_3 -edge x-ray absorption spectroscopy (XAS) study of the local atomic structure and lattice dynamics around lead ions in PbS polycrystals and nanocrystals. The obtained results give direct evidence of strong nonuniform atomic structure relaxation in nanosized PbS.

Optical absorption spectra of our PbS quantum dots show well defined excitonic peak centered at about 760 nm (1.63 eV). Using this value and the energy gap dependence on the particle size [3], one could estimate the average size of nanoparticles to be about 2.4 nm, being in good agreement with our findings from XAS.

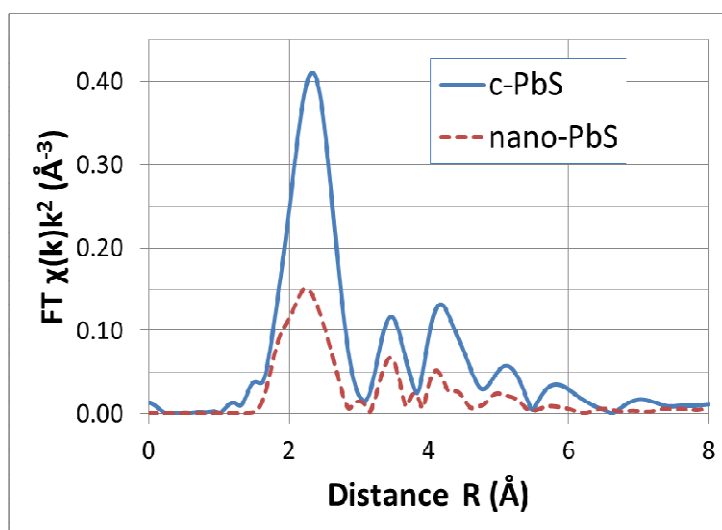


Fig. 1. Fourier transform of the Pb L_3 -edge EXAFS spectra for PbS quantum dots (dashed line) and polycrystalline PbS (solid line).

References

1. R.B. Schoolar and J.R. Dixon, Phys. Rev. **137**, A667 (1965).
2. S.A. McDonald, G. Konstantatos, S. Zhang, et al., Nature Materials **4**, 138 (2005).
3. I. Moreels, K. Lambert, D. Smeets, et al., ACS NANO **3**, 3023 (2009).

Nanocrystals for Solar Cell Applications

P. Kulis, J. Butikova, B. Polyakov, I. Tale

Institute of Solid State Physics, University of Latvia, Latvia

e-mail: p.kulis@cfi.lu.lv

Several nanocrystals (NC) based solar cell architectures were demonstrated in recent time. Main architectures are Schottky type [1], blend of two different NC materials [2], Gratzel type solar cell [3] and blend of NC and polymer [4]. One of most significant advantage of NC based solar cell technology is synthesis from solution, which is much cheaper in comparison with conventional vacuum technologies used for silicon solar cells.

It is well known that band gap of nanocrystals may be tailored in wide range varying its size due to quantum confinement effect. Sulphide materials have rather large Bohr radius (18 nm for PbS and 2.4 nm for CdS). Another important material characteristic for solar cell engineering is work function. Ability to modify work function of NC is essential for increasing solar cell efficiency.

In this study we report on various methods of the synthesis of PbS, CdS, Cu₂S and ZnO nanocrystals and their investigations with optical absorption methods and Kelvin probe measurements of work function of chemically synthesized nanocrystal thin films.

Acknowledgements

P.K. and J.B. were supported by ESF Grant no.2009/0202/1DP/1.1.1.2.0/09/APIA/VIAA/141.

References

1. J. Luther, M. Law, M. Beard, Q. Song, M. Randy, J. Ellingson, A. Nozik *Nanoletters* **8**, 2008, 3488-3492
2. Y. Wu, C. Wadia, W. Ma, B. Sadler, A. Alivisatos *Nanoletters* **8**, 2008, 2551-2555
3. B. Hyun, Y. Zhong, A. Bartnik, L. Sun, H. Abrun, F. Wise, J. Goodreau, J. Matthews, T. Leslie, N. Borrelli *ASC NANO*, **2**, 2008, 2206-2212
4. J. Choi, Y. Lim, M. Santiago-Berrios, M. Oh, B. Hyun, L. Sun, A. Bartnik, A. Goedhart, G. Malliaras, H. Abruna, F. Wise, T. Hanrath *Nanoletters* **9**, 2009, 3749-3755

Metallothermic Synthesis of Nanocrystalline Powders and Nanorods of Chromium Silicides

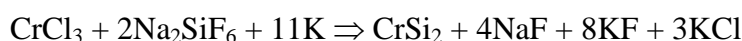
V. Malyshev, D. Shakhnin, L. Molotovska, O. Podyman, M. Sushinskiy

V.I. Vernadskii Institute of General and Inorganic Chemistry of NAS of Ukraine, Kiev, Ukraine

e-mail: victor_malyshev@mail.ru

Metallothermic reduction of chromium and silicon halides by alkali and alkali-earth metals is proposed as promising method of chromium silicides synthesis.

Process of simultaneous metallothermic reduction of CrCl_3 and Na_2SiF_6 by potassium could be presented as follows:



Molten phase formed at synthesis temperatures (923-1023 K) facilitates nanocrystalline product formation. Obtained by metallothermic reduction method powders consist of hexagonal chromium disilicide phase. Average size of CrSi_2 particles obtained by metallothermic method is 35-60 nm.

Thermostability of synthesized powder was studied in air at up to 1273 K by TGA and DTA methods. Results analysis allow one to stipulate that obtained powders are stable up to 973 K. Further temperature increase causes significant oxidation of powders leading to formation of protective oxide layer at their surface.

Change of metal-reductor with different reaction ability in metallothermic synthesis leads to changes in structure of nascent silicides nanoparticles. Instead of nanopowders, nanorods are formed.

Process of simultaneous metallothermic reduction of CrCl_3 and SiCl_4 by magnesium could be presented as follows:



All peaks at the X-ray diffractogram of this process product can be attributed to the cubic Cr_3Si phase.

According to the results obtained by methods of TEM and transmission electrons diffraction, all the investigated samples contain primarily nanorods 30-90 nm in diameter and up to 500 μm long.

Production of Nanopowders Using Nanosecond Electron Beam from Gas and Liquid Precursors

S.Yu. Sokovnin^{1, 2}, M.E. Balezin¹

¹Institute of Electrophysics, Ural Branch RAS, 106 Amundsen St., Yekaterinburg, Russia; 620216

²Ural Federal University named after First President of Russia B.N. Yeltsin, 19, ul. Mira, Yekaterinburg

e-mail: sokovnin@iep.uran.ru

Frequency nanosecond electron accelerators type URT have been developed for use in radiation technologies [1]. The accelerators include a thyatron, a pulse transformer and a semiconductor opening switch. The accelerating voltage is up to 0.9 MV, FWHM pulse length is up to 60 ns, and the repetition rate is up to 250 Hz (Table). A metal ceramic cathode, which is used in the accelerator, provides an electron beam cross section up to 16 cm in diameter or rectangular with the dimensions of 45*5cm² at a maximum density of the pulse current equal to 2 A/cm².

Table. Parameters of URT accelerators

Accelerator	U, kV	Pulse energy, J	T _p , ns	Repetition rate, pps
YPT-0.2	200	1.75	35	250
YPT-0.5	500	6.25	50	200
YPT-1	900	25	60	50

Thus, a family of nanosecond electron accelerators has been developed for use in radiation technologies applied to layers up to 0.4 g/cm² thick, such as production of nanopowders from gas and liquid precursors.

Experiments on the irradiation of silver nitrate solutions in various liquids by a URT-0.5 accelerator facilitated the development of technology for producing silver nanopowders (NPs). The powder yield and particle size as a function of the irradiation mode has been established. An increase in the adsorbed dose results in an increased powder yield; however, the particle size decreases and the powder agglomeration rate increases. Therefore, the targeted production of silver NPs with a mean particle size in the range of 90-1100 nm is possible. Besides to produce TiO₂ and SiO₂ NPs the gas precursors were used.

References

1. S. Yu. Sokovnin, Nanosecond Electron Accelerators and Radiation Technologies Based on Them (Ural Branch of the Russian Academy of Sciences, Yekaterinburg, 2007) [in Russian]

The Effects of Cold Deformation and Electron Irradiations of Zr-1%Nb Alloy on Temperature Range Deuterium Desorption

V.O. Mats, O.M. Morozov, V.G. Kulish, V.I. Zhurba, O.V. Mats

National Science Center "Kharkov Institute of Physics and Technology", Kharkov, Ukraine

e-mail: Vyacheslav_mats@mail.ru; morozov@kipt.kharkov.ua

Nanostructured condition of the alloy Zr-1%Nb was received by deformation cool rolling (~300 K). The degree to deformation was formed ~96%. The average size of grain after deforming was $d \approx 61$ nm. For such nanostructure typical high concentration three-dimensional concentration borders (~3,4 %) and significant level microstrains. The high degree of unsoundness and spottiness of the sharing the internal voltages conditions change the thermal desorption spectra of deuterium. In thermal desorption spectra of ion-implanted deuterium this reveals itself as additional low-temperature area desorption of deuterium within the range of the temperature 770-1000 K (see fig. 1, curve b).

The irradiation by electron with energy 10 MeV and by fluence $\sim 6 \times 10^{17} \text{ cm}^{-2}$ brings about active development of the revocable processes in nanostructure alloy. Density of dislocations falls in grains object. The most intensive displacement dislocations occurs in top of the ragged borders - in places of the maximum concentration of the voltages. The dislocation glide and microslip is occurs because of interaction them with flow point defects of radiation origin. As a result is occurring of shaping new polygonal borders. The transformation nanostructure occurs in the manner of reduction of the average grain size ($\sim d \sim 58$ nm) and increase to concentrations of the borders (~8,8 %). This reveals itself in increase temperature range of deuterium isotope retention and appearance additional peaks with the temperature in maximum ~700 and ~800 K (see fig.1, curve c). This reflects the structured changes of Zr-1%Nb alloy.

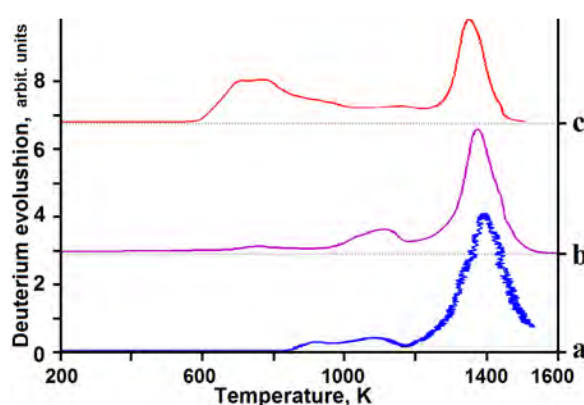


Fig.1. Thermal desorption spectra of deuterium (dose $\sim 1.3 \times 10^{17} \text{ D/sm}^2$) implanted in Zr-1%Nb alloy: (a) - source, (b) - deformed by cool rolling RT under on ~96%; (c) - deformed by cool rolling RT under on ~96% and irradiated by electron beam fluence $\sim 6 \times 10^{17} \text{ cm}^{-2}$

Reference

1. I.M. Neklyudov, O.M. Morozov, V.G. Kulish, V.I. Zhurba, P.A. Khaimovich, A.G. Galitskiy. Hydrogen diagnostics of structural states in 18Cr10NiTi steel. Journal of Hydrogen Energy, 36 1192 (2011).

Deposition of Cu and Pt Nanoparticles on the Surface of Metallic Aluminum and Impedance Spectra of these Complex Electrodes

J. Katkevics¹, A. Lescinskis¹, D. Erts², A. Viksna¹

¹Faculty of Chemistry, University of Latvia, Kr. Valdemara Str. 48, Riga, LV-1013, Latvia

²Institute of Chemical Physics, University of Latvia, Kronvalda blvd. 4, Riga, LV-1586, Latvia

e-mail: arturs.viksna@lu.lv

Cu and Pt nanoparticles are perspective materials for application as catalysts, photocatalysts, adsorbents, sensors. Different methods have been previously applied for fabrication of nanoparticle arrays on the surface, for example, Pt nanoparticles were fabricated by electron beam lithography on oxide surfaces [1] or by the reductions of H_2PtCl_6 in ethylene glycol [2]. Cu nanoparticles were deposited on the ultrathin polypyrrole film by constant current electrolysis [3] and on Al surfaces by internal electrolysis methods [4].

In the present study, the deposition of Cu and Pt nanoparticles on metallic Al surface were performed by electrolysis at constant electrode potential in acidic electrolyte media, by internal electrolysis method in the acidic electrolyte media and combination of these methods. Combination of electrolysis at constant electrode potential with internal electrolysis method was found most effective for fabrication of nanoparticle arrays.

Firstly Cu or Pt nanoparticles in the solution were synthesized by reduction of CuSO_4 or H_2PtCl_6 using reducing agent and then Cu or Pt nanoparticles were deposited on the surface of metallic aluminum by electrolysis at constant potential with short controlled time and formation process of nanoparticles was completed by internal electrolysis. Then we described the formation mechanism of Cu and Pt nanoparticles during the internal electrolysis. The contact area of Cu and Pt nanoparticles with aluminium was analyzed by electrochemical impedance spectroscopy. The composition of deposited material was approved by equivalent circuit analysis, optical and scanning electron microscope methods.

References

1. Zhu. J., Somorjai G.A. Nano Lett. **1**, 2001, 8.
2. Long N. V., Ohtaki M., Nogami M. J. Novel of Carbon Resource Sci., **3**, 2011, 40.
3. Zhou X. J., Harmer A. J., Heinig N. F., Leung K. T. Langmuir, **20**, 2004, 5109.
4. Denisova J., Katkevics J., Erts D., Viksna A. IOP Conf. Series: Mater. Sci. Eng., **23**, 2011, 012040.

Zirconia Nanoparticles as Submicro-Level Label for Biological Applications

K. Smits¹, J. Liepins², M. Gavare², M. Grube², A. Gruduls³, D. Jankovica^{1,4}

¹Institute of Solid State Physics, University of Latvia, Latvia

²Institute of Microbiology and Biotechnology, University of Latvia, Latvia

³Faculty of Biology, University of Latvia, Latvia

⁴Institute of Inorganic Chemistry, Riga Technical University, Latvia

e-mail: Janis.Liepins@lu.lv

Great variety of measurement methods is used in now day's biology and pharmacology; however the demand for more measurement possibilities is permanent. Recent advances in high throughput microcultivation systems have greatly increased the possibilities to screen effects of any particular chemical (or potential drug) in the level of cell or few cells (lab on chip concept), however – the amount of parameters available for online analyses has remained limited. Until now – mainly integrative parameters are used - optical density (OD) measurements for cell count and color assays for cell enzymatic activity. On the other hand - there are many online parameters used in small-scale reaction systems (e.g. dissolved oxygen, CO₂ production, temperature, etc.), which, usually due to lack of adequate methodology, are poorly covered in microcultivation systems.

Already now rare earth doped ZrO₂ are used successfully as sensors in bioreactor systems (both in lab and industrial scale). We propose to expand usage of these materials also to microcultivation systems by employing subsequent material's nanocrystals.

Effects of ZrO₂ nanocrystals on live cells growth parameters were tested on baker's yeast *Saccharomyces cerevisiae* - traditional eukaryotic cell and one of the “basic test organism” for pharmacology studies used for drug screening in microcultivation systems.

A set of undoped as well as Er and Yb doped ZrO₂ samples at different concentrations were prepared by sol-gel method. The optimal rare-earth ion concentration was determined. The up conversion luminescence for free standing and for nanocrystals with baker's yeast cells was studied and the differences in up-conversion luminescence spectra were analyzed.

Carl Zeiss optical microscope was modified to use in up-conversion luminescence imaging. For the first time (to our knowledge) the images with sub micro up-conversion luminescent particles in biologic media were made.

Optical Properties of Metal Nanoparticle Arrays Deposited Through Ultrathin Anodized Aluminum Membranes

R. Poplauskis¹, U. Maļinovskis¹, V. Rutkovskis¹, I. Apsite¹, J. Prikulis¹, F. Lombardi², D. Ertis¹

¹Institute of Chemical Physics, University of Latvia

²MC2, Chalmers University of Technology, Goteborg, Sweden

e-mail: raimonds.poplausks@lu.lv

Metal nanoparticle arrays are potential materials for novel sensor development and applications in electronic and optical devices. One of the array production technique is use of porous ultra thin anodized aluminum oxide (AAO) template (mask) through which material is deposited to form arrays of 20-80 nm diameter nanoparticles on a substrate [1,2].

We have successfully developed the technology of membrane production [3] as well as metal nanoparticle deposition on various surfaces including silicon and glass. The nanoparticle materials tested include Ag, Au/Pd alloy, Au with Ti layer for improved adhesion. The goal of present work is development of a recipe for uniform coverage of large areas with metal nanoparticle arrays.

Metal nanoparticle arrays on transparent substrates form optically active systems, which respond to various stimuli in sensor applications. Their spectral properties can be tailored for particular need by changing particle shape and array density.

Here we present optical scattering measurements of nanoparticle arrays of various metals and alloys produced by the above method; Optical imaging allows assessment of the uniformity and overall quality of deposited metal nanoparticle arrays and determines applicability for particular device design. The optical properties are compared to array structure analysis using electron and scanning probe microscopy techniques.

References

1. Ding G. Q., Zheng M. J., Xu W. L., Shen W. Z., Nanotechnology, 2005, Vol. 16 , 1285–1289
2. Woo L., Hee H., Lotnyki A., Schubert M., Hesse D., Baik S., Gosele U., Nature Nanotechnology, 2008, Vol. 3 402-407.
3. I. Pastore, R. Poplauskis, I. Apsite, I. Pastare, F. Lombardi, D. Ertis, IOP Conference Series: Mater. Sci. Eng. 23, 012025 (2011)

Superparamagnetic Iron Oxide Based Nanostructures Bearing Organosilicon Heterocyclic Choline Analogues as Original Approach to Double Pro-Drugs

I. Segal¹, A. Zablotskaya¹, A. Mishnev¹, M. Maiorov²

¹Latvian Institute of Organic Synthesis, Latvia

²Institute of Physics, University of Latvia, Latvia

e-mail: seg@osi.lv

One of the problems in searching of magnetic nanostructures for biomedical application is to obtain particles with sufficiently hydrophilic surfaces and small average size so they can evade the reticuloendothelial system *in vivo*.

Magnetic iron oxide based mixed-covered nanostructures bearing organosilicon heterocyclic choline analogues have been prepared to provide their physico-chemical investigation. The compounds, which were chosen as a cover for magnetite nanoparticles, are environmentally friendly substances, namely, widely spread in nature oleic acid and biologically active organosilicon heterocyclic choline analogues, so-called, silyl pro-drugs.

According to the developed procedure [1-2] the structures assembling the final product composed of magnetite, an oleic acid and N-methyl-N-(2-decyl- and 2-hexadecyldimethylsiloxyethyl)-1,2,3,4-tetrahydroisoquinolinium iodide as biocompatible shell have been obtained. This complex compositions can be accepted as double pro-drugs due to its original unusual magnetosome-like structure containing non-covalently linked silyl pro-drug (the second surfactant) with oleic acid (the first surfactant).

Structural conclusions and size determination for synthesized magnetic nanoparticles are drawn based upon methods of magnetogranulometry, DLS and X-ray diffraction analysis. Most expected iron oxide core diameter was 5.0–5.5 nm.

The procedure for the preparation of water soluble nanoparticles has been modified. The micelles size in aqueous solution of nanoparticles, bearing N-methyl-N-(2-decyldimethylsiloxyethyl)-1,2,3,4-tetrahydroisoquinolinium iodide, obtained according to the modified procedure, was determined by DLS, which gave the value of about 30 nm.

References

1. A. Zablotskaya, I. Segal, E. Lukevics, *Appl. Organomet. Chem.*, **24**, 150 (2010).
2. A. Zablotskaya, I. Segal, M. Maiorov, D. Zablotsky, A. Mishnev, E. Lukevics, I. Shestakova, I. Domracheva, *J. Magn. Magn. Mater.* **311**, 135 (2007).

Synthesis of Ferrite Nanoparticles for the Magnetic Fluids of Various Practical Applications

G. Kronkalns, M. Maiorov

Institute of Physics, University of Latvia, Latvia

e-mail: kron@sal.lv

Magnetic fluids (MF) are stable colloidal solutions consisting of magnetic nanoparticles dispersed in a carrier liquid and a surfactant acting as a dispersant. The unique ability to control and manipulate the flow and energy transport processes, using an external magnetic field, makes MF an attractive media for potential technological applications in a variety of fields, such as electronics, mechanical engineering, thermal engineering, aerospace, and bioengineering. However, the application of a magnetic fluid in a particular area requires its specific properties. To produce a magnetic fluid with the desired properties for use in a particular area is possible by changing the materials of the magnetic nanoparticles, carrier medium and surfactant [1]. For an efficient heat transfer highly temperature sensitive MF is required with high pyromagnetic coefficient $\beta = (\partial M / \partial T)_H$. For this purpose, we have synthesized nanoparticles of complex $\text{Fe}_2\text{Mn}_{0.3}\text{Zn}_{0.6}\text{Ca}_{0.1}\text{O}_4$, $\text{Fe}_2\text{Zn}_{0.7}\text{Cu}_{0.3}\text{O}_4$, $\text{Fe}_{1.9}\text{Gd}_{0.1}\text{Mn}_{0.6}\text{Zn}_{0.4}\text{O}_4$ ferrites. These particles were coated with oleic acid (surfactant) and dispersed in tetradecane. Many industrial applications require the use of thermally stable, chemically inert, magnetic fluid having a low vapor pressure. For the preparation of such magnetic fluid as the carrier medium castor oil and di(ethylhexyl) sebacate was used. Oleic and lauric acids are used as the surfactants and nanoparticles of magnetite as a dispersion medium. MF containing hard magnetic nanoparticles is characterized by the considerable heating effects in AC magnetic fields due to various energy loss mechanisms. These effects are of interest for technical heating processes. Hard ferrite CoFe_2O_4 particles are synthesized and dispersed in tetradecane ($\text{C}_{14}\text{H}_{30}$) for this purpose. Octadecanol ($\text{C}_{18}\text{H}_{38}\text{O}$) was used as the surfactant. Magnetic properties of colloids are measured by a vibration sample magnetometer in fields up to 1 T.

References

1. G.Kronkalns, M. Maiorov, and E. Blums. *Magneto hydrodynamics*, vol. 33 no. 1, 92(1997).
2. A. Grants, A. Irbitis, G. Kronkalns, M.M. Maiorov. *J. Magn. Magn. Mat.*, vol. 85, 129(1990),

Nonisothermal Transport of Ferrocolloid Particles through Porous Membrane under Transversal Magnetic Field

V. Sints¹, E. Blums¹, G. Kronkalns¹, A. Mezulis¹

¹Institute of Physics, University of Latvia, Latvia

e-mail: viesturs.shints@gmail.com

Transport properties of magnetic nanoparticles are important characteristics which determine the colloidal stability of magnetic fluids in various applications. At present there are considered several applications of ferrofluids under nonisothermal conditions. If strong temperature gradients are presented, there appears a new transport phenomenon – particle thermomagnetoforesis. Experiments on magnetic Soret effect usually are accompanied by uncontrollable thermal or solutal magnetic convection which strongly influences the measurement results. In present work the measurements of thermophoretic particle transport are performed using porous media thereby excluding the possible influence of convection. Thermophoretic mobility of nanoparticles is determined from measurements of particle concentration in two chambers which are located on both sides of the porous layer. The chambers are kept at different temperatures. Homogeneous magnetic field is oriented transversally to the membrane, it is induced by a water cooled solenoid. In frame of linear irreversible thermodynamics the flux densities of solvent, particles flux and heat flux contain summands proportional to the gradients of thermodynamic potentials: pressure, particle chemical potential and temperature. The measured dynamics of both, the particle separation and the thermoosmosis induced pressure difference allows evaluating the membrane transport parameters: the filtration coefficient, the coefficient of solutal osmosis and the coefficient of thermoosmosis. Onsager relations allow evaluation also the coefficient of particle reverse osmosis. Besides, from particle separation curves it is possible to calculate the fluid transport coefficients: mass diffusion and thermodiffusion. The magnetic field causes an increase in mass diffusion and a decrease in particle thermodiffusion. It is shown in the work that the origin of both effects is the magnetic pressure difference on borders of the layer due to breakdown of particle concentration (porosity of the filter is 0.8). Evaluations say that the conventional magnetic Soret effect due to magnetophoresis of particles is significantly smaller than the proposed here effect of magnetic barophoresis.

Direct and Indirect Determination of the Ferrite Nanoparticles Size Distribution

M. Maiorov¹, V. Šints¹, M. Lubane², E. Blums¹

¹Institute of Physics, University of Latvia, Latvia

²Institute of Inorganic Chemistry, Riga Technical University, Latvia

e-mail: maiorov@sal.lv

The polydispersity of nanoparticle systems give rise to special requirements of the particle size description. The size distribution function gives the most perfect presentation of particle sizes, although its determination is a very laborious way. There are direct and indirect methods of polydispersity analysis. The direct method is based on statistical analysis of transmission electron microscopy pictures (TEM). The indirect methods are based on analysis of various macroscopic phenomena which are related to particle sizes. For example, there may be used methods based on realization of inverse task: $y(x) = \int g(x,r) \cdot f(r) \cdot dr$, where y is the observed intensity, g is the intensity for one particle and $f(r)$ is the size distribution function. The present work is devoted to comparison of results of direct polydispersity analysis with those of indirect ones for superparamagnetic

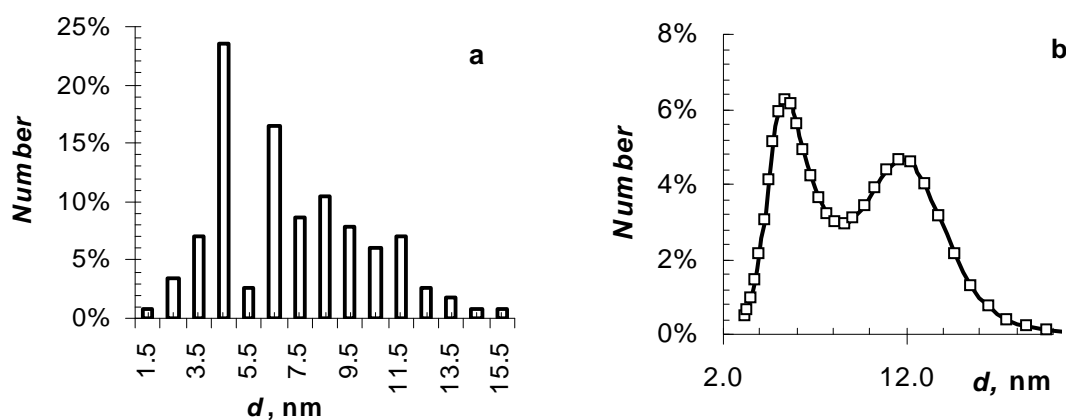


Fig.1 The size distribution of the ferrite nanoparticles: a- histogram from ferrite nanoparticle TEM, b-size distribution function from the sample magnetization analysis.

magnetic nanocolloids. In this case the function $g(x,r)$ means the macroscopic magnetization curve of colloid which is represented as a superposition of Langevin functions. Such approximation may be employed for colloids of small magnetic interaction parameters (low concentrations small particle sizes).

The Relaxation Time of the Ferrofluid Optical Anisotropy as an Indicator of the Ferrite Nanoparticles Fractionation

M. Maiorov, A. Mežulis

Institute of Physics, University of Latvia, Latvia

e-mail: maiorov@sal.lv

A ferrofluid is a colloidal solution of the magnetic nanoparticles in the liquid carrier. Usually it is a polydisperse system with wide size distribution. Under some conditions, such as gravitation, acceleration, gradient magnetic field, gradient of the temperature, the redistribution of the magnetic nanoparticles occurs in the volume.

As a result not only particle concentration but also the mean particle size of the colloidal solution varies with taken part of the solution volume i.e. a fractionation take place.

The optical anisotropy occurs in the liquid colloidal solution of the magnetic nanoparticles under external magnetic field [1].

The nature of the phenomenon is orientation of the colloidal particles along direction forced by

external magnetic field. The relaxation regards so called Brownian type rotation. The time of the particle rotation depends on the colloidal particle size. Owing to this feature, the study of the relaxation of the optical anisotropy in the pulse magnetic field may be a sensitive and quick way to observe the fractionation process in the ferrofluid.

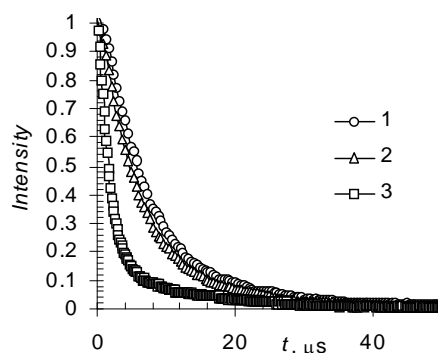


Fig.1 The relaxation of the ferrofluid optical anisotropy from different place of volume after fractionation: 1,2-bottom and top of the gravity column accordingly, 3- top of the centrifuge cell.

References

1. E.Blums, A. Cebers, M. M. Maiorov, Magnetic Fluids, Walter de Gruyter & Co., Berlin -- New-York, 1997, 416 pages

Sedimentation of Suspended Nanoparticles

A. Mezulis, E. Blums, M. Maiorov, A. Lickrastina

Institute of Physics, University of Latvia

e-mail: ansis@sal.lv

If in the particle transport a constant velocity U takes place, the concentration distribution of particles $c = c(x, t)$ can be obtained by solving the equation $\frac{\partial c}{\partial t} = D \frac{\partial^2 c}{\partial x^2} + U \frac{\partial c}{\partial x}$ with its initial and boundary conditions. Assuming that the diffusion coefficient D is known, this equation actually allows to study U . The simplest way to get a constant non-zero U is to subject suspended particles to gravitation. In this case the sedimentation velocity can be calculated as:

$$U = \frac{2g(\rho - \rho_0)d^2}{9\eta_0}, \quad (1)$$

where d is the hydrodynamic diameter of a particle, ρ its density, ρ_0 and η_0 the density and the viscosity of solvent. The real hindrance of sedimentation experiments is very low values of U , and thus very small changes of concentration $c(x, t)$ per moderate time unit.

Sedimentation experiments become reasonable at studying polydisperse suspensions, moreover, if stability of the particles is ensured by a surfactant layer of different density, and formation of aggregates is not eliminated. Properly measured U allows to conclude about mean hydrodynamic values of ρ and d , Eq.(1).

We carried out a sedimentation experiment with suspended ferromagnetic nanoparticles. Polydispersity of nanoparticles obeys log-normal distribution, proved by independent measurements with the vibrating sample magnetometer (VSM) and the size analyzer (DSL). We measured the concentration of magnetic nanoparticles by measuring the inductance with two coils, placed at the top and at the bottom of the test-tube. 7 days were enough to evaluate U , however the experiment proceeded for 24 days with the aim to find the difference in size distributions between the top and the bottom of the test-tube by DSL.

Measured mean sedimentation velocity $U = 0.017$ mm/h is in good agreement with that, estimated by Eq.(1). Polydispersity curves, taken by DSL, allow to perform more detailed analysis over the sizes of nanoparticles, $U = U(\rho, d)$.

References:

1. G. K. Batchelor, C.-S. Wen, J. Fluid Mech., 124, 495-528 (1982)

Characterization of Au Nanodots and Azobenzene Derivative Films by Kelvin Probe Force Microscopy

Z. Alute¹, A. Pastare¹, J. Katkevičs^{1,2}, A. Vīksna^{1,2}, I. Muzikante³, D. Erts¹

¹Institute of Chemical Physics, University of Latvia, Latvia

²Department of Chemistry, University of Latvia, Latvia

³Institute of Solid State Physics, University of Latvia, Latvia

e-mail: zanda.alute@lu.lv

During the last decade there has been increasing interest for design and fabrication of extra small addressable electrodes, sensors and other devices for nanoelectronics and nanophotonics applications. Such device prototypes require investigation of relevant material properties in nanoscale. Atomic Force Microscopy (AFM) and its modifications have proven to be excellent tools for material parameter determination and device prototype testing and characterization.

Kelvin probe force microscopy (KPFM), which is an application of the non-contact atomic force microscope, was used for measuring the contact potential difference between the conductive probe and sample simultaneously with the topography measurements [1]. In this study surface potential maps of electrodeposited Au nanodot array and the self-assembled film of azobenzene derivatives located on the Au film were acquired. The surface potential values of various materials with a lateral resolution below 50nm and potential resolution lower than 10mV were obtained. Also the comprehensive investigation of the influence of the main experimental parameters during KPFM has been analyzed. The effects of varying the tip-sample distance from 10 to 60 nm and the applied V_{AC} from 500 to 2000 mV were investigated [2, 3]. Work functions of investigated surfaces are determined.

References

1. M. Nonnenmacher, M. P. O'Boyle, H. K. Wickramasinghe, S. Sadewasser, T. Glatzel, Appl. Phys. Lett. **58**, 2921 (1991)
2. W. Melitz, J. Shen, A. C. Kummel, S. Lee, Surf. Sci. Rep. **66**, 1 (2011)
3. A. Liscio, V. Palermo, K. Müllen, P. Samori, J. Phys. Chem. C **112**, 17368 (2008)

Optical Properties of Nanostructured Ag-Al₂O₃ Granular Thin Films

L. Poperenko, M. Biednov, Y. Irina

Taras Shevchenko National University of Kyiv, Ukraine

e-mail: kolybmw@yandex.ru

We made a comprehensive research of nanostructured thin films, consisting of silver nanoparticles, embed in dielectric matrix (Al₂O₃) with different Ag volume concentrations. Thickness and optical constants of the films were measured with the help of ellipsometry. Measured angular dependences reveal, that optical conductivity changes from metallic to dielectric with decrease of silver volume fraction [1], (Fig. 1). We show, that optical properties of samples with $f > 0.4$ can be extracted using semifinite medium approximation if thickness of film is higher than 300 nm, and that optical constants of samples with $f < 0.4$ can be described, using effective medium approximation.

Complex dielectric function was measured within 295-825 nm wavelength range. We observed a red shift of silver particle's plasma frequency with decrease of filling factor and suggest a mechanism that can explain such behavior. Average values of complex index of refraction $n+ik$ for samples with $f=0.08-0.2$ is

$n=1.4-1.8$; $k=0.2-0.6$. It means that thin films consisting of silver nanoparticles, embedded in dielectric matrix can perform a strong light absorption in broad spectral region [2], and such materials can be used to increase efficiency of photovoltaic elements and photo detectors.

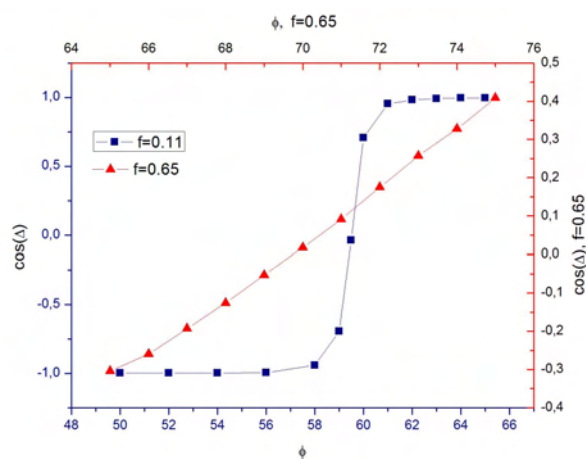


Fig.1 Dependences of ellipsometric parameters $\Psi(\phi)$ and $\Delta(\phi)$ of samples with different silver volume fractions $f=0.65$ and $f=0.11$

References

1. L.V. Poperenko, V.S. Stashuk *Diagnostics of the surface by the polarized light* (Kyiv University, Kyiv 2007)
2. V.G. Kravets, F. Schedin, and A.N. Grigorenko, *Phys. Rev. B* 78, 205405 (2008)

Diamond synthesis using Plasma Chemical Vapour Deposition method

E. Elksnis¹, A. Skudra², A. Viksna¹

¹Faculty of Chemistry, University of Latvia

²Institute of Atomic Physics and Spectroscopy, University of Latvia

e-mail: elksn@inbox.lv

Our work is concerned with the preparation and investigation of low pressure DC plasma chemical vapour deposition systems for diamond synthesis. A variety of chemical vapor deposition (CVD) methods have been developed over the last years to obtain layer of diamond at low pressure. These methods have led to many applications taking advantage of the exceptional properties of a diamond. However, their properties have to be improved and operational costs reduced.

In this work we used low power (60W) DC plasma discharge system in order to deposit rare modification of nanostructural „cauliflower-like” high-quality diamond films from hydrocarbon–hydrogen gas mixtures at low pressure on tungsten substrate. Discharge was operated for 100 hours, during whom coating on substrate was made.

Analysis of tungsten substrate surface was performed by SEM-EDX and data showed that main component of the coating is carbon. There were also oxygen pollution traces. Obtained diamond coating image was very similar to that produced in University of Bristol (Fig. 1 a and b).

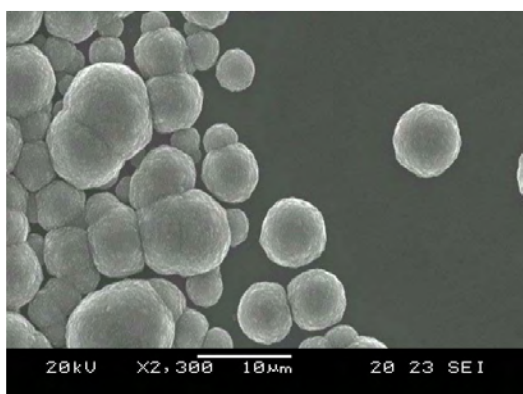


Fig. 1a Image of „cauliflower-like” diamond particles produced in University of Bristol

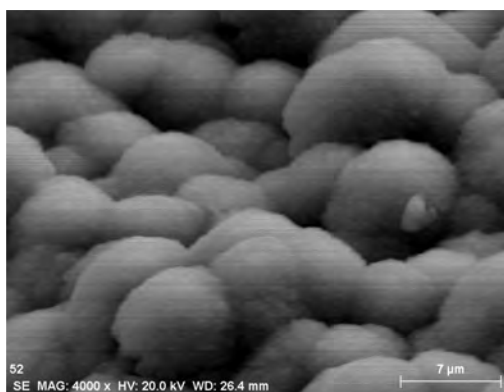


Fig. 1b Image of our „cauliflower-like” diamond coating on tungsten

Acknowledgements

The work was partly supported by National Research Program in Materials Science Project #1 Multifunctional materials.

References

1. Bristol University CVD Diamond Group <http://www.chm.bris.ac.uk/pt/diamond/semflat.htm>

Deposition and Characterization of Graphene Oxide Films Obtained by Langmuir-Blodgett Technique

L. Gerca¹, K. Kundziņš¹, M. Knite², M. Rutkis¹

¹Institute of Solid State Physics, University of Latvia, Latvia

²Institute of Technical Physics, Riga Technical University, Latvia

e-mail: martins.rutkis@cfi.lu.lv

Nowadays a huge attention is paid to single-sheet graphene (SG), an outstanding transparent material with a high electrical and thermal conduction. Due to these properties, replacement of traditional transparent electrodes by SG could lead to enhanced performance of optoelectronic devices. Large area substrates should be covered by SG for future applications like solid state lighting and solar cells. One of the possible routes of obtaining such films is to use dispersion of single-sheet graphene oxide (SGO) what can be produced in large scale by use of the different liquid phase graphite exfoliation methods. The challenging part is how to transfer SGO from dispersion on to large area substrate in controlled manner. One of such possibilities is to obtain Langmuir monolayer of SGO at the air/water interface and then transfer it to substrate by Langmuir-Blodgett (LB) or Langmuir-Schaefer deposition method¹. Optimization of optical and electrical properties could be achieved within a thickness control of GO films upon repeated deposition process².

In presentation we would like to show LB deposition results achieved by commercially available (Cheap Tubes Inc.) submicron size dried SGO with thickness 0.7 – 1.2 nm by AFM. Suspension treatment, spreading an LB deposition process parameter impact on film morphology and properties will be discussed.

References

1. L. J. Cote, F. Kim, J. Huang, J. Am. Chem. Soc., **131**, 1043–1049 (2009)
2. Q. Zheng, W. H. Ip, X. Lin, N. Yousefi, K. K. Yeung, Z. Li, J-K. Kim, ACS NANO, **5**, 7, 6039-6051, (2011)

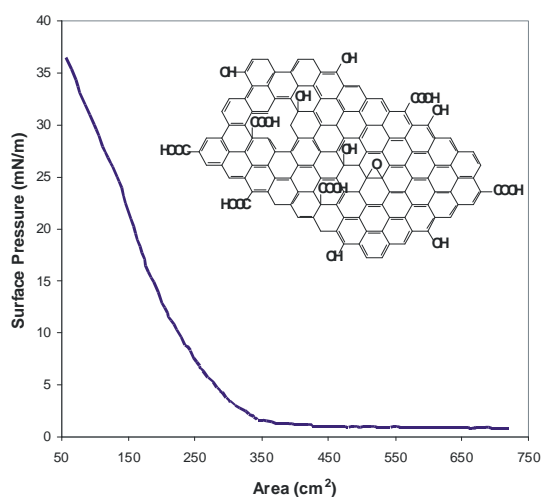


Fig.1 Compression isotherm of single sheet graphene oxide (SGO) monolayer on air/water interface.

Structure of Nanoporous Carbon Materials for Supercapacitors

A. Volperts¹, G. Dobele¹, N. Mironova-Ulmane², I. Sildos³

¹Latvian State Institute of Wood Chemistry, Latvia

²Institute of Solid State Physics, University of Latvia, Latvia

³Institute of Physics, University of Tartu, Estonia

e-mail gdobele@edi.lv

Technical large scale implementation of super capacitors (EDLC) is being hindered by high costs of electrodes, which is an important factor in their acceptance at the world markets. Many researches use activated carbon electrodes due to their lower costs, wide working conditions range and high potential comparing to electrodes made from other carbon materials (fullerenes, nanotubes, etc.).

The main goals of our work is the obtaining of effective nanoporous carbon materials with high specific surface using thermocatalytical synthesis with sodium hydroxide and their testing by X-ray scattering technique and micro-Raman spectroscopy. It was experimentally established that temperature 500°C is not sufficient ($S_{\text{BET}} 1200 \text{ m}^2/\text{g}$) to reach the maximum porous structure of carbon materials. At 700°C specific surface maximum ($S_{\text{BET}} 3570 \text{ m}^2/\text{g}$) is being achieved after 90 minute synthesis. The hypothesis of the possible pore size formation mechanism has been drawn – it is proposed that graphene planes are being consequently removed from the reaction zone.

On the X-ray scattering plots of the carbon materials obtained two diffraction maximums are being observed at 21.7 and 42.8 degrees, which is characteristic for the materials with partially ordered molecular structure. It was established that positions of diffraction maximums do not correspond to the ones observed in the case of graphite-like carbon materials. Average coherent scattering areas sizes $L=1.2$ and $L=1.9$ nm can be attributed to the average crystallites sizes. Raman spectra of the obtaining nanoporous carbon materials display two broaden bands: G-band (1333 cm^{-1}), D-band (1585 cm^{-1}). Raman spectra have also the second order overtone of the D band and G band: broaden 2D band (2785 cm^{-1}) corresponding to the graphite and sharp G `band (2685 cm^{-1}) corresponding to the graphene

Effect of Annealing Temperatures and Substrate Surface Treatment on the Properties of Nickel Containing Titania Thin Sol-Gel Films

U. Joost^{1,2}, R. Pärna¹, E. Nõmmiste¹, T. Käämbre¹, A. Kikas¹, I. Kuusik¹, I. Kink^{1,2}, M. Hirsimäki³,
V. Kisand¹

¹Institute of Physics, University of Tartu, Riia 142, 51014 Tartu, Estonia

²Estonian Nanotechnology Competence Center, Riia 142, 51014 Tartu, Estonia

³Surface Science Laboratory, Tampere University of Technology, P.O. Box 692 FIN-33101, Tampere, Finland

e-mail: urmas.joost@ut.ee

Titania (TiO₂) is a material that has attracted great attention for many advanced applications using the sunlight. It has been studied extensively as a promising photocatalyst [1], solar energy cell material [2], antifogging and self-cleaning coating [3,4]. Unfortunately, it absorbs only a fraction of sunlight, which restricts the use of titania. Nickel containing titania thin films have been prepared on HF or methanol cleaned Si(100) substrate by using the sol-gel method and annealed in the air at 450 to 1150 °C. Several experimental techniques (Atomic Force Microscopy, X-ray Diffraction, X-ray Reflection, Raman spectroscopy, Energy Dispersive X-ray Analysis, X-ray Photoelectron Spectroscopy, X-ray Absorption Spectroscopy, UV-VIS Spectroscopy and Hydrophilicity measurements) have been applied to characterize these films. The morphological and structural properties of nickel containing titania were found to be dependent on substrate treatment. The thin films deposited on methanol cleaned Si(100) substrates, compared to similar films on HF cleaned Si(100) substrates, were more uniform, did not contain large pores and had smaller RMS roughness, especially when annealed below 650 °C. Also films on methanol cleaned substrate were more crystalline and anatase transformation to rutile phase occurred at 150 °C lower temperature. When films were annealed above 650 °C, nickel was found mainly in the NiTiO₃ crystallites. Nickel compounds segregated to the surface of the film, forming islands. Nickel addition red-shifted the titania fundamental absorption edge further into the visible range.

References

1. M. Keshmiri, M. Mohseni, T. Troczynski, Appl. Catal. B: Environ. **53** 209-219 (2004).
2. G. M. Keima, M. J. Colgan, M. J. Brett, Solar Energy Mater. Solar Cells **85** 321-331 (2005).
3. R. Wang, K. Hashimoto, A. Fujishima, M. Chikuni, E. Kojima, A. Kitamura, M. Shimohigoshi, T. Watanabe, Nature **388** 431-432 (1997).
4. R. Wang, K. Hashimoto, A. Fujishima, M. Chikuni, E. Kojima, A. Kitamura, M. Shimohigoshi, T. Watanabe, Adv. Mater. **10** 135-138 (1998).

Characterization of Elastic and Dissipative Nanocomposite Material Properties via Using of Small Dimension Specimens

P. Akishin, E. Barkanov

Institute of Materials and Structures, Riga Technical University, Latvia

e-mail: pavels.akisins@rtu.lv

Carbon nanotubes (CNT) and their mechanical properties have been closely investigated since the late 1990s. Initially researches were mainly focused on using of CNTs to reinforce polymer and ceramic matrices, later – on the reinforcing of metallic matrices. Thus, CNT-reinforced aluminium has potential applications in the aerospace, automotive and sports industries where light weight combined with high stiffness and strength is desired.

Technologies of nanocomposite metals production are expensive and complex. For this reason it is perspective to apply non-destructive methods and to use specimens with small dimensions for determination of material properties. The specimens with cross-section 10x2 mm and a length of 60, 70, 80 mm was used in the research. Two methods have been used to determine the elastic material properties: an impulse excitation method and a method, based on the three-point-bending tests. Peak-picking method has been applied to determine dissipative material properties. Specimens machined from large billets made of aluminium alloy LM24 with CNT volume content of 0.0, 0.1, 0.3, 0.5 and 1.0% have been tested to determine the influence of the CNT on elastic and dissipative properties of the LM24 alloy.

Specimens with free-free boundary conditions simulated by handing the specimens on thin threads have been used in the experiments conducted by the impulse excitation and peak-picking methods. The experimental results show that anchoring of specimen in the upper corners instead of the nodal lines of bending modes didn't influence values of eigenfrequencies and the dependency of loss factor on the frequency, but increased values of loss factor to constant value of 0.00025.

The addition of CNT to the aluminium alloys did not yield a visible increase in their elastic properties, but decreased their dissipative properties. If for bending modes the maximal average deviation (in comparison with pure LM24 alloy) is 32%, for twisting modes it is 45%. It is necessary to note that material investigated did contain pores that have considerable influence on the elastic and dissipative material properties. Therefore it was not possible to obtain clear dependences of the material properties on CNT content.

Synthesis of Silica-Carbon Nanotube Composite Materials and Their Application for Laser Systems

J. Pilipavicius, D. Sakalauskas A. Beganskiene, A. Kareiva

Vilnius University, Department of General and Inorganic Chemistry

e-mail: jurgis.pilipavicius@chf.vu.lt

Carbon nanotubes (CNT) have been widely investigated by researchers to improve understanding of the unique electric mechanism and optical properties. Semiconducting, single-walled carbon nanotubes (SWCNT) are a promising material for saturable absorbers in laser mode locking. Furthermore, SWCNT-based saturable absorbers can be fabricated by simple and economical methods, such as spray, spin coating or horizontal evaporation methods. However, application of those techniques requires dissolution of CNT's. Unfortunately, CNTs are insoluble in any solvents and forming bundles due to strong van der Waals interactions that tightly hold them together. CNT's insolubility decrease the overall yield of usable material and interfere with most of the desired properties of the CNT's. The use of various surfactants and polymers can highly increase solubility of CNT in polar and non-polar media.

Currently, fabrication of CNT and polymer composites for saturable absorbers is very popular. But due to nature of organic polymer matrix, these composites are unstable on higher temperatures or in high energy light expositions. Therefore a sol-gel process for the fabrication for inorganic (i.e. silica) or semi-organic (organic-modified silica) matrix can be a promising way to produce photo-chemically and thermally stable CNT composites.

The aim of this work - using spin-coating technique make a SWCNT's and silica composites. So foremost SWCNT's solubility in ethanol was investigated using different surfactants – Triton (X-100 and X-305), polyvinylpyrrolidone (PVP 360 000M and PVP 24 000M) and Poly(4-vinylpyridine) (P4VP 40 000M). Most stable colloidal solution was obtained using a P4VP as surfactant – solutions were stable up to 6 weeks. Therefore this surfactant was used for the fabrication of SWCNT/Silica composite coatings. SWCNT's was directly dispensed in a colloidal silica sol and coatings made by spin-coating technique. All samples were investigated under optical, atomic force microscopy methods, and optical non-linearity was measured.

Mechanical and Electrical Properties of PE Nanocomposites with Carbon Nanotubes

J. Zicans¹, R. Merijs Meri¹, J. Bitenieks¹, R. Maksimovs², M. Knite³

¹Institute of Polymer Materials, Riga Technical University, Latvia

²Institute of Polymer Mechanics, Latvia

³Institute of Technical Physics, Riga Technical University

e-mail: zicans@ktf.rtu.lv

In this work, the influence of multi-walled carbon nanotubes (MWCNTs) and commercial polyethylene/carbon nanotube masterbatch on mechanical and thermal properties of CNT reinforced linear low density polyethylene (LLDPE) nanocomposites is studied. The composites were obtained by using melt mixing.

Tensile elastic modulus of the nanocomposites rapidly increase, by raising CNT content up to 2 wt. %. Above 2 wt. % concentration of CNT gradual decrease in elastic modulus can be observed due to agglomeration. This shows that 2 wt. % is limiting CNT concentration for used mixing technique to achieve good dispersion of the nanofiller throughout the LLDPE volume. Greater modulus and yield stress increase is observed for polyethylene masterbatch filled composites.

By analyzing calorimetric data of the investigated nanocomposites it was observed that the effect of nanofiller on the crystallization behavior is stronger in the case of the composites modified with the masterbatch.

Thermogravimetric analysis measurements show that weight loss curves of the investigated nanocomposites shift to higher temperatures along with increasing CNT content. Thus 50% weight loss of LLDPE is reached at 470°C while that for the nanocomposite with 5 wt.% of CNT – at ~ 500°C, most probably due to better heat dissipation of the material. This indicates about increased thermal stability of the CNT modified nanocomposites.

Investigated LLDPE nanocomposites show percolation threshold of electrical conductivity at 2 wt. % or 1 wt. % of the nanofiller, depending upon whether neat CNTs or masterbatch is used. Permittivity measured in the frequency range from 10⁻² to 10⁶ Hz is independent from the frequency for unfilled polymer. For nanocomposites noticeable dielectric polarization is observed and the dielectric constant is higher for samples with higher CNT content. There is also similar increase in imaginary part of permittivity at higher CNT concentrations.

The Effect of Nanosize ZnO on the Structure and Properties of the Selected Polymer Blend Composites

A. Grigalovica¹, I. Bochkov¹, R. Merijs Meri¹, J. Zicans¹, J. Grabis², C. Berger³, H.P. Heim³

¹Institute of Polymer Materials, Riga Technical University, Latvia

²Institute of Inorganic Chemistry of Riga Technical University, Riga, Latvia

³Institut für Werkstofftechnik - Kunststofftechnik, University of Kassel, Germany

e-mail: zicans@ktf.rtu.lv

In the prevailing “nanoage” in science there are multiple evidences about development of nanostructured materials and composites on it bases. In many researches it is reported about modification of broad range of thermoplastic and thermosetting polymers with various inorganic and organic nanofillers such as cellulose whiskers and nanofibers [1], nanoclay [2], precious metals and metal oxides [3], various carbon allotropes (graphene, carbon nanotubes, nanodiamond etc) [4]. Considerably less effort, however, is devoted to the development of polymer blend nanocomposites.

In the current research the effect of ZnO nanoparticles on the structure and properties of common thermoplastic polymers - polyoxymethylene (POM), polypropylene (PP), ethylene- octane copolymers (EOC) - and their binary blends is investigated. Composites have been obtained in a broad component wt.-to-wt. ratio (0-50 % by EOC weight content) by using twin screw extruder. The amount of nanostructured ZnO filler in the composites is changed in the interval from 0 to 5 wt. %.

Structure as well as quasistatic and dynamic stress-strain characteristics of ZnO modified nanocomposites has been investigated. In general results show that at small amount of EOC impact strength as well as superelasticity of the investigated nanocomposites increase. In the same time addition of ZnO improve heat resistance and mechanical properties of the investigated polymers and their blends to certain extent.

References:

1. H.P.S. Abdul Khalil, A.H. Bhat, A.F. Ireana Yusra, Carbohydrate Polymers 2012, 87, 963.
2. S. Pavlidou, C.D. Papaspyrides, Progress in Polymer Science 2008, 33, 1119.
3. S. P. Gubin, Yu. A. Koksharov, G. B. Khomutov, G. Yu. Yurkov, Russian Chemical Reviews 2005, 74, 489
4. Z. Spitalsky, D. Tasis, K. Papagelis, C. Galiotis. Progress in Polymer Science 2010, 35, 357.

Measurement of Static Friction Force of Complex Shaped ZnO Nanowires on a Flat Surface

M. Antsov¹, L. Dorogin¹, B. Polyakov^{1,2}, S. Vlassov¹, R. Lõhmus¹

¹Institute of Physics, University of Tartu, Estonia

²Institute of Solid State Physics, University of Latvia, Latvia

e-mail: antsof@gmail.com

Complex shaped nanowires (NW) bent on a flat substrate by static friction force are investigated theoretically and experimentally. Zinc oxide NWs on oxidized silicon wafer are used for the experiments inside a scanning electron microscope (SEM). The complex shapes of NW's are obtained by a nanomanipulation device as an actuator and an atomic force microscope (AFM) tip attached to it as a probe, in order to push the NW. Series of manipulations were conducted, where the NW was manipulated in steps to acquire different complex shapes, for example S- or arc-shapes of the same NW. NW bent profile is preserved due to balance of intrinsic elastic force and external lateral friction force from the substrate.

Strus et. al [1] introduced a method, where an AFM image of a carbon nanotube was obtained and used as a basis for determining the static friction and elastic stresses in the framework of the elastic beam theory. The drawbacks of that method were the unconsidered boundary conditions and reduced equilibrium equations.

Model based on elastic beam theory is proposed that enables to solve coupled equations of equilibrium for the NW, taking into account boundary conditions of free NW ends[2]. That method demonstrated successful interpretation of bent NWs of simple arc-shapes. In the present study we have developed a improved algorithm of NW skeletonization for analysis of complex shaped NWs. Calculation of distributed friction force, elastic energy and elastic stress along the complex shaped NWs from experimentally obtained SEM image is demonstrated. Depending on the shape of the NW, different degrees of interpolation polynomial functions can be applied.

References

1. M. Strus, R.Lahiji, P.Ares, V.Lopez, A.Raman, R.Reifenberger: *Nanotechnology*, **20**, 385709 (2009).
2. L. M. Dorogin, B. Polyakov, A. Petruhins, S. Vlassov, A. E. Romanov, *J. Mater. Res.* **27**, 580 (2011)

Mechanical Properties of Antimony Sulfide Nanowires

L. Jasulaneca¹, R. Meija¹, J. Prikulis¹, J. Varghese², J.D. Holmes², D. Erts¹

¹Institute of Chemical Physics, University of Latvia, Raina blvd. 19, Riga, LV-1586, Latvia

²Department of Chemistry, National University Ireland, Cork, Ireland

e-mail: ljasulaneca@gmail.com

Characterization of the fundamental mechanical properties of individual nanowires is crucial for their application in nanometer size devices. Young's modulus defined as the ratio of tensile stress to tensile strain is one of the most important parameters used to determine material's mechanical properties. It has been observed experimentally as well predicted by theory that Young's modulus of nanowires of different materials may be size dependent, however measurements results show opposing trends.

Antimony sulfide has attracted interest for its high photosensitivity and thermopower [1]. Mechanical properties of antimony sulfide nanowires to our knowledge have not been measured.

Antimony sulfide nanowires were fabricated by reaction between SbCl_3 and thiourea at 195° C temperature. Experiments were performed *in situ* by means of a nanomanipulation system compatible with scanning electron microscope. The advantage of this method is the possibility to directly investigate mechanical reaction of individual nanowires at the moment when an external force is applied.

In our experiment Young's modulus of antimony sulfide nanowires has been determined by two approaches – by measuring nanowire resonance frequency and nanowire deflection by an external electrostatic field. Young's modulus has been determined for nanowires of varying cross sections and results compared to that of bulk antimony sulfide.

References

1. B. Roy, B.R. Chakraborty, R. Bhattacharya, A.K. Dutta, Solid State Commun. **25**, 937 (1978)

Properties and Applications of Well-Ordered and Individual V-VI Group Semiconductor Nanowires

G. Kunakova¹, P. Birjukovs¹, R. Meija¹, J. Andzane¹, J.D. Holmes², D. Erts¹

¹Institute of Chemical Physics, University of Latvia

²National University of Ireland, Cork, Ireland

e-mail: Gunta.Kunakova@lu.lv

Semiconductor nanowires are perspective 2D materials for the applications in the future technologies. Band gaps of Bi_2S_3 (1.3 eV) and Sb_2S_3 (1.6-1.8 eV) cover the visible and near infrared ranges of the solar spectrum. Thus these nanowires are optimal candidates for the conversion of sunlight into energy. Another possible application is integration of individual nanowires and nanowire arrays in other functional devices, for example field effect transistor (FET) chemical sensors.

In our experiments, we used Bi_2S_3 and Sb_2S_3 nanowires and highly ordered nanowire arrays. Nanowire arrays were grown inside AAO membrane pores with pore diameters of 50-200 nm. Here we present some results on our experimental work.

Recently, Bi_2S_3 nanowire array based field effect transistor was demonstrated by our group. To make it possible to use such FETs as chemical sensors, it is important to increase a sensing surface. This can be done by providing a suitable arrangement of the nanowire in FET. To proof that we have manufactured an individual nanowire based transistor on a flat surface using lithography techniques. Characteristics of individual nanowire based and nanowire array based transistors were measured and compared.

Also, we have investigated photoconductive properties of highly ordered Sb_2S_3 nanowires encapsulated in AAO matrix. Samples were illuminated with light in the range from ultraviolet to the infrared. For the sample illumination both LED diodes and laser beam were used. Photocurrents, kinetic components, response and decay times and stability for the different wave lengths were measured and compared.

Improved Method of Nanowire Disconnection for Application in NEM Switches

R. Meija¹, J. Andzane¹, J. Prikulis¹, A. Livshits¹, J.D. Holmes², D. Erts¹

¹Institute of Chemical Physics, University of Latvia

²Department of Chemistry, University College Cork, Ireland

e-mail: Raimonds.Meija@lu.lv

Recently, some research groups including our group presented individual nanotube or nanowire based two-terminal nanoelectromechanical *on-off* devices [1,2]. The operation of these devices is based on the fine balancing between electrostatic, elastic and adhesion forces. For the successful operation of such device, one must rely on the elastic force of the bended nanowire. This force must be strong enough to overcome adhesion in the nanowire-electrode contact area and to tear the nanowire from the contact. The problem to be solved is to find improve the method for the nanowire detachment from the contact. Nanowire's detachment should not be dependent only on elastic force of the bended nanowire. Thus it will be less dependent on the nanowire's mechanical properties and the system configuration.

In this work we present application of DC and AC electrical fields to help the elastic force of the nanowire to disconnect it from the contact. These methods were developed for the systems with two and more input electrodes and one output electrode. The experiments were carried out *in situ* by using nanomanipulation systems inside SEM. Ge nanowires were used as active elements and electrochemically etched gold tips was used as opposite electrodes.

The first way to go is to combine the elastic force with the DC electrostatic field. The DC field must be applied between the second input electrode and output electrode. Although the experiments were successful, the nanowire disconnection required operating voltages up to 200V. So high voltages lead to the fast damage of the nanowire. This approach can be improved by applying AC field "on top" of DC field. With combined AC+DC electric field the detachment of the nanowire can be achieved at the AC field frequency nearly the same as the resonant frequency of the double-clamped nanowire. The AC and DC voltages in this case are in the range of just 3-25 V. Neither melting nor degradation of the nanowire is observed during repetitive switching of the nanowire by combined AC+DC method.

References

1. Andzane, J., Petkov, N., Livshits, A., Boland, J.J., Holmes, J.D., Erts, D., Two Terminal Nanoelectromechanical Devices Based on Germanium Nanowires. *Nano Lett.*, 2009, Nr. 5, p. 1824–1829.
2. Andzane, J., Prikulis, J., Dvorzek, D., Mihailovic, D., Erts, D, Mo₆S₃I₆ nanowire based two-terminal nano-electromechanical switch, *Nanotechnology*, 2010, Nr. 21. pp. 6 (125706).

Au Electrodeposition into AAO Pores and on the Bi₂S₃ Nanowires

A. Pastare¹, J. Katkevics^{1,2}, Z. Alute¹, A. Viksna^{1,2}, D. Erts¹

¹Institute of Chemical Physics, University of Latvia, Kronvalda blvd. 4, Riga, LV-1586, Latvia

²Faculty of Chemistry, University of Latvia, Kr. Valdemara Str. 48, Riga, LV-1013, Latvia

e-mail: Anita.Pastare@lu.lv

Au nanowires (NW) and nanoparticles (NP) are perspective for application as biosensors, DNS detectors, in nanoelectronics and for other purposes [1] In the current study, the deposition of Au NW in pores of anodized aluminium oxide (AAO) template and on the ends Bi₂S₃ of NW was performed in miniature (2-3 drops of electrolyte, in a few mm² AAO) electrochemical cell. Effectiveness of developed cell was examined. Electrolyte composition containing H[AuCl₄], K₄[Fe(CN)₆] was successfully used in the electrochemical synthesis of gold NW and NP. Active component, (K[Au(CN)₂]) responsible for the electrochemical formation of Au NW, is produced in the electrolyte during chemical reaction between K₄[Fe(CN)₆] and H[AuCl₄]. The products of chemical reaction between K₄[Fe(CN)₆] and H[AuCl₄] are characterized and evaluated by UV-VIS molecular absorption spectrometry.

The obtained Au NW and Au NP were characterized by scanning electron microscopy (SEM) and by atomic force microscopy (AFM).

Electrodeposition of Au by using said electrolyte system is compared

with electrodeposition by commonly used K[Au(CN)₂] in citrate solution as electrolyte [2]. It was stated that generation of electrochemical active component during chemical reaction in electrolyte solution have several advantages such as electrolyte is non-cyano component electrolyte and growth nanowires is equally uniform. As presented in Figure 1, the developed method is suitable for the electrofabrication of Au nanowires and particles on the Bi₂S₃.

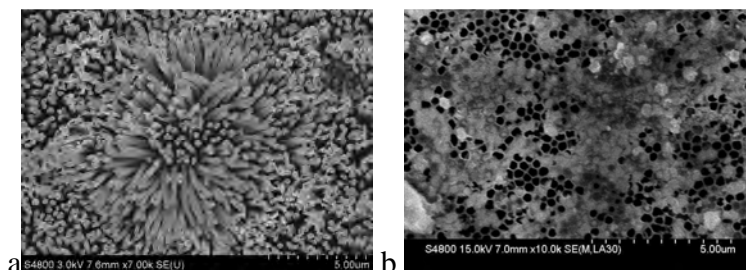


Fig 1. SEM images of Au NW (a) and Au particles (white spots) on the ends of Bi₂S₃ NW(b).

References

- Griehaber D., MacKenzie R., Voros J., Reimhult E. *Sensors*, **8**, 1400 (2008).
- Lui J., Duan J. L., Toimil-Molares M. E., Karim S., Cornelli T. W., Dobrev D., Yao H. J., Sun Y. M., Hou M. D., Mo D., Wang Z. G., Neumann R. *Nanotechnology*, **17**, 1922 (2006).

Carrier Dynamics in Nanostructures of Ternary AlGa_xN with Tunable Bandgap

R. Aleksiejūnas¹, S. Nargelas¹, S. Miasojedovas¹, P. Ščajev¹, K. Jarašiūnas¹, L. Trinkler²,
J. Grigorjeva², B. Berzina², K.H. Chen³, Li-C. Chen³

¹Institute of Applied Research, Vilnius University, Sauletekio Ave. 9 - III, Vilnius 10222, Lithuania

²Institute of Solid State Physics, University of Latvia, 8 Kengaraga, 1063 Riga, Latvia

³Center for Condensed Matter Sciences, National Taiwan University, Taipei 106, Taiwan

e-mail: ramunas.aleksiejunas@ff.vu.lt

Quasi one-dimensional semiconductor nanostructures of ternary Al_xGa_{1-x}N compounds open a possibility to tailor their electrical and optical properties by combining both the composition (molar concentration of Al) and size-dependent electronic confinement. This novel approach for bandgap engineering is promising for sensing and optoelectronic applications, while requires detail studies of structural, optical and photoelectrical properties.

In the given report we present an optical study of carrier dynamics in MBE-grown Al_xGa_{1-x}N nanorod structures on Si(111) substrate with Al content 1.5% or 6.6 %. The typical nanorod diameter was 55-60 nm. For comparison, carrier dynamics in 0.5 μm thick Al_xGa_{1-x}N/Al₂O₃ layers with x = 6.7 – 13% has been investigated. Photoluminescence (PL), time-resolved transient grating (TG), and differential transmission (DT) techniques were applied to monitor recombination rates of excess carriers. We found out that the PL peak position in nanorod samples depends on Al content determined by XRD. Varying excitation wavelength in 250 - 310 nm, time-integrated PL spectra at low injections revealed the strongest response in 355 - 370 nm (3.46 - 3.35 eV) range for differently grown ternary nanostructures.

Time-resolved DT and TG experiments revealed two components of injected carrier decay in nanorods: the first one of 15 - 25 ps, which decay correlated with Al content, being faster at higher Al content. The second component of 0.4 – 1.6 ns varied across the layers. The reference AlGa_xN on sapphire layer (with x = 0.068) also revealed two-component relaxation with characteristic times of 25 ps and 500 ps. DT spectral response at 330 nm excitation was found in 360-375 nm range and decayed with 14 ps time.

Correlation of observed features with XRD data and Al content will be also discussed.

Evaluation of Polymer-Nanostructured Carbon Composites Response to Chemical Stimuli

S. Stepina¹, G. Sakale¹, M. Knite¹, V. Tupureina²

¹Institute of Technical physics, Riga Technical University, Latvia

²Institute of Polymer materials, Riga Technical University, Latvia

e-mail: Santa.Stepina@rtu.lv

Nowadays scientific progress and improving of chemical industry has made a big step forward. That means, the possibility of various organic solvents to come in tracheas of workers is growing and it can make irreversible damage to workers organism. Therefore there is a need to design, elaborate and investigate polymer-nanostructured carbon composite (P-NCC), which would serve in factories as a sensor material and would warn workers about health risks or it can help manufacturers control production processes.

Sensor material is made of polymer matrix (polyethylene glycol (PEG) and ethylene-vinyl acetate (EVA)) and conductive ingredient (high structured carbon black nanoparticles). Used polymer matrixes differ with structure and polarity. PEG is highly crystalline and polar polymer, while EVA has amorphous structure and is non-polar polymer. Specifically formed sensor material structure enables chemical vapour detection in the air.

PEG-NCC and EVA-NCC percolation thresholds are determined. PEG-NCC percolation curve shows unexpected behavior, instead of one percolation threshold we observed two thresholds at 3 and 8 mass parts of carbon black. EVA-NCC percolation threshold is around 7 mass parts of carbon black. Conclusion is that linear polymer macromolecules, like PEG have, promoted faster conductive channel formation between carbon black nanopartilces.

PEG-NCC and EVA-NCC chemical vapour sensitivity depending on concentration of carbon black have been evaluated. As expected both composites show the best ethanol vapour sensitivity slightly above percolation thresholds. PEG-NCC highest response is observed at 8 mass parts of carbon black. It can be explained with PEG crystalline structure reduction when increase the concentration of carbon black in the composite content.

Sensing Effects in Polymer/Thermoexfoliated Graphite and Polymer/Multiwall Carbon Nanotube Composites

M. Knite¹, L. Matzui², J. Zavickis¹, G. Sakale¹, A. Linarts¹, K. Ozols¹

¹Institute Riga Technical University, Institute of Technical Physics, Latvia

²Kyiv National Taras Shevchenko University, Department of Physics, Ukraine

e-mail: knite@latnet.lv

Recently we have elaborated polyisoprene/high structured carbon black composites with excellent piezoresistivity effect [1] as well as chemoresistivity effect [2]. The task of this study is to test the thermoexfoliated graphite (TEG) as well as multiwall carbon nanotubes (with high (LMWCNT) and low (SMWCNT) aspect ratio) for their application in design of new sensitive polymer composites. TEG has been synthesized in Department of Physics of KNTSU. Polyisoprene/TEG and polyisoprene /MWCNT composites were prepared in Institute of Technical Physics of RTU.

Piezoresistivity (Fig. 1) and chemoresistivity (Fig. 2) DC and AC tests of composites show promising results. Polyisoprene/TEG composite has higher sensitivity to chemicals (Fig.2) than polyisoprene/LMWCNT. It allows to expect all the better sensitivity of polymer/single graphene composites in future.

References

1. J.Zavickis, M.Knite, G.Podins, A.Linarts, R.Orlovs, *Sensors and Actuators. A: Physical* **171**, 38 (2011)
2. G.Sakale, M.Knite, V.Teteris, *Sensors and Actuators. A: Physical* **171**, 19 (2011)

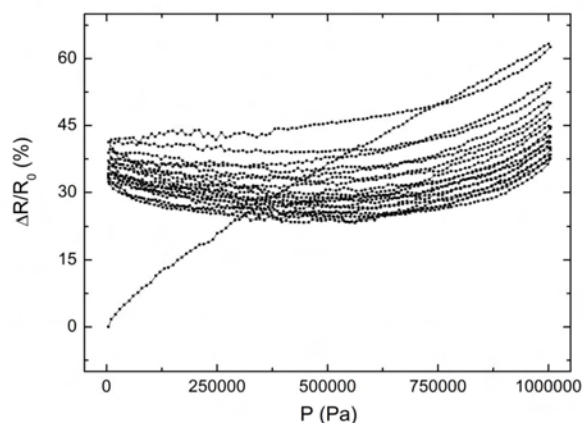


Fig. 1 Piezoresistivity DC test of polyisoprene/TEG composite by 10 cycles of loading at room temperature. 10 phr TEG.

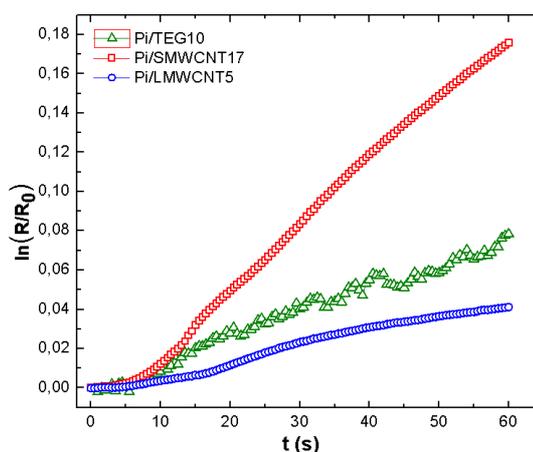


Fig. 2 Chemoresistivity DC test of polyisoprene/TEG composite and polyisoprene/MWCNT composites at room temperature for ethyl acetate vapour.

Completely Hyperelastic Pressure Sensing Mat with Structurally Integrated Piezoresistive Sensors

A. Linarts¹, J. Zavickis¹, M. Knite¹, Ā. Solovjovs¹

¹Institute of Technical Physics, Riga Technical University, Latvia

e-mail: artis.linarts@rtu.lv

Previous studies of polyisoprene nanostructured carbon black composites (PNCBC) have proven that this material could be used to produce cheap pressure, impact or vibration detection units – sensors [1]. Depending on the carbon black concentration and filler dispersing methods PNCBC reveals higher or lower piezoresistive properties as well as good electrical conductivity [2]. In this article we try to elaborate completely hyperelastic pressure sensitive mat (CHPSM) capable of large scale pressure mapping using layered composite approach.

The CHPSM were made from raw PNCBC compositions with variable electroconductive carbon black concentrations.

Each element of CHPSM was semi-vulcanized separately so it could maintain its shape during final vulcanization when these elements were cured together to form a uniform sensor. The CHPSM consists of 6 separate piezoresistive elements with hyperelastic electrodes incorporated into non-conductive natural polyisoprene rubber shell. The piezoresistivity of each CHPSM element was determined under operational pressures up to 1 and 10 atmospheres. Dimensions of the elaborated CHPSM are 100x70x5 mm but they can be easily tailored for a specific requirement.

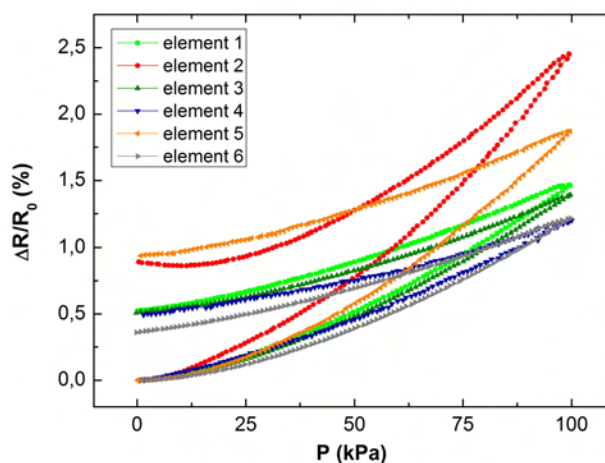


Fig.1 Piezoresistive behavior of separate similar CHPSM elements under 1 atmosphere of pressure

References

1. M.Knite, V.Teteris, A.Kiploka, J.Kaupuzs, *Sensor.Actuator A* **110**, 142 (2004)
2. J. Zavickis, A. Linarts and M. Knite, *Energetika* **8**, 44 (2011)

Effect of the Plasticizers on Chemoresistivity of Polyvinylacetate-Nanostructured Carbon Composite

G. Sakale¹, E. Liepa¹, V. Tupureina², M. Knite¹, D. Jakovlevs³

¹Institute of Technical Physics, Riga Technical University, Latvia

²Institute of Polymer materials, Riga Technical University, Latvia

³Biomaterial Innovation and Development Center, Riga Technical University, Latvia

e-mail: elinaLiepa@gmail.com

It is progressive to look for ecology, health and air quality nowadays. People, who work in factories and laboratories, are taken precautions to avoid serious health problems that are related with exposure to various volatile organic compounds (VOC) concentration in the air.

A sensor material polyvinylacetate – nanostructured carbon composite (PVAc-NCC) was created to detect various VOC. Its working principle is related to the ability of composite matrix to absorb VOC molecules that causes swelling and subsequent increase of composite electrical resistance. When the leak of VOC is removed, the composite relax fully to the initial electrical resistance value.

Experimental results showed that PVAc-NCC cannot determinate lower ethanol concentration than 10000 ppm because the sensor electrical resistance drift was comparable with the sensor response to VOC. To improve the sensitivity of the composite we used several plasticizers (polyethylene glycol (PEG) with low molecular weight (300; 400; 1000; 6000) and di-n-octyl sebacate (DOS)). We compared sensitivity in ethanol vapour of produced sensor materials and evaluated the significance of used plasticizer.

Of all tested composites the largest electrical resistance increase was observed for PVAc-NCC_PEG 300 20%, when exposed to ethanol vapour. That is related to decrease of composite glass transition temperature (T_g) due to addition of PEG 300 20%. The T_g of PVAc-NCC is 42,87⁰C, but for the composite composition with PEG 300 T_g is -63,35⁰C. It is known from the polymer glass transition theory that molecules have a great deal of freedom to move at temperatures well above T_g . Chains are free to take up all the conformations allowed by rotations around single bonds [1].

The possible lower detection threshold (130 ppm) of ethanol vapour has been determined for PVAc-NCC_PEG 300 20% (with thickness 30 μ m). Selectivity of PVAc-NCC_PEG300 20% to polar VOC has been determined as well.

References

1. David I. Bower. An Introduction to Polymer Physics. Cambridge University Press, 2002, p. 209.

Molecular Dynamics 1,4-DHP-Lipid as a Gene Transfection Agent

V. Duka¹, C. Czaplewski², A. Liwo², G. Duburs¹, I. Liepina¹

¹Latvian Institute of Organic Synthesis, Latvia

²University of Gdansk, Poland

e-mail: vita.duka@gmail.com; inta@osi.lv

Self-assembling biomaterials are used to enwrap a gene or drug and deliver through a membrane into a cell. Molecular dynamics (MD, Amber 9.0, f99 force field) of a gene transfection agent 1,1'-{[3,5-bis(dodecyloxycarbonyl)-4-phenyl-1,4-dihydro-pyridin-2,6-diyl] dimethylene} bispyridinium dibromide (1,4-DHP lipid, Fig. 1.) showed that it forms tubular [1] and spherical supramolecular structures, and not planar bilayers. 1,4-DHP lipid tubomicellae is stable in water, but in smaller 1,4-DHP lipid concentrations a classic micellae can split from the tubomicellae, which is in agreement with electron microscopy showing both tubular and round structures. MD shows that the DNA could be bound between two tubular micellae. The 1,4-DHP-lipid aryl rings tend to take tangential position towards the tubular micellae's surface (Fig. 2).



Fig.1 1,4-DHP lipid.

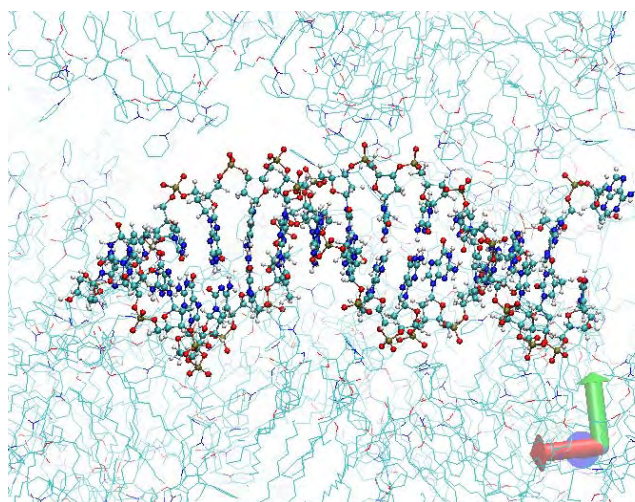


Fig.2 1,4-DHP lipids binding with the DNA

Acknowledgments

Supported by ESF project 2009/0197/1DP /1.1.1.2.0/09/ APIA/VIAA/014, Gdansk Academic Computer Center TASK.

References

- Inta Liepina, Cezary Czaplewski, Adam Liwo, Gunars Duburs. 1,4-DHP-lipid parameters and rod like micellae. *Journal of Biophysical Chemistry*, v. 2, No4, 386-394, 2011.

Investigation of Electric Properties of Nanocomposites in Frequency Domain – Compact Measurement Data Representation

I. Matīss¹, Ē. Pentjušs¹, O. Krievs¹, J. Zicāns¹

¹Institute of Polymer Materials, Riga Technical University, Latvia

e-mail: oskars.krievs@rtu.lv

The paper presents a procedure for mapping large amounts of experimental measurement data in a compact and representable form, preserving information on the properties of the research object for further investigations. The experimental data comprise measurements of the complex dielectric permeability of nanocomposite samples, carried out over frequency range of 100Hz to 15MHz. The raw data are reduced to one of mathematical descriptions of dielectric relaxation – Debye or Havrilaki-Negami. The conformity between experimental and theoretical coherencies is determined by correlation factor. Statistical significance of the experimental data is verified by measurement standard deviation and variation factor.

The Debye model provides a more adequate representation of measurement data and tracks the experimental coherencies of real and imaginary components of dielectric permeability relatively precisely (see Fig.1.). The curves of Havrilaki-Negami model are of explicitly monotonous type – the model is applicable in cases where integral characteristics of the material or its components are of interest.

The implemented dielectric relaxation model provides a possibility to recover the frequency characteristics for any argument value, even extrapolating outside the actual measurement range to some extent.

Acknowledgements

The research was carried out within the project No.2010/0209/2DP/ 2.1.1.1.0/ 10APIA/VIAA/028 financially supported by ERDF.

References

1. Mohan G. R. et al. Dielectric properties of polycrystalline mixed nickel–zinc ferrites, *Materials Letters* 40, 1999, 39–45
2. Matiss, I. Purvinsh A., Measurement of Frequency Dependent Dielectric Properties by the Capacitance Technique, IEEE-ISIE-2006 (IEEE International Symposium on Industrial Electronics), Canada, 2006.

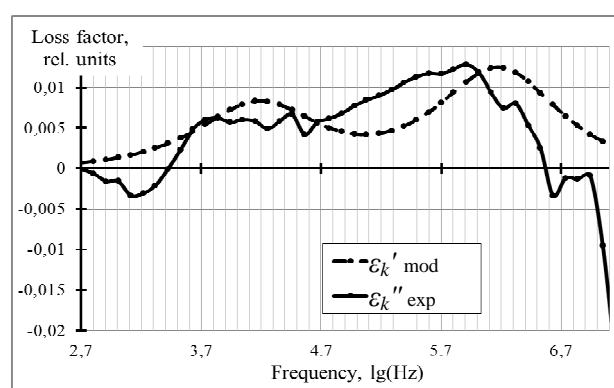


Fig.1. Frequency dependences of dielectric loss factor: $\varepsilon_k' \text{ mod}$ -theoretical data, $\varepsilon_k'' \text{ exp}$ - experimental data

Glycerol Oxidation by Molecular Oxygen in Presence of Novel Supported Platinum Catalysts

S. Čornaja¹, K. Dubencovs¹, V. Serga², L. Kulikova², V. Kampars¹, E. Sproģe¹, O. Stepanova¹,
A. Cvetkovs², S. Žižkuna¹

¹Riga Technical University

²RTU Institute of Inorganic Chemistry, Riga Technical University, Latvia

e-mail: Svetlana@ktf.rtu.lv

Glycerol is a bio-fuel production by-product. This work studies novel supported Pt contained catalyst, prepared by extractive-pyrolytic method [1], activity and selectivity in process of glycerol oxidation in alkaline water solutions. In the process of catalysts preparation the support nature, the time of support dispersion in the precursor solution, drying temperature, temperature and duration of pyrolysis, as well as Pt concentration in the catalyst, were varied. Research revealed that catalysts activity and selectivity depends on catalyst support nature, pyrolysis temperature and duration as well as on Pt concentration in catalyst. The most active catalysts are Pt/AlO(OH), Pt/ZrO₂, Pt/Y₂O₃, Pt/Lu₂O₃ and Pt/Al₂O₃. Depending on the catalyst composition and its synthesis conditions main oxidation products obtained were either glyceric or lactic acids

The highest selectivity by glyceric acid 55-61% with glycerol conversion 85-90% has been achieved by use of 5%Pt/Al₂O₃ catalyst prepared from precursor with concentration 0.4 M, support dispersion time 10 min, drying temperature 80-100 °C and time 10 min, pyrolysis temperature and duration are equal correspondingly 300 °C and 120 min. Glycerol oxidation conditions: c₀(glycerol) = 0.3 M, c₀(NaOH) = 0.7-1.5 M, n(glycerol)/n(Pt) = 210-300, t = 60 °C, P(O₂) = 1 atm, oxidation time is 4-8 hours.

The highest selectivity by lactic acid 63% with glycerol conversion 86% has been achieved by use of 1.25%Pt/Y₂O₃ catalyst prepared from precursor with concentration 0.4 M, support dispersion time 10 min, drying temperature 80-100 °C and time 3 min, pyrolysis temperature and duration are equal correspondingly 400 °C and 5 min. Glycerol oxidation conditions: c₀(glycerol) = 0.3 M, c₀(NaOH) = 1.5 M, n(glycerol)/n(Pt) = 300, t = 60 °C, P(O₂) = 1 atm, oxidation time is 7 hours.

Acknowledgements

This work was supported by the ERAF project Nr. 2DP/2.1.1.1.0/10/APIA/VIAA/087.

References

1. Latvian patent application Nr P-11-174 (23.12.2011).

Cobalt Cementation in Ethanol-Water System: Kinetics and Morphology of Metal Aggregates

C. Larosa¹, P. Nanni¹, A.P. Reverberi²

¹CNR-IENI, Via De Marini 6, 16100 Genova (ITALY)

²DICheP, Department of Chemical Engineering and Process, University of Genova, via Opera Pia 15, 16145 Genova (ITALY)

Cementation has long been recognized as a valid technique to remove undesired elements from solutions in electrodeposition processes [1] or in the recovery of rare metals from various sources [2-3]. A cobalt cementation process in a mixture of ethanol-water solvent at different temperatures is presented. A new theoretical model is proposed taking into account the depletion of the less electropositive metal undergoing solubilization. The kinetics [4-5] of cementation of Cobalt from hit complex are investigated and the relevant activation energy of the reaction suggests the onset of a chemical control regime for all experimental runs. Finally, the cemented phase is chemically characterized by means of energy dispersive spectroscopy and the size distributions of the relevant metal aggregates are determined by means of both dynamic light scattering in solution and atomic force microscopy after drop casting onto a solid substrate.

Reference

1. Bøckman, O.; Østvold, T.; Voyiatzis, G.A.; Papatheodorou, G.N. Raman spectroscopy of cemented cobalt on zinc substrates. *Hydrometallurgy* **2000**, *55*, 93-105.
2. Fabián, M.; Baláž, P.; Briančin, J. Study of the silver ions cementation after mechanical activation of cementator. *Hydrometallurgy* **2009**, *97*, 15-20.
3. Viramontes Gamboa G.; Medina Noyola M.; López Valdivieso A. Fundamental considerations on the mechanisms of silver cementation onto zinc particles in Merrill-Crowe process. *J. Colloid Interf. Sci.* **2005**, *282*, 408-414.
4. Bøckman, O.; Østvold, T. Products formed during cobalt cementation on zinc in zinc sulfate electrolytes. *Hydrometallurgy* **2000**, *54*, 65-78.
5. Younesi, S.R.; Alimadadi, H.; Keshavarz Alamdari, E.; Marashi, S.P.H. Kinetic mechanism of cementation of cadmium ions by zinc powder from

Structure and Zeta-Potential Analysis of Particulate Matter

M. Baitimirova¹, A. Osite¹, J. Katkevich¹, A. Viksna¹

¹University of Latvia, Latvia

e-mail: puma3b@inbox.lv

The particulate matter and smoke has very different content, size and type. The particles of smoke can include pollutants such as heavy metallic elements (Zn, Cu, Fe, Pb etc.). Nowadays the airborne solid particles and smoke can collect fractionating them by size. Fractions of particulate matter can be characterized by physical (size, shape etc.), chemical (components, pollutants etc.) and electrochemical (impedance, zeta-potential etc.) parameters. It allows investigating properties of particulate matter including black carbon. In this research the fractionated collection of particulate matter from Riga city air is continued. Also solid particles of smoke are collected from burning of various combustibles in a laboratory system.

A structure of solid particles of petrol smoke is determined by optical and scanning electron microscope (SEM). The average size of petrol smoke particles is from 1 to 10 μm (Fig. 1). From this it can be concluded - the solid particles of petrol smoke are fractals of Aitken and accumulation mode particles.

Zeta-potential of petrol smoke particles in water [1] is negative for one part of particles (from -10 to -30 mV) and it is positive for other part of particles (from +12 to +30 mV). Such distribution of zeta-potential promotes particles flocculation in petrol smoke. As a result, particles are forming large and heavy. They settle down adhering components of tar to the particle surface. Whereas airborne particulate matter have another electrochemical character. One part of airborne particles have very high negative zeta-potential (from -50 to -150 mV), but other part have very low zeta-potential (from +8 to +9 mV). Particles with such distribution of zeta-potential can overcome tens kilometres of distance by air flow.

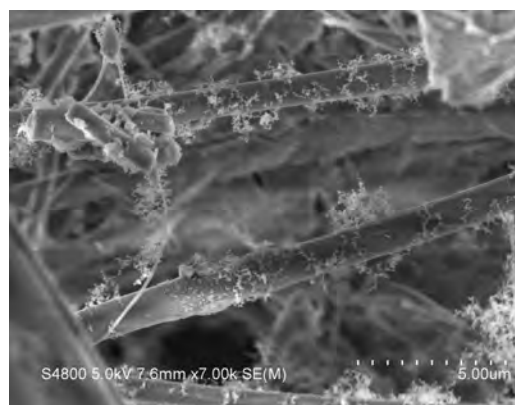


Fig.1. A SEM micrograph of a petrol smoke

References

1. H.-J. Jacobasch, G. Baubock, J. Schurz. Polymer Science. Problems and results of zeta-potential measurements on fibres. Colloid & Polymer Science, Vol. 263, No. 1 (1985)

Quantum Chemical Simulations of Doped TiO₂ Nanotubes for Photocatalytic Hydrogen Generation

O. Lisovski¹, S. Piskunov^{2,3,4}, Yu. Zhukovskii⁴, J. Ozolins¹

¹Faculty of Materials Science and Applied Chemistry, Riga Technical University

²Faculty of Computing, University of Latvia

³Faculty of Physics and Mathematics, University of Latvia

⁴Institute of Solid State Physics, University of Latvia

e-mail: oleg.lisovski@gmail.com

TiO₂ (band gap ~3 eV) is the most attractive photocatalyst proposed for water-splitting applications. To dissociate water and to obtain hydrogen under influence of visible light, the band gap ($\Delta\varepsilon_g$) of efficient photocatalysts must be adjusted into the range of $1.23 < \Delta\varepsilon_g < 2.5$ eV. When comparing with conventional catalysts, titania nanotubes (NTs) possess larger specific surface area and, consequently, have better adsorption capacity and higher photocatalytic activity. Although pristine NTs tend to have larger $\Delta\varepsilon_g$ with respect to the bulk, recent experimental studies suggest that low-dimensional structures of TiO₂ with $\Delta\varepsilon_g > 3.0$ eV are better starting point for doping which leads to the formation of the induced mid-gap states and adjusting the band gap width.

Since the experimental synthesis and characterization of nanostructured materials is quite complicated and expensive procedure, in order to perform reliable band gap engineering of doped and co-doped TiO₂ NTs we propose relatively cheap, but efficient large-scale *ab initio* calculations on the electronic structure. Using hybrid exchange-correlation functional within the density functional theory (DFT) we have calculated parameters of morphology for the energetically stable TiO₂ tubular structure. This nanotube possesses negative strain energy being attractive for doping. We carried out calculations on real band structures of titania nanotubes doped by either light elements (C, N, S – as a substitute for O), or Fe substituting for Ti. Nanotubes containing O vacancies have also been modeled. Based on the results of our simulations we conclude that O vacancies reduce the band gap greatly and shift the band edges far above the required levels. Doping with Fe and C does not induce impurity levels in the band gap able to shift the band edges to required positions. Finally, sulfur doped titania NT with the bottom of conduction bands positioned slightly above normal hydrogen electrode level and the band gap close to 2.5 eV is predicted to be the most suitable catalyst for photocatalytic hydrogen generation under influence of visible light.

Atomic and Electronic Properties of Ni Filament Encapsulated Inside Single-walled Carbon Nanotubes of Different Chiralities

J. Kazerovskis^{1,2}, S. Piskunov^{2,3,4}, Yu.F. Zhukovskii², P.N. Dyachkov⁵, S. Bellucci⁶, M. Utinans¹

¹Faculty of Materials Science and Applied Chemistry, Technical University of Riga, Latvia

²Institute of Solid State Physics, University of Latvia, Riga, Latvia

³Faculty of Computing, University of Latvia

⁴Faculty of Physics and Mathematics, University of Latvia

⁵Kurnakov Institute of General and Inorganic Chemistry, Russian Academy of Sciences, Moscow

⁶National laboratory of Frascati, National institute of nuclear physics, Italy

e-mail: Gio.GmbH@gmail.com

In this study, we consider monoatomic chains of nickel atoms encapsulated into single-walled carbon nanotubes (CNTs) of zigzag-type ($n,0$) and armchair-type (n,n) chiralities with varied n indices. Performing large-scale calculations within the Density Functional Theory (DFT) as implemented in *CRYSTAL-09* code [1] we obtain the equilibrium geometry of single Ni filament inside CNTs. For verification, we compare results of our calculations with those obtained using the DFT formalism of Linear Augmented Cylindrical Waves (LACW) [2]. In all the cases, Ni filament preserves a ferromagnetic ground state. Our calculations show that CNTs with Ni filament exhibit metallic behavior (Fig. 1), even if pristine nanotube is semiconductor (*i.e.*, zz -type, Fig. 2). Therefore, we predict that encapsulation of Ni filament inside CNTs is a way for reliable creation of stable conductive quasi-one-dimensional hybrid nanostructures.

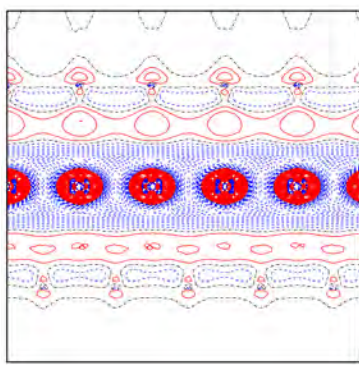


Fig. 3. Charge redistribution inside Ni-CNT(5,5) hybrid nanostructure.

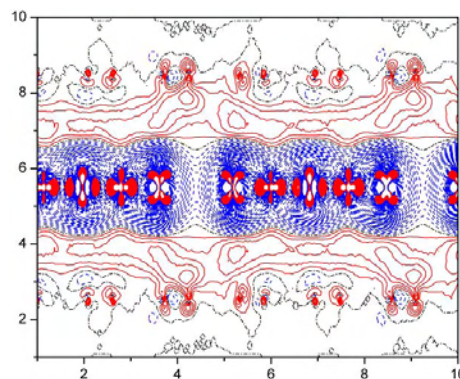


Fig. 2. Charge redistribution inside Ni-CNT(10,0) hybrid nanostructure.

Ni-*ac*-CNTs are found to be a more stable, with a stronger interatomic Ni-C bonding than Ni-*zz*-CNTs, due to a smaller mismatch in the former system. The most preferable for Ni filament insertion are found to be CNT(5,5) and CNT(10,0).

References

1. R. Dovesi, V.R. Saunders, C. Roetti, *et al.* *CRYSTAL-2009 User Manual*. Turin: University of Torino (2009).
2. P.N. Dyachkov and D.V. Makaev, *Phys. Rev. B* 76 (2007) 195411.

Quantum Chemical Simulations of Doped SrTiO₃ Nanotubes for Application in Photocatalytic Reactions

J. Begens¹, S. Piskunov^{2,3,4}, Yu.F. Zhukovskii², E. Spohr⁵, M. Utinans¹

¹Faculty of Material Science and Applied Chemistry, Riga Technical University

²Institute of Solid State Physics, University of Latvia, Riga, Latvia

³Faculty of Computing, University of Latvia

⁴Faculty of Physics and Mathematics, University of Latvia

⁵Department of Theoretical Chemistry, University of Duisburg-Essen, Germany

e-mail: jevgenijs.begens@gmail.com

SrTiO₃ nanotubes (NTs) have attracted considerable recent interest because of their unique physical properties and promising novel functionalities compared with bulk materials [1]. Quantum confinement effects typical for nano-sized materials lead to a widening of the energy band gap of single-walled SrTiO₃-NTs (~6.1 eV) as compared to the bulk (~3.6 eV), and, thus, makes them attractive for further band gap engineering through doping. Induced mid-gap states may enhance the reactivity of high-performance photo-electrochemical electrodes under influence of visible light. Therefore, photocatalysts made of doped SrTiO₃-NTs are potential candidates to be used in future dye-sensitized solar cells or for photocatalytic hydrogen production.

Analyzing results of calculations performed using the *CRYSTAL-09* code based on the hybrid density functional theory within the LCAO approach [2], we predict that the most energetically favorable single-walled SrTiO₃-NTs with negative strain energy can be folded from SrTiO₃ (110) nanosheets of rectangular morphology [3]. Because SrTiO₃ is a model material for a number of quasi-cubic perovskites, we suggest that NTs with the rectangular morphology may be produced from other types of ABO₃ perovskites too. The increase of the Ti-O bond covalency in the outer nanotube shell may lead to an enhancement of adsorption properties. This would imply that nanotubes can be used in gas-sensing devices. The band gap structures of the SrTiO₃-NTs doped by C, N, S, and Fe, as well as of NTs containing oxygen vacancies are thoroughly discussed in our presentation.

References

1. R.A. Evarestov, A.V. Bandura, IOP Conf. Ser.: *Mater. Sci. Engineering* **23** (2011) 012013
2. R. Dovesi, V.R. Saunders, C. Roetti, *et al. CRYSTAL User Manual*: University of Torino: Turin (2009).
3. S. Piskunov, E. Spohr, *J. Phys. Chem. Lett.* **2** (2011) 2566.

Parametric Simulation of CNT *dc*- and *ac*-Conductivity for Various Nanotube Chiralities

Y. Shunin^{1,2}, V. Gopeyenko², P. Dyachkov³, N. Burlutskaya², Yu. Zhukovskii¹, S. Bellucci⁴

¹Institute of Solid State Physics, University of Latvia, Latvia

²Information Systems Management Institute, Latvia

³Kurnakov Institute of General and Inorganic Chemistry, Russian Academy of Sciences, Moscow

⁴INFN-Laboratori Nazionali Di Frascati, Frascati, Italy

e-mail: viktor.gopejenko@isma.lv

Usually two basic electron conductivity mechanisms in CNT-based structures are considered. The ballistic mechanism is engaged in electron transport within CNTs while the collisional mechanism is characteristic of CNT-substrate interconnects. Hence the general conductivity σ_{gen} is evaluated as follows: $\frac{1}{\sigma_{gen}} = \frac{1}{\sigma_{coll}} + \frac{1}{\sigma_{bal}}$. For pure CNTs, we clearly observe that $\sigma_{bal} \gg \sigma_{coll}$. In the framework of multiple scattering theory formalism and effective medium approximation, we can evaluate both factors of conductivity. A special question for modeling is the dependence of both conductivity mechanisms on the electron free path length which, in the case of pure CNT, is usually considered as the nanotube length. The case of CNT-Metal interconnects has been parametrically investigated within the recent three years (e.g., [1,2]). We present here the results of numerical research of *dc*- and *ac*-conductivity for pure CNTs of various chiralities using multiple scattering theory principles and Kubo-Greenwood formula [1]:

$$\sigma_E(\omega) = \frac{2\pi e^2 \hbar^2 \Omega}{m^2 \omega} \int_{E_F - \hbar\omega}^{E_F} [f(E) - f(E + \hbar\omega)] |D_E|^2 \rho(E) \rho(E + \hbar\omega) dE, \text{ where } \omega \text{ is the real frequency parameter}$$

of Fourier transform for the time-dependent functions, $f(E)$ Fermi-Dirac distribution function, $D_{E,E'} = \int_{\Omega} \Psi_{E'}^* \nabla \Psi_E dr$, $\Psi_{E(\mathbf{K})}$ the wave function of the system, \mathbf{K} the complex wave vector of effective medium and $\rho(E)$ the electronic density of states [1,3]. The analysis of Kubo-Greenwood's conditions in respect of CNT morphology is also present taking into account *dc* ($\omega = 0$), *ac* ($\omega \neq 0$) regimes and the temperature factor of electron transport. Parametrical numerical simulations of conductivity have been carried out for zig-zag ($m,0$), arm-chair (m,m) and chiral (m,n) CNTs.

References

1. Yu.N. Shunin, Yu.F. Zhukovskii, S. Bellucci, *Computer Modelling & New Technologies* 12, No.2 66 (2008).
2. Yu.N. Shunin, Yu.F. Zhukovskii, N. Burlutskaya, S. Bellucci, *Central Eur. J. Phys* 9, No.2, 519 (2011).
3. P. N. D'yachkov, D. Z. Kutlubaev, D. V. Makaev, *Phys. Rev. B* 82, 035426 (2010).

Cluster Embedding Method for Quantum-Chemical Simulation of Nanodevices

E.K. Shidlovskaya^{1,2}

¹Information Systems Management Institute, Latvia

²Institute of Chemical Physics, University of Latvia, Latvia

e-mail: shidlovsk@inbox.lv

When we theoretically describe nanodevice we have to treat the whole quantum system as two subsystems: small finite fragment of the system containing nanodevice (cluster) and the rest of the system containing electrodes. Problem "cluster in the field of the rest of system" is successfully solved in the frameworks of embedded molecular cluster (EMC) model [1] with *orthogonal* wave functions. We have developed modified EMC model [2] treating cluster embedding problem in the frameworks of one-electron approximation with *non-orthogonal* wave functions.

Applicability of cluster embedding method with non-orthogonal wave functions for theoretical study of processes in nanodevices is studied. Processes in nanodevices are treated in the frameworks of time-dependent DFT (TDDFT) and quantum transport theory [3]. We demonstrate [4] that our cluster embedding method is compatible with DFT Kohn-Sham method. Therefore we may use TDDFT-based quantum transport theory if electron transitions are described correctly. For this purpose we need occupied and vacant cluster states of the same localization. Our initial embedding equations [2] are established to give localized in the cluster region occupied states and delocalized vacant ones [5]. To get the same localization degree for the both states, modified equations are proposed [5]. We conclude that our embedding scheme with modified cluster embedding equations may be combined with quantum transport theory based on TDDFT. We demonstrate that approach for electric current calculation [3] developed for orthogonal wave functions may be applied for non-orthogonal wave functions [4] if we transform initial equations assuming that overlaps are small ($S^2 \ll S$).

References

1. L.N. Kantorovich, *J. Phys. C: Solid State Phys.* **21**, 5041 (1988).
2. E.K. Shidlovskaya, *Int. J. Quantum Chem.* **89**, 349 (2002).
3. S. Kurth, G. Stefanucci, C.-O. Almbladh, A. Rubio, and E.K.U. Gross, doi: 10.1103/PhysRevB.72.035308
4. E.K. Shidlovskaya, *NATO Science for peace and security Series – B: Physics and Biophysics*, Springer, 2012.
5. E.K. Shidlovskaya, *Computer Modelling and New Technologies* **10**, No 4, 17 (2006).

Finite Temperature Effects in Single-Parameter Non-Adiabatic Electron Pumps

P. Nazarovs¹, V. Kashcheyevs^{1, 2, 3}

¹Faculty of Computing, University of Latvia, Latvia

²Faculty of Physics and Mathematics, University of Latvia, Latvia

³Institute of Solid State Physics, University of Latvia, Latvia

e-mail: nazarow@gmail.com

Quantized charge pumping is transfer of an integer number of electrons per cycle through a periodically modulated nano electronic structure. It finds applications both in fundamental and applied areas of physics: metrology, quantum information, single-electronics, quantum dot spectroscopy etc. [1]. A significant goal for high-accuracy quantum pumps is the realization of new current standard which is based on electron counting. Thus theoretical understanding of charge dynamics and underlying processes in electron pumps are essential for improvement of experimental devices [2].

We develop a systematic generalization of the kinetics equations method [3] for strongly non-adiabatic charging of quantum dots [4] that takes place single-parameter charge pumps [1, 4]. Our primary goal is to connect the microscopic parameters of a quantum dot model (such as level spacing, charging energy and tunneling rates) to the experimentally measurable quantities (primarily the average pumped current).

We explore the case of a multi-level quantum dot in good thermal contact with environment and separate fast (energy) and slow (electron number) variables. The resulting set of kinetic equations for the probability distribution of the number of captured electrons is formulated for the constant interaction model of Coulomb interactions on the dot. We present analytical expressions for kinetic equations' coefficients in and develop numerical solutions that classify of possible temperature influence scenarios on the I-V characteristics of single-gate non-adiabatic quantum pumps.

References:

1. K. Nishiguchi, A. Fujiwara, et al., Appl. Phys. Lett. 88, 183101 (2006).
2. M. D. Blumenthal et al., Nature Physics 3, 343 (2007)
3. C.W.J. Beenakker, Phys. Rev. B 44, 1646 (1991)
4. B. Kaestner, V. Kashcheyevs, et al., Phys. Rev. B 77, 153301 (2008);

Modeling of Non-Adiabatic Quantum Pumping

J. Timoshenko^{1,3}, V. Kashcheyevs^{1,2,3}

¹Faculty of Computing, University of Latvia, Latvia

²Faculty of Physics and Mathematics, University of Latvia, Latvia

³Institute of Solid State Physics, University of Latvia, Latvia

e-mail: janis.timoshenko@gmail.com

Quantum pumps are electrostatically controlled nano-sized current sources that produce an integer number of electrons per cycle and therefore can be used, for example, as current standards. A common setup for a quantum pump consists of a quantum dot, attached to leads and separated from them by potential barriers that are controlled by time-dependent voltages applied to gate electrodes [1].

The loading and unloading of the quantum dot are essentially time-dependent and often non-adiabatic processes; therefore an appropriate mathematical description of charge transfer through the quantum pump is a challenging task.

In this work we present a theory for the description of the non-adiabatic loading of a quantum dot with one energy level. Using non-equilibrium Green function approach [2] we calculate the time-dependence of the average number of electrons on the dot as well as the fluctuations of this number. We are able to isolate the essential parameters that affect the charge transfer in the quantum pump (Fig. 1). The presented model can be used to analyze experimentally obtained volt-ampere characteristics of real quantum pumps and to enhance the precision of currently available devices.

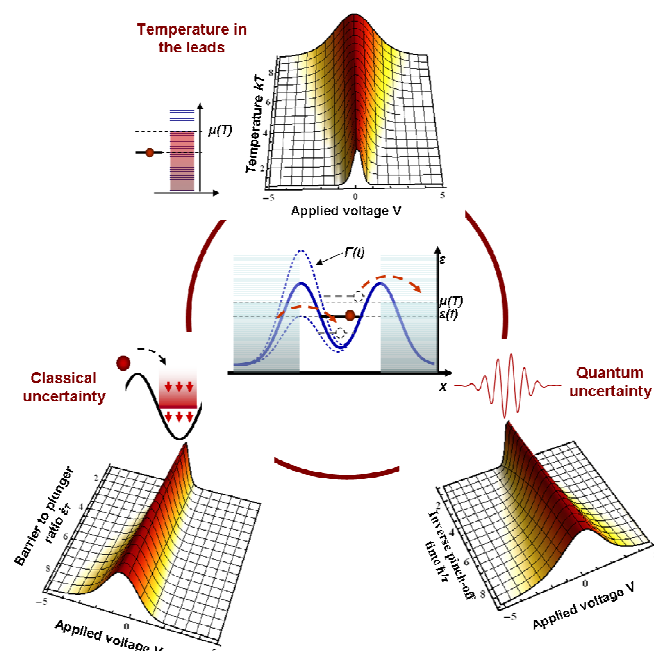


Fig.1 Schematic depiction of our model of non-adiabatic quantum pump (*in the centre*) and of three basic factors that determine the fluctuations of the pumped current: **temperature in the leads**, **inverse pinch-off time** (speed of barrier closing) and the **barrier-to-plunger ratio** (frequency-independent measure for the speed of changes of the energy on dot). In the 3D plots the dependencies of the occupation fluctuations (second moments of the distribution of electron number) on applied control voltage and the dominating parameters are shown.

References

1. V. Kashcheyevs, B. Kaestner, Phys. Rev. Lett. **104**, 186805 (2010).
2. A. Jauho, N. Wingreen, Y. Meir, Phys. Rev. B **50**, 5528 (1994)

Analysis of Void Superlattice Formation in CaF₂

P. Merzlyakov¹, G. Zvejnieks¹, V.N. Kuzovkov¹, E.A. Kotomin¹, K.D. Li², L.M. Wang²

¹Institute of Solid State Physics, University of Latvia,

²Dept. Materials Science & Engineering, and Department of Nuclear Engineering & Radiological Sciences, University of Michigan, USA

e-mail: pavel.merzlyakov@gmail.com

Irradiation of many metallic and insulating solids with energetic particles, such as heavy ions, neutrons, electrons, can result in a formation of ordered structures including periodic defect walls, bubble lattices, void lattices and periodic compositions in alloys [1-3]. The particular ordered structures arising in such open dissipative systems far from equilibrium depend on a type, energy, and flux of the energetic particles as well on the temperature. It was noticed [3] that despite the difference in the appearance, a similar underlying mechanism may be invoked to explain the selforganization behavior of these structures.

In this work, we quantitatively analyze the experimental results of halogen gas void formation in an electron-irradiated CaF₂. Two filters based on different assumptions are developed that digitalize the TEM micrographs and determine both void cluster distribution and characteristic void spacing (superlattice) depending on irradiation dose. Both approaches demonstrate that superlattice spacing increases with irradiation dose. Moreover, we propose a microscopic model for interstitial and vacancy creation, diffusion and recombination that uses pair interactions between reactants. The kinetic Monte Carlo simulations performed in 3D demonstrate that the model could describe the initial stage of experimentally observed void lattice formation.

Acknowledgements

P.M. and G.Z. greatly acknowledge the financial support of ESF project 2009/0202/1DP/1.1.1.2.0/09/APIA/VIAA/141

References

1. W. Jaeger and H. Trinkaus, J. Nucl. Mater. 205, 394 (1993)
2. A. M. Stoneham, Rep. Prog. Phys. 70, 1055 (2007)
3. H.C. Yu and W. Lu, Acta Mater. 53, 1799 (2005)

Atomistic Theory of Mesoscopic Pattern Formation Induced by Bimolecular Surface Reactions between Oppositely Charged Molecules

G. Zvejnieks, V.N. Kuzovkov, E.A. Kotomin

Institute of Solid State Physics, University of Latvia, Latvia

e-mail: guntars@latnet.lv

The kinetics of mesoscopic pattern formation is studied for a reversible $A + B \leftrightarrow 0$ reaction between mobile oppositely charged molecules at the interface [1]. Using formalism of the joint correlation functions, non-equilibrium charge screening and reverse Monte Carlo methods [2], it is shown that labyrinth-like percolation structure, Fig. 1, can be induced by even moderate reaction

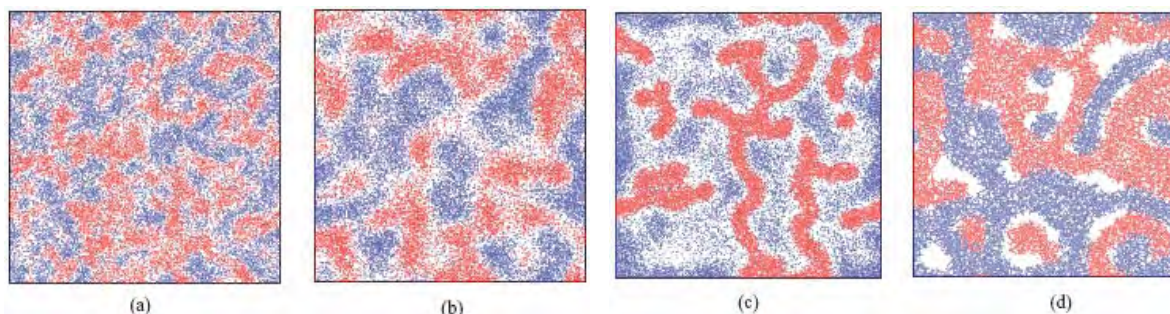


Fig.1 Calculated labyrinth-like structures (Reverse Monte Carlo snapshots) in the absence of Coulomb interactions. Reactants A are shown in red. B in blue.

rate. The driving force for the formation of principally nonsteady-state percolating structure is associated with both (i) permanently growing segregation of dissimilar reactants and (ii) aggregation of similar reactants into mesoscopic size domains. A role of short-range and long-range reactant interactions in pattern formation is discussed.

References

1. V.N. Kuzovkov, E.A. Kotomin, G. Zvejnieks, J. Chem. Phys. **135**, 224503 (2011)
2. V.N. Kuzovkov, E.A. Kotomin, G. Zvejnieks, M. Olvera de la Cruz, Phys. Rev. E **82**, 021602 (2010)

Numerical Investigation of the Stability of Photoinduced Microconvective Structures in Ferrofluid Layers

D. Zablotzky¹, E. Blums¹

¹Institute of Physics, University of Latvia, Latvia

e-mail: dmitrijs.zablockis@gmail.com

Ferrofluids are colloidal suspensions of magnetic nanoparticles in liquid carrier. Apart from the superparamagnetic properties of the dispersed phase, the ferrocolloid exhibits strong Soret effect under the applied temperature gradient.

We consider a periodic concentration grating induced through photoabsorption and thermodiffusion in a thin layer of ferrofluid by interfering laser beams ([1, 2]) under the action of externally applied uniform magnetic field. The demagnetizing fields created by the complex interaction of the nonuniform perturbation of concentration and the external magnetic field cause the appearance of the magnetic force, which in turn promotes microconvection.

We describe a stationary system of periodic convective rolls emerging within the photoinduced concentration grating under the action of the external magnetic field. The parasitic microconvection attempts to either suppress or enhance the induced grating depending on the orientation of the applied field. We investigate the stability of the stationary convective-diffusive structures and determine the critical control parameter and the wave-number of the critical perturbation of the instability of the primary system of periodic convective rolls in the first approximation via a combined crossroll-square type perturbation.

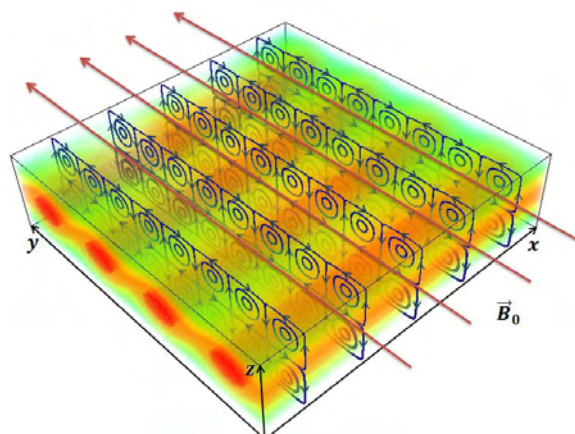


Fig.1 Photoinduced convective rolls in a layer of ferrofluid under laterally applied magnetic field.

References

1. J. C. Bacri, A. Cebers, A. Bourdon, G. Demouchy, B. M. Heegaard, B. Kashevsky, and R. Perzynski, Phys. Rev. E, 52, pp. 3936-3942, 1995.
2. J. Lenglet, A. Bourdon, J.-C. Bacri, G. Demouchy, Phys. Rev. E, 65, pp. 3936-3942, 2002.

The Non-equilibrium Charge Screening Effects in Diffusion-Driven Systems

V. Kuzovkov¹, E. Kotomin¹, M.O. de la Cruz²

¹Institute of Solid State Physics, University of Latvia, Latvia

²Northwestern University, Evanston IL 60208, USA

e-mail: kuzovkov@latnet.lv

The effects of non-equilibrium charge screening in mixtures of oppositely charged interacting molecules on surfaces are analyzed in a closed system. The dynamics of charge screening and the strong deviation from the standard Debye-Hückel theory are demonstrated via a new formalism based on computing radial distribution functions suited for analyzing both short-range and long-range spacial ordering effects. At long distances the inhomogeneous molecular distribution is limited by diffusion, whereas at short distances (of the order of several coordination spheres) by a balance of short-range (Lennard-Jones) and long-range (Coulomb) interactions. The non-equilibrium charge screening effects in transient pattern formation are further quantified. It is demonstrated that the use of screened potentials, in the spirit of the Debye-Hückel theory, leads to qualitatively incorrect results [1].

References

1. V.N. Kuzovkov, E.A. Kotomin, and M. Olvera de la Cruz, *J. Chem. Phys.* **135**, 034702 (2011)

The Anderson Localization Problem, the Fermi–Pasta–Ulam Paradox and the Generalized Diffusion Approach

V. Kuzovkov

Institute of Solid State Physics, University of Latvia, Latvia

e-mail: kuzovkov@latnet.lv

Half a century ago two celebrated papers were published temporally close to each other which gave birth to two fundamental directions of theoretical physics. In 1955 the Fermi-Pasta-Ulam (FPU) paradox was formulated which suggested the nonequipartition of energy among normal modes of an anharmonic atomic chain. This phenomenon is closely connected with the problems of ergodicity, integrability, chaos and stability of motion. A few years later, in 1958, Anderson suggested the possibility of electron localization (AL) in a random system, provided that the disorder is sufficiently large. This idea is one of the foundations for the understanding the electronic properties of disordered systems.

Our purpose is to establish a close connection between the two fundamental problems [1]. That is, the AL is nothing else but the FPU effect in a modified dynamical system with interacting normal modes. Besides, the delocalized states in the AL problem are analogous to the stable quasi-periodic motion (recurrence in the FPU problem) and, respectively, the localized states are similar to the thermalization (motion instability) in the FPU. Our FPU modification includes:

- (i) non-trivial change of the mode ensemble. In the FPU without interactions all normal modes are stable. In contrast, in the AL both stable and unstable modes also exist.
- (ii) a modified mode interaction: the stochasticity in the AL is introduced directly, through random forces linear in coordinates and rather indirectly, through nonlinear terms in the dynamical equations.

References

1. V.N. Kuzovkov, Phys. Scripta **84**, 065002 (2011)

Light Induced Self Assembly of Switchable Colloids

P. Jha¹, V. Kuzovkov², B. Grzybowski¹, M.O. de la Cruz¹

¹Northwestern University, Evanston IL 60208, USA

²Institute of Solid State Physics, University of Latvia, Latvia

e-mail: kuzovkov@latnet.lv

Dynamic self-assembly aims at producing ordered structures in otherwise disordered materials by controlled energy influx into the system. This strategy has been widely successful in the design of nanoscale components - where the conventional mechanical design methods cannot be used. From a theoretical perspective, dynamic self-assembly processes pose several difficulties because of their intrinsic non-equilibrium nature, since the well-established toolset of equilibrium thermodynamics cannot be applied. Non-equilibrium thermodynamics is a field in its infancy, and one is often faced with computational challenges associated with tracking the dynamics of infinitely many particles, that are needed to explain the mesoscale behavior of systems. We are working on a novel method of kinetic Monte Carlo simulations, applied to the study of aggregation phenomenon in a model system of colloidal particles under periodic light forcing [1].

References

1. P.K. Jha, V.N. Kuzovkov, B.A. Grzybowski, and M. Olvera de la Cruz, *Soft Matter* **8**, 227 (2012)

Institute of Physics, University of Tartu in Baltic Sea Region Cooperation Network Technet_nano – New Challenges for Academia and Industry

T. Plank, M. Kirm

Institute of Physics, University of Tartu, Estonia

e-mail: toomas.plank@ut.ee

In all countries public research institutions offer high-level and expensive innovation- and development resources in the field of micro- and nanotechnology: scientific competence centers and clean rooms. However, the potential customers, including small and medium sized enterprises (SME), are not fully aware about those possibilities. Even more, the potentially suitable clean room might situate not in the same but in the neighboring country.

To address these problems, a Baltic Sea Region (BSR) project [1] “Technet_nano – Transnational network of public clean rooms and research facilities in nanotechnology making accessible innovation resources and services to SMEs in the BSR” – was launched. The main goals of the project are: to create a transnational cooperation network of research institutions and developers in the field of micro- and nanotechnology; to give the SMEs and public bodies a cross regional access to nanotechnology facilities in the whole BSR; to communicate the SMEs and public community about the innovation potential of micro- and nanotechnology. Twelve partners from Denmark, Estonia, Germany (3), Latvia, Lithuania (3), Poland and Sweden (2) participate in this project funded by the BSR programme [1].

Why Estonia participates in the project? The corresponding nanotechnology investigation areas already exist in Estonia or are in the stage of active development. The competent research staff working at Tartu University and in Tallinn University of Technology contributes to the field of nanoscience. Knowledge based Estonian enterprises have reached the stage that clean room technologies are needed to unlock their full innovation potential and to develop advanced products and technologies.

At late 2011, the construction of brand-new clean room facility was finalised at premises of Tartu Science Park [2]. At the moment, Nanotechnology Competence Center and Institute of Physics are in the process of furnishing the clean room. In year 2014 is scheduled an opening of a second clean room in Tartu, in new building of Institute of Physics.

References

1. The Baltic Sea Region Programme 2007-2013 <http://eu.baltic.net/>
2. Tartu Science Park <http://www.teaduspark.ee/en>

Magnetic and Electric Field Effects on the Growth of Ferrite Films in Spray Pyrolysis Process

A. Knoks¹, I. Dirba², A. Sutka³, M. Majorovs⁴, J. Kleperis², G. Mezinskis³

¹Faculty of Physics and Mathematics, University of Latvia, Latvia

²Institute of Solid State Physics, University of Latvia, Latvia

³Institute of Silicate Materials, Riga Technical University, Latvia

⁴Institute of Physics, University of Latvia, Latvia

e-mail: ainars.knoks@gmail.com; kleperis@latnet.lv

Functionalized magnetic nanoparticles are technologically important materials with a wide range of applications, such as magnetic storage and microwave devices, gas sensing devices, for biorecognition and medical diagnostics. Nanocrystalline zinc ferrite is also of considerable interest in both research and technological fields due to its unique magnetic properties due to the dominant role of the surface magnetic ions that differ substantially from their bulk counterparts. Spray pyrolysis method make it possible to change the cation distribution and crystallite size of mixed metal ferrite thin film coatings, affecting their magnetic and catalytic properties.

Experimental setup is made in our work to investigate the influence of magnetic and electric field on spray pyrolysis thin film growth process. The structure, morphology, magnetic and optical properties of different thin ZnFe_2O_4 films are investigated with X-ray diffractometer, X-ray fluorescence (XRF) spectrometer, Raman scattering spectrometer, SEM and optical microscopes, magnetic susceptibility stand, spectrophotometer. The growth mechanism of nano-grains on hot substrate includes the nonequilibrium process which enables the formation of a variety of metastable phases (Zn and Fe interstitials, changing coordination number of oxygen around the cation) what lead to a random distribution of Zn and Fe ions on the tetragonal (A) and octahedral (B) crystal sites.

Acknowledgements

Authors (ID and AS) acknowledge ESF for the research scholarship. JK acknowledge support from National Research Program in Energy&Environment for financial support.

Light Sensitivity Enchase of TiO₂ Thin Films with Ferrite Nanoparticles Using Multi-source Spray Pyrolysis Method

L. Grinberga¹, I. Liepina², A. Sutka³, J. Kleperis¹, G. Bajars¹, G. Mezinskis³

¹Institute of Solid State Physics, University of Latvia, Latvia;

²Faculty of Chemistry, University of Latvia, Latvia;

³Institute of Silicate Materials, Riga Technical University, Latvia

e-mail: kleperis@latnet.lv

Energy crisis is the main stimulus for the design of structurally organized and functionally integrated artificial nanomaterial systems capable of harvesting solar energy. Titanium dioxide (TiO₂) as environmentally friendly and photo-catalytic material is attractive for numerous technological applications: gas sensors, pigments in foodstuffs, paints, cosmetics, in dye solar cells etc. The absorption edge of TiO₂ is in the blue part of visible light; therefore efficiency to solar light is low. ZnFe₂O₄ is another catalyst with a relatively small band gap (1.9 eV), which is used as co-catalyst to shift the TiO₂ absorption edge to visible light region of the spectrum, and simultaneously an effective photocatalyst due to its capability of utilizing visible light and good photochemical stability [1].

ZnFe₂O₄ nanoparticles obtained by auto-combustion method [2] can be used to synthesize TiO₂/ZnFe₂O₄ composites. In our work a spray pyrolysis method was used to obtain well-crystallized TiO₂/ZnFe₂O₄ thin films on ITO coated glass substrates heated above 350°C. We used two spray guns to obtain multi-layer TiO₂/ZnFe₂O₄ thin film structures. Optical properties and photo-activity of multilayer structures were measured.

Acknowledgements

LG acknowledges European Social Fund project Nr. 2009/0202/1DP/ 1.1.1.2.0/09/APIA/VIAA/141 and other authors acknowledge National Research Program in Energy&Environment for financial support.

References

1. S. Padikkaparambi, Y. Zahira, S. Viswanathan et al, Internat. Journal of Photoenergy, **20**, 19 pages (2012).
2. A. Šutka, G. Mežinskis, A. Plūdonis, S. Lagzdina, Power Engineering, **56**, 254-259 (2010).

Preparation and Photoactivity of Electrophoretic TiO₂ Coating Films

I. Liepina, G. Bajars, J. Gabrusenoks, L. Grinberga, J. Kleperis, A. Lūsis

Institute of Solid State Physics, University of Latvia, Latvia

e-mail: liepina.ineta@gmail.com

Titanium dioxide (TiO₂) is considered as a good photocatalyst for hydrogen generation due to its excellent resistance to chemical and photochemical corrosion in aggressive aqueous environments. It is also less expensive than other photo-sensitive materials. Traditionally, the photoactive coatings are deposited by sol-gel, spin coating, chemical vapor and sputter deposition methods which are suitable for flat substrates. For coating of irregular conductive surfaces the electrochemical methods are most eligible. The advantages of electrophoresis over other coating methods are the homogeneity of deposition for complex shapes, reduction of material usage and high production rates, low contamination level and negligible initial capital investment, as well as easy transfer from the research laboratory to industry [1].

In this paper TiO₂ thin films were prepared by sol-electrophoretic process on various substrates – Cu, Ti, Pt and In₂O₃. The as-deposited thin films were annealed at 500 °C for 2 h to increase their crystallinity. Obtained TiO₂ thin films were characterized by phase composition, morphology and their microstructures using X-ray diffraction, Raman spectroscopy, as well as scanning electron microscopy. Photoactivity measurements were carried out in two electrode cell as described in [2]. The possible correlations between the photoactivity and various parameters such as substrate material, preparation method, structural properties and thickness of thin films are discussed. The use of electrophoretic deposition enables to modify physical characteristics of TiO₂ films such as film grain size and roughness is demonstrated.

Acknowledgements

LG thanks European Social Fund project Nr. 2009/0202/1DP/1.1.1.2.0/09/APIA/VIAA/141 and other authors thanks European Regional Development Fund project No.2010/0243/2DP/2.1.1.1.0/10/APIA/VIAA/156 for financial support.

References

1. A. Abdel Aal, M. A. Barakat and R. M. Mohamed, Applied Surface Science **254**, 4577 (2008)
2. J. Linitis, A. Kalis, L. Grinberga and J. Kleperis, IOP Conf. Series: Materials Science and Engineering **23** (2011) 012010

Structural Studies of Titanium Oxide after Thermal Treatment

I. Narkevica¹, K. Rubenis¹, N. Borodajenko¹, J. Ozolins¹, L. Berzina-Cimdina¹, D. Jakovlevs¹,
N. Mironova-Ulmane², I. Sildos³

¹Institute of General Chemical Engineering, Riga Technical University, Riga, Latvia

²Institute of Solid State Physics, University of Latvia, Riga, Latvia

³Institute of Physics, University of Tartu, Estonia

e-mail: inga.narkevica@rtu.lv

The present work describes the results of investigation of structure TiO₂ depending on temperature and thermal treatment conditions. The structural characteristics of the samples were evaluated using X-ray diffraction, SEM and Raman spectroscopy. Cylindrical-shaped TiO₂ ceramic specimens were prepared from plastic TiO₂ ceramic mass by extrusion. Plastic ceramic mass was obtained by mixing the required components (TiO₂ (anatase) powder, distilled H₂O, binder and oil). Dried samples were sintered in air followed by thermal treatment in high vacuum conditions (2×10^{-3} Pa). XRD patterns of all samples treated in vacuum, showed the presence of rutile crystalline structure. To compare morphology of the raw materials and obtained samples SEM was used. Raman spectra were measured using Renishaw inVia micro-Raman spectrometer equipped with argon laser (514.5 nm, max cw power $P_{ex}=10$ mW). The spectral signal was dispersed by the 2400 grooves/mm grating onto Peltier-cooled (-60°C) CCD detector. Raman spectrum for anatase at room temperature consists of following allowed bands 144 cm⁻¹, 197 cm⁻¹, 399 cm⁻¹(B_{1g}), 513 cm⁻¹(A_{1g}), 519 cm⁻¹(B_{1g}), and 639 cm⁻¹. The Raman spectrum of rutile, exhibited dominant peaks at 140, 235, 446, 610 and 820 cm⁻¹ after thermal treatment in air. But Raman spectra of rutile after vacuum thermal treatment have additional bands. The origin of these additional bands will be discussed.

Acknowledgements

This work has been supported by the European Regional Development Fund within the project “Development of innovative water processing technology using nanostructured ceramic“, No. 2010/0257/2DP/2.1.1.1.0/10/APIA/VIAA/012.

Hydrogen Adsorption in Zeolite Studied with Sievert and Thermogravimetric Methods

P. Lesnicenoks¹, A. Sivars², L. Grinberga², J. Kleperis²

¹Faculty of Materials Science and Applied Chemistry, Riga Technical University, Latvia

²Institute of Solid State Physics, University of Latvia, Latvia

e-mail: peteris.lesnicenoks@gmail.com; kleperis@latnet.lv

The sample camera of thermogravimetric analyzer Shimadzu DTG - 60/60H may be considered as almost sealed container; also sample chamber of Sievert type adsorption/desorption analyzer PCTPro-2000 is container with constant volume. Temperature is changed in both analyzers, but hydrogen is applied at constant pressure in thermogravimetric analyzer and at high pressure in PCTPro-200. Heating of a gas in a closed constant-volume container is an isochoric process where the system does no work and all the energy added as the heat or pressure remains in the system as an increase in internal energy only. Thermogravimetric analyzer used to study hydrogen adsorption in zeolite was adapted to two gases (Ar and H₂) through the gas flow system. Next setup of experiments was performed: 1) heating to 200 (300) °C in argon atmosphere at the speed 10 deg/min, 2) cooling down in automatic mode to room temperature in hydrogen atmosphere. In PCTPro-2000 hydrogen adsorption/desorption in zeolite was measured at different pressures (1-10 bar) and temperatures (RT-200 °C). The applicability of both methods was tested on palladium powder reference sample. It is known that palladium metal absorbs hydrogen at given temperature in exothermic reaction and palladium hydride PH_{0.7-0.8} forms, which was fully observed in our experiments for both analyzers.

There are a lot of controversial reports about applicability of zeolite as appropriate material for hydrogen storage. We have shown that natural zeolite can adsorb hydrogen up to 4 wt% of zeolite at room temperature. Zeolite samples were prepared from natural clinoptilolite (Ukraine), supplied as a coarse, medium and fine powder material. Activation of the samples was carried out in ion-exchange process by soaking zeolite powder in the solution, and in pyrolysis process, coating palladium nanoparticles on zeolite powder particles.

Acknowledgements

Authors acknowledge financial support of ERDF project Nr. 2010/0188/2DP/2.1.1.1.0/10/APIA/ VIAA/031.

Threshold Character of Temperatures on Hydrogen Desorption from the Mg-V Composite

I.M. Neklyudov, O.M. Morozov, V.G. Kulish, V.I. Zhurba, A.G. Galitskiy, N.S. Lomino,

V.D. Ovcharenko, A.S. Kuprin, E.N. Reshetnyak

National Science Center "Kharkov Institute of Physics and Technology", Kharkov, Ukraine

e-mail: morozov@kipt.kharkov.ua

Alloys based on magnesium are promising in the view of present-day requirements to the low-cost metal-hydride hydrogen storage systems. However, the use of these alloys presents some difficulties, e.g. a high temperature (between 500 and 600 K) during hydrogen desorption from the alloys.

In our opinion an attention should be given to composite materials which have a low solubility or do not interact with composite components at all. According to the phase diagram of the Mg-V system there is no compounds of these components.

The plasma evaporation-sputtering method was used to manufacture composite materials of the Mg-V system. The ion-implanted deuterium desorption temperature variations depending on the component concentrations were studied. It has been established that the introduction of a V impurity to magnesium leads to the significant decrease of the deuterium desorption temperature (300-330 K) as compared to the release from Mg samples (fig. 1).

A step-like form of the curve of the deuterium desorption temperature testifies to presence of two various structural conditions at composite Mg-V depending on the relation of components. The hydrogen desorption data obtained using Mg-V and Mg-Zr [1] composites can be used for the further investigations into the hydrogen storage materials containing chemical elements with a low solubility in the alloy components.

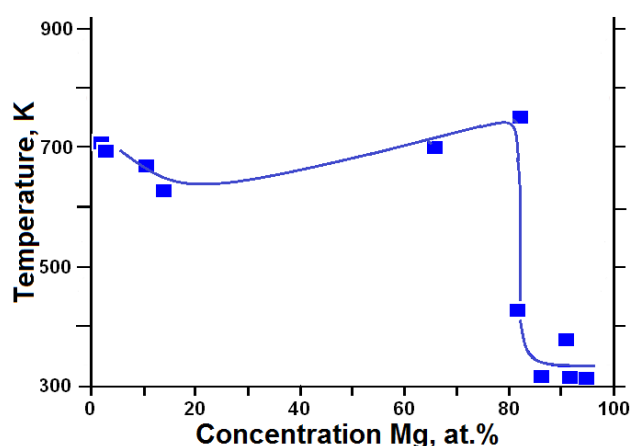


Fig.1. Thermoactivated deuterium desorption temperature of maximum versus the composition of Mg-V on the ratio of components concentration. Deuterium dose is $\sim 7.3 \times 10^{17} \text{ D/cm}^2$, $T_{\text{irrad.}} \sim 100 \text{ K}$

Reference

1. I.M. Neklyudov, O.M. Morozov, V.G. Kulish, V.I. Zhurba, N.S. Lomino, V.D. Ovcharenko, O.S. Kuprin. IOP Conf. Ser.: Mater. Sci. Eng. 23 (2011) 012028 doi:10.1088/1757-899X/23/1/012028.

Boron – the Extrinsic Trap for Atoms of Hydrogen in Electrochemical Systems

A.V. Zvjagintseva

The Voronezh state technical university, 394026, the Moscow avenue, 14, Voronezh, Russia

e-mail: zvygincevaav@mail.ru

Experimental results about behaviors of hydrogen in electrochemical systems on the basis of nickel are considered at its doping by atoms of boron. It is shown that concentration of hydrogen in electrochemical system on the basis of nickel is defined by probability of formation of defective structures in metal and is function of parameters of electrolysis. Mathematical modeling of interaction of atoms of hydrogen with extrinsic and structural traps is made. The kinetics of capture of atoms of hydrogen is defined by structural traps. The physical model of formation of pulling stresses in a vicinity of atoms of boron is offered.

Abundance of boron in system Ni-B makes 0,5-1 %. It means that on each 10-15 atoms Ni 1 atom of boron [1] joins. In places of lattice imperfections atoms of hydrogen, forming connection with nickel and boron are deployed. It is possible in that case when boron is impurity of replacement of small atomic radius and at doping Ni by boron reduction of lattice constants is observed. In its vicinity there is a pulling stress that causes interaction of atoms of boron with hydrogen (extrinsic traps for atoms of hydrogen), (fig. 1.). Hydrogen unlike boron is impurity of introduction and increases nickel lattice constants. Hydrogen is located tetra – and oktapores nickeliferous covering.

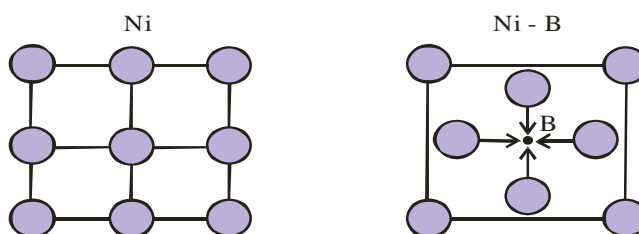


Fig.1 The scheme of displacement of atoms of nickel in a vicinity of an impurity of a pine forest. (● - Atom Ni; ● - Atom B)

References

1. A.V.Zvjagintseva, J.N.Shalimov. Doping of electrolytic alloys by the components raising degree hydrogen absorption. Scientific notes of Taurian national university of V.I.Vernadskogo. A series «Biology, chemistry». Volume 24 (63). №3. Simferopol: THY. 2011. c.96 – 102.

Comparison of Electrodes with Smooth and Nanostructured Surfaces in Pulse and DC Electrolysis

M. Vanags¹, P. Aizpurietis², J. Kleperis¹, G. Bajars¹

¹Institute of Solid State Physics, University of Latvia, Latvia

²Faculty of Physics and Mathematics, University of Latvia, Latvia

e-mail: sf11053@gmail.com; kleperis@latnet.lv

Hydrogen is one of the most important gases which is highly demanded in chemical industry as well as in hydrogen economics. On commercial scale it is produced by steam reforming of hydrocarbons; however hydrogen of high purity can be obtained in a process of water electrolysis. Effective electrolyzers are necessary to produce hydrogen as much as possible using a given quantity of electricity. The economics of electrolysis process can be improved only by efficient electrocatalysis so as to minimize the overpotentials on electrodes. The applied voltage to produce a given current and hence the desired amount of hydrogen is a sum of electrode potentials on both electrodes (cathode and anode), E_e - equilibrium cell voltage for decomposition of water 1.23 V and heat losses in electrolyte: $E_{\text{appl}} = E_e + |\eta_c| + \eta_a + IR$. Nanostructuring and modification of electrode surfaces can reduce both electrode potentials η_c and η_a and thus decrease applied voltage and heat loss in electrolysis cell.

In our work the research is done how to make an alkali electrolysis more efficient using nanostructuring of electrode surface, electrocatalyst metal and modified supply voltage. Porous electrodes are obtained by plasma spray coating a Ni-Al alloy (ratio 4:1) layer onto 316L stainless steel plate as substrate, and etching it in the hot alkaline solution of KOH. Volt-ampere and impedance characteristics are measured for electrodes in 5M KOH solution and calomel electrode as reference, using potentiostat Voltalab 310. Electrochemical characteristics (value of exchange current, corrosion stability, hydrogen evolution potential) are compared for both fresh and long time exposed to electrolysis electrodes. It is found that the Ni-Al coating increases the electrolysis efficiency and stability of the electrode during the electrolysis.

Acknowledgements

Authors acknowledge financial support of ERDF project Nr. 2010/0188/2DP/2.1.1.1.0/10/APIA/ VIAA/031

Measuring In-Plane and Through-Plane Conductivities of Polymer Electrolyte Membranes

J. Hodakovska, J. Kleperis

Institute of Solid State Physics, University of Latvia, Latvia

e-mail: julia_h_lv@yahoo.co.uk

Much of attention is paid by researchers to membrane-electrode assembly (MEA) and its parts, when new materials are investigated to improve fuel cell performance. Ion conductivity is one of the most important properties which need to be determined for membrane. In our work the membrane's through-plane conductivity is measured using MEA in the direction as it is used in an operating fuel cell. This is called a two-electrode method, and AC impedance or current interrupt techniques are used to obtain the conductivity values. In this method measured conductivity can be affected by contact resistances between the gas diffusion layer/current collector or catalyst layer; the resistance of ion diffusion media, interactions within the catalyst layer and interface catalyst/membrane. Moreover the treatments of the membrane during manufacturing MEA (stretching and hot-pressing) will change not only its structure, thickness, but also its proton conductivity.

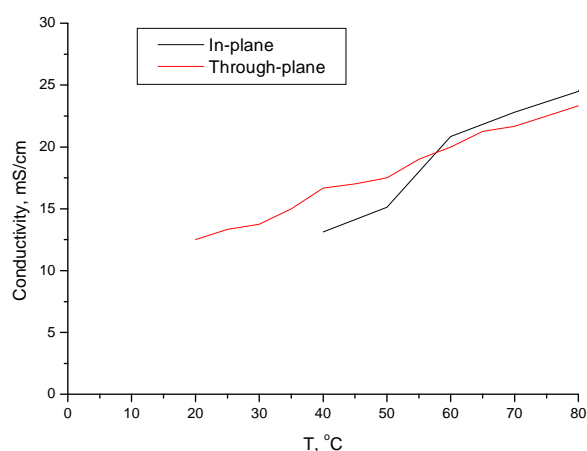


Fig.1. In-plane and through-plane conductivity results for SPEEK polymer membrane.

The other option to measure the membrane conductivity is four-electrode, in-plane conductivity when the bulk conductivity of a membrane is obtained using AC impedance or a DC voltage sweep techniques. Two different electrode positions can be used: current electrodes placed in the bottom of the membrane, but the voltage electrodes - at the top, and all four electrodes are on one side of membrane. The advantage of four-electrode method appears when comparison of synthesized sample series necessary - even if the absolute conductivity value is not exact, it is possible quickly determinate the differences between samples.

Acknowledgements

Author (JH) acknowledges LZP project Nr.09.1553 ‘Nanostructured materials for environmental friendly technologies and energy’ for financial support.

Synthesis and Photocatalytic Properties of Modified TiO₂ Nanotubes

R. Drunka^{1,2}, J. Grabis¹, A. Patmalnieks³

¹Institute of Inorganic Chemistry, Riga Technical University, Latvia

²Institute of Solid State Physics, University of Latvia, Latvia

³Institute of Microbiology and Biotechnology, University of Latvia, Latvia

e-mail: reinis_drunka@inbox.lv

Titanium dioxide is very promising material for photocatalysts, decomposition of organic compounds, splitting of water, for manufacturing self-cleaning materials and dye-sensitized solar cells. It is generally concluded that the photocatalytic activity depends on the specific surface area, phase composition and presence of dopants, which promotes absorption of visible light.

Self-organized TiO₂ nanotube-layers were formed by electrochemical anodization of titania foil in a (NH₄)₂SO₄/HF electrolyte (Fig.). The prepared by anodization TiO₂ nanotubes were fully X-ray amorphous.

Doped with sulfur nanotubes and nanopores were prepared by their treatment at 380°C in H₂S flow or by using method of micro arc oxidation in sulfur containing electrolyte.

Doped with nitrogen nanotubes were obtained by their treatment at 500 °C per 2h in NH₃ or N₂ flow.

The catalytic activity was determined by degradation of MB solution under UV and visible light illumination. The prepared photocatalysts have higher activity with respect to pure TiO₂ nanotubes. Sulfur doped nanotubes have higher activity with respect to nitrogen doped nanotubes.

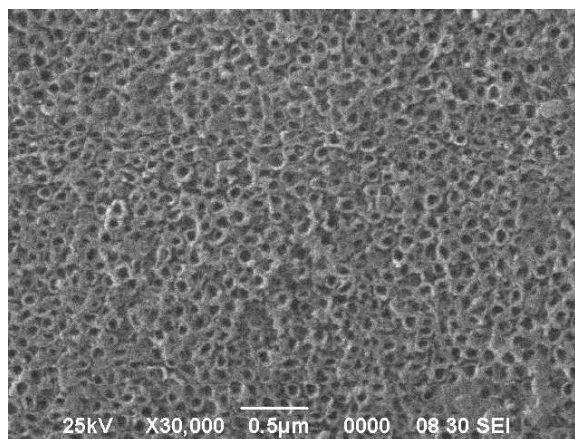


Fig.1. SEM image of TiO₂ nanotubes.

References

1. Vitiello, R.P., Macak, J.M., Ghicov, A., Tsuchiya, H., Dick, L.F.P., Schmuki, P. *Elec. chem. Commun.*, **8**, 544 (2008).
2. J.Li, L. Wan, J. Feng. *J. Mat. Pro. Tech.* **209**, 762 (2009).

EPM Fine-Disperse Platinum Coating on Powder Carriers

V. Serga, L. Kulikova, A. Cvetkov, A. Krumina

Institute of Inorganic Chemistry, Riga Technical University, Latvia

e-mail: antonzweig@hotmail.lv

Advantages of the extractive-pyrolytic method (EPM) for the synthesis of oxide materials are demonstrated when metal extraction systems with monocarboxylic acids are used [1]. With reference to the extraction systems with the anion-exchange extractant tri-n-octylamine (C_8H_{17})₃N, we studied possibilities of the EPM to produce palladium nanoparticles on α -Al₂O₃ micro granules [2] and platinum nanocrystalline films on glass substrates [3]. Platinum has been widely used in many applications, especially for catalysis and fuel cell technology.

In the present investigation, in order to coat platinum particles, a carrier sample was dispersed in a solution of the platinum-containing organic precursor $[(C_8H_{17})_3NH]_2PtCl_6$ in toluene, then it was dried and thermally treated. As carriers, we used powders of Al₂O₃, γ -AlO(OH), Y₂O₃, CeO₂, SiO₂.

The influence of the specific surface area (SSA) of the carriers, parameters of thermal treatment (pyrolysis temperature and annealing time) and the concentration of metal in the precursor solution on the mean size of platinum crystallites (\bar{d}_{Pt}) in the produced composites was investigated. It has been found that with the platinum content ≤ 2.4 wt.%, X-ray diffraction do not allow to get information on \bar{d}_{Pt} for all studied carriers except for amorphous SiO₂. It is shown (Fig. 1) that with the given carrier, the decrease in metal concentration in the precursor solution leads to a noticeable decrease of \bar{d}_{Pt} in the composite.

The decrease of the platinum particles' size was also observed with the increase of the carrier SSA (4.8 wt.% metal concentration in composites): from 20 nm (Al₂O₃ plasma processed nanopowder, SSA = 41 m²/g) to 10 nm (γ -Al₂O₃, SSA = 122 m²/g) and 5 nm (γ -AlO(OH), SSA = 146 m²/g). Metal particles with $\bar{d} \approx 10$ nm have been accordingly obtained on CeO₂ and Y₂O₃ nanopowders with the relatively small SSA of 26 m²/g and 21 m²/g.

Acknowledgments

This work was supported by ERAF project No. 2DP/2.1.1.1.0/10/APIA/VIAA/087.

References

1. A.I Kholkin, T.N. Patrusheva. Extractive pyrolytic method. M., "Com Book" (2006)
2. V. Serga, L. Kulikova, E. Palcevskis, M. Maiorov, A. Krumina. FM&NT, Book of abstracts, 158 (2009)
3. V. Serga, L. Kulikova, V. Grekhov, J. Kalnacs, A. Murashov, A. Vilken. FM&NT, Book of abstracts, 245 (2011)

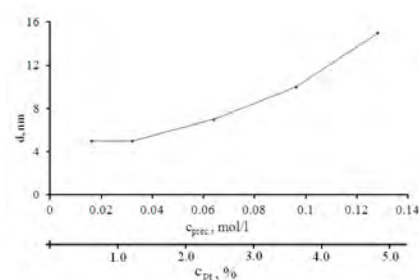


Fig.1. Influence of the platinum concentration in the precursor solution on d_{Pt} in Pt/ SiO₂ composites.

Quantification of Impurities in Solar Silicon

G. Kolosovska¹, A. Viksna¹, G. Chikvaidze², A. Osite¹, A. Opalais¹

¹Faculty of Chemistry, University of Latvia, Latvia

²Institute of Solid State Physics, University of Latvia, Latvia

e-mail: gunita.kolosovska@delfi.lv

Solar energy is potentially capable of supplying most of the global need for primary energy, and it is expected to become an alternative source for fossil fuels as a clean energy, but the economic aspect of the system is a major hindrance to its growth.

About 95% of the current solar cell module market is based on solar cells using silicon as raw material, of which about 60% is polycrystalline silicon. The key element in a solar cell energetics is technology of purification of solar silicon. The power conversion efficiency of solar cells is largely dependent on impurity levels in the silicon. With the recent significant growth of solar cell production, the demand for high purity and cheap silicon as a principal raw material is rapidly increasing, eliciting a shortage of high purity silicon.

Silicon matrix does not contain organic matter. There two methods had been applied for preparation of Silicon samples – wet mineralization at atmospheric pressure and mineralization by using the closed microwave technology. Earlier studies show that the mineralization, performed with the help of microwave technology, is three times more effective than the one – done at atmospheric pressure. Silicon dissolves only in HF and HNO₃ acids mixture. Hydrogen peroxide is also added to the acid mixture, to increase nitric acid oxidation capacity.

It was experimentally found that optimal sample amount for the microwave mineralization is about 0.5 g and optimal ratio of HF and HNO₃ acids mixture is 3 to 5. Special attention was paid to the B and P determination in solar Silicon. It is required specific sample preparation due to volatility of boron and special requirements for the phosphorus quantification by inductively coupled plasma mass spectrometry. Additionally 1 mL 1% mannitol was added for the sample preparation of boron because Boron with mannitol forms complex, which is stable up to 80 °C. For the determination of phosphorus it is necessary to add 0.5 mL of concentrated H₂SO₄.

References

1. J. Takahashi. Agilent Technologies. **6** (2008)

P-n Junction in Intrinsic Semiconductor Formed by Laser Radiation

A. Medvid^{1,2}, R. Rimsa¹, P. Onufrievs¹, E. Dauksta¹, G. Mozolevskis¹, T. Puritis¹

¹Institute of Technical Physics, Riga Technical University, Riga, Latvia

²Institute of Semiconductor Physics NAS of Ukraine, Kyiv, 03028, Ukraine

e-mail: onufrievs@latnet.lv

P-n junction is the most important component of many semiconductor devices. Thermodiffusion, ion implantation and molecular beam epitaxy are only a few methods to form a p-n junction. The main drawback for these methods is high cost per p-n junction. A possibility of p-n junction formation by laser radiation was shown in several semiconductors: p-Si[1,2], p-CdTe[3], p-InSb[4,5], p-InAs[6], p-PbSe[7] and p-Ge[8]. Different mechanisms have been proposed to explain the nature of inversion of conductivity type: impurities' segregation, defects' generation, amorphization and oxygen related donor generation. However, the proposed mechanisms have many lacks and even contradictions; therefore the mechanism of p-n junction formation by laser radiation is not clear until now. For the understanding it, i-Ge crystal was irradiated by Nd:YAG laser with different energy of quantum. The crystal was used in the experiments as a model material because the concentration of impurities in this material is lower than the concentration of intrinsic point defects at RT. Increase of rectification ratio of I-V characteristics and barrier height with intensity of the laser radiation, energy of laser radiation quanta and numbers of pulses were observed in this experiment. The mechanism of this phenomenon is explained by generation and redistribution of intrinsic point defects in temperature gradient field, which causes strongly absorbed laser radiation. The redistribution of defects takes place because interstitial atoms drift towards the irradiated surface, but vacancies drift in the opposite direction – in the bulk of semiconductor according to Thermogradient effect. Since interstitials in Ge crystal are of n-type and vacancies are known to be of p-type, a p-n junction is formed.

References

1. Y. Mada et al. Appl. Phys. Lett., **48**, 1205 (1986).
2. J. Blums et al. Physics Status Solidi (a), **K91**, (1995).
3. A. Medvid' et al., Radiat. Meas., **33**, 725 (2001).
4. I. Fujisawa, Jap., J. Appl. Phys, **19**, 2137 (1980).
5. A. Medvid' et al. Vacuum, **51**, 245 (1998).
6. L. Kurbatov et al. Reports of Acad. Sc.USSR, **268**, 594 (1983)
7. K.D. Tovstyuk et al. Ukrainian Journal of Physics, **21**, 1918 (1984).
8. S.G. Kiyak et al. Physics and Technics of Semiconductors, **18**, 1958 (1984).

Properties of the Nafion Membrane Impregnated With Hydroxyl Ammonium Based Ionic Liquids

V. Garaev¹, G. Vaivars^{1,2}, J. Kleperis², S. Pavlovica¹

¹Department of Chemistry, University of Latvia, Latvia

²Institute of Solid State Physics, University of Latvia, Latvia

e-mail: valery.garaev@gmail.com

The Nafion (*DuPont*) membrane is one of the most common and commercially available proton conducting membrane. Also, it is characterized by significant thermal, mechanical and chemical stability. Due to its good properties, Nafion membrane is widely used in fuel cells and other electrochemical applications. However, the temperature range is limited and typically do not exceed 100 °C since the ion conductivity is very sensitive to the water content changes. There are few options to solve the problem. It's possible to produce the composite membranes using zirconium phosphate [1], heteropolyacids or inorganic oxides [2] to stabilize the water content. Recently, the room temperature ionic liquids due to their excellent chemical, electrical and thermal properties are used to impregnate the polymer membranes.

In this work, the Nafion 112 membrane impregnated with nine various ionic liquids have been investigated. The used ionic liquids were combined from hydroxyl ammonium cations (2-hydroxyethylammonium/HEA, bis(2-hydroxyethyl)ammonium/BHEA, tris(2-hydroxyethyl)ammonium/THEA) and carboxylate anions (formate, acetate, lactate). (Fig. 1.) These ionic liquids are highly biodegradable and non-toxic.

The dependence of the membrane ion conductivity and thermal stability on ionic liquid content is presented.

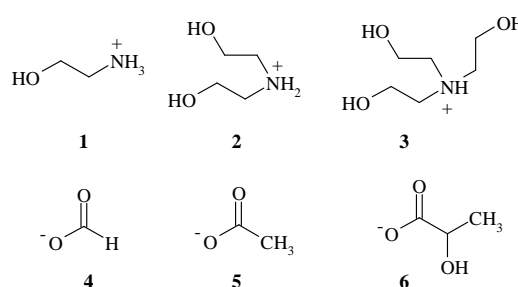


Fig. 1 In the first row: 1 - HEA, 2 - BHEA, 3 - THEA; in the second row: 4 - Formate, 5 - Acetate, 6 - Lactate

References

1. C. Yang, P. Costamagn, S. Srinivasan, J. Benziger, A.B. Bocarsly, J. Power Sources **103**, 1 (2001)
2. Z. Shao, H. Xu, M. Li, I. Hsing, Solid States Ionics **177**, 779 (2006)

Multiscale Modeling of Silicon Crystal Growth: From Molecular Dynamics to Macroscopic Features

G. Barinovs¹, A. Sabanskis¹, A. Krauze¹, A. Muiznieks¹

¹Faculty of Physics and Mathematics, University of Latvia, Latvia

e-mail: girts.barinovs@lu.lv

Industrial silicon crystal growth from a melt is largely determined by macroscopic properties of the crystal-melt system such as temperature field or capillary effects. However, the growth mechanisms at atomic scale can significantly affect the crystal growth even at macroscale. This is well pronounced by external faceting of conical crystal surface, Fig. 1, or formation of ridges and constrictions on cylindrical external crystal surface due to the presence of atomically smooth internal facets in the vicinity of triple point. In order to realistically describe the physical processes at different spatial scales, *sequential multiscale modeling* approach was used. The following steps were included:

1) Molecular dynamics calculations on atomic scale in order to calculate the dependence of free surface energy of interfaces on the crystallographic orientation.

2) Wulff's figures construction to solve the Herring's equation describing interface angles for equilibrium crystal growth.

3) The use of the solution to construct the Voronkov's angular diagrams in order to find the orientation of the external crystal surface depending on the melt orientation.

4) The prediction of the crystal edge behavior in a macroscopic model.

5) The use of a macroscopic model to predict the macroscopic physical crystal growth parameters.

The results of the multiscale modeling are in agreement with the observed behavior of facets and ridges on the silicon crystal surface.



Fig.1 Formation and the shape of atomically flat {111} facets on the external crystal surface have to be explained by simultaneous description of crystal growth at atomic and macroscopic scales. Crystal growth direction is $\langle 100 \rangle$.

Acknowledgements

The research has been supported by the European Regional Development Fund, contract No. of the project at University of Latvia 2011/0002/2DP/2.1.1.1.0/10/APIA/VIAA/085

Ab Initio Modeling of Uranium Nitride Grain Boundary Interfaces

D. Bocharov^{1, 2}, Yu.F. Zhukovskii³, D. Gryaznov³, E.A. Kotomin³

¹Faculty of Computing, University of Latvia

²Faculty of Physics and Mathematics, University of Latvia

³Institute of Solid State Physics, University of Latvia

e-mail: bocharov@latnet.lv

Uranium mononitride (UN) is considered nowadays by the Generation IV International Forum of nuclear reactors [1] as one of the most promising nuclear fuels alternative to UO_2 . However, it reveals unwanted oxidation in air which could affect the fuel fabrication process and its performance [2]. Recently, we performed a detailed study on oxygen interaction with UN surface using density functional theory calculations (see [3], and references therein) as implemented in VASP computer code [4]. We were able to identify a mechanism of UN surface oxidation consisting of several important steps starting from oxygen molecule dissociation and finishing with oxygen atom incorporation into vacancies on the surface. Taking into account the fact that synthesized specimens of polycrystalline fuel powder contains particles with differently oriented crystallographic facets and a wide variety of interfaces between the grains [5], we consider here a role of grain boundaries (GB) in UN oxidation.

In the present study, we present the results of first calculations on oxygen behavior in the UN GBs. We focus our study on simplest interface models to describe oxygen behaviour in such complex objects. We, thus, suggest a model of $(310)[001](36.8^\circ)$ tilt grain boundary used previously for describing of electron-trapping in other rock-salt compounds like MgO, NaCl and LiF [6]. We have considered three positions of incorporated O atoms, enumerated with 1-3 in Fig. 1. We have observed a clear trend for vacancy segregation at the interfaces (surface and GBs). The formation energies of N vacancy inside the GB (3.3-3.5 eV) and on the surfaces (2.9-3.7 eV) are smaller than those in the bulk material (~ 4.4 eV). Also, the O incorporation into and solution energies in the vacancies inside the GBs ($-5.6 \div -5.9$ vs. $-2.3 \div -2.5$ eV, respectively) are close to those for the UN surfaces ($-5.7 \div -6.2$ eV for O atom incorporation and $-2.4 \div -2.8$ for O atom solution).

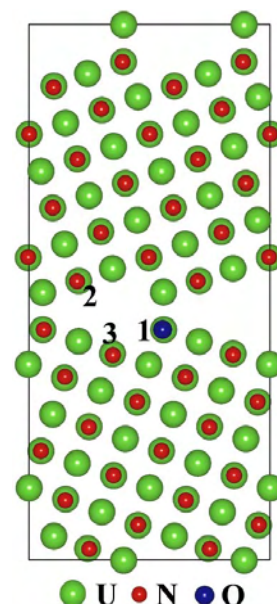


Fig. 4. Cross-section of the $(310)[001](36.8^\circ)$ tilt grain boundary for UN slab model with oxygen incorporated into position 1.

References

1. www.gen-4.org
2. Y. Arai, M. Morihira, and T. Ohmichi, *J. Nucl. Mater.* 202, 70 (1993).
3. D. Bocharov, *PhD thesis Summary*, LU, ISBN 978-9984-45-437-5 (2012).
4. G. Kresse and J. Hafner, *VASP the Guide* (University of Vienna, 2007).
5. G.W. Chinthaka Silva, Ch.B. Yeaman, L. Ma, G.S. Cerefice, K.R. Czerwinski, and A.P. Sattelberger, *Chem. Mat.*, 20, 3076 (2008).
6. K. McKenna and A. Shluger, *Nature Mater.*, 7, 859 (2008).

***Ab Initio* Calculations of Bulk and Surface Defects in MgF₂ Crystals**

F.U. Abuova¹, A.F. Fix¹, A.T. Akilbekov¹, S. Piskunov², E.A. Kotomin^{2, 3}, R.I. Eglitis²

¹L. N. Gumilyov Eurasian National University, 3Munaitpasova, Astana, Kazakhstan

²Institute of Solid State Physics, 8 Kengaraga str., University of Latvia, Riga

³Max Planck Institute for Solid State Research, Heisenbergstr.1, Stuttgart, Germany

MgF₂ with rutile structure is important wide-gap optical material with numerous applications. We present and discuss the results of calculations for basic colour centers (F-, H-, Frenkel defects) in the bulk and at surface [1, 2]. This study is based on the large scale ab initio DFT calculations using hybrid B3PW exchange-correlation functional as implemented into CRYSTAL code. In order to understand the behaviour of the material with respect to irradiation and its optical properties, we analyzed the electronic structure, atomic geometry, charge density distribution as well as defect- and surface formation energies using several types of supercells. We compare also properties of close and well separated F-H (Frenkel) defect pairs and migration of defects.

References

1. A. F. Vassilyeva, R. I. Eglitis, E. A. Kotomin, A. K. Dauletbekova, *Physica B* 2010, 405, 2125
2. A.F. Vassilyeva, R.I. Eglitis, E.A. Kotomin, A. K. Dauletbekova, *Centr. Eur. J. Phys.*, 2011, 9, 515.

Quantum Chemical Simulation on Binding Energies of Pair- and Triple-Wise Defects in Fcc-Fe Lattice for ODS Steels

A. Gopejenko¹, Yu.F. Zhukovskii¹, P.V. Vladimirov², E.A. Kotomin¹, A. Möslang²

¹Institute of Solid State Physics, University of Latvia, Riga, Latvia

²Karlsruhe Institut für Technologie, Institut für Materialforschung-I, Karlsruhe, Germany

e-mail: agopejen@inbox.lv

Reduced activation ferritic-martensitic steels (RAFM) are promising structure materials for future fusion reactors. These materials possess better thermal conductivity, higher swelling resistance and lower damage accumulation than austenitic steels. Also these materials were developed to reduce the pollution and decrease the requirements for the facilities of the waste storage of the radioactive structures of the fusion reactors after service. Some elements that are contained in martensitic steels were substituted by other elements with faster decay of the induced radioactivity. One of the most used oxides used to reinforce RAFM steels is Y_2O_3 . The RAFM steels strengthened by Y_2O_3 particles are being tested to evaluate the possibility of their implementation at temperatures of 650°C and higher instead of RAFM steels in combination with the advantages of the RAFM steels. Compared with the conventionally produced RAFM steels ODS RAFM steels have better tensile and creep properties.

The work is aimed at theoretical study on atomic scale mechanisms of yttria particle nucleation and growth. For study of these mechanisms, it is necessary to investigate the interaction of yttrium solute atoms with vacancies and with oxygen atoms in interstitial positions as well as in substitute positions of Fe atoms. This stage requires systematic large-scale first principle calculations. The data set obtained at this stage [1,2] is used for further kinetic Monte Carlo simulations of yttria particle nucleation and growth. Deep understanding of the kinetics of ODS particle formation gained in this project would support the new ways for further improvement of the properties of ODS steels advancing their development for fusion and numerous high-temperature applications as well as increasing their radiation resistance.

References

1. A. Gopejenko, Yu.F. Zhukovskii, P.V. Vladimirov, E.A. Kotomin, A. Möslang, Ab initio simulation of yttrium oxide nanocluster formation on fcc Fe lattice. - J. Nucl. Mater., 2010, 406, p. 345–350.
2. A. Gopejenko, Yu.F. Zhukovskii, P.V. Vladimirov, E.A. Kotomin, A. Möslang, Modeling of yttrium, oxygen atoms and vacancies in γ -iron lattice. - J. Nucl. Mater., 2011, 416, p. 40-44.

Influence of SiO₂ Admix on Radiolysis of Powders of Li₄SiO₄

A. Zarins¹, G. Kizane¹, A. Supe¹, L. Baumane², A. Berzins³, Dz. Rašmane⁴, I. Steins⁴

¹Institute of Chemical Physics, University of Latvia, Latvia

²Latvian Institute of Organic Synthesis, Latvia

³Faculty of Chemistry, University of Latvia, Latvia

⁴Institute of Inorganic Chemistry, Riga Technical university, Latvia

e-mail: arturs.zarins@lu.lv

Lithium orthosilicate pebbles with 2.5wt% SiO₂ additions (Li₄SiO₄+2.5 wt% SiO₂) have been selected as one of possible breeder material for the European Helium Cooled Pebble Bed (HCPB) blanket module [1]. Most of all previous research of radiolysis of Li₄SiO₄ was done with “pure” Li₄SiO₄ ceramics [2]. Aim of our research was to investigate influence of additions of SiO₂ on radiolysis of ceramics of Li₄SiO₄ in air atmosphere.

Paramagnetic radiation defects - SiO₃³⁻ and SiO₄³⁻, which are characteristic for “pure” Li₄SiO₄, also mostly forms in powders of Li₄SiO₄ with 2.0 wt% SiO₂ additions under action of γ radiation ($D_{\text{absorb.}}=56$ kGy, $P=14$ kGy·h⁻¹),

(Fig. 1.). Approximately two times less concentration of radiation defects forms in powder of Li₄SiO₄ with SiO₂ additions ($2.7 \cdot 10^{18}$ radicals per gram), than in “pure” powder of Li₄SiO₄ ($4.6 \cdot 10^{18}$ radicals per gram).

Higher concentration of radiation defects in “pure” powder of Li₄SiO₄, comparing with powder with SiO₂ additions, might be caused by accumulation of chemisorption products of H₂O and CO₂. In support of a hypothesis, that on particles of powder Li₄SiO₄ with SiO₂ additions forms a layer of SiO₂, which delays chemisorptions of gases, is the fact that in ESR spectra of “pure” powder of Li₄SiO₄ after irradiation forms signals of radiation defects of products of chemisorptions. In powder of Li₄SiO₄ accumulate two radiation defects of radiolysis of Li₂CO₃ and one radiation defect (atomic hydrogen) of radiolysis of LiOH or (H₂SiO₃)_n (Fig. 1.).

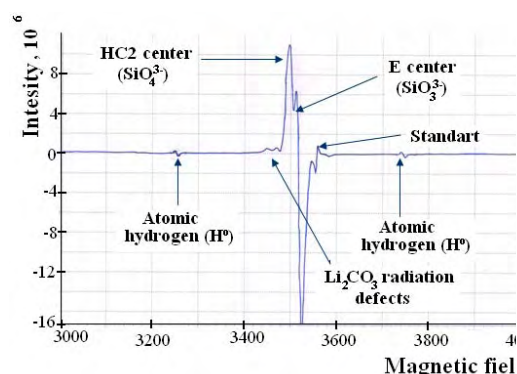


Fig.1. ESR spectra of “pure” Li₄SiO₄ powder after irradiation by γ radiation ($D_{\text{absorb.}}=56$ kGy, $P=14$ kGy·h⁻¹, air atmosphere)

References

1. M. Zmitko et. al., Jour. of Nucl. Mat. **417**, 678-683 (2011).
2. J. E. Tiliks et. al., Fus. Eng. and Des. **17**, 17-20 (1991).

Comparison of Tritium Accumulation in Various Divertor Tiles Depending on the Geometrical Positioning in the Divertor Structure

M. Halitovs, G. Kizane, A. Vitins, E. Pajuste, L. Avotina, J. Jansons

Institute of Chemical Physics, University of Latvia, Latvia

e-mail: mihails_halitovs@inbox.lv

The research experiments compare tritium mass activity in various divertor tiles of JET fusion device MkII-SRP type divertor. The two tiles examined (Fig. 1) are of the same divertor sector but having different plasma interaction therefore also different tritium accumulation conditions. Carbon fiber composite (CFC) divertor tile 14IN G3B is under direct plasma interaction while tile 14BW G4B is only partially interacting with plasma because of the different geometric positioning in the divertor structure.

Because of the positioning tile 14IN G3B should have higher mass activity of tritium. Yet, it also has a higher erosion ratio as plasma actively re-interacts with the erosion material layer on the top of CFC tile. What concerns tile 14BW G4B, it has less plasma interaction on the surface and part of it is geometrically covered from plasma interaction by tile 14IN G3B. Therefore a part of tile 14BW G4B is covered with stable erosion material layer. This layer additionally accumulates tritium and later on it diffuses into the bulk of CFC tile.

Tritium mass activity on surface of tile 14IN G3B is around $2.6 \cdot 10^6$ Bq·g⁻¹ (Cyl4e and Cyl6e) while for tile 14BW G4B surface activity varies from $1.2 \cdot 10^6$ Bq·g⁻¹ (2Cyl1) up to $1.6 \cdot 10^8$ Bq·g⁻¹ (1Cyl10). The same tendency remains in the bulk – the layer below 1 mm depth has activity around $2 \cdot 10^4$ Bq·g⁻¹ for tile 14IN G3B, while it is mostly $8 \cdot 10^3$ Bq·g⁻¹ for tile 14BW G4B (Fig. 2, a) Top slice activity, b) Bulk activity).

References

1. E. Pajuste et al., J. Nucl. Mat. 415, S765–S768 (2011)

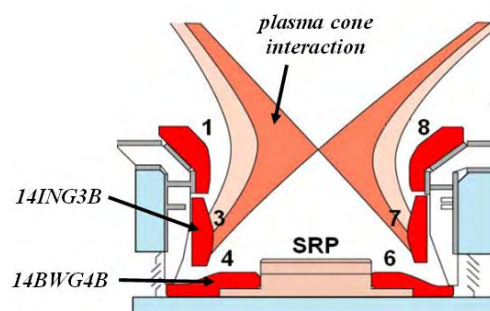


Fig.1 The scheme of MkII-SRP type divertor and position of examined tiles

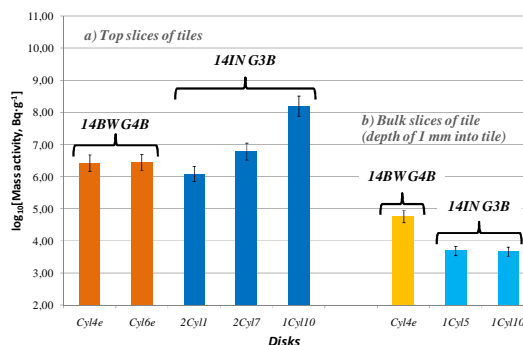


Fig.2 Tritium mass activity in CFC tiles

Methane Emissions by Combustion of Biomass

J. Kalnacs, V. Grehov, D. Grigale, A. Murashov, A. Orupe, A. Vilken

Institute of Physical Energetics, Latvia

e-mail: jkalnacs@edi.lv

Emission factors for solid biomass fuels are determined taking into account fuel consumption in natural units at the same moisture content in fuel used for reporting on fuel consumption to the Central Statistical Bureau. In determining emission factors, the IPCC 1996 Revised Guidelines for National Greenhouse Gas Inventories and the 2000 Good Practice Guidance and Uncertainty Management in National Greenhouse Gas (GHG) Inventories, as well as physico-chemical characteristics of solid biomass fuels used in Latvia are taken into account. For integral determination of concentration of individual components in the GHG emissions, Fourier infrared spectrometer IR Prestige-21, Shimadzu, Japan, graduated (calibrated) by the corresponding gases was mainly used. The results are summarized in Table 1.

Table 1. CH₄ emission factors, g/ MWh obtained energy

Heat unit Fuel		1	2	3	4	5	6
		1	Firewood	18.7	31.8	39.3	296
2	Wood chips	7.4	17.8	28.2	229.9	–	–
3	Wood waste	18.9	17.2	44.7	278.5	–	–
4	Wood briquettes	–	29.7	–	355.1	348.7	297
5	Wood pellets	1588.88*	–	574.44	330.00	–	–
6	Charcoal	–	–	–	778.71	740.21	–

Notes:

* - The result was obtained for automatic boiler working in the smouldering mode as warm weather conditions determined a small actual power of boiler.

1-Central heating boilers; 2. Hot water boilers; 3. Combined (two-functional) central heating and hot water boilers; 4. Room stoves; 5. Economic stoves; 6. Kitchen ovens.

Conclusions

1. CH₄ emissions have been detected for practically all furnaces and can be assessed as minor, but precise result can be obtained only for the particular furnace in the particular circumstances.
2. CH₄ emissions are more dependent from combustion circumstances, but not from biomass quality.

Characterisation of Biomass Ashes

J. Kalnacs, V. Grehov, D. Grigale, A. Murashov, A. Orupe

Institute of Physical Energetics, Latvia

e-mail: jkalnacs@edi.lv

The enhancement of biomass-derived energy plays an important role in the Europa energy and climate strategies. The use of new and upgraded biomass fuels, has become more common in recent years. Although municipal heating become still the most popular heating systems in Latvia.

Currently biomass ash is a waste product, disposed of in landfills or stored elsewhere. Ash disposal generates costs for energy, and so also expenses for ash producers.

The aim of investigation is to gate the content of different biomass ashes and to understand its influence on melting behaviour and possibilities for utilisation ashes as fertilising and liming agent in agriculture. Biomass ash usually contains mineral plant nutrients, especially base cations (e.g. Ca, Mg, K), and has a strongly alkaline pH. Thermogravimetric and diferential thermo analyse – fig. 1 is used for analysing thermal behavior of biomas ashes . Tthere are obtained dependences between different biomass ash composition and qualities, detrmined fusion, liming and fertilising.

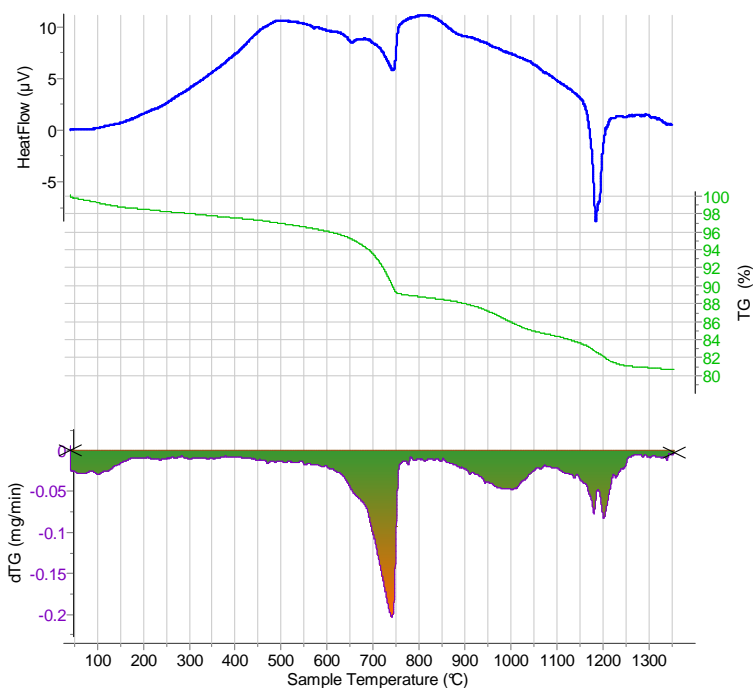


Fig.1 Tipicle temperature dependance of heat flow and weight looses for biomass ashes.

Growth and Properties of Strained Epitaxial Nanolayers of Lead Selenide

A.M. Pashaev¹, O.I. Davarashvili², Z.G. Akhvlediani², M.I. Erukashvili², R.G. Gulyaev²,
V.P. Zlomanov³

¹National Aviation Academy of Azerbaijan, Baku

²Iv. Javakhishili Tbilisi State University

³M. V. Lomonosov Moscow State University

The investigation of semiconductor layers with a large mismatch with the substrate (>0.01) has become a rather interesting problem in physics and material science of semiconductors. In the case of strained layers grown on the substrates with larger lattice constants (when they are subjected to tension), two basic problems are distinguished [1]: 1. The defects also causing tension of the layers are pushed to the surface, forming the conditions for runoff defects and the decrease in the layer entropy, which is often necessary in the nanotechnology of semiconductors. 2. In IV-VI semiconductors, for instance, in the heterostructure PbSe/KCl ($\alpha_{PbSe} = 6.126 \text{ \AA}$, $\alpha_{KCl} = 6.290 \text{ \AA}$), the forbidden gap width must increase with the tangential lattice constant. Such conditions correspond to the effective “negative” pressure in lead selenide. This work is devoted to the investigation of the mentioned problem.

The epitaxial PbSe layers were obtained on KCl substrates by the method of molecular epitaxy with a “hot wall”. The temperature of the polycrystalline PbSe source was in the interval from 450 to 510°C. The substrate temperature was relatively low, 240-300°C. The growth rate of the layers was controlled from 1 to 10 nm/s by varying the intensity of the molecules flow on the substrate. The thicknesses of the layers were 20-2000 nm, but special attention was given to the layers < 100 nm thick.

The investigation of the layers with the decrease of their thicknesses to 20 nm showed that the tangential lattice constant of PbSe increased up to 6.220 \AA [2].

By optical characterization of the layers, by the data on IR transmission the forbidden gap width over a wide range of thicknesses of the layers was determined. In the thin PbSe layer 72 nm thick, the forbidden gap width increased by 117 meV as compared with a thicker unstrained PbSe layer 1.8 \mu m ($E_g=286 \text{ meV}$).

References

- 1 A.M. Pashaev, O.I. Davarashvili, M. I. Erukashvili, R. G. Gulyaev and V. P. Zlomanov *Georgian Engineering News*, 2,88,(2011).
2. O.I. Davarashvili, R. G. Gulyaev, M. I. Erukashvili and M. A Dzagania *Bulletin Nat. Georg.Akad. Sci*, 36, 1, 39, (2010).

TABLE OF CONTENTS

A

Abdukadyrov	207
Abele	48, 189
Abuova	305
Aizpurietis	296
Akhvlediani	311
Akilbekov	127, 207, 305
Akishin	159, 255
Albertini	49
Albino	141
Aleksanyan	50
Alekseeva	200
Aleksejeva	178
Aleksiejūnas	264
Alfimov	34
Alute	249, 263
Anan'ev	210
Andersone	194
Andzane	51, 261, 262
Anspoks	231, 233, 234, 235
Antisari	40, 42
Antonova	137, 138, 139, 140, 147, 201, 221
Antsov	259
Aoki	223
Apsite	242
Augustovs	110
Aurora	40
Avotina	308
Azamat	52
Azens	161

B

Badalyan	52
Bagaturyants	34, 198
Bagdzevičius	140, 141
Baitimirova	274
Bajars	162, 163, 165, 290, 291, 296
Bakulin	73, 123
Balezin	238
Baluyan	181
Bandura	53
Banys	74, 140, 141, 143, 144, 145
Baranauskas	86
Baranov	58
Barczak	183
Barinovs	303
Barkanov	150, 158, 159, 255
Bauermeistere	193
Baumane	307
Bdikin	38
Beganskiene	256
Begens	277
Bellucci	90, 132, 276, 278
Belous	130
Bennetsen	70
Bensalah	153
Berger	258
Bergfelds	119
Berkowski	69

Berzina	264
Berzina-Cimdina	219, 292
Berzins A.	307
Berzins Dz.	226, 227
Bester	97
Biednov	250
Bikhert	206
Bilalov	155
Birjukovs	261
Birks	139, 140
Bitenieks	257
Blokhin	67, 115, 116
Blums	245, 246, 248, 284
Bocharov	125, 304
Bochkov	258
Bogdanov	210
Bokov	143
Bolesta	220
Bonetti	42
Bormanis	133, 134, 135, 142, 145, 149, 154, 155, 156
Borodajenko	292
Boscherini	42
Bosne	38
Boyko	62
Brik	54, 69, 72, 78, 83
Brilingas	145
Bujakiewicz-Korońska	148
Bulanovs	199
Burkhanov	156
Burlutskaya	90, 278
Butikova	55, 236
Bychanok	79
Bykov	56
Bystrov	38, 122
Bystrova	122

C

Castel	141
Ceragioli	86
Chate	192
Chen	264
Cherepakhin	82
Chernenko	217
Chernyshev	229
Chikin	269
Chikvaidze	119, 300
Christensen	35
Chub	269
Chubarov	57
Chudoba	77
Churmanov	58
Cielavs	180
de la Cruz	99, 285, 287
Cvetkov	151, 272, 299
Czaplewski	184, 185, 270
Čornaja	272

D

D'yachkov	59
Dacenko	223

Dauksta.....	153, 301
Daletbekova.....	206, 207, 208
Davarashvili.....	311
Dec.....	152
Dehtjars.....	76
Dejneka.....	44, 52
Dekhtyar.....	87, 122
Delgadillo.....	38
Denys.....	66
Dieguez.....	153
Dimza.....	146, 147, 201, 221
Dindune.....	162
Dirba.....	289
Dizhbite.....	194
Dobele.....	194, 253
Dobrovolsky.....	269
Doke.....	203, 204, 205
Dolgov.....	61, 62
Dorogin.....	259
Dovbeshko.....	62
Drozd.....	95
Drunka.....	298
Dubencovs.....	272
Duburs.....	270
Duka.....	185, 270
Dunce.....	139, 140
Duzynska.....	95
Dyachkov.....	276, 278

E

Ecis.....	161
Efimov.....	229
Efimova.....	229
Efremov I.....	134, 154
Efremov V.....	133, 134, 154
Eglitis.....	63, 124, 305
Eiras.....	144
Elksnis.....	251
Enukashvili.....	311
Erts.....	48, 51, 114, 189, 240, 242, 249, 260, 261, 262, 263
Etier.....	91
Evarestov.....	30, 53, 67, 98, 115, 116, 232

F

Fabeni.....	209
Fedorovskis.....	48, 189
Fedotovs.....	226, 227
Feldbach.....	50
Ferreira.....	88
Fesenko.....	62
Fidelus.....	95
Fitting.....	64, 131
Fix.....	305
Flerov.....	65, 82
Fomins.....	171, 172, 174
Foret.....	48
Franckevičius.....	108
Freidzon.....	198
Frolov.....	132
Fuks.....	71
Fursikov.....	66

G

Gabrusenoks.....	121, 165, 291
Galimov.....	75
Galitskiy.....	294
Garaev.....	302
Garbarz-Glos.....	136, 137, 138, 148
Garibin.....	217
Gattia.....	40
Gavare.....	241
Gavars.....	212
Geraldies.....	38
Gerbreders.....	177
Gerca.....	180, 252
Gertners.....	176
Gluhihs.....	192
Gnatyuk.....	223
Goettmann.....	84
Golant.....	211
Gopejenko A.....	306
Gopeyenko V.....	90, 278
Gorelik.....	62
Gorev.....	65, 82
Grabis.....	95, 222, 258, 298
Gracheva.....	44
Grafov.....	269
Grandjean.....	84
Granqvist.....	36
Grazulevicius.....	102
Grechishkin.....	149
Grehovs.....	180, 309, 310
Grigalaitis.....	141, 143, 145
Grigale.....	309, 310
Grigalovica.....	188, 258
Grigorjeva J.....	264
Grigorjeva L.....	128, 200, 201, 202, 225
Grinberga.....	290, 291, 293
Grīva.....	76
Gross.....	191, 193
Grossin.....	191
Grube J.....	203, 204, 205
Grube M.....	241
Gruduls.....	241
Grudis.....	102
Gruzdev.....	58
Gryaznov.....	67, 81, 115, 126, 304
Grzybowski B.....	287
Gržibovskis R.....	111
Gubaev.....	44
Guillot.....	84
Gulbinas.....	108
Gulyaev.....	311

H

Halitovs.....	308
Hanschmidt.....	168, 170
He.....	63
Heim.....	258
Henry.....	57
Heredia.....	38
Heremans.....	41
Hirsimäki.....	254
Hmelnickis.....	48, 189
Hocker.....	73, 123
Hodakovska.....	297
Hodkiewicz.....	49

Högberg	57
Holmes	51, 260, 261, 262
Hoop	182
Høvik	37
Hrubiak	95
Hussainov	170
Hussainova	169

I

Il'ves	92
Irina	250
Isaenko	85
Ivanov M.	140
Ivanov V.	200
Ivanov V. Yu.	58
Ivanova A.	149
Ivanova A.	180
Ivashkevich	132

J

Jablonskas	143
Jakovlevs	160, 228, 268, 292
Janeliukštis	164
Janisels	120
Jankovica	202, 205, 241
Jankovskis	160
Jansons	308
Jarašiūnas	264
Järvekülg	70, 167, 168, 224
Jastrabik	44, 52
Jasulaņeca	260
Jekabsone	165
Jershova	191
Jha	287
Jia	63
Joost	254
Josse	141
Jurģis	111
Jursenas	102, 195, 197
Juška	103

K

Käämbre	254
Kaemmer	218
Kalendarev	161, 231, 233
Kalinko	230, 231, 232, 233, 234, 235
Kalkis	179, 188
Kallaev	155
Kalnacs	180, 309, 310
Kalnin	68
Kalvane	18, 138, 142, 146, 148, 149, 155, 156
Kaminska	69, 95, 148
Kampars	109, 111, 196, 197, 272
Kanepe	162
Kangur	70, 224
Kanygin	79
Kaplunova	149
Karbovnyk	220
Kareiva	193, 256
Kärner	209
Karpicz	195
Kartashev	82

Kashcheyevs	280, 281
Kassymkanova	208
Katashev	87
Katkevics	240, 249, 263, 274
Kaulachs	180
Kazerovskis	276
Kazlauskas	102
Kazuss	94
Kędzierska	77
Khanin	217
Khenkin	181
Kholkin	38
Kiisk	61, 62, 70, 224
Kikas	72, 254
Kink	167, 170, 254
Kinka	141, 142
Kirilov	199
Kirilova	199
Kirm	31, 50, 85, 288
Kisand	254
Kiselova	226, 227
Kityk	54, 220
Kizane	307, 308
Kleemann	152
Kleperis	162, 163, 289, 290, 291, 293, 296, 297, 302
Klopov	117
Klotins	118, 221
Knite	186, 252, 257, 265, 266, 267, 268
Knoks	289
Kokars	110, 196
Kolobjonoks	177
Kołodziejczyk	77
Kolosovska	300
Konsin	157
Korepanov	206, 208
Kosmaca	51
Kotlov	221, 230
Kotomin	67, 68, 71, 81, 99, 116, 126, 127, 282, 283, 285, 304, 305, 306
Kourkoutis	64
Kovalovs	150, 158, 159, 192
Kozlovs	94
Krasilnikova	194
Krasnenko	72
Krasnikov	209, 213
Krauze	119, 120, 303
Kreichberga	197
Kreuer	97
Krievs	271
Kronkalns	244, 245
Krotkus	102
Krumina	151, 299
Kucins	189
Kucinskis	162, 163
Kukle	166
Kukli	50
Kuklja	71, 81
Kulda	39
Kulikova	151, 272, 299
Kulis	235, 236
Kulish	239, 294
Kulkova	73, 123
Kunakova	261
Kundzina	147
Kundzins K.	128, 146, 147, 252
Kundzins M.	147
Kuprevics	48, 189
Kuprin	130, 294
Kurilin	132

Kuusik	254
Kuzhir.....	74, 79, 132
Kuzmin 96, 116, 125, 215, 222, 229, 230, 231, 232, 233, 234, 235	
Kuznetsov.....	74
Kuznetsova.....	88
Kuzovkov	99, 282, 283, 285, 286, 287

L

Laguta.....	209
Läheranta	75
Laipniece	196
Lancere.....	76
Lancok.....	52
Lange.....	50
Lapidus.....	184, 185
Lapko.....	132
Larosa.....	273
Lashkul.....	75
Latvels.....	187
Lauberts.....	194
Lācis.....	120
Lescinskis.....	240
Lesnicenoks.....	293
Lesnikovich.....	132
Lewandowska-Szumieł.....	77
Li.....	282
Lickrastina.....	248
Liepa.....	268
Liepina Ineta.....	290, 291
Liepina Inta.....	184, 185, 270
Liepina V.....	225
Liepins.....	241
Linarts.....	266, 267
Lisitsyn.....	206, 208
Lisitsyna.....	206, 208
Lisovski.....	275
Lisunov.....	75
Liu.....	104
Livinsh.....	136, 138, 147, 201, 221
Livshits.....	262
Liwo.....	184, 185, 270
Lobanov.....	85
Lobjakas.....	170
Löhmus A.....	70, 168, 169, 170, 182
Löhmus R.....	167, 259
Lojkowski.....	77
Lombardi.....	242
Lomino.....	130, 294
Lomonosov.....	132
Loot.....	61
Lubane.....	246
Łukasiewicz.....	152
Lupascu.....	91
Luse.....	171
Lushchik.....	89
Lusis.....	163, 164, 165, 291

M

Ma.....	69, 78
Macevskis.....	94
Macka.....	48
Mackeviciute.....	144
Macutkevic.....	74

Mäeorg.....	170, 182
Maevsky.....	122
Maglione.....	141
Maier.....	67, 71, 81, 115, 116
Maiorov.....	151, 243, 244, 246, 247, 248, 289
Makarova.....	135
Maksimenko.....	74, 79, 132
Maksimov.....	210
Maksimovs.....	257
Malyshev.....	237
Malyshkina.....	149
Maļinovskis.....	242
Manika.....	129
Maniks.....	129
Mannsberger.....	80
Marcins.....	55
Marcos.....	108
Mastrikov.....	71, 81
Matīss.....	271
Mats O.V.....	239
Mats V.O.....	239
Matzui.....	266
Medvid.....	153, 301
Meija.....	260, 261, 262
Merijs Meri.....	179, 188, 257, 258
Merkle.....	81
Merzlyakov.....	282
Mezinskis.....	289, 290
Mezulis.....	245, 247, 248
Miasojedovas A.....	102
Miasojedovas S.....	197, 264
Mihailova.....	199
Mihailovs.....	197
Mihashenok.....	82
Mikhaleva.....	82
Millers.....	200, 201, 202, 225
Mironova-Ulmane 83, 160, 194, 214, 219, 222, 228, 253, 292	
Mishnev.....	243
Moiseyenko.....	62
Molotovska.....	237
Montone.....	40, 42
Monty.....	95, 225
Morozov.....	130, 239, 294
Moskvin.....	58
Möslang.....	306
Mourabit.....	84
Mozolevskis.....	301
Muhins.....	55
Muiznieks.....	119, 120, 303
Muizzemnieks.....	179
Mukhyshbaeva.....	207
Muktepavela.....	128
Murashov.....	180, 309, 310
Muzikante.....	111, 187, 195, 249
Mychko.....	153

N

Nagirnyi.....	85
Naidoo Q.....	190
Naidoo S.....	190
Nanni.....	273
Nargelas.....	264
Narkevica.....	292
Nazarovs.....	280
Ndungu.....	190
Nechaev.....	190
Neklyudov.....	294

Nemilov.....	210
Nielsen.....	41
Nikl.....	89, 209
Nömmiste.....	254
Novakova.....	181
Nunney.....	80
Nunzi.....	104

O

Odinokov.....	198
Okotrub.....	79
Omarov.....	155
Omelkov.....	85
Onufrievs.....	301
Opalais.....	300
Ornicane.....	109
Orupe.....	309, 310
Osite.....	274, 300
Ovcharenko.....	130, 294
Ozolins J.....	275, 292
Ozolins V.....	41
Ozolins M.....	171, 172, 173, 174
Ozols A.....	110
Ozols K.....	186, 266

P

Paalo.....	170
Paddubskaya.....	74, 79
Pajuste.....	308
Palatnikov.....	133, 134, 135, 154
Pankratov.....	215, 216, 220, 221, 230
Paramonova.....	122
Pärna.....	254
Part.....	168
Pascarelli.....	229
Pashaev.....	311
Pasquini.....	42
Pastare.....	249, 263
Pastors.....	109, 111
Paszkwicz.....	95
Patmalnieks.....	298
Paulins.....	173
Pavlovica.....	302
Pazzi.....	209
Pedersen.....	57
Pentjuss.....	164, 165, 271
Peterlevitz.....	86
Petrik.....	190
Piekarczyk.....	137
Pietrzykowska.....	77
Pikker.....	61
Pikuly.....	135
Pilipavicius.....	256
Pilmane.....	175
Pishtshev.....	117
Piskunov.....	125, 275, 276, 277, 305
Plank.....	288
Plaude.....	146, 147
Plushch.....	79
Podyman.....	237
Polakovs M.....	219, 228
Poletaev.....	66
Polyaka.....	122
Polyakov B.....	55, 235, 236, 259

Ponomarenko J.....	194
Ponomarenko N.....	160
Poperenko.....	223, 250
Poplauskis.....	48, 189, 212, 242
Popov.....	215, 220, 221, 229, 230
Prikulis.....	242, 260, 262
Pudzis.....	187
Purans.....	96, 116, 125, 126, 127, 161
Puritis.....	301
Pustovarov.....	58, 85

R

Rašmane.....	307
Reedo.....	169, 182
Reemann.....	70
Reinholds E.....	228
Reinholds I.....	179, 188
Reisfeld.....	87
Reiterov.....	206
Reshetnyak.....	130, 294
Reszka.....	95
Reverberi.....	273
Rey.....	191
Ribeiro.....	88
Riikjärv.....	168
Rimsa.....	301
Rodionov.....	44
Rodnyi.....	43, 217
Romanova.....	87
Romanyuk.....	62
Ronis.....	162
Rovetsky.....	220
Rubenis.....	292
Rucevskis.....	150
Rudnitskaya.....	38
Rusan.....	210
Russakova.....	207
Rutkis.....	111, 114, 196, 197, 252
Rutkovskis.....	242
Ryškevič.....	195

S

Saal.....	167, 168
Saar.....	70
Sabanskis.....	120, 303
Sablina.....	82
Saharov.....	110
Sakalauskas.....	256
Sakale.....	265, 266, 268
Salak.....	88
Salakhov.....	44
Salma-Ancane.....	219
Salundi.....	167, 168
Samulionis.....	141, 142
Saraidarov.....	87
Sarakovskis.....	202, 203, 204, 205, 216, 226, 227
Sartinska.....	132
Savikhin.....	89
Saxena.....	95
Scherbina.....	154
Schmauder.....	73, 123
Schmidt.....	64
Schwartz.....	89
Sedyshev.....	132

Segal	243
Seliverstov	217
Serga	151, 272, 299
Serrano	108
Seyedhosseini	38
Shakhnin	237
Shalapska	213
Shcherbina	133, 134
Shi	63
Shidlovskaya	279
Shimane	177
Shipkovs	180
Shirmane	215, 216, 221, 230
Shlihta	180
Shuba	79
Shugai	89
Shunin	90, 278
Shvartsman	91, 152
Shvetsov	132
Sidorov	133, 134, 135, 154
Sikolenko	229
Sildos	50, 61, 62, 83, 219, 222, 224, 253, 292
Silenko	132
Sints	245
Sitko	148
Sivars	293
Sīpols	111
Skagers	175
Skagestad	37
Skudra	212, 251
Skuja	197
Skvortsova	214, 228
Smejkal	48
Smeltere	136, 137, 138
Šmiga	136, 137, 148
Smirnov	217
Smits J.	163
Smits K.	201, 202, 225, 241
Smolen	77
Sokolov	58
Sokovnin	92, 238
Solonin	132
Solovjovs	267
Sorkin	157
Sorokin	126, 127
Sozańska	93
Spohr	277
Springis	203, 204, 205
Sproģe	272
Stalidzane	87
Steins	307
Stepanova	272
Stepina	265
Sternberg	114, 139, 140, 145
Stonkus	185
Strazdina	94
Stryganyuk	213
Suchocki	69, 95, 148
Supē	307
Sursajeva	128
Sushinskiy	237
Susinskis	48, 189
Sutka	289, 290
Svagere	212
Svane	35
Svirskas	140
Swieszkowski	77
Sybilski	69
Syrnikov	44

Ščajev	264
Šints	246

T

Tale	55, 236
Tamanis	128
Tamm	50
Tarasov	66
Tätte	168, 170
Tedim	88
Teisseyre	95
Telysheva	194
Teófilo	86
Teteris	112, 176, 177, 178, 211
Tikhomirov	198
Timoshenko	96, 231, 233, 234, 235, 281
Timusk	167, 168
Titkov	75
Tokmakovs	196
Tolmachova	130
Tomkeviciene	102
Touzin	131
Traskovskis	110, 196
Trefilova	208
Trepakov	44, 52
Trinkler	264
Troyanchuk	229
Trukhin	211
Trukša	174
Tuckerman	97
Tumanov	156
Tupureina	265, 268
Turovska	111

U

Uimin	58
Ukshe	269
Umalas	169
Useinov	127
Utinans	276, 277
Utt	224

V

Vaišnoras	108
Vaivars	190, 302
Välbe	182
Valkunas	105
Valusis	74
Vamze	175
Vanags	296
Varghese	260
Vasil'chenko E.	89
Vasylechko L.	148
Velgosh	220
Velķere	164
Vembris	187
Ventura	184, 185
Vieira	88
Vihodceva	166
Viksna	191, 193, 240, 249, 251, 263, 274, 300
Vilčiauskas	97
Vilken	309

Vilnis	161
Vitins	308
Vladimirov	306
Vlassov	259
Voitkans	55
Voloshinovskii.....	213
Volperts	253
Voss.....	203, 204, 205

W

Walsh.....	48
Wang	282
Weizman.....	71
Wojtas.....	38

Y

Yartys	66
Yavorska.....	48
Ye	143
Yermakov	58
Yermekova	208
Yue	63
Yurgelevych	223
Yusupov	44

Z

Zabels.....	129
Zablotskaya.....	243
Zablotsky	284
Zandersons.....	164
Zanin.....	86
Zanriba.....	48, 189
Zarins A.	307
Zarins E.....	196
Zavickis.....	266, 267
Zazubovich	209, 213
Zdorovets	207
Zheludkevich	88
Zherebtsov	75
Zhgun.....	125
Zhukovkii.....	304
Zhukovskii	90, 98, 126, 127, 275, 276, 277, 278, 306
Zhumazhanova.....	207
Zhurba.....	130, 239, 294
Zhydachevsky	148
Zicans.....	179, 188, 257, 258, 271
Zlomanov	311
Zorina.....	212
Zubkins	161
Züttel.....	45
Zvejnieks.....	99, 118, 282, 283
Zvjagintseva.....	295
Žižkuna	272

Notes

Notes